

Alma Mater Studiorum – Università di Bologna  
in cotutela con Université Claude Bernard Lyon 1

**DOTTORATO DI RICERCA IN**

**Bioingegneria**

Ciclo XXVII

**Settore Concorsuale di afferenza:** 09/G2

**Settore Scientifico disciplinare:** ING-INF/06

**THE RECONSTRUCTION OF SKELETAL MOVEMENT:  
THE SOFT TISSUE ARTEFACT ISSUE**

PhD Thesis

**Presentata da:** Tecla Bonci

**Coordinatore Dottorato**

Prof. Elisa Magosso

**Relatore**

Prof. Aurelio Cappozzo

**Relatore**

Prof. Laurence Chèze

ESAME FINALE ANNO 2015

“Obstacles are those frightful things you see  
when you take your eyes off your goal”

- Henry Ford -

## Abstract

In 3D human movement analysis performed using optoelectronic stereophotogrammetric systems and skin markers, bone pose estimate can only be carried out in an indirect fashion. During a motor task, the deformation of the soft tissues makes the skin markers move with respect to the underlying bone generating the so called soft tissue artefact (STA). In general, STA is caused by skin sliding associated with joint movement, soft tissue volumetric deformation due to muscular contraction, gravity and inertial effects on soft tissue masses (wobbling). This movement has a frequency content similar to the bone movement and it is, therefore, not possible to distinguish them using any filtering techniques. In addition, STA is subject-, task-, and location-specific. Therefore, STA is the main problem in optimal bone pose estimate and its compensation remains an open question.

The aim of this PhD thesis was to contribute to the solution of this crucial issue. Modelling this phenomenon based on measurable trial-specific variables is a fundamental prerequisite for its removal from skin marker trajectories. This model can be incorporated in future optimal bone pose estimators thus reducing relevant inaccuracies and significantly improve the estimate of joint kinematics.

Two model architectures of STA are proposed. Initially, a model of the thigh artefact at marker-level is presented. STA was modelled as a linear combination of angular kinematics of the joints involved in the movement. This model was calibrated using both ex-vivo and in-vivo invasive measures (pin markers) of the STA. The considerable number of model parameters to be identified led to the approximation of the STA phenomenon. The STA of a body segment can be represented as a vector field composed by the displacement of each skin marker during the task with respect to its reference position in the anatomical reference frame. A modal approach was then used for the STA approximation and three STA definitions were proposed to represent the phenomenon as a series of modes: individual marker displacements, marker-cluster geometrical transformations, and skin envelope shape variations. It is important to point out that the marker-cluster geometrical transformations definition allows to separate the rigid component of the artefact from its non-rigid component. Modes obtained with the three above-mentioned definitions were selected using two different criteria: those that represent a certain percentage of the total STA energy (ranking) or those that describe the rigid component of the artefact which can be chosen *a priori*. Following the latter approach, it was empirically demonstrated with simulated data that only the rigid component of the artefact affects joint kinematics, regardless of the amplitude of the non-rigid component. For this reason, a model of the rigid component of the STA (at cluster-level) was then defined, using the marker-cluster geometrical transformation, for the thigh and shank segments. The selected rigid

modes were modelled as linear combination of the joint angles involved in the movement. This STA representation, by reducing the degrees of freedom of the STA field, allows reducing the number of the model parameters to be identified. An acceptable trade-off between STA compensation effectiveness and number of model parameters can be obtained using this STA modelling. This improves bone pose estimation and, therefore, joint kinematics accuracy.

The main potential applications of the results of this thesis are the following. First, the proposed STA models can be used to generate, at both marker- and cluster-level, realistic STAs which can be effectively used for simulation purposes when comparatively assessing skeletal kinematics estimators. Second and more importantly, by focusing only on the rigid component of the artefact, the model attains a satisfactory reconstruction of the artefact by using a reduced number of parameters. This circumstance makes incorporating the model in an optimal bone pose estimator feasible.

## Sommario

Quando la stima del movimento scheletrico viene condotta utilizzando un sistema non invasivo come quello stereofotogrammetrico e dei marcatori posti sulla cute, la stima della posa dell'osso può essere ottenuta utilizzando metodi indiretti.

Durante l'esecuzione di gesto motorio, la deformazione dei tessuti molli causa un movimento reale dei marcatori cutanei rispetto all'osso sottostante, generando il cosiddetto artefatto da tessuto molle (STA). In generale, lo STA è causato dallo stiramento della cute associato al movimento articolare, alla deformazione volumetrica dei tessuti dovuta alla contrazione muscolare, alla gravità ed ad effetti inerziali delle masse dei tessuti molli (il cosiddetto *wobbling*). Questo movimento ha un contenuto in frequenza simile a quello dell'osso sottostante e, quindi, non è possibile distinguerli usando tecniche di filtraggio. Inoltre, lo STA varia da soggetto a soggetto, varia al variare del movimento e della posizione del marcatore sul segmento in esame. Per questi motivi, lo STA è il problema principale nella stima ottima del movimento scheletrico e la sua compensazione rimane un problema, ad oggi, tuttora irrisolto.

Lo scopo di questa tesi è stato quello di dare un contributo alla soluzione di questo problema. Modellare questo fenomeno utilizzando delle variabili misurabili durante un dato esperimento è un prerequisito fondamentale per la rimozione dell'artefatto dalle traiettorie dei marcatori acquisite con un sistema stereofotogrammetrico. Questo modello può essere inserito in futuri stimatori ottimi della posa per ridurre l'inaccuratezza e per migliorare significativamente le stime di cinematica articolare.

Due architetture di modello di artefatto sono state proposte. Inizialmente, viene presentato un modello di artefatto di coscia per ogni singolo marcatore (*marker-level*). L'artefatto su ogni marcatore è stato modellato come combinazione lineare della cinematica articolare delle articolazioni coinvolte nel gesto motorio. Questo modello è stato calibrato utilizzando misure dirette ed invasive dell'artefatto di coscia (pin intracorticali) ottenute da dati *in-vivo* ed *ex-vivo*. Il considerevole numero di parametri del modello da identificare ha condotto a considerare soltanto un' approssimazione dell'intero fenomeno. In particolare, l'artefatto su di un segmento corporeo può essere rappresentato come un campo vettoriale composto dallo spostamento di ogni marcatore, durante l'esecuzione del movimento, rispetto alla sua posizione di riferimento nel sistema di riferimento anatomico. Un approccio modale è stato quindi utilizzato per approssimare l'intero STA e tre definizioni matematiche sono state proposte per la sua rappresentazione come una serie di modi: *individual marker displacements*, *marker-cluster geometrical transformations*, e *skin envelope shape variations*. È importante evidenziare che la definizione *marker-cluster geometrical transformations* consente di separare la componente rigida dell'artefatto da quella non-rigida. I modi ottenuti con le definizioni sopraindicate sono stati selezionati utilizzando due diversi criteri: quelli che rappresentano una certa percentuale dell'energia totale del fenomeno (*ranking*) o quelli che descrivono la componente rigida dell'artefatto e che possono essere definiti *a priori*. Utilizzando l'ultimo approccio, è stato empiricamente dimostrato utilizzando dati simulati che soltanto la componente rigida dell'artefatto influenza la posa dell'osso, e quindi la cinematica articolare, indipendentemente dall'ampiezza della componente non-rigida dello STA. Per questo motivo, è stato poi definito un modello della componente rigida dell'artefatto considerando l'intero cluster di marcatori (*cluster-level*), utilizzando la *marker-cluster geometrical transformations*, per i

segmenti di coscia e di gamba. I modi rigidi così selezionati sono stati modellati come combinazione lineare degli angoli articolari coinvolti nel movimento. Questa rappresentazione dell'artefatto, che riduce i gradi di libertà del campo STA, permette di ridurre il numero di parametri del modello che devono essere identificati. Utilizzando questa modellazione per l'artefatto, si ottiene un compromesso accettabile tra compensazione del fenomeno e numero di parametri del modello. Ciò migliora la stima della posa dell'osso e, quindi, l'accuratezza della stima della cinematica articolare.

Le potenziali e principali applicazioni dei risultati presentati in questa tesi sono di seguito indicati. Prima di tutto, i modelli proposti possono essere utilizzati per generare artefatti realistici, sia a livello di singolo marcatore che per l'intero cluster di marcatori, che possono essere utilizzati in simulazione, come quando devono essere confrontati diversi stimatori della posa dell'osso. Inoltre, e principalmente, focalizzandosi soltanto sulla componente rigida dell'artefatto, il modello ottiene una ricostruzione soddisfacente dell'artefatto utilizzando un numero ridotto di parametri. Questa circostanza rende possibile l'inserimento del modello in uno stimatore ottimo della posa dell'osso.

## Résumé

En analyse 3D du mouvement humain, lorsqu'elle est effectuée à l'aide de systèmes stéréophotogrammétriques optoélectroniques et de marqueurs cutanés, l'estimation de la position et de l'orientation des os ne peut être effectuée que de façon indirecte. Au cours d'une tâche motrice, la déformation des tissus mous engendrent le déplacement des marqueurs cutanés par rapport à l'os sous-jacent, générant ce que l'on appelle un artefact des tissus mous (STA). En général, le STA est causé par le glissement de la peau associé aux mouvements des articulations, à la déformation volumétrique des tissus mous due à la contraction musculaire, à la gravité et aux effets inertiels sur les masses molles (oscillations). La fréquence de ces mouvements est similaire à celle du mouvement des os, rendant, de ce fait, ces mouvements impossibles à distinguer par technique de filtrage. En outre, le STA est sujet-, tâche-, et position-spécifique. Par conséquent, le STA représente le principal problème lors de l'estimation de la position et de l'orientation optimales des os, et la question de leur compensation reste ouverte.

Le but de cette thèse de doctorat a été de contribuer à solutionner ce problème crucial. Modéliser ce phénomène à partir de variables essai-spécifiques mesurables est une condition fondamentale afin d'en soustraire les effets à la trajectoire des marqueurs cutanés. Ce modèle doit être introduit dans un estimateur de position et d'orientation des os, afin de réduire de façon appropriée les inexactitudes et d'améliorer significativement l'estimation de la cinématique articulaire.

Deux architectures de modèle de STA sont proposées. Pour commencer, un modèle d'artefact de la cuisse au niveau des marqueurs est présenté. Le STA a été modélisé comme une combinaison linéaire de la cinématique angulaire de l'articulation impliquée dans le mouvement. Ce modèle a été calibré en utilisant à la fois des mesures ex-vivo et in-vivo invasives (vis intra-corticales) de STA. Le nombre considérable de paramètres du modèle à identifier a conduit à la simplification du champ de STA. Ce dernier a été défini comme le déplacement de chaque marqueur cutané pendant la tâche par rapport à sa position de référence dans le repère anatomique de référence. Une approche modale a ensuite été utilisée pour approximer le STA, pour lequel trois définitions ont été proposées afin de représenter le phénomène par une série de modes : déplacements individuels des marqueurs, transformations géométriques d'un cluster de marqueur, et variations de la forme de l'enveloppe cutanée. Il est important de souligner que la définition par transformations géométriques du cluster de marqueurs permet de dissocier la composante rigide de l'artefact de sa composante non-rigide. Les modes obtenus grâce aux trois définitions susmentionnées ont été sélectionnés selon deux critères différents : ceux représentant un certain pourcentage de l'énergie totale du STA (classement) ou ceux décrivant la composante rigide de l'artefact, qui peuvent être choisis a priori.

En suivant cette dernière approche, il a été démontré empiriquement avec des données simulées que seule la composante rigide de l'artefact affecte la cinématique articulaire, indépendamment de l'amplitude de la composante non-rigide. Pour cette raison, un modèle de la composante rigide du STA (au niveau du cluster) a été défini, en utilisant la transformation géométrique du cluster de marqueurs, pour les segments de la cuisse et de la jambe. Les modes rigides sélectionnés ont été modélisés par une combinaison linéaire des angles articulaires impliqués dans le mouvement. Cette représentation du STA, en réduisant les degrés de liberté du champ de STA, permet de réduire le nombre de paramètres du modèle à identifier. Un compromis acceptable entre l'efficacité à compenser le STA et le nombre de paramètres du modèle peut être obtenu en utilisant cette modélisation du STA. Ceci améliore l'estimation de la position et de l'orientation des os et, par conséquent, l'exactitude de la cinématique articulaire.

Les principales applications possibles des résultats de cette thèse sont les suivants. Tout d'abord, les modèles proposés permettent de générer, tant au niveau du marqueur que du cluster, des STAs réalistes qui peuvent ensuite être utilisés efficacement à des fins de simulation lors de l'évaluation comparative d'estimateurs de la cinématique du squelette. En second lieu et surtout, en se concentrant uniquement sur les composantes rigides de l'artefact, le modèle permet une reconstruction satisfaisante de l'artefact à l'aide d'un nombre réduit de paramètres. Cette caractéristique rend faisable l'introduction du modèle dans un estimateur de position et d'orientation des os.

## Scientific writing

### *Full length articles*

- “Generalized mathematical representation of the soft tissue artefact”. R. Dumas, V. Camomilla, T. Bonci, L. Cheze, A. Cappozzo. *Journal of Biomechanics*, 2014, 47 (2), 476–481.
- “A soft tissue artefact model driven by proximal and distal joint kinematics”. T. Bonci, V. Camomilla, R. Dumas, L. Cheze, A. Cappozzo. *Journal of Biomechanics*, 2014, 47 (10), 2354–2361.
- “A model of the soft tissue artefact rigid component”. V. Camomilla, T. Bonci, R. Dumas, L. Cheze, A. Cappozzo.  
*Submitted for publication (under first review in Journal of Biomechanics).*
- “What portion of the soft tissue artefact requires compensation when estimating joint kinematics?”. R. Dumas, V. Camomilla, T. Bonci, L. Cheze, A. Cappozzo.  
*Submitted for publication (under first review in Journal of Biomechanical Engineering).*

### *Abstract to national conference*

- “Different approaches for in-vivo soft tissue artefact modelling”. T. Bonci, V. Camomilla, R. Dumas, L. Chèze, A. Cappozzo. Congress: GNB 2014 (Pavia, 2014).

### *Abstracts to international conferences*

- “A modal approach for soft tissue artefact mathematical representation and compensation”. T. Bonci, V. Camomilla, R. Dumas, L. Chèze, A. Cappozzo. Congress: 7<sup>th</sup> World Congress of Biomechanic (Boston, 2014);
- “A modal approach for the soft tissue artefact mathematical representation in optimal joint kinematics estimators”. T. Bonci, V. Camomilla, R. Dumas, L. Cheze, A. Cappozzo. Congress: 13th International Symposium on 3D Analysis of Human Movement (Lausanne, Switzerland, 2014) ***Withaker-Allard Innovation Award for the oral presentation***;
- “Pelvis soft tissue artefact assessment during 3-d hip movements”. V. Camomilla, T. Bonci, A. Cappozzo. Congress: 1st Clinical movement analysis world conference (Rome, 2014).

*Abstracts to international conferences published on international journal*

- “Generation of realistic thigh soft tissue artefacts as a function of hip and knee kinematics”.  
T. Bonci, V. Camomilla, R. Dumas, A. Cappozzo. Congress: ESMAC (Glasgow, 2013).  
Published in *Gait & Posture*, Vol. 39, S72–S73, June 2014.
- “A qualitative analysis of soft tissue artefact during running”. R. Dumas, V. Camomilla, T. Bonci, L. Chèze, A. Cappozzo. French speaking congress: 39ème congrès de la Société de Biomécanique (Valenciennes, 2014).  
Published in *Computer Methods in Biomechanics and Biomedical Engineering* Vol. 17, No. S1, 124-125, 2014.

# Contents

<i>Abstract</i>	<b>i</b>
<i>Sommario</i>	<i>iii</i>
<i>Résumé</i>	<i>v</i>
<i>Scientific writing</i>	<i>vii</i>
<b>1. Chapter 1: INTRODUCTION</b>	<b>1</b>
1.1. <i>Area of interest of the research</i>	1
1.2. <i>Context</i>	1
1.3. <i>Objective and structure of the thesis</i>	3
<b>2. Chapter 2: SOFT TISSUE ARTEFACT: STATE OF ART</b>	<b>6</b>
2.1 <i>Theoretical background</i>	6
2.2 <i>STA measure</i>	8
2.2.1 <i>Intracortical pins</i>	9
2.2.2 <i>External fixators</i>	15
2.2.3 <i>Percutaneous trackers</i>	18
2.2.4 <i>Imaging</i>	22
2.3 <i>Non-invasive statistical approach</i>	36
2.4 <i>Soft tissue artefact minimization and compensation</i>	37
2.4.1 <i>The “solidification” procedure</i>	38
2.4.2 <i>Multiple anatomical landmark calibration</i>	39
2.4.3 <i>Pliant surface modeling</i>	40
2.4.4 <i>Dynamic calibration</i>	41
2.4.5 <i>Point cluster technique</i>	42
2.4.6 <i>Global optimization</i>	43
2.5 <i>Conclusions</i>	49
<b>3. Chapter 3: A SOFT TISSUE ARTEFACT MODEL DRIVEN BY PROXIMAL AND DISTAL JOINT KINEMATICS</b>	<b>52</b>
3.1 <i>Introduction</i>	53
3.2 <i>Methods</i>	55
3.2.1 <i>Model architecture and calibration</i>	55
3.2.2 <i>Experimental data</i>	56
3.1.1 <i>STAs and reconstructing hip and knee joint kinematics</i>	57
3.1.2 <i>Model calibration and model feasibility assessment</i>	58
3.1.3 <i>Generalizability of the STA estimate</i>	58
3.1.4 <i>Statistical analysis</i>	59
3.2 <i>Results</i>	59
3.2.1 <i>Range of joint movement</i>	59
3.1.1 <i>Amplitude of the soft tissue artefacts</i>	60
3.1.2 <i>Model calibration and architecture feasibility assessment</i>	62
3.1.3 <i>Assessment of model generalizability</i>	68
3.2 <i>Discussion</i>	68
3.2.1 <i>Model feasibility</i>	69
3.2.2 <i>Model generalizability</i>	70
<b>4. Chapter 4: GENERALIZED MATHEMATICAL REPRESENTATION OF THE SOFT TISSUE ARTEFACT</b>	<b>72</b>
4.1. <i>Introduction</i>	73
	<b>ix</b>

4.2.	<i>Generalized mathematical formulation</i>	74
4.3.	<i>Ranking and selection of modes</i>	75
4.4.	<i>Experimental data</i>	77
4.4.1.	Ex-vivo dataset	77
4.4.2.	In-vivo dataset	78
4.5.	<i>STA definition and interpretation</i>	79
4.5.1.	Individual marker displacements	79
4.5.2.	Marker-cluster geometrical transformations	82
4.5.3.	Skin envelope shape variations	86
4.6.	<i>STA mathematical representations: impact on knee kinematics</i>	88
4.1.	<i>Single ranking of thigh and shank modes: impact on knee kinematics</i>	89
4.2.	<i>Discussion</i>	92
4.2.1.	STA definitions	92
4.2.2.	Ranking and selection of modes	93
4.2.3.	Towards STA mathematical modelling	94
4.2.4.	STA reduction and knee kinematics	95
<b>5.</b>	<b>Chapter 5: GEOMETRICAL TRANSFORMATION OF A MARKER-CLUSTER AND ITS IMPACT ON BONE POSE ESTIMATION</b>	<b>97</b>
5.1.	<i>Introduction</i>	98
5.2.	<i>Material and Method</i>	100
5.2.1.	Gait data	100
5.2.2.	Running data	102
5.2.3.	Marker-cluster geometrical transformation	102
5.2.4.	STA components	103
5.2.5.	Impact of RM and NRM on bone pose estimation: reference	104
5.2.6.	Impact of RM and NRM on bone pose estimation: Monte Carlo Simulation framework	104
5.3.	<i>Results</i>	106
5.3.1.	Marker-cluster geometrical transformation and number of markers	106
5.3.2.	Monte Carlo Simulation: gait data	107
5.3.3.	Monte Carlo Simulation: running data	110
5.4.	<i>Discussion</i>	111
	<i>Appendix Chapter 5</i>	113
<b>6.</b>	<b>Chapter 6: WHAT PORTION OF THE SOFT TISSUE ARTEFACT REQUIRES COMPENSATION WHEN ESTIMATING JOINT KINEMATICS?</b>	<b>117</b>
6.1.	<i>Introduction</i>	118
6.2.	<i>Material and methods</i>	119
6.2.1.	Experimental data	119
6.2.2.	STA approximations and compensation	120
6.2.3.	Errors on knee joint kinematics estimate	122
6.2.4.	Statistical analysis	122
6.3.	<i>Results</i>	122
6.3.1.	Energy and number of the selected modes	122
6.3.2.	Knee joint kinematics	123
6.4.	<i>Discussion</i>	130
<b>7.</b>	<b>Chapter 7: A MODEL OF THE SOFT TISSUE ARTEFACT RIGID COMPONENT</b>	<b>134</b>
7.1.	<i>Introduction</i>	135
7.2.	<i>Materials and Methods</i>	137
7.2.1.	STA rigid component model architecture	137
7.2.2.	Experimental data	141
7.2.3.	STA model calibration	142
7.2.4.	STA compensation	142
7.2.5.	Evaluation of calibration feasibility and compensation effectiveness	142
7.3.	<i>Results</i>	144
7.3.1.	STA assessment	144
7.3.2.	STA modelling: selection of angle time histories	145
7.3.3.	STA model calibration	148
7.3.4.	STA compensation	155

7.4.	<i>Discussion</i>	157
7.4.1.	STA assessment	157
7.4.2.	STA model calibration	160
7.4.3.	STA compensation	160
7.5.	<i>Conclusion</i>	161
	<i>Soft tissue artefact: from cluster-level to marker-level</i>	163
<b>8.</b>	<b>Chapter 8: CONCLUSION</b>	<b>166</b>
8.1.	<i>A possible model of thigh STA</i>	166
8.2.	<i>STA degrees of freedom reduction</i>	168
8.3.	<i>STA characterization</i>	169
8.4.	<i>Mode selection criteria</i>	170
8.5.	<i>STA rigid modelling</i>	170
8.6.	<i>Future work and perspective</i>	171
	<i>References</i>	173
<b>Appendix A1.1: SOFT TISSUE ARTEFACT MODELLING USING THE SKIN ENVELOPE SHAPE VARIATION DEFINITION: IMPACT ON HIP JOINT CENTRE ESTIMATION DURING THE STAR-ARC MOVEMENT</b>		
	<i>Introduction</i>	A1.1
	<i>Material and Methods</i>	A1.2
	<i>Results</i>	A1.5
	Analysis of modes in terms of STA energy	A1.5
	Hip joint centre position estimation	A1.6
	Model architecture to link hip joint kinematics to modes	A1.9
	<i>Discussion</i>	A1.16
	<i>References – A1</i>	A1.19
<b>Appendix A2.1: PELVIS SOFT TISSUE ARTEFACT ASSESSMENT DURING 3-D HIP MOVEMENTS</b>		
	<i>Introduction</i>	A2.1
	<i>Materials and methods</i>	A2.2
	Subjects and digital bone	A2.2
	Marker placement	A2.6
	Data acquisition	A2.7
	Data processing	A2.10
	<i>Results</i>	A2.11
	<i>Discussion</i>	A2.15
	<i>References – A2</i>	A2.16

## ***1. Chapter 1***

### ***“INTRODUCTION”***

#### **1.1. Area of interest of the research**

Expert clinicians, physiotherapists and trainers perform a qualitative diagnosis\evaluations that can be a fast and useful instrument. However, during some instances, as occurs for comparisons performed in different periods of time to evaluate the rehabilitation strategy or to obtain an objective evaluation, the problem to perform quantitative measurements characterized by high precision arises.

The skin marker-based stereophotogrammetry is most frequently used to analyse human motions for its advantages in safety and usability. This technique consisting in gluing reflective or light-emitting markers on the skin and obtains their three dimensional positions using two or more calibrated cameras. Compared with radiographic and fluoroscopic techniques, stereophotogrammetry does not expose subjects to radiation and takes less time and effort in measuring activities. An accurate analysis of the human movement has an important role in the medical and sport field. In the medical field, the human movement analysis can be an useful support for the clinical evaluation of new prosthesis implant, for rehabilitation programs or therapeutic protocols, while in the sport field it can be useful to evaluate the motor task performed or the effect of a new training protocol.

The aim of the human movement analysis is to give the optimal estimation of the skeletal movement during the execution of different motor tasks. Nevertheless, there are some limitations due to limited awareness of the methodological fundamentals and experiments associated with the use of instruments for the study of the biological system.

#### **1.2. Context**

The application of quantitative studies of human locomotion has contributed substantially to the improvement in the treatment of injury and disease of the musculoskeletal system. In particular, the treatment of neuromuscular disorders has been improved by analysing dynamic gait characteristics of patients prior to treatment (Andriacchi and Alexander, 2000). Optoelectronic stereophotogrammetric systems and skin markers are used to analyse human movement in the three

dimensional (3D) space. The movement of the markers is typically used to infer the underlying relative movement between two adjacent segments (as occurs for knee joint) with the goal of precisely defining the movement of the joint. The reconstruction of the 3D human skeletal system using this method is affected by two sources of errors. The first concerns the instrumental errors due to the system used and on the methods used to cope this source of inaccuracy. The second is associated with the erroneous assumption that markers and body segments are rigidly connected. It is well known that skin markers move with respect to the underlying bones for the interposition of soft tissue. During a motor task, the deformation of the tissue surrounding the bone makes the markers move with respect to the underlying bone, causing the so called soft tissue artefact (STA). This movement generates landmark mislocation and STAs.

Its compensation is the main problem when aiming at optimal bone-pose estimate. In recent years, applied researches have become increasingly interested in the compensation of STAs: using optoelectronic stereophotogrammetry and skin markers, the inaccuracy involved with STAs still represents an unsolved problem (Leardini et al., 2005; Peters et al., 2010).

In general, an STA is caused by:

- skin sliding associated with joint movement,
- soft tissue volumetric deformation due to muscular contraction and gravity,
- inertial effects on soft tissue masses (wobbling).

This phenomenon have a frequency content similar to the bone movements and it is, therefore, not possible to distinguish between them using any filtering techniques. Moreover the STA is subject-specific, task-specific, location-specific. For this reasons, STA have been recognized as the major source of error in human motion analysis and several studies have been performed to better understand and measure the STA in different motor tasks. What has been done in the literature has been reviewed and reported in the *Chapter 2*. In order to compensate for this phenomenon, its characterization and modelling is a crucial issue. We can represent the STA as generated by the sum of two contributions: the deformation of the surface marker cluster (normally not uniform with respect to the centroid of the cluster) and the rigid displacement, translation and rotation, of the cluster with respect to the underlying body segment. Several studies have been carried out to compensate for STA, focusing on the deformation of the marker cluster (Andriacchi et al., 1998; Ehrig et al., 2006; Taylor et al., 2005). This approach showed a limited efficacy, since, as recently quantified, the most important part of the STA is produced by the rigid movement of the cluster rather than by its deformation (Andersen et al., 2012; Barré et al., 2013; Grimpampi et al., 2014).

### 1.3. Objective and structure of the thesis

A bone pose estimator embedding an STA model that might compensate also for the rigid movement of the marker cluster remains to be assessed. Based on a quasi-linear relationship of the STA with the closest joint angles (Akbarshahi et al., 2010; Camomilla et al., 2013; Cappozzo et al., 1996), a model able to generate realistic thigh STA for both simulation and compensation purposes during multi-articular movements has been devised and assessed. Model feasibility was assessed using both skin and pin markers, *in-vivo* during running and from *ex-vivo* experimental data (*Chapter 3*).

In the perspective to embed an STA model in bone-pose estimator, the noticeable number of relevant parameters could cause difficulties in convergence during the optimization process, therefore this number has to be decreased. For this purpose, a modal approach (Dumas et al., 2014a) with different STA definitions (individual marker displacements; marker-cluster geometrical transformations; or skin envelope shape variations) was proposed and it was applied to the experimental data (*Chapter 4*). STA were represented using modes, composed by a direction and an amplitude, which can be selected or ranked according a chosen criterion. Some quantitative conclusions about that were drawn for each STA definition using information available in the literature and *ex-vivo* experimental data used also in the previous chapter of the thesis. In addition, the impact of different STA approximations, using the different STA definitions, was evaluated on the accuracy of knee joint kinematics estimates using running data.

Among the proposed STA definitions, the marker-cluster geometrical transformations, which addresses the rigid and non-rigid transformations of the cluster of skin markers, from the result reported in the Chapter 3, allows for the best trade-off between STA compensation effectiveness and number of modes, relative to knee kinematics accuracy and the number of parameters. Recent studies quantified these cluster STA components in different motor tasks (Andersen et al., 2012; Barré et al., 2013; de Rosario et al., 2012; Grimpampi et al.), showing that the cluster rigid motion (RM) is predominant with respect to the cluster non-rigid motion (NRM). The results obtained in these studies suggest that the cluster RM is the main component which affects the estimation of the bone pose, mostly for its amplitude with respect to its counterpart. Based on this observation, it is concluded, either explicitly or implicitly, that cluster non-rigid motion has a limited impact on bone pose estimation and that STA compensation should concentrate on the cluster rigid motion. In *Chapter 5* it has been disputed the message carried by this statement and it has been demonstrated that the cluster non-rigid motion does not have a limited effect on BPE accuracy, but, rather, it has no effect whatsoever and that this is the case independently from its magnitude relative to the

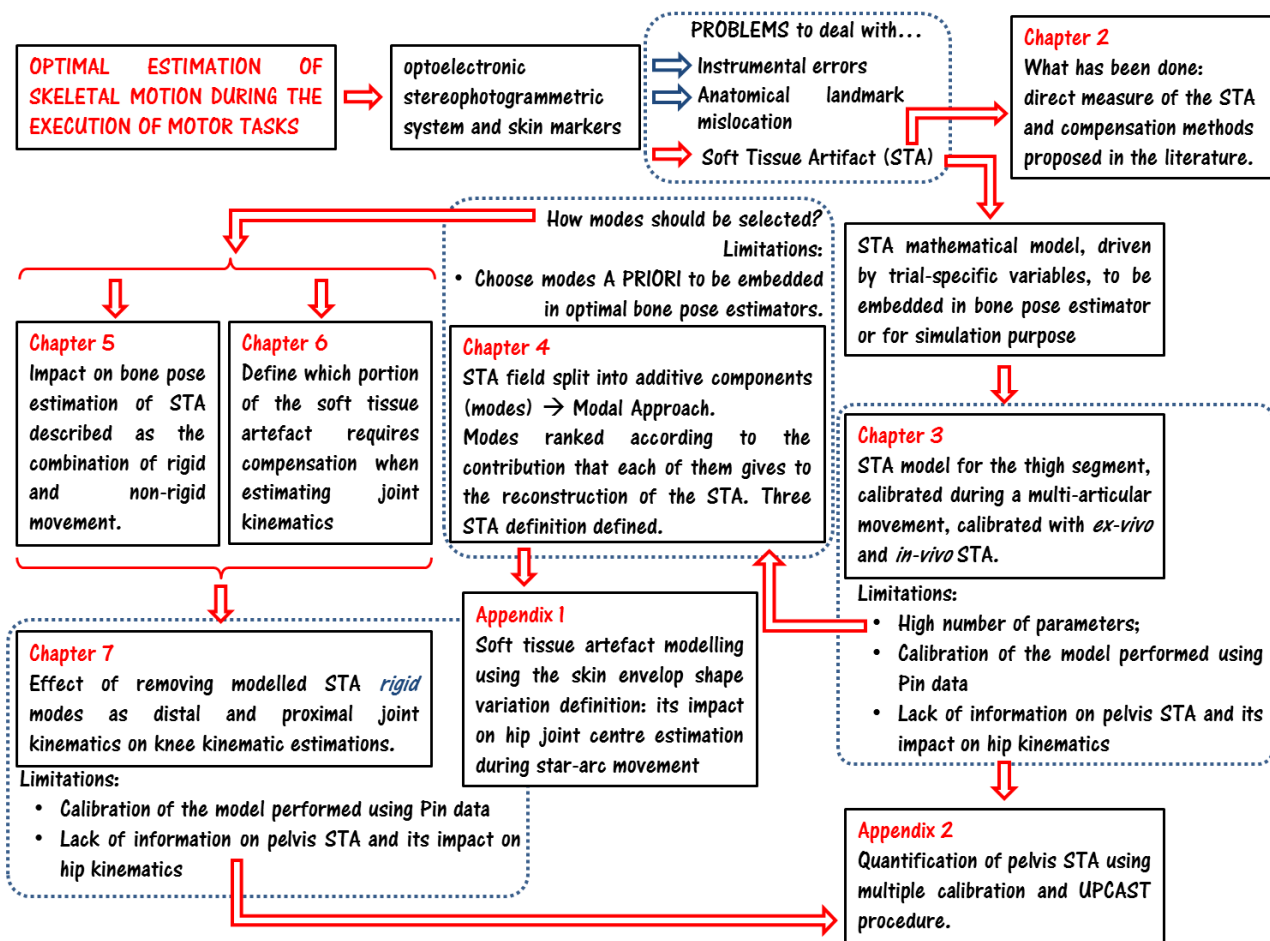
cluster rigid motion. For this reason, the only STA component to be compensated for is the cluster rigid motion. Simulated data were used for the empirical demonstration.

Given the importance to estimate the bone pose with high accuracy, and therefore the joint kinematics, the impact of selected removal of modes representing the soft tissue artefact has been evaluated on the knee joint kinematics. In particular, it is evaluated the effect of removing a selected threshold of the STA or selected modes decided a priori (*Chapter 6*), as described in the previous thesis chapter.

The STA model based on the marker-cluster geometrical transformations (GT) definition has been developed for the propriety of the basis of vectors that can be defined a priori and for the numerical results shown in the thesis. Moreover, the impact of such model has been evaluated on the knee joint kinematics (*Chapter 7*).

The soft tissue artefacts have also an impact on the estimation of the hip joint centre (HJC) position during the star-arc movement, although an algorithm for its compensation, such as the quartic sphere fit method, proposed by Gamage and Lasenby (2002) with the correction term introduced by Halvorsen (2003), can be used. This method gave the best results compared with the symmetrical centre of rotation estimation method proposed by Ehrig et al. (2006), as shown in the study performed by Cereatti et al. (2009). Based on this results, HJC estimations were performed on *ex-vivo* data (Cereatti et al., 2009), selecting a distal and proximal skin marker cluster removing STA, modes by modes, using the skin envelope shape variations for the STA modal approach. In addition, the impact of STA on the HJC estimations has been evaluated modelling the thigh artefact, for its removal, as linear combination of the hip kinematics measured during the experiment (*Appendix 1*).

The study performed in the Chapter 7, and all the others presented here, lack of the information on the pelvis STAs, which are probably as important as the thigh STA, and their impact on hip kinematics and bone poses. To date, only one study assessed STA with reference to markers located on the pelvis. This was done by determining how the local position of anatomical landmarks (ALs) varied, as determined through manual palpation, while the hip assumed different flexion/extension angles, using a multiple anatomical calibration (Hara et al., 2014). A study has been presented using the same approach, but through a different anatomical calibration method which allowed for a better reliability (UP-CAST, Donati et al., 2008) and for different hip flexion/extension and ad-abduction angles (*Appendix 2*).



**Scheme 1.1** – Structure of the thesis. Main limitations of some chapter are also shown.

Finally, conclusions and suggestions for future studies are presented in *Chapter 8*.

## 2. Chapter 2

### “SOFT TISSUE ARTEFACT: STATE OF ART”

#### Nomenclature

	STA	Soft Tissue Artefact
	RSA	Roentgen Stereophotogrammetric Analysis
	HJC	Hip Joint Centre
	DOF	Degree of Freedoms
	AL	Anatomical Landmark
	CAST	Calibration Anatomical System Technique
	AF	Anatomical Frame
	CTF	Cluster Technical Frames
	PCT	Point Cluster Technique
	PST	Percutaneous Skeletal Trackers
	FHA	Finite Helical Axis
	CT	Computed Tomography
	RMS	Root Mean Square
	MRI	Magnetic Resonance Imaging
	LSTAD	Local STA Deformation
	RSTAM	Rigid STA Movement
	BMI	Body Mass Index
	SVD	Single Value Decomposition
	PSM	Pliant Surface Modeling
	RBM	Rigid Body Modelling
	GO	Global optimization
Joint degrees of freedom	FE	Flexion/Extension
	AA	Abduction/Adduction
	IER	Internal/External Rotation
	LM	Medio/Lateral
	AP	Anterior/Posterior
	PD	Proximal/Distal

#### 2.1 Theoretical background

To analyze human movement in the three dimensional space, the instantaneous position and orientation of the different bones involved in the motor task have to be defined. Optoelectronic stereophotogrammetric systems and skin markers can be used for this aim.

The muscle-skeletal system reconstruction and the computation of its kinematics, using a model of the human body, exhibits a number of crucial problems. Firstly, there are issues concerning

instrumental errors, e.g. camera calibration and filtering or smoothing of marker position data (Chiari et al., 2005) along with the limitations introduced by the mechanical model used (as, for instance, the assumption of rigidity of the bones or the number of degrees of freedom of the joints involved in the analysis). Secondly, there are issues related to experimental errors. Actually, the muscle-skeletal system generates the most important errors in the reconstruction of the movement: the poor repeatability associated with the identification of the anatomical landmarks (Della Croce et al., 2005) and the relative movements between markers and the underlying bone (Soft Tissue Artefacts – STAs) (Andriacchi and Alexander, 2000; Leardini et al., 2005; Peters et al., 2010). The nature of this relative movement between the markers, glued on the external surface of the segment, and the underlying bone is associated with the specific marker set and experimental protocol adopted.

In recent years, applied researchers have become increasingly interested in the compensation of STAs, however the problem is still seeking for a satisfactory solution. During the execution of a motor task, the measurement of the motion of different body segments is mostly influenced by the real movement of the surrounding soft tissue leading to inaccurate estimates of the poses of the underlying bones (Leardini et al., 2005). This movement is generated by muscle contraction, skin stretching, and wobbling caused by the inertia of the limbs. Describe exactly the effect on the bone pose estimation is very difficult due to the complex nature of the human body. For example, depending on the location of the markers on the lower-limb and the analysed activity, a marker can move more than 30mm compared to its initial position (Cappozzo et al., 1996). This can affect the position and the orientation of the segments (thigh and shank) up to 31 mm and 15 deg, respectively (Sangeux et al., 2006). Then, propagated to the estimation of the tibio-femoral joint kinematics, the STA can introduce measurement error more than 18 mm and 8 deg on the estimated displacements and angles of the knee, respectively (Cappozzo et al., 1996). Moreover, movements of the body segments and the STAs have the same frequency content, so it is impossible to apply any filtering technique to eliminate this phenomenon. Then, a good knowledge and characterization of the STA is required to compensate it during different motor tasks. The measured STA depends on many factors such as the anatomical properties of the body segments and joints, the motor task performed. Hence, the acquisition protocol for the measurements is as critical as the parameters to be assessed. Their interpretation and the derived hypotheses are also dependent to the number of subjects analyzed. It is then interesting to know how the STA has been assessed, for which activity, number of subjects and what are the hypotheses formulated for the STA.

Based on the literature, the STA in the lower limb is:

- the largest measurement error in *in-vivo* movement analysis;
- maximum in the thigh;
- both systematic and random error;
- subject dependent;
- task dependent.

This chapter section addresses, first, at reviewing the studies aimed at assessing STA in the lower limb with different methods. Proposed techniques designed to minimize these effects are also reported. All the studies in the different sections are reported in a chronologic order.

## 2.2 STA measure

To directly measure the amplitude of soft tissue artefact on a segment of interest during experimental data acquisitions, the movement of the underlying bone has to be acquired.

For this purpose the following methods can be used: bone pins, external fixator devices, skeletal trackers, or medical imaging.

### 2.2.1 Intracortical pins

The major limitation of this method is its invasiveness and the mechanical issues related to the pins

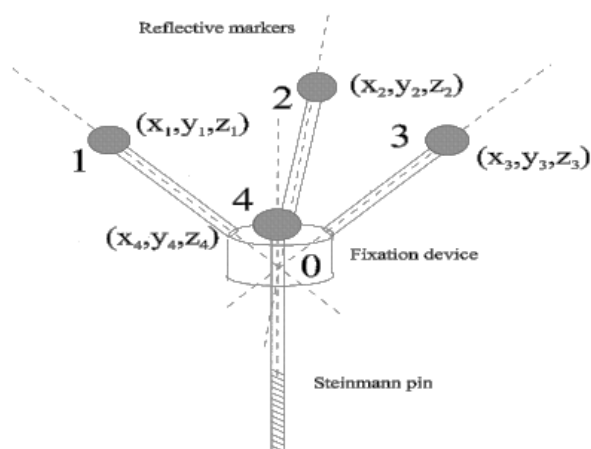


**Figure 2.1** – Schematic of a target cluster used by Lafortune (1984).

(Figure 2.1). Some studies had concerns about possible bending effects on the pins (Ramsey and Wretenberg, 1999; Ramsey et al., 2003; Reinschmidt et al., 1997b) which can reduce the quality of the reference data: the pins may cause discomfort and the anaesthetics may alter the perception of the subject. To minimize the restriction of the movement of the skin marker, they should be glued not close to the bone pin insertion (Reinschmidt et al., 1997a). The worst

case scenario with the use of the intracortical pins is when they break. Indeed, two studies reported the loss of data due to breakage or loosening of the pins (Benoit et al., 2006; Reinschmidt et al., 1997b). All these technical and ethical issues explain the limited number of subjects and the difficulty to recruit volunteers. Six is the maximum number of subjects analysed with intracortical pins in a study (Benoit et al., 2006).

Lafortune, 1984; Levens et al., 1948 were the pioneering using intracortical pins to analyse skeletal motion during walking. This method gave the opportunity to track directly the motion of bones with the insertion of pins equipped with reflective markers. After a local anaesthesia around the insertion site, a surgery is required to cut the skin, pass the pin around the muscles, tendons, or ligaments and then screw the pin in the bone. The advantage of this method is the employment of the same acquisition system as used for reflective markers attached on the skin. In addition, the same acquisition volume can be acquired for the reference and the skin marker system. This gives for example the possibility to analyse the STA on a full gait cycle.

The use of X-ray video-fluoroscopy and intracortical pins to quantify STA magnitude was described by Lafortune and Lake, in 1991. In this preliminary experiment using fluoroscopy, three cycles of unloaded flexion-extension of the knee were analysed. A 21 mm distal and a 23 mm posterior displacement was exhibited by a marker placed on the proximal tibia, and this displacement was found to be linearly related to knee flexion. In a second experiment, the STA magnitude was analysed at heel strike during running. Data were obtained from a marker attached to a cortical pin inserted into the tibia and from a marker glued on the skin of a volunteer over the lateral tibial condyle. The relative movement between these two markers reached 10 mm, and was

dependent also upon the type of impact. The same authors, in another study (Lafortune et al., 1992) showed the tibio-femoral 3D kinematics during walking using target clusters fixed directly into the bones, without providing information on STA.

External marker devices, each consisting of a bone screw and an aluminium tripod instrumented with three reflective spherical markers, were anchored on the distal femur and on the proximal tibia (Karlsson and Lundberg, 1994). In addition, three skin markers were glued on the distal thigh and on the proximal shank. While standing, the two volunteers performed a hip internal-external rotation with extended knee. The knee joint rotations obtained with bone-anchored and skin-attached markers showed a great difference: the knee internal-external rotation when measured with the cluster of markers linked with the bone showed a range of about 20 degrees, which was observed to be about 50 degrees when measured with the skin marker cluster. Moreover, the skin displacement tracked by thigh markers was found to be higher than that by shank markers.

The impact of the STA during the stance phase of a level walking task on both knee and ankle was assessed by (Reinschmidt et al., 1997a). Intracortical Hofmann pins with triads of reflective markers were inserted into the lateral femoral condyle, the lateral tibial condyle and the postero-lateral aspect of the calcaneus (Figure 2.2a) in five male volunteers (age:  $28.6 \pm 4.3$  years, mass:  $83.4 \pm 10.2$  kg, height:  $185.1 \pm 4.5$  cm). The task was performed by each subject three times. Six skin markers were also glued on the lateral and anterior aspects of the thigh, shank and shoe. The knee and ankle joint kinematics were described using standard conventions (Cole et al., 1993; Grood and Suntay, 1983). Only the data from three subjects were valid for the measurement of the knee joint kinematics due to issues with the pins for the two other subjects. The maximal difference between bone- and skin-marker based knee rotations were 4.4 deg, 8.4 deg and 4.3 deg (obtained as the mean value over all the volunteers), in the frontal, transverse and sagittal plane, respectively. In the same anatomical planes the maximal difference between bone- and skin-marker ankle rotations were 5.4 deg, 5.1 deg and 5.9 deg. It was shown that the thigh is the most affected segment by the STA due to muscle movements during the stance phase and may be even higher during the swing phase, through segmental error analysis (the average difference between the bone- and skin marker-based motion). It was concluded that only the knee flexion/extension (FE) can be measured using skin markers, seeing as the error introduced by the STA can almost be as high in magnitude as the real joint motion for the knee abduction/adduction (AA) and internal/external rotations (IER).

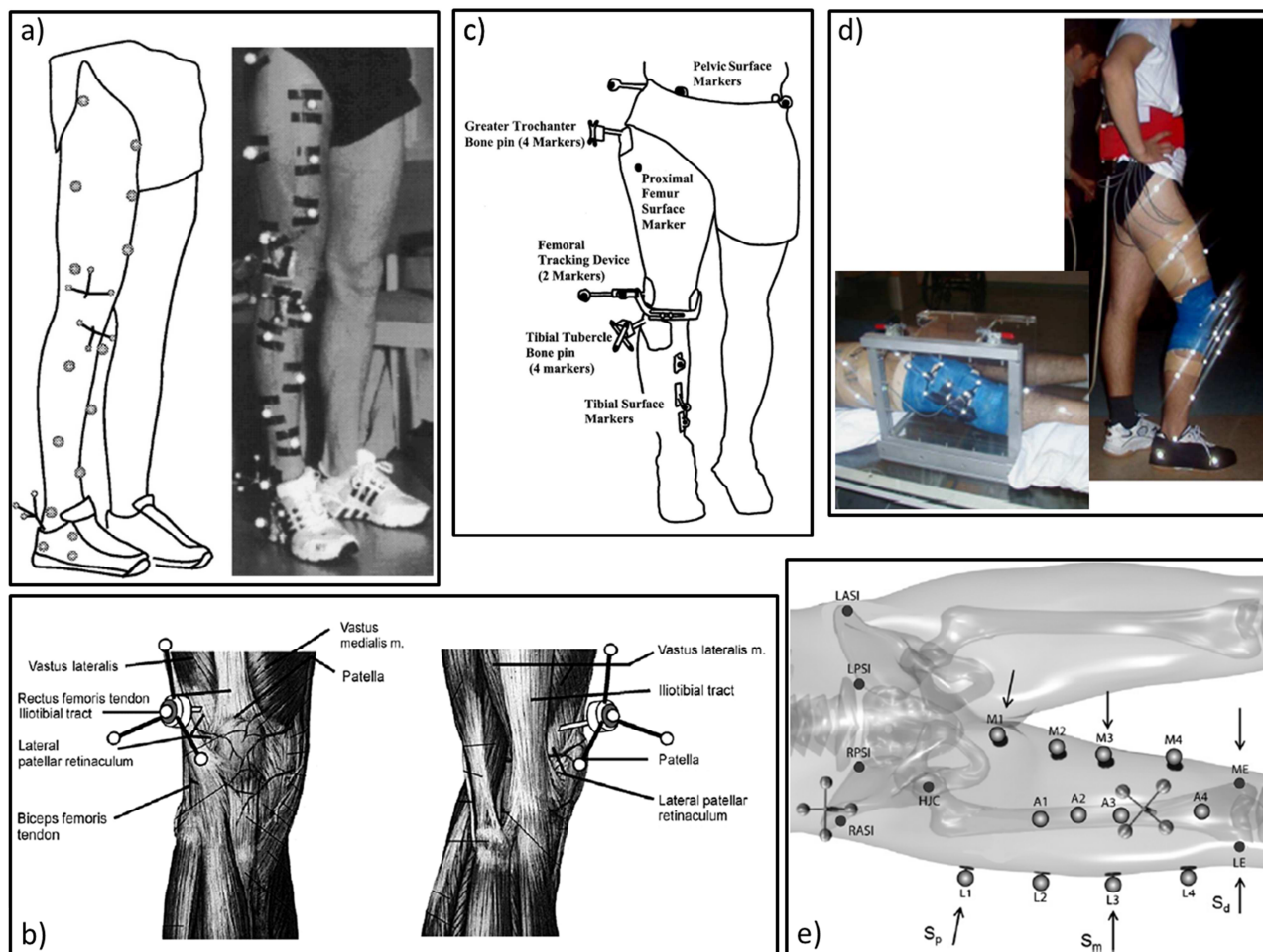


**Figure 2.2** – Experimental setup with intracortical pins implanted in lower limbs. **a)** Reinschmidt et al., 1997c; **b)** Ramsey et al., 2003; **c)** Houck et al., 2004; **d)** Benoit et al., 2006; **e)** Camomilla et al., 2013.

The effect of STA on 3D joint rotations was assessed also in the stance phase of five running trials by the same authors (Reinschmidt et al., 1997c). The same acquisition protocol was used for 3 subjects (age:  $25.7 \pm 2.1$  years; mass:  $85.5 \pm 9.6$  kg; height:  $1.87 \pm 0.10$  m). As in the previous work, the knee kinematics was defined using the Cardan angles calculated from both the external and skeletal markers. For the knee FE again a good agreement was found between skin- and bone-based knee patterns, while for the other two angular degrees of freedom (*i.e.*, AA and IER), the difference between the two kinematics had similar amplitude with respect to the amplitude of the corresponding physiological motion. Such errors, expressed in percentage of the relative full range of motion were 21%, 70%, and 64%, for FE, AA and IER, respectively. Therefore, it was shown that skin markers lead to an overestimation of joint motion. When the impact of the STA was evaluated on the single segment, the error analysis for the shank did not exceed 5 degrees for all subjects and all rotations; while for the thigh the errors were consistently values higher. Not surprising the errors due to the relative movement between skin markers and the underlying bone were higher in running than in walking, due to muscle contraction that occurs during the running stance. Moreover, the

authors also concluded the possibility that the skin set may can move as a unit relative single unit relative to the underlying bone. Thus, a compensation method reducing only the relative movement between markers may be not enough to reduce the impact of STA on the pone pose estimation, and, therefore, joint kinematics.

Several different motor tasks were analysed using an instrumented leg with two arrays of six markers inserted directly into the tibial tubercle and the greater trochanter (Fuller et al., 1997). Twenty markers were also glued all over the thigh and shank segments. In this study two experiments were performed. One volunteer (age between 35 and 40 years; mass 91 kg; height 1.905 m) walked two times: one time only with skin markers glued on the segments and another time with also intracortical pin mounted markers. This was performed to determine the frequency of the transient oscillation, which occurs at heel strike: it was suggested that STA introduces high frequency artefact. On another volunteer (age: between 35 and 40 years; mass: 104 kg; height: 1.88 m) it was assessed the effect of the STA on the computation of the instantaneous knee helical axis during different activities: cycling, squatting, normal gait, and voluntary swing movement. It was shown that the displacement with respect to the underlying bone of the skin markers could exhibit values up to 20 mm. Moreover, STA was found to be task-dependent, showing different patterns among the tasks analysed. It was also shown that the power spectra for skin- and pin-markers cover similar frequency bands, indeed there was not a distinct soft tissue noise transient. Therefore no evidence of a distinct frequency domain for the STA: attempt to remove STA through traditional filtering techniques can result in loss of information or in introduction of spurious motion patterns. It was concluded that the skin marker trajectories are not appropriate for representing motion of the underlying bones, particularly of the femur.

In 1998, Ball and Pierrynowski modelled the STA as a time varying affine transformation of 12 degrees of freedom (three orientations, three position, three shears, three scales) between the technical frame and the anatomical frame based on the trajectories of at least 4 markers glued on a segment, moreover, 20 and 16 skin markers were glued on the surface of the thigh and the shank, respectively. The validation of such modelling was realized using intracortical pins inserted in the femur and the tibia. Three volunteers (age:  $37 \pm 3$  years; height:  $1.81 \pm 0.07$  m; mass:  $82.7 \pm 4.5$  kg) walked for 20 seconds on a treadmill at three velocities: slow ( $0.66 \text{ms}^{-1}$ ), medium ( $1.10 \text{ms}^{-1}$ ), and fast ( $1.54 \text{m s}^{-1}$ ), collecting from 12 to 20 strides of gait. Bone poses and knee joint kinematics were analysed comparing the intracortical pins measurements, the traditional method using a fixed rigid transformation and the proposed method that will be described in details in the section 2.4.3. However, no numerical measurement about STA were shown in this study.

A new femoral tracking device was proposed by Houck et al., 2004 to measure the relative motion between the skin and the femur, and therefore, to improve the measure of the knee joint kinematics during gait trials. This device is a U shaped frame of aluminium and the femoral epicondyles were clamped with two pads. Intracortical pins were inserted into the proximal-lateral aspect of the right femur and tibia, equipped with four infrared light emitting diodes to validate this device. Three skin markers were glued along the crest of the tibia. The femoral tracking device was clamped over the femoral condyles and on its lateral extension two diodes were attached. A third diode was placed on the skin, distal with respect to the greater trochanter. Two subjects were involved in this study but only the results of one subject (age: 35 years; height: 1.73 m; mass: 80 kg) were compared in terms of knee joint kinematics obtained by the skin markers, the new device and the intracortical pins (Figure 2.2c). A ‘reasonable validity’ was claimed for the device by the authors over 85% of the stance phase of gait. Rotation error values were of few degrees, but during terminal stance and during the swing phase (*i.e.*, when maximum knee flexion occurs) these errors increased substantially. In this study, they found absolute differences of up to 2.2 deg in the sagittal plane, 2.7 deg in the frontal plane and 1.8 deg in the transversal plane, while up to 13.9 mm of linear displacements was observed during walking.

The difference in ankle complex motion during the stance phase of walking was measured in three volunteers using skin- and bone-anchored markers in Westblad et al., 2000. Three skin markers were glued laterally on each shank, heel, and forefoot and their trajectories were acquired during a barefoot walking trial. Hoffman pins, equipped with four markers (*i.e.*, bone-anchored markers) were inserted into the tibia, fibula, talus and calcaneus. The mean maximal differences between the skin- and bone- based joint rotations were smaller than 5 degrees. The smallest absolute difference was found for plantar/dorsiflexion. This finding was in contrast to a previous report (Reinschmidt et al., 1997a) where knee abduction/adduction showed the lowest error magnitude. This difference may be explained by the fact that subjects assessed in the latter study wore shoes.

STA was also quantified during the stance phase of gait and during cutting motion by Benoit et al., 2006 (Figure 2.2d). Eight volunteers (age: 26 years; height: 1.78 m; mass: 78.1 kg) were recruited in this study but only six of them were analysed (age:  $26\pm 4.7$  years; height:  $1.77\pm 0.04$  m; mass:  $76.3\pm 12.3$  kg; BMI:  $24.4\pm 3.8$ ). The information acquired from the intracortical pins were combined with a Roentgen stereophotogrammetric analysis (RSA) to remove the error due to the misplacement of the anatomical landmarks (Della Croce et al., 2005). During the foot-strike, mid-stance and toe-off of all the motor tasks performed by the volunteers the STAs were quantified in term of absolute error values in the knee kinematics, and to measure differences between both

systems, *i.e.*, marker- and pin-based. The impact of the STA on the joint kinematics was between  $2.4 \pm 2.2$  deg to  $4.4 \pm 3.2$  deg for the knee angles and between  $3.3 \pm 2.4$  mm to  $13.0 \pm 5.0$  mm for the knee displacements, during the stance phase of the gait. In particular, during the toe-off, only the anterior/posterior displacement showed a high error, otherwise, all the other errors were between  $3.3 \pm 2.4$  mm and  $8.0 \pm 5.7$  mm, even for proximal/distal displacement. During the second motor task performed by the volunteers (cutting motion) the impact of the STA on knee kinematics was more marked: the absolute difference between the two knee kinematics were from  $3.3 \pm 1.8$  deg to  $13.1 \pm 9.8$  deg (the latter was measured for AA during toe-off) for the knee angles, while for the knee displacements these errors were from  $5.6 \pm 5.1$  mm to  $16.1 \pm 8.9$  mm. Moreover, the direction of the skin movement artefact was not repeatable across subjects as observed in other studies (Houck et al., 2004; Manal et al., 2000; Reinschmidt et al., 1997c).

The impact of the STA on the determination of the hip joint centre (HJC) obtained with a functional calibration using a star-arc-movement (flexion/extension-abduction/adduction of the hip in different planes followed by a half circumduction) was analysed by Cereatti et al., 2009. Intracortical pins, equipped with four reflective markers, were inserted in the pelvis and the femur, eight markers were glued on the thigh. In this study, four fresh cadaveric specimens were used. The calibration movement was repeated three times for each specimen. The HJC estimations were performed with two different approaches (constrained three-degrees of freedom or an unconstrained six-degrees of freedom: DOF) and compared. The maximum error was the same for both algorithms for the subject with largest thigh circumferences. The relative motion between the skin markers and the underlying bone was between 1.0 mm and 10.6 mm. The proximal markers, which were closer to the hip joint, were significantly ( $p < 0.05$ ) more influenced by the STA. For this reason, HJC estimation errors computed using the distal marker clusters were significantly lower ( $p < 0.001$ ).

Andersen et al., in 2012, analysed the components of skin markers: rigid-body (translation and rotation) and deformation components. The aim of the study was to determine which component influenced more the pose estimation of the femur and tibia, using the experimental data described in Benoit et al., 2006. Three tasks were analysed: walking, cutting, and hopping. A linear model of the STA was proposed using the principal component analysis to describe the twelve degrees of freedom of the four markers glued on the segment. The results shown that the motion of the skin marker cluster relative to the underlying bone was dominated by rigid-body motions rather than deformations. Therefore, they concluded that all the STA compensation techniques focused on the marker cluster deformation will not be effective at removing the rigid body movement.

Recently, a model that provides the thigh STAs as a function of hip joint kinematics was identified, calibrated, and validated (Camomilla et al., 2013). This model estimates the STA which occurs on thigh markers in the anatomical reference frame, during a mono-articular movement (star-arc-movement). The proposed model was calibrated and assessed using experimental data obtained in a previous *ex-vivo* study (Cereatti et al., 2009): four intact fresh adult cadaver subjects positioned supine with steel pins, equipped with four-marker clusters, implanted into tibia, femur and hip-bones. In addition, 12 markers were glued on the thigh (Figure 2.2e). The model was calibrated and tested on the mono-articular movement performed for three times by an operator. The model calibration was performed for each marker using a global optimization based on the root mean square of the displacement difference between the measured skin marker and the estimated one. Different calibrations were realized to evaluate the effect of the trial-specific, subject-specific, and hip joint movement (HJM) on the estimation of the STA. The accuracy of subject-specific model estimates and the HJM independency, suggested the validity and generalizability of the model for a given subject and marker location. Besides, the large inter-subject variability of the model parameters confirmed the fact that STA is subject-dependent. The median root mean square distance values slightly increased when moving from trial- to subject-specific estimates: from 0.8 mm to 0.9 mm. Regarding HJM-dependency, these median value for all subjects was 1.0 mm. The results obtained were also different among the analysed subjects (*i.e.*, the third subject showed moderate correlations with respect to the others in all the calibration procedures performed).

### 2.2.2 External fixators

To treat bone fracture, external fixators (Figure 2.3) can be used. These devices are rigidly associated with the underlying bone, giving the opportunity to directly access to bone kinematics. In some studies reflective markers were located on this device, and the same acquisition system as for the skin markers was used. However, this device was typically located on only one segment (femur or tibia) for the rarity to have fractures in both bones. Therefore, the STA of only one segment was measured. The maximum number of subjects analysed using this method was seven (Cappozzo et al., 1996). When using external fixators, as occurs for the pin insertion, the STA assessment is limited by skin sliding restrictions (Leardini et al., 2005).

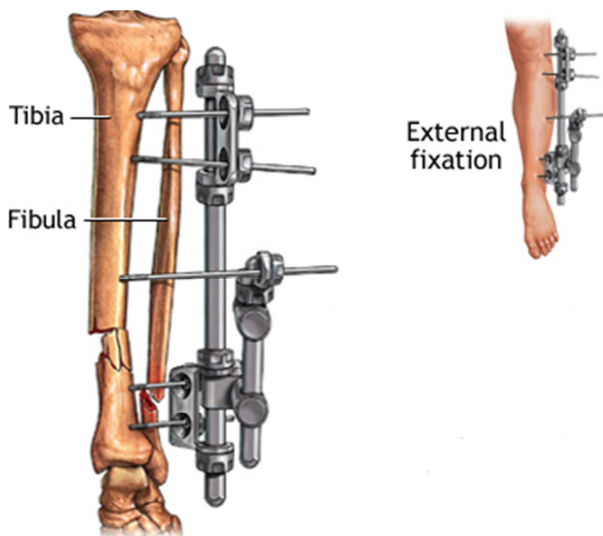


**Figure 2.3** – Example of an external fixator used to treat bone fracture.

The first study performed to analyse STA with patients wearing external devices for fracture fixation at either the femur or the tibia was done by Angeloni et al., 1992. These devices are rigidly associated with the underlying bone: a set of axes can be defined (Figure 2.4a). Markers were glued on the skin over the following four anatomical landmarks (ALs): greater trochanter, lateral epicondyle, head of the fibula, lateral malleolus. Using large elastic bands and Velcro fasteners, markers were placed on rigid plates in the proximal half of the thigh and the shank. The

range of displacement of these plate-mounted markers with respect to underlying bones during walking was lower than that of the markers located on the ALs. Similar results were obtained using a semi-quantitative video-fluoroscopic analysis.

The same authors showed more detailed results using the same methods in Cappozzo et al., 1996. The STA effects were investigated on seven subjects (age:  $23.3 \pm 5.7$  years; height:  $1.67 \pm 0.16$  m; mass:  $66.9 \pm 14.4$  kg) while performing different motor tasks: level walking at a natural speed, cycling on an exercise bike, flexion of the lower limb while standing, repetitive isometric muscular contraction and hip external rotation while standing with the knee in full extension. Each task was repeated at least for four times. The CAST (calibration anatomical system technique) method was used to define the anatomical frames (AFs), associated with skin- and fixator- marker cluster technical frames (CTF). A stereophotogrammetric system was used to track the motion of the markers on the external fixator and the skin markers, located on the ALs, as described in the previous work (Figure 2.4a). Markers on the fixator were assumed to provide instantaneous positions and orientations (*i.e.*, pose) of the corresponding rigidly associated bone. Other skin markers were glued on the body segment, as compatible with the presence of the fixator and camera visibility. The marker displacement with respect to the underlying bone showed remarkable magnitudes (up to 40 mm), as much as an order of magnitude larger than stereophotogrammetric errors. During the level walking task, the marker displacement due to STA was in the range of 10-30mm. The results were detailed for each subject and not averaged. However, it was clearly presented that in general, the STA associated with the markers on thigh and shank ALs showed magnitude that varies approximately linearly with respect to the joint flexion angle, irrespective of

the motor task performed. Bone orientation affected by STA caused an error between 6 deg and 20 deg for the femur, and between 4 deg and 10 deg for the tibia. Moreover, during hip external rotation, the error in femur orientation caused by STA reached magnitudes from 6 deg to 28 deg. Therefore, estimating the knee joint kinematics using skin marker data, FE, AA and IER might be affected with inaccuracy that can be respectively as large as 10%, 20%, and 100% of the relevant expected range of motion.

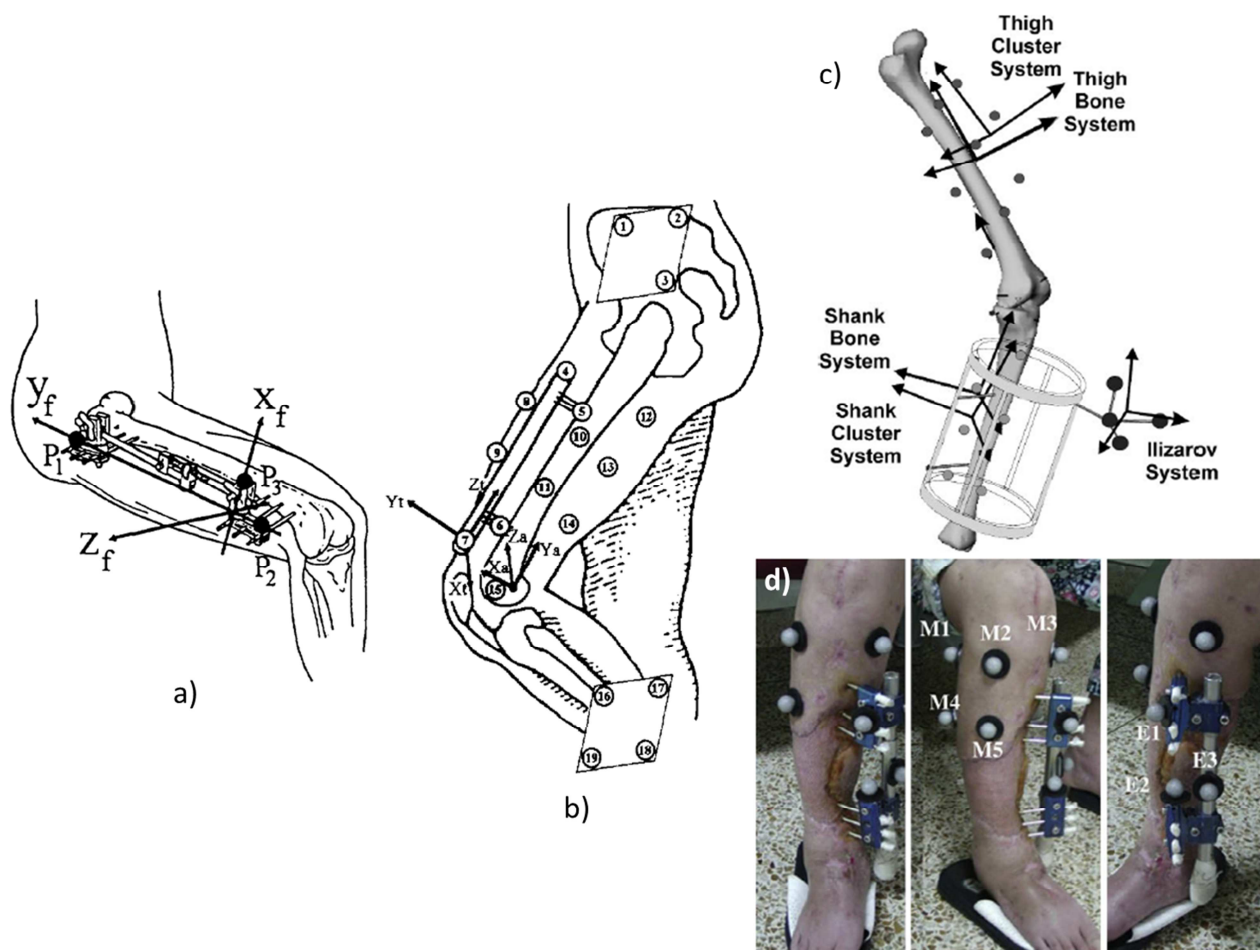


**Figure 2.4** – External fracture devices used in: **a)** Cappozzo et al., 1996; **b)** Cappello et al., 1997; **c)** Alexander and Andriacchi, 2001; **d)** Ryu et al., 2009.

To reduce the impact of STA on the bone pose estimation, Cappello et al., 1997 proposed a multiple anatomical landmark calibration protocol repeating such calibration in different postures. For its validation, a cycling test on a patient wearing a femoral external fixator was performed (Figure 2.4b). This technique will be described in section 2.4.2. Eight skin markers were glued on the thigh. A subset of three or more of them were used to define a CTF. In addition, four skin markers were located on the external fixator. With a CAST experimental protocol (Cappozzo et al., 1995), using a pointer, the coordinates of the femur ALs were defined. The amplitude of the STA was between 3.9 mm and 9.4 mm. Estimating the femur AF with the CAST protocol for two static postures analysed (*i.e.*, maximal hip and knee flexion and extension) the error in the femur pose estimation (position

and orientation) compared with the reference obtained with the external fixator was 5.00-5.10 deg, for the orientation components, while for the position vector the error was 6.9-7.0 mm. When the double calibration procedure was used, this error decreased to 3.50 deg for the orientation and 4.4 mm for the position.

The validation of the compensation method for the STA proposed by Alexander and Andriacchi, 2001, improving the point cluster technique (PCT) (Andriacchi et al., 1998), was realized on one subject (age: 46 years; height: 1.75 m; mass: 84.1 kg). The method will be discussed in the section 1.2.5. The point cluster marker set (six markers) was glued on the shank of the subject, four markers were rigidly attached to the Ilizarov device (an external fixator), which was rigidly connected to the tibia (Figure 2.4c). The subject, which exhibited a limited range of motion, performed a 10 cm step-up onto a platform. The proposed method reduced the impact of the STA on the pose of the shank from 0.25 mm to 0.08 mm and from 0.370 deg to 0.083 deg, values obtained as average location error. However, higher errors were obtained with this method in another study (Stagni et al., 2003) tested on two subjects (age: 67 and 64 years, height: 1.55 and 1.64 m, mass: 58 and 60 kg) during a step up/down test repeated three times.

To reduce the error caused by STA on the AL positions, Ryu et al., 2009 proposed a compensation method and used it on one subject (age: 42 year.; height: 1.63 m; mass: 56 kg; BMI: 21.1) with an external fixator in the tibia for its validation (Figure 2.4d). A linear relationships between the displacement of ALs and skin markers expressed in TFs, was proposed to be used. The STA during an active knee flexion/extension had an amplitude of 4.0 mm-18.3 mm, affecting the tibia pose with errors around 3 deg-4 deg and 20 mm-65 mm on each axis of the reference frame. With the proposed compensation methods, the effect of the STA on the tibia pose was reduced of 39-83%, with error around 0.6 deg-2.4 deg and 11 mm-31 mm on each axis of the reference frame.

### 2.2.3 Percutaneous trackers

Percutaneous skeletal trackers (PST) were metal devices designed specifically for the fixation to the skeleton using a number of halo pins inserted into the periosteum on opposite sides, instead into the bone, as occurs using intracortical pins (Holden et al., 1997). Nevertheless, using this device, a local anaesthesia is required. The issue about the limitation of the skin displacement around the area of the insertion when this device is used to measure the STA arises (Leardini et al., 2005). Seven was the maximum number of subjects acquired with this instrument (Manal et al., 2000).

Three healthy male volunteers (age: 28, 36, and 35 year; height: 1.80, 1.91, and 1.77 m; mass: 95.0, 91.6, and 69.2 kg; BMI: 29.4, 25.24, and 22.2) participated in the study performed by Holden et al.,

1997. The PST was fixed in the distal part of the tibia and fibula and it was instrumented with reflective markers (Figure 2.4a). Additional markers were attached to shells mounted on the lateral surface of the mid-shank and on the dorsal aspect of the mid-foot, instead of gluing the reflective markers directly on the skin. The volunteers walked at self-selected speed for six times along a corridor, including a platform. The AF associated with the bone was defined with a static anatomical calibration with both skeletal- and surface-based markers. The impact of the STA was calculated defining the relative 3D difference between the skeletal- and the surface-based AFs. In the volunteers analysed, a peak of the rotation error had a mean magnitude of 4 deg at the 8% of the gait cycle. Additional error rotation occurred during the terminal stance and during most of the swing phase with a magnitude 8 deg in one volunteer. Maximum absolute displacements of the skin-based AF, with respect to the reference AF obtained using the skeletal data, were less than 6.0 mm in the transverse plane but reached 10.5 mm longitudinally. The displacement between skin markers and the underlying bone was reproducible within subjects, but poor among subjects. Inverse dynamics were also analysed in the three volunteers during the stance phase. The impact of STA on knee moments was considered relatively small, seeing as the largest difference between two estimations was only 9 Nm. Moreover, the greatest errors occur in similar phase of the gait cycle, certainly due to the muscle activation.

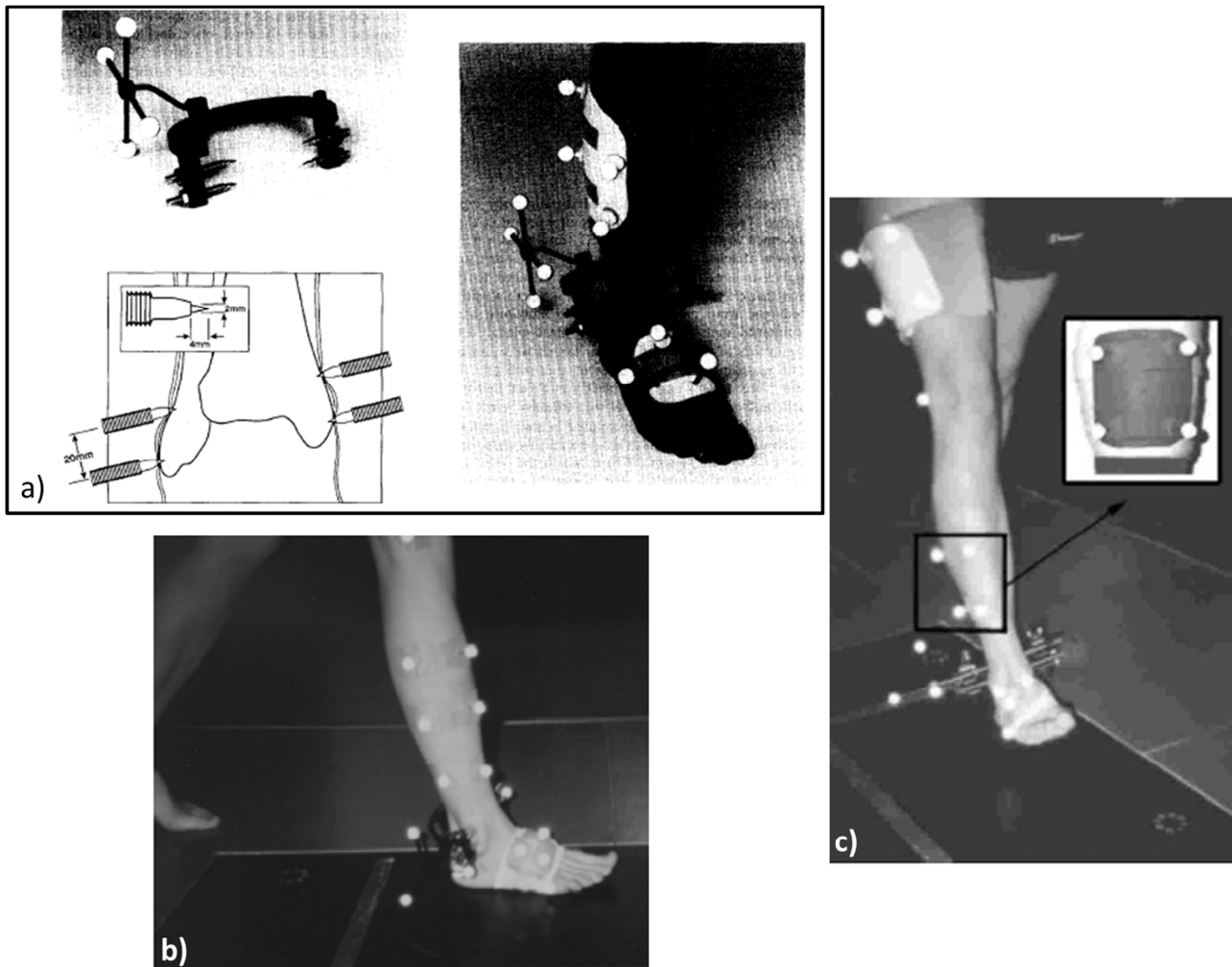


**Figure 2.5** – Percutaneous skeletal trackers used in: **a)** Holden et al., 1997; **b)** Manal et al., 2000; **c)** Manal et al., 2002.

In another study aimed at defining an optimal marker set to track the movement of the tibia, also further information were provided about the STA (Manal et al., 2000). Seven subjects (age:  $25.6 \pm 1.9$  years) performed several walking trials with eleven different configurations of markers glued on the shank, obtained by combining geometry, location (proximal/distal) and attachment (underwrap/overwrap) factors for the array of markers (Figure 2.4b). As reference, a tracker was clamped to the two malleoli and AFs were defined for the foot, shank and thigh using markers located over ALs. The differences between the PST and the marker sets were quantified using the root mean square deviation of the relative helical angle based on the three most similar trials of each subject and for each marker set. When the marker arrays over the lateral shank were placed more distal than proximal, better estimates of tibial rotation were noted. No significant difference were measured between overwrapped or underwrapped surface mounted markers, but as the trend was in favour of the underwrapped attachments. The best performance was observed for an underwrapped rigid shell with four markers located distally, as much as possible. However, even when using the

best set of markers, rotational deviations of  $\pm 2$  deg about the medio–lateral and antero–posterior axes and  $\pm 4$  deg about the longitudinal axis were noted in the individual subject data. The largest errors were measured in the first and last thirds of stance. Although the average peak deviation was just slightly greater than 2 deg, when these deviations were analyzed subject by subject, such errors increase at 7–8 deg. These large errors were masked when the data were averaged across subjects. This was caused by the following reasons: peak deviations did not occur at the same time for the different subjects; and the deviation direction was not always the same. This complicates future efforts to model soft tissue movement, since the model must not only account for the magnitude and timing of the rotational deviation, but it must also account for the direction of the deviation.

In Manal et al., 2002 the effect of STA was evaluated on knee moments in level walking, by comparing relevant calculations obtained using the same tracking targets and the surface cluster defined in the above-mentioned study. Six subjects (age:  $25.6 \pm 1.9$  year; height:  $1.78 \pm 0.05$  m; mass:  $77.8 \pm 14.0$  kg) were involved in the study. The more relevant difference in the estimation of the knee moments was 3 Nm. Therefore, based on these small and non-significant differences between PST and the cluster defined as described above, the authors assessed that the STA has a very small effect on the knee joint moment.

On seven healthy subjects (height  $1.78 \pm 4.7$  m; mass  $77.8 \pm 14.0$  kg) a PST was anchored to the medial and lateral malleoli of each subject using two modified halo pins on each side (Manal et al., 2003) to measure estimating tibial translation during natural cadence. Three spherical retro reflective tracking targets were then secured to the PST device. Both the PST device and the tracking targets were assumed rigid with the tibia. A second array of four targets was mounted to a Velcro backed contour molded shell, which was attached superficially to the distal lateral shank using an elasticized band (*i.e.*, surface-mounted) as shown in Figure 2.4c. The subjects performed three walking trials at a self-selected speed. Results shown found average error peaks difference of 7.1 mm, 3.7 mm and 2.1 mm, while individual peak differences were 14.1 mm, 11.8 mm, and 8.3 mm along the X, Y, and Z axes of the global coordinate system, respectively. The ensemble-averaged curves masked the magnitude of individual subject errors for the reason explained also in the previous study performed by the same authors. The authors presented the STA as two sources of errors. First, the deformation of the shape of the soft tissue, and second the movement of the soft tissue relatively to the underlying bone. In this study, the first one was avoided due to the use of the underwrapped rigid shell with markers. So, all of the difference due to the STA should come from the second error source.

### 2.2.4 Imaging

Imaging techniques are non-intrusive methods to measure skin movement with respect to the underlying bone *in-vivo*. The main limitation of these methods is the small volume of acquisition. Moreover, when radiographs (static) are acquired, only 2-D information can be acquired. All the acquired measures are dependent on the pose of the segment within the system. A wrong orientation will influence the reported measurement.

The accuracy of skin markers for the prediction of skeletal locations in the foot and ankle was assessed using radiographs from ten volunteers (age: 18-35 years; height:  $1.70 \pm 0.075$  m; mass:  $69.2 \pm 12.1$  kg) for the first time by Maslen and Ackland, 1994. The relationship between skin and skeletal markers was examined during rear foot inversion/eversion maneuver (a 10 deg calcaneal inversion position, a neutral alignment, and a 5 deg calcaneal eversion position). Small steel markers were placed over the two malleoli, the navicular tuberosity, the sustentaculum tali and the base of the fifth metatarsal. Lateral view radiographs were collected and analyzed for all the volunteers, including compensation for X-ray magnification. For the inversion and the eversion, the initial offsets measured during the neutral pose were removed to measure only the effect of the pose of the foot on the position of the steel markers. The markers on the two malleoli shown the largest artefact, mean displacement between the skin markers and the underlying bones was between 2.7 mm and 14.9 mm.

The first study that used a standard fluoroscopy to assess the STA was performed by Sati et al., 1996. On the medial and lateral condyles and on the lateral aspect of the thigh, small metallic markers were individually taped. Several markers were placed on the skin in each of these regions to find regions of minimal skin movement. The video fluoroscopy was employed to visualize the X-ray projection of both the radio-opaque metallic markers placed on the surface of the skin and the underlying bone (Figure 2.6a). An active knee flexion from the upright posture was performed by three male subjects and acquired using a calibrated X-ray fluoroscope in order to represent the swing phase of gait. The radio-opaque skin marker positions, recorded during the active knee flexions, were measured with respect to the reference axes defined in the knee image, taking into account both the effects of magnification and the 3D nature of the knee movement. Root mean square values of lateral marker movements were between 2.5 mm and 16.8 mm. The maximum displacement measured along the antero-posterior direction was 42.5 mm, while along the vertical direction this value was 20.6 mm. The STA along the medial direction shown root mean squared values between 2.1 mm and 17.1 mm. Moreover, the results showed that the largest STA was measured for markers located closest to the joint line, providing useful information for marker

placement in routine movement analysis. In this study, also a correction method for orientation error is proposed, nevertheless it is efficient only for small rotations ( $\pm 5$  deg).

A similar study of the one conducted by Maslen and Ackland, 1994 was performed by Tranberg and Karlsson, 1998. On six healthy subjects (mean age 39) were analysed different ankle positions: neutral position, 20 deg dorsi/flexion and 30 deg plantar/flexion. Spherical lead markers were glued on the skin over the following ALs: medial malleolus, navicular bone, the medial part of the calcaneus, and the base and the head of the first and fifth metatarsal heads. During the experiment, a specially constructed platform was used (Figure 2.6b). On the proximal markers (ones close to the medial malleolus and to the calcaneus) the largest STA was measured: more than 4 mm. These skin markers underwent the largest skin sliding caused by the largest angular motion exhibited by the talocrural joint. The smallest STA was found for the metatarsal bones (less than 1.8 mm). However, using this technique, the STA can be measured only in the sagittal plane.

A high-accuracy cine-radiographic method, to directly evaluate the 3D skeletal kinematics during stressful sport activities, as running and hopping, was used in Tashman and Anderst, 2002. This method was used to characterize the nature of the motion between the skin surface markers located over the femoral condyles and the underlying bone during impact movements. Tibio-femoral kinematics were defined *in-vivo* for two subjects. For the first time, impact movement was analysed: one-legged forward hopping. Reference femur and tibia motion was tracked in two patients after implantation of three 1.6 mm diameter tantalum beads at the time of knee surgery. A very noticeable “bounce” relative to the bone was observed after the impact on both skin markers. The peak-to-peak magnitude of the STA ranged from 5 to 31 mm, after foot impact. The timing, frequency and magnitude of the transient component of the STA was dependent on subject, marker and direction. Therefore, the STA motion in this study was complex, time-varying and correlated to the movement: methods based on Gaussian noise modelling to reduce STA (Alexander and Andriacchi, 2001) should be applied with caution for studies which address rapid movements and impacts.

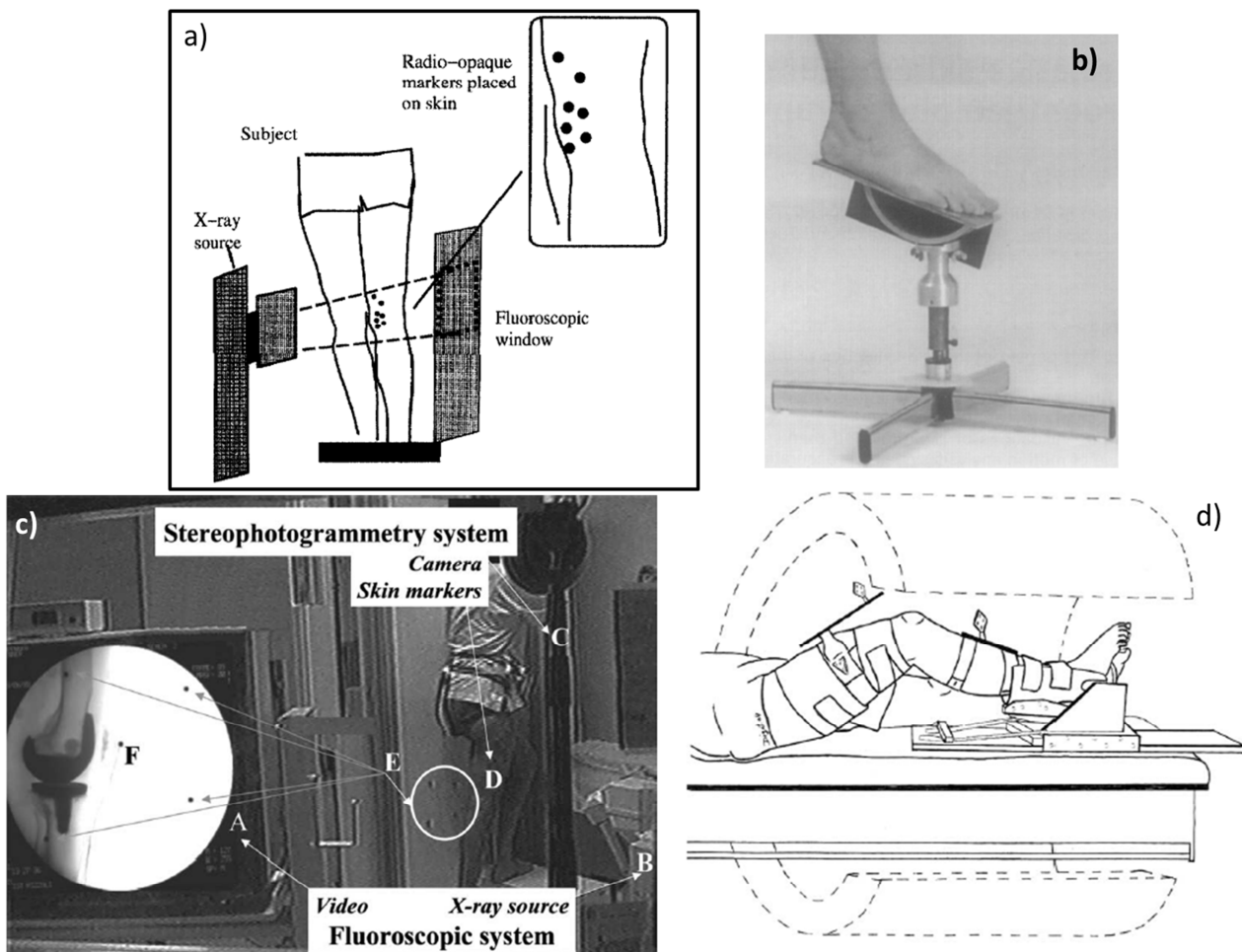


**Figure 2.6** – Different imaging system used in: **a)** Sati et al., 1996; **b)** Tranberg and Karlsson, 1998; **c)** Stagni et al., 2005; **d)** Sangeux et al., 2006.

In Stagni et al., 2005 the STA was characterized combining two techniques: stereophotogrammetry and 3D fluoroscopy (Figure 2.6c). Experimental data were acquired from two subjects (age: 67 and 64 years; height: 1.55 m and 1.64 m; mass: 58 kg and 60 kg; BMI: 24 and 22), with total knee replacement, during stair climbing, step up/down, sit-to-stand/stand-to-sit, and extension against gravity. Reference 3D kinematics of the femur and tibia was reconstructed from fluoroscopy-based tracking of the relevant prosthesis components. Soft tissue artefact was quantified as the motion of a grid of retro-reflecting markers attached to the thigh and shank with respect to the underlying bones, tracked by optoelectronic stereophotogrammetry. A different number of markers were glued on the thigh of the two subjects: nineteen and twenty-five markers were uniformly attached laterally on the skin. Moreover, ten skin markers were also attached to the lateral aspect of the shank. The reconstruction of each 2D fluoroscopic projection using an iterative procedure using a shape matching technique based on the knowledge of corresponding CAD models, allowed the definition of the 3D pose of the prosthesis components. The trajectory of the skin markers acquired with the stereophotogrammetric system were represented in the relevant prosthesis component reference

frames. STA was fully quantified for the first time in 3D and without any constraint to skin motion during the execution of activities of daily living in the whole thigh and shank. The STA on skin markers glued on the thigh was found up to 31 mm, while for the markers located on the shank the STA amplitude was up to 21 mm. During all the motor tasks skin markers on the thigh exhibited a larger displacement, except during the leg extension against gravity, where the displacements of the markers on the shank were larger. In this case, the gravitational contribution to STA is not time dependent and the inertial one is negligible, while the muscles of the shank are poorly contracted. Thus, the skin markers attached on the relaxed soft tissues are particularly prone to gravity and inertia during the extension of the knee. Moreover, the impact of the STA on knee rotations was also measured: the ab/adduction and internal/external rotation angles were the most affected by STA propagation, with root mean square errors up to 192% and 117% of the corresponding range, respectively.

Another non-invasive technology that can assess the relative movement between the bone and the markers on *in-vivo* data is the Magnetic Resonance Imaging (MRI), which can acquire soft tissue as well as bone image. The study performed in 2006 by Sangeux et al. used such technology on eleven volunteers (mean age 33 years) which performed an actively loaded knee extension, using a foot drive device (Figure 2.6d). The impact of the STA in the estimation of the Finite Helical Axis (FHA) was assessed. Four capsuled, filled with a liquid visible in MRI, were fixed through Velcro bands on the thigh and shank. FHAs were defined for each segment. The whole volume of the knee of the subject was processed for four sequentially held knee flexion positions during the knee movement. The bones and external marker sets geometry were reconstructed from magnetic resonance images. Then a registration algorithm was applied to the bones and the relative movement of the thigh and shank marker sets with respect to their underlying bones was computed. The measured STAs were greater for the thigh (2-22 mm) than for the shank (1-9 mm). Thigh marker sets relative movement expressed the same trend for all the subjects: an increase of the relative movement distance with the flexion angle. On the tibia, instead, STAs did not show this features. Relative movement rotation parameters for the thigh (range: 0–11 deg) and the shank marker (range: 0–15 deg) did not express a trend with the flexion angle. Marker displacements affected the knee movement finite helical axes direction (range 10–35 deg) and localization (range 0–40 mm).

Eight normal subjects (age:  $23.3 \pm 2.3$  years; mass:  $69.7 \pm 12.1$  kg; height:  $172.0 \pm 3.6$  cm) received a computed tomography (CT) scan of the knee joint for the study performed by Tsai et al., (2009). The CT data were segmented using a threshold filter to obtain volumetric models of the individual

bones: femur, tibia, fibula and patella. These subject-specific volumetric bone models, including their external surfaces and internal structures, were then used for the registration with the fluoroscopic images. Skin markers were glued on the thigh and the shank segment. Three tasks were tested (isolated knee flexion/extension, level walking, and sit-to-stand), simultaneously acquired using a 3D motion capture system and a dynamic fluoroscopy system (Figure 2.7a). The registered poses of the femur and tibia during subject standing calibration were used to define the local coordinate systems for each of the bones, with positive X-axis directed anteriorly, Y-axis superiorly, and Z-axis laterally. The marker positions relative to the local coordinate systems were then taken as the reference positions with no STA. Then, the STA of the markers was calculated as the movement of the markers from their reference positions and was expressed as total magnitude. For each motor task, the peak and root mean square (RMS) of the STA of each marker over the movement cycle were calculated for each subject, which were then averaged across all the subjects. The STA were also expressed in terms of the knee flexion angle to examine the relationship between the STA and the knee joint motion. In contrast to previous results on patients with external fixators or intracortical pins, the STA of markers were found to be in nonlinear relationships with knee flexion angles and some of their patterns were different between activities. For this reason, the authors suggested that correction of STA using a linear error model based on STA measured from static isolated joint positions may not produce satisfactory results for normal subjects during activities considered in this study. Moreover, the authors assessed that the movement of the overlying skin could also be affected by movements of more than one joint. Therefore, the STA of the markers on the thigh are directly affected by the poses of the knee and hip at the same time, and those on the tibia by the poses of the knee and ankle. In addition, the STA of the markers close to the knee joint were greater than those away from the joint (total STA RMS for the markers MCF and T2 were 27.1 mm and 9.7 mm, respectively, during the isolated knee flexion/extension, Figure 2.7a).

The aims of the study performed by Akbarshahi et al., in 2010, were to quantify lower limb soft-tissue artefact in young healthy subjects during functional activity (open-chain knee flexion, hip axial rotation, level walking, and a step-up), and to determine their effect on the calculation of knee joint kinematics. Four healthy males (age:  $30\pm 3$  years, mass:  $71\pm 7$  kg, height:  $178\pm 2$  cm) participated in this study. Magnetic resonance imaging (MRI) data were used to generate subject-specific bone models. Ten reflective markers were placed on each subject's leg and located on the anterior and lateral aspects of the mid and distal third of the thigh, the mid anterior and lateral aspects of the shank, the lateral femoral epicondyle and the patella. Kinematic data were collected

simultaneously from an X-ray fluoroscopy unit and a video motion capture system. Three radio-opaque reflective markers, visible in both systems, were placed on a plane parallel to the image plane of the X-ray unit, and were used to synchronize data between the two systems and to perform relevant reference frame transformations (Figure 2.7b). Knee joint kinematics was derived using the anatomical frames from the MRI-based, 3D bone models together with the data from video motion capture and X-ray fluoroscopy. STA was defined as the degree of movement of each marker in the antero-posterior, proximo-distal and medio-lateral directions of the corresponding AF. 180 different skin-marker clusters were used to calculate knee joint rotations, and the results were compared against the reference one (obtained from fluoroscopy). Although a consistent pattern of soft-tissue artifact was found for each task across all subjects, the magnitudes of STA were subject-, task- and location-dependent. Thigh STA were substantially greater than that measured on the shank. Markers positioned close to the knee joint showed considerable movement, with RMS values as high as 29.3 mm. The largest amount of STA for the thigh occurred in the proximo-distal direction during the step-up task ( $12.6 \pm 4.7$  mm), whereas that for the shank occurred in the medio-lateral direction during the open-chain knee flexion task ( $8.6 \pm 2.7$  mm). The maximum RMS error measured for knee joint rotations occurred for the open-chain knee flexion task and were 24.31 deg, 17.81 deg and 14.51 deg for FE, IER and AA, respectively. Moreover, AA and IER calculated with skin-marker clusters showed misleading patterns, with average RMS errors that were substantially greater than their respective total range of motion (ROM) for three of the four tasks

In 2011, Kuo et al., quantified the STA of selected markers on the thigh and shank, and their effects on the calculated joint centre translations, angles and moments of the knee during sit-to-stand. Ten patients (age:  $77.7 \pm 6.5$  years; mass:  $63.4 \pm 10.1$  kg; height:  $151.0 \pm 7.0$  cm), with total knee replacements performed a sit-to-stand movement. Experimental data were simultaneously acquired using a motion capture system, a force-plate and a fluoroscopy system (Figure 2.7c). Fifteen infrared retro-reflective markers frequently used in human motion analysis (Cappozzo et al., 1996) were used to track the motion of the pelvis, and the thigh, shank and foot of the tested limb. Three additional technical markers were also attached to the thigh. The real poses of the thigh and shank were defined by those of the femoral and tibial components obtained using a 3-D fluoroscopy method. The STA were measured on the following markers: medial and lateral femoral epicondyles (MFC and LFC), thigh markers (T1, T2, T3, and T4), tibial tuberosity (TT), and fibular head (FH). The STA of the skin markers were calculated as their movement relative to the underlying prosthesis components. The MFC and LFC were displaced posteriorly and proximally from their true positions when the subjects sat on the chair, and moved anteriorly and distally with the knee

extending during the task. The magnitudes of STA of the thigh markers were greater than those of the shank in these patients during the sit-to-stand, in agreement with the literature and the previous study performed by the same authors on healthy subjects (Tsai et al., 2009). The joint center translations, angles and moments at the knee were also calculated separately using skin markers and the registered prosthesis poses. Considerable STA were found, leading to significantly underestimated flexion and internal rotation angles, and extensor moments, but overestimated joint center translations and adduction angle. In this study, accurate data of the kinematics and kinetics of total knee replacements during sit-to-stand were provided. For the first time in the literature, the effects of STA on the calculated joint center translations, joint angles and moments were also quantified.

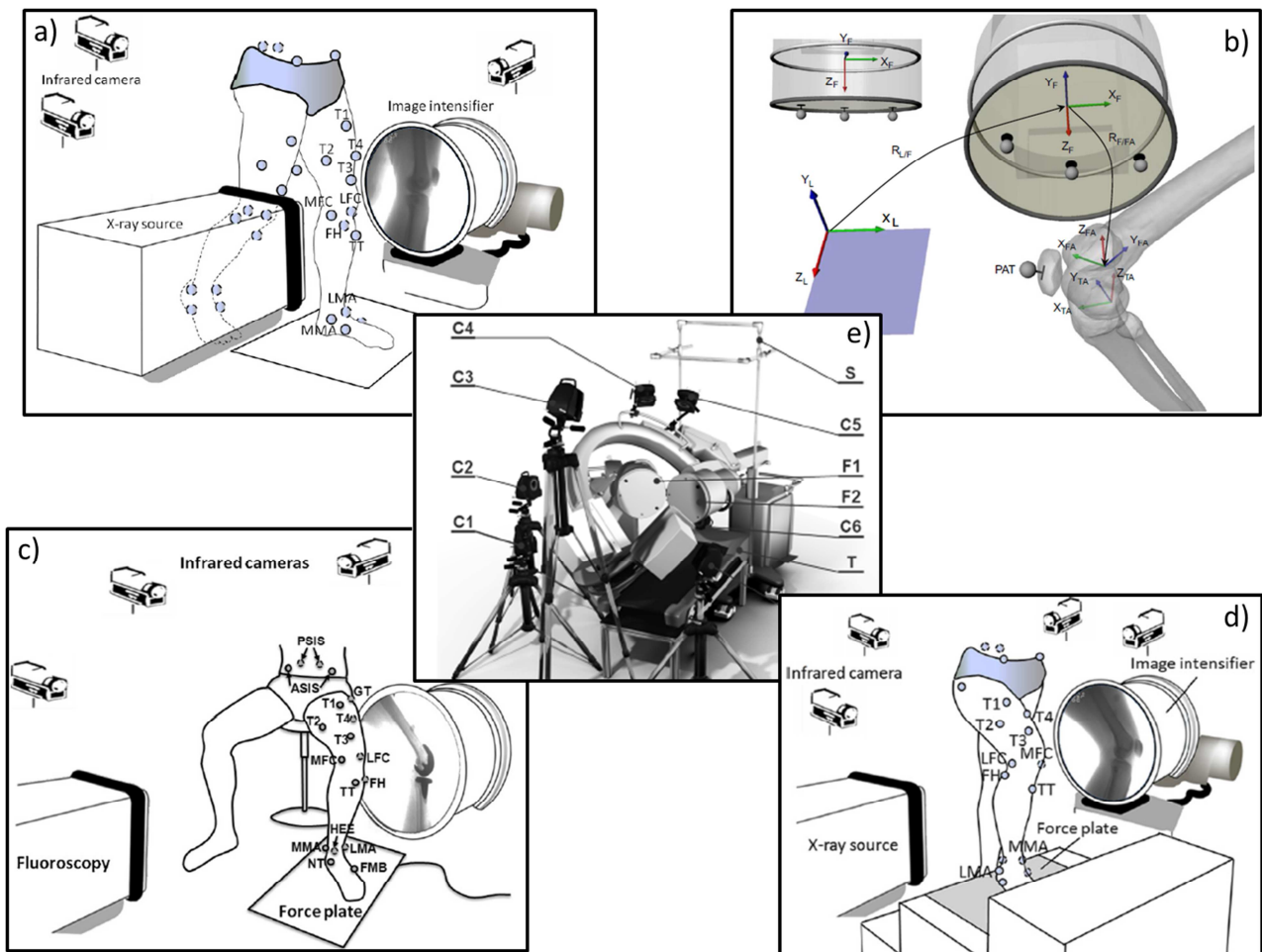


**Figure 2.7** – Different imaging system used in: **a)** Tsai et al., 2009; **b)** Akbarshahi et al., 2010; **c)** Kuo et al., 2011; **d)** Tsai et al., 2011; **e)** Barré et al., 2013.

The effects of STA were greatest in the peak values of the joint angles and moments: the mean error in the peak knee flexion angle and peak extensor moment were found to be about 10 deg and 10.5%, respectively. The authors declared that the results obtained in this study could help in

developing guidelines for using skin markers and in establishing databases in the biomechanical assessment of sit-to-stand in patients with total knee replacements.

The STA were measured during stair-ascent and their effects on the calculated joint centre translation, angles and moments at the knee in normal subjects during this activity were assessed in the study performed by Tsai et al., in 2011. Twelve young adults (age:  $22.3 \pm 1.4$  years; mass:  $75.8 \pm 7.9$  kg; height:  $171.2 \pm 2.7$  cm) walked up a three-step stair while data were acquired simultaneously from a 3-D motion capture system, a force plate and a dynamic fluoroscopy system (Figure 2.7d). The real poses of the knee were obtained using a 3D fluoroscopy method. From CT images of the knee joint of each subject, the subject-specific volumetric models of the femur, tibia, fibula and patella were obtained for subsequent registration with fluoroscopic images. Eighteen infrared retro-reflective markers were used to track the motion of the pelvis, and the thigh, shank and foot of the tested limb (Figure 2.7d). The STA of the thigh markers were greater than those on the shank, leading to significantly underestimated flexion and extensor moments, but overestimated joint centre translations during the first half of the stance phase. The STA of the markers had significant effects on the measured knee angles during the first half of stance phase: at 10%, 20% and 30% of stance phase, knee flexion, abduction and internal rotation angles calculated from skin markers were all significantly smaller than the real kinematics. Significantly smaller knee flexion was also found at 40% of stance phase. Knee joint centre translations calculated from skin markers were significantly greater than those from the virtual bone markers at 10%, 20%, 30%, 40% and 50% of stance phase for posterior components; similarly, at 10%, 20%, 30% and 40% for distal components and at 10% of stance phase for medial components. The results obtained in this study can be useful for a better understanding of the normal biomechanics of the knee during stair-ascent, as a baseline for future clinical applications and for developing a compensation method to correct for the effects of STA.

Barré et al., in 2013, measured the STA on nineteen subjects (age:  $70 \pm 6$  years; mass:  $80 \pm 14$  kg; height:  $168 \pm 9$  cm) with knee arthroplasty that walked on a treadmill while a bi-plane fluoroscopic system (X-rays) and a stereophotogrammetric system (skin markers) recorded their knee movement (Figure 2.7e). A static calibration was performed during a standing posture to obtain AF-TF rigid transformations to compute the knee joint kinematics of the prosthesis AF from the TF defined on the skin markers clusters. During the treadmill gait, the markers trajectory, segments' pose and knee joint kinematics were obtained. The two components of the STA, *i.e.* the local displacement of the markers (LSTAD) and the rigid body motion of the skin marker cluster relative to the underlying bone (RSTAM, defined as the rigid movement of the cluster of skin markers relative to the

prosthesis), were separated and quantified during the stance and swing phases. The results obtained in this study showed that the RSTAM amplitude was approximately 80-100% of the STA, while LSTAD magnitude was around 35-50%, confirming the importance of the RSTAM relative to LSTAD. The authors considered the RSTAM as the main source of STA error. For this reason, the amplitude and the pattern of the RSTAM were studied. It was shown that RSTAM was more pronounced during the swing phase than the stance phase. The vertical axis of the anatomical frame of the femur was influenced the most by RSTAM. Combined with tibial error, internal/external rotation angle and distraction-compression were the knee kinematics parameters most affected by RSTAM during the gait cycle, with average RMS values of 3.8 deg and 11.1 mm. This study highlighted higher RSTAM during the swing phase particularly in the thigh segment and suggested new features for RSTAM such as the particular shape of some RSTAM waveforms and the absence of RSTAM in certain kinematics during the gait phases. In order to evaluate whether RSTAM is dependent on gait speed or body mass index (BMI), Pearson coefficients were computed between the range, the standard deviation of RSTAM waveforms and BMI and gait speed: some similarities were observed for the RSTAM between subjects, while some correlations were found with gait speed and BMI.

The following tables (Tables 2.1-2.5) synthesize the main features and conclusions of the studies aimed at the STA quantification with the different methods described (intracortical pins, external fixators, percutaneous trackers and imaging).

<i>STA Measure</i>	<i>Study</i>	<i>Motor Task</i>	<i>Subject</i>	<i>Marker Location</i>	<i>STA Quantification</i>	<i>Impact of STA on bone pose or joint kinematics</i>
<b>Bone-Pins</b>	Lafortune and Lake, 1991	Unloaded knee flexion-extension	1	Marker placed on the proximal tibia	<ul style="list-style-type: none"> <li>• 21 mm distal and a 23 mm posterior displacement</li> <li>• displacement linearly related to knee flexion</li> </ul>	-
		Heel strike during running		Marker placed on the lateral tibial condyle	STA magnitude of 10 mm	-
	Karlsson and Lundberg, 1994	Hip internal-external rotation (extended knee)	2	Three skin markers glued on the distal thigh and on the proximal shank	thigh STA > shank STA	Knee IE measurement: 20 deg (pin) vs 50 deg (skin markers)
	Reinschmidt et al., 1997a	Stance phase of a level walking	5	Six markers glued on the thigh, shank and shoe	thigh is most by the STA due to muscle movements during the stance phase than shank	Error introduced by the STA can almost be as high as the magnitude of the real knee AA and IER
	Reinschmidt et al., 1997c	Running stance phase	3		-	Skin markers overestimate joint motion. Errors due to STA were higher in running than in walking
	Fuller et al., 1997	Walking	1	Twenty markers glued on the thigh and shank segments	<ul style="list-style-type: none"> <li>• STA values up to 20 mm</li> <li>• STA was task-dependent</li> <li>• Power spectra for skin- and pin-markers there was not a distinct transient</li> </ul>	-
		Cycling, squatting, normal gait, and swing movement	1			
	Ball and Pierrynowski, 1998	Walking (20 s on a treadmill, three velocities)	3	Twenty and sixteen markers glued on the thigh and the shank	-	The Pliant Surface Modelling for STA compensation is proposed. Using the traditional rigid body modelling errors the position of femur and tibia, were 4.8 mm and 3.8 mm
	Houck et al., 2004	Gait	1	Three markers were glued along the crest of the tibia	-	Tibiofemoral angles: maximum errors (0-85% of stance) of 1deg and 4.2 deg
	Westblad et al., 2000	Stance phase of barefoot walking	3	Three markers glued on shank, heel, and forefoot	-	Ankle complex motion: mean maximal differences < than 5 deg

- Table 2.1 -

<i>STA Measure</i>	<i>Study</i>	<i>Motor Task</i>	<i>Subject</i>	<i>Marker Location</i>	<i>STA Quantification</i>	<i>Impact of STA on bone pose or joint kinematics</i>
<b>Bone-Pins</b>	Benoit et al., 2006	Stance phase of gait and cutting motion	6	Four markers glued on thigh and shank	the direction of the skin movement artefact was not repeatable across subjects	Average rotational errors up to 4 deg and 13 deg and translational errors up to 13 mm and 16 mm for the walk and cut, respectively
	Cereatti et al., 2009	Star-arc-movement	4	Eight markers glued on thigh	<ul style="list-style-type: none"> <li>• STA between 1.0 mm and 10.6 mm</li> <li>• HJC determination using different clusters and methods</li> </ul>	HJC errors highly varied among subjects, methods, and skin marker clusters (between 1.4 and 38.5mm)
	Andersen et al., in 2012	walking, cutting, and hopping	6	Four markers glued on thigh and shank	STA quantified using the principal component analysis	-
	Camomilla et al., 2013	Star-arc-movement	4	Twelve markers glued on thigh	• STA between 1.0 mm and 35 mm	-
<b>External fixators</b>	Cappozzo et al., 1996	Walking, cycling, knee flexion, isometric muscular contraction and hip external rotation	7	Four skin markers glued on anatomical landmarks of the leg	<ul style="list-style-type: none"> <li>• STA magnitude up to 40 mm</li> <li>• STA showed magnitude that varies approximately linearly with respect to the joint flexion angle (different tasks)</li> </ul>	Error bone orientation due to STA: 6 deg and 20 deg for the femur, and between 4 deg and 10 deg for the tibia
	Cappello et al., 1997	Cycling	1	Eight markers glued on the thigh	STA magnitude between 3.9 mm and 9.4 mm	The multiple anatomical landmark calibration protocol is proposed: estimating the femur pose, the orientation error decreased from 5 deg to 4 deg, and the position one from 7 mm to 4.5 mm
	Alexander and Andriacchi, 2001	A 10 cm step-up onto a platform	1	Six markers glued on the shank	-	Improvement of the Point Cluster Technique: STA error of the shank pose reduced from 0.25 mm to 0.08 mm and from 0.370 deg to 0.083 deg
	Ryu et al., 2009	Active knee flexion/extension	1	Five markers glued on the shank	The magnitude of the STA was 4-18 mm, depending on the location of the markers	STA error for shank pose: 4 deg and 65 mm

- Table 2.2 -

<i>STA Measure</i>	<i>Study</i>	<i>Motor Task</i>	<i>Subject</i>	<i>Marker Location</i>	<i>STA Quantification</i>	<i>Impact of STA on bone pose or joint kinematics</i>
<i>Percutaneous trackers</i>	Holden et al., 1997	Walking	3	Markers were attached to shells mounted on the lateral surface of the mid-shank	STA was reproducible within subjects, but poor among subjects	Maximum positional STA thigh error was less than 6.0 mm in the transverse plane and 10.5 mm longitudinal one
	Manal et al., 2000	Walking	6	Six markers glued on the shank	-	The largest errors STA were measured in the first and last thirds of stance. Rotational errors can reach 7–8 deg
	Manal et al., 2002	Walking	6	Six markers glued on the shank	-	STA has a very small effect on the knee joint moment
	Manal et al., 2003	Walking	7	Six markers glued on the shank	-	Average peak difference in the tibia position were 7.1, 3.7 and 2.1 mm along the X, Y and Z axes of the global coordinate system respectively. Individual subject peak differences were as large as 14.1, 11.8 and 8.3 mm (same axes)
<i>Imaging</i>	Maslen and Ackland, 1994	Rear foot inversion/eversion maneuver	10	Marker glued on the shank and feet (radiographs)	The markers on the two malleoli shown the largest STA (mean STA was between 2.7 mm and 14.9 mm)	-
	Sati et al., 1996	Knee flexion	3	Several markers glued on the medial and lateral condyle and on the lateral aspect of the thigh (fluoroscope)	rms STA from 2 to 17 mm. Largest movement occurred on markers placed on the joint line	A correction method for orientation error is proposed, nevertheless it is efficient only for small rotations ( $\pm 5$ deg)

- Table 2.3 -

<i>STA Measure</i>	<i>Study</i>	<i>Motor Task</i>	<i>Subject</i>	<i>Marker Location</i>	<i>STA Quantification</i>	<i>Impact of STA on bone pose or joint kinematics</i>
<b>Imaging</b>	Tranberg and Karlsson, 1998	Different ankle positions	6	Skin markers glued on foot anatomical landmarks	On the proximal markers (close to the medial malleolus and to the calcaneus) the largest STA was measured: more than 4 mm.	-
	Tashman and Anderst, 2002	One-legged forward hopping	2	Markers glued on the medial and lateral condyle	The peak-to-peak magnitude of the STA ranged from 5 to 31 mm, after foot impact. The timing, frequency and magnitude of the transient component of the STA was dependent on subject, marker and direction.	-
	Stagni et al., 2005	Stair climbing, step up/down, sit-to-stand/stand-to-sit, and extension against gravity	2	Several markers glued on the thigh and shank	The magnitude of thigh STA was found up to 31 mm, while for shank STA was up to 21 mm	Knee AA and IE angles were the most affected by STA propagation, with root mean square errors up to 192% and 117% of the corresponding range, respectively
	Sangeux et al., 2006	Loaded knee extension, using a foot drive device	11	4 markers (capsuled, filled with a liquid visible in MRI) fixed on thigh and shank	STA magnitude thigh of 2-22 mm and shank of 1-9 mm. Thigh STA increased with the flexion angle.	Marker displacements affected the knee movement finite helical axes direction (range 10–35 deg) and localization (range 0–40 mm)
	Tsai et al., 2009	Knee flexion/extension, level walking, and sit-to-stand	8	Skin markers were glued on the thigh and the shank segment	the STA were found to be in nonlinear relationships with knee flexion angles and sometimes different between activities	STA on the thigh are directly affected by the poses of both knee and hip, and those on the tibia by the poses of both knee and ankle

- Table 2.4 -

<i>STA Measure</i>	<i>Study</i>	<i>Motor Task</i>	<i>Subject</i>	<i>Marker Location</i>	<i>STA Quantification</i>	<i>Impact of STA on bone pose or joint kinematics</i>
<b>Imaging</b>	Akbarshahi et al., in 2010	open-chain knee flexion, hip axial rotation, level walking, and a step-up	4	Ten reflective markers were placed on thigh and shank	<ul style="list-style-type: none"> <li>• Consistent pattern of STA found for each task, the STA magnitudes were subject-, task- and location-dependent</li> <li>• Thigh STA &gt; Shank STA</li> <li>• Markers located close to the knee showed considerable movement (29 mm)</li> </ul>	AA and IER calculated with STA-affected data showed misleading patterns (average RMS errors > their respective total range of motion)
	Kuo et al., 2011	Sit-to-stand	10	Six markers glued on thigh, and two on shank	Magnitude thigh STA > shank STA	STA significantly underestimated flexion and internal rotation angles, and extensor moments, but overestimated joint centre translations and adduction angle
	Tsai et al., in 2011	Stair-ascent	12	Eighteen infrared retro-reflective markers were used to track the motion of pelvis, thigh, shank and foot	<ul style="list-style-type: none"> <li>• STA magnitude up to 40 mm</li> <li>• Thigh STA &gt; Shank STA</li> </ul>	Thigh STA were greater than those on the shank, leading to significantly underestimated flexion and extensor moments, but overestimated joint centre translations during the first half of the stance phase
	Barré et al., in 2013	Walking	19	Eighty markers spread on the lower limb (thigh and shank)	The rigid movement of the of skin marker cluster amplitude was approximately 80-100% of the STA, while the local displacement of the markers magnitude was ~ 35-50%	The vertical axis of the anatomical frame of the femur was influenced the most by RSTAM

- Table 2.5 -

### 2.3 Non-invasive statistical approach

The study performed by Camomilla et al., 2009, showed the possibility to characterize the STA for any marker location, subject and motor task, providing an estimate of the STA vector in the relevant bone-embedded frame. It can be applicable *in-vivo* using only stereophotogrammetry. On the surface of the segment, the largest possible number of skin markers have to be glued. Any given STA vector is observed from all the marker cluster frames, built using all the available markers. A subset of the latter cluster frames is identified as made of frames that undergo with uncorrelated local movements. The method is based on the construction of multiple local independent observers of the STA vector and on the determination of its best estimate through an ensemble coherent exercise. The STA estimation is performed averaging the vectors reconstructed using the above-mentioned independent cluster frames. For the method validation, experimental data provided by stereophotogrammetry and simultaneous 3D fluoroscopy during a step up/down movement (Stagni et al., 2005) were used. The displacement vector due to the instrumental error is negligible with respect to the STA and therefore it is not considered (Chiari et al., 2005). The STA estimations obtained with the proposed method had root mean square values in the range 2.5-23.0 mm and was consistent with those measured with the fluoroscopy. Moreover, the STA estimated and measure showed high correlation values ( $0.83 \pm 0.13$ ) and normalized root mean square distance of  $27\% \pm 16\%$ . The authors claimed the following limits: the method estimates the STA minimising, through averaging, the contribution of the displacements relative to the bone of independent observers. However, for the determination of their mutual uncorrelation, only information on cluster deformation and not on cluster rigid translation, and rotation, is available. For this reason, the performance of the method will be limited if the selected clusters present a common rigid translation dominant with respect to the deformation. The high number of clusters available and their different positions on the thigh confidently reduces this probability. Moreover, the method do not give information on the phase of the signal, it provides only an estimate of the deformation pattern and magnitude. In addition the author claimed that the proposed method could be validated with other experimental data, as during other motor tasks with higher acceleration. Such assessment could provide information on the deformation pattern in different location of the thigh and, therefore, it could allow for optimal marker placement and constitutes an indispensable prerequisite for bone pose estimator design and assessment.

In a recent study, the pelvic STA was quantified in multiple static positions (Hara et al., 2014). The multiple calibration (described in section 2.4.3) is a technique used to reduce the impact of STA on kinematic data, which involves several calibrations through the range of motion of the joint of

interest. Through this technique, the magnitude and the direction of the pelvic marker displacement was assessed in different static positions. Although many studies have investigated STA on the thigh, shank and foot (Cappozzo et al., 1996; Fuller et al., 1997; Garling et al., 2007; Maslen and Ackland, 1994; Peters et al., 2009; Reinschmidt et al., 1997c; Sangeux et al., 2006; Stagni et al., 2006, 2005), knowledge of the STA at the pelvis is particularly scarce. This study investigated how skin-mounted pelvic markers were displaced in relation to anatomical bony landmarks in multiple static positions, and the corresponding influence on the pelvic angles in healthy young adults (age:  $28.8 \pm 3.8$  years; height:  $1.71 \pm 9.0$  m; mass:  $67.2 \pm 12.3$  kg; BMI:  $22.8 \pm 2.7$ ). Joint kinematics were obtained using fourteen markers located according to requirements of the Plug-in-Gait (Vicon, UK) with a Davis hip joint and a trunk model. Markers were also glued over bilateral ASIS and PSIS in the reference standing position. For all the subjects, multiple anatomical calibration trials were acquired in six positions: maximum anterior and posterior pelvic tilt, trunk forward, hip flexed of 90 deg, maximum hip extension, and limb alignment to replicate a typical gait initial contact position. In addition, eleven subjects were tested on other three positions: pelvic obliquity, lateral flexion and hip flexed at 45 deg. In each calibration position, the pelvic AL location were manually palpated by experienced physiotherapists. When the AL differs from the surface marker position, the AL location was identified with a pointer device. Such calibration, was repeated three times for each position. The average of these trials was used to represent the data of each subject. Results showed that ASIS markers showed highest displacements than PSIS markers. Moreover, displacements particularly evident (up to 17 mm) were observed in positions where the hip was flexed. A strong correlation was found between the hip flexion angle and marker displacement. Although STA measured in this study may differ from STA that occurs during activities such as walking, the results of this study provide reference information of pelvic STA, which may lead to application in kinematic and kinetic data as a function of joint angle: results suggest that activities with large hip flexion would cause larger STA. Moreover, the inter-ASIS distance measured in supine found to be smaller than the distance measured in standing, that may place the hip joint centre more medially in the Plug-in-gait model.

#### 2.4 Soft tissue artefact minimization and compensation

A diffuse use of gait or motion analysis has been limited in the diagnosis of patient with locomotor pathology and the following planning and assessment of the treatment for its reliability, particularly for joint components which undergo small variation. Non-invasive marker set can be used for tracking motion of human body segments, typically tracked using technique used in the field of geometric morphometrics. The latter studies the statistical variation and covariation of the shapes of

marker cluster (cluster set glued on the segment). The notion of shape of used here is that of the relative positions of points corresponding to the marker-cluster model. The positions of the points can be captured with the stereophotogrammetric system. The coordinates must, of course, be recorded in a way such that they are unaffected by variation in orientation, and scale. Bookstein (1991) gives a comprehensive account of the field of geometric morphometrics. Dryden and Mardia (2002) cover many aspects of shape statistics. The fundamental advances of geometric morphometrics over traditional approaches (multivariate morphometrics) are in the development of powerful statistical methods based on models for shape variation rather than the use of standard multivariate methods on ad hoc collections of distances, angles, and ratios. The statistical analysis of shape methods can be interpreted in terms of the differences in the coordinates of the markers after the configurations of points have been optimally superimposed (usually using least-squares). These methods use the Procrustes distance (the square root of the sum of squared differences) as a metric for comparing shapes. Note that the thin-plate spline methods (Bookstein, 1989) are based on this approach. The Procrustes distance is a type of shape distance between a pair of configurations of landmark points (measured skin marker position and cluster-model in each instant of time) is usually computed by first centring the two configurations of landmarks on the origin and scaling each configuration to unit centroid size (the square root of the sum of their squared coordinates, Bookstein, 1991). One of the configurations is then rotated to align it with the other so that the square root of the sum of squared differences between corresponding coordinates, is as small as possible. This quantity is often called a “Procrustes distance”.

However, STA strongly affects AL trajectories and, consequently, the Procrustes superimpositions, and the relevant segment AFs and finally joint kinematics and kinetics. Techniques for minimizing its contribution and compensating for the relevant effects are certainly fundamental in human movement analysis. Several methods have been proposed and are described in the present section, they will be reported in chronological order.

#### 2.4.1 *The “solidification” procedure*

In 1995, Chèze et al., proposed the “solidification” to facilitate the kinematic analysis using video system data, which addresses only the deformation of the cluster during a movement. The skin markers trajectories were defined as consistent with the rigid body assumption. At least three non-collinear markers are sufficient for the bone pose determination and the first step of this procedure is to identify the subset of three markers which defines the least-perturbed triangle throughout the entire motion. An iterative procedure identify the ‘solid’ shape which best fits this time-varying triangle: the mean value for each vertex angle are measured for the triangles during the movement

and the most deformed frames are eliminated step-by-step, until 75% of the frames are retained. Then, to solve a least-squares positioning problem, the best fit of the solid to each measured triangle is determined choosing appropriate points on the triangle and by using the standard Single Value Decomposition (SVD) algorithm (Söderkvist and Wedin, 1993). Nominal trajectories of markers rigidly assembled in two clusters located on the thigh and shank segment were used for the model validation. Such trajectories were generated from experimental data acquired during the swing phase of gait and were perturbed by typical STA during gait using artificial noise. The nominal knee kinematics was compared with that obtained using the proposed method. The results obtained showed that this compensation works just as using an existing least-squares method in reducing kinematic errors: it does not yield substantial numerical improvements. Although that, it still possesses several advantages. First, the method is conceptually simple, providing a geometric interpretation of numerical approaches. Second, it provides a straightforward way to identify erroneous or highly deformable images, which could reduce the accuracy of kinematics calculation. Third, and biggest advantage, is that the solidification procedure permits the unambiguous application of the rigid body theory while the improved kinematic accuracy of a least-squares method is maintained. One disadvantage of the method claimed by the authors is that the mean shape calculation and fitting become more complex when the number of solidified markers increased beyond three.

#### *2.4.2 Multiple anatomical landmark calibration*

In the same year of the above mentioned study, Cappozzo et al., proposed a technique for a more rational determination of AFs: the CAST. A single static calibration of ALs is required to identify their local coordinates in the relevant CTF, which are accurately identified using a pointer equipped with markers in known positions. Using this technique, a constraint of rigidity between the CTF and the ALs was assumed. During an experimental study (Cappozzo et al., 1996), the AL local coordinates in the relevant CTF were observed to change consistently over the flexion cycle of the relevant joint and based on it, Cappello et al., proposed an improvement of the CAST technique, to compensate for the skin sliding associated with joint flexion during the execution of the target motor task. An interpolation between two known positions at the extremes of the range of flexion can be performed. This technique overcomes the constraint of rigidity used in the CAST method and recommends a double calibration of the ALs, at the two extremes of the expected range of joint motion. A cycling exercise described in section 2.2.2 was used, using reference data obtained from a femoral external fixator which moved rigidly with the underlying bone for the validation of the proposed method. The traditionally femur ALs used in gait analysis were calibrated during maximal

hip and knee flexion and extension. During the two calibration postures, the pose of the CTF and the positions of the ALs in the global reference frame were defined. With a SVD technique (Söderkvist and Wedin, 1993), the optimal rigid transformation of the CTF poses in the calibration postures was estimated. The obtained transformation was also applied to the global coordinates of the ALs. Therefore, two different geometrical configurations of the cluster and anatomical markers were obtained. Both were expressed in the reference frame of one of the calibration position: information on cluster shape variation and AL displacements were provided when passing from a calibration posture to another. Through linear interpolation between these two configurations, a time-varying overall model, which includes also the calibration parameters, was obtained. The time was assumed as the independent variable. The skin marker trajectories acquired during cycling were used to estimate the bone pose. The FE angles was used to register the model. Using the double calibration, the error in the reconstruction of the GT position was reduced from more than 15 mm (obtained using the CAST procedure, *i.e.*, single calibration) to less than 10 mm. While when the pose of the femur was estimated, the error for the orientation decreased from 5 deg to 4 deg, and for the position from 7 mm to 4.5 mm. The preliminary implementation of the proposed method used for cycling provided encouraging results, therefore, for other motor tasks, compensation methods based on multiple AL calibrations should be designed according to the expected range of joint rotations. The authors consider that this technique can be enhanced using more sophisticated methods to characterize skin sliding and deformation while a joint is flexing using non-linear interpolation methods or a larger number of calibration positions. However, such enhancement, should be defined by any specific application by limiting the corresponding number of necessary additional AL calibrations. However, the authors claimed that it is important to emphasise that even when four well distributed markers are selected to form the technical skin cluster, errors in bone orientation and positions components show a root mean square value of about 3 deg and 3 mm. These residual errors, due to inertia and muscular contraction and to interpolation errors, require further analysis and attention to avoid an overwhelming negative influence on the description of joint mechanics.

#### 2.4.3 *Pliant surface modeling*

Ball and Pierrynowski, in 1998, proposed the Pliant Surface Modeling (PSM) for STA compensation with a new non-rigid, 12 DOF method. This method quantified ‘pliant’ (scales and shears) motion accounting for deformation of the marker cluster associated with skin stretching, muscle activity and inertial phenomena in addition to rigid rotations and translations. In particular, deformations were described with affine deformation matrices made up of rotation, scaling,

shearing and translation. The proposed method was compared with the traditional rigid body modelling (RBM), which assumes body segment, surface rigidity and 6 DOF. Typical methods of movement analysis have only offered the ability to model the rigid characteristics of a body segment (3 rotations and 3 translations), while PSM is designed to quantify 6 additional DOF (3 scales and 3 shears). Experimental data were obtained from three volunteers with pin, equipped with circular cluster of markers, inserted in the femur and tibia and skin markers glued on the surface of the two segments as described in section 2.2.1. The volunteers walked at slow, medium and fast speed for 20 second on a treadmill. When the RMB was used to obtain the position of femur and tibia, the errors were 4.8 mm and 3.8 mm, respectively. Instead, when the new approach was used, these errors were reduced of the 45% and 56%, respectively. For the error in orientation, it was found less than 0.5 deg, which is considered a minimal error. When the bone pose was defined at different speed, no significant difference were observed between the two methods, although higher speeds caused slightly higher errors. The PSM method, of course, cannot account for rigid cluster displacement with respect to the underlying bone. Moreover, the PSM offers superior “rigid” estimates of the knee motion with the ability to quantify “pliant” surface changes.

#### 2.4.4 *Dynamic calibration*

In the same years of the above-mentioned method for the STA compensation, Lucchetti et al., suggested an analytical procedure to be included in routine movement for subject- and task- specific STA assessment and for its compensation using a dynamic model of the relationship between the CTF and the relevant ALs. Experimental data were obtained from two able-bodies male volunteers and one male patient. Four markers were fixed on a rigid plate on a Milwaukee orthosis located on the pelvis. Five skin markers were glued on the thigh and four on the shank. For the pelvis, thigh, shank and shank-thigh segments CTF were defined. The following motor tasks were then performed: 1. orthonormal posture; 2. right hip FE followed by AA, with the knee hyperextended; 3. right lower limb swing, with the knee hyperextended, as occurs during the swing phase of walking; 4. Level walking at natural cadence. The thigh-shank CTF was defined using the markers on the shank, which were supposed to be more reliable than the thigh CTF when the knee is blocked (*i.e.*, for the position 1, 2 and 3). The position of the medial and lateral epicondyle were estimated in the latter CTF. Using the postures with knee-locked leg as a reference, the displacement of these ALs in the thigh CTF and the relevant relation to hip FE, AA and IER were computed and stored in the “artefact table”. When the walking task was analyzed, approximate values of hip rotation were estimated using the traditional joint kinematics methods. For each of these rotation, the corresponding least distant values in the “artefact table” were sought. The AL final local positions

were corrected by subtracting the corresponding artefact component. The new ALs were used to define the corrected AF. From this AF, compensated knee translations and rotations were computed.

The model validation was performed on the patient with a single dof knee prosthesis. Femur and tibia pose were defined using a traditional least-squares optimal estimator. Error for knee joint translations was up to 14 mm, while error for knee rotations was 6 deg. When the proposed method was used, these errors were reduced to less than 4 mm and 3 deg. Using this method, the strong correlation between STA and hip rotations was successfully removed. The knee kinematics estimated through two different thigh clusters on a normal subject were compared as a further validation. When no compensation was applied, the knee rotations that undergo moderate variations during walking (AA and IER) showed significantly different patterns for the two clusters. Through compensation, errors diminish to magnitudes which may allow extraction of information even from those joint movement components which undergo small variations and which have always been concealed by overwhelming inaccuracies. Even better results may be expected if the procedure is extended to both segments adjacent to the target joint. While, when the compensation method was applied, the two estimates were much more similar. For this reason, the dynamic calibration significantly contributed to the compensation of STA. In order to achieve the presented results, the subject performed an ad hoc movement that, to some extent, makes the entire experimental and data reduction procedure more cumbersome. However, it appears that benefits are greater than costs.

#### 2.4.5 Point cluster technique

In 1998, a new method for obtaining limb segment motion from markers located on the skin was proposed by Andriacchi et al. The method is based on a cluster of markers uniformly distributed on the limb segment. Each marker has an assigned arbitrary mass. The center of mass and the inertia tensor of the cluster are calculated. The eigenvalues and eigenvectors of the inertia tensor are the principal moments of inertia and the principal axes of the 'point cluster'. The eigenvalues of the inertia tensor do not change if the segment is a rigid body. In order to minimize the changes of the eigenvalues, the mass of each marker is adjustable at each frame: the cluster has a time-invariant distribution matrix like that for rigid bodies. The eigenvectors establish a transformation between the segment and the global coordinate system. For the model validation, a simulation model where systematic and random errors were introduced into a fixed cluster of points was used. The simulation demonstrated, that using the proposed method, the error due to the non-rigid body movement could be substantially reduced. In addition, the model was also tested in a group of ten subjects with intracortical pins placed into the femur and tibia, which allowed to evaluate its applicability to *in-vivo* testing. The results obtained in the *in-vivo* comparison to previous studies

where intracortical pins were placed also demonstrated the point cluster technique produces a reasonable approximation to *in-vivo* knee joint movement. However, the author claimed that there are some practical limitation of this method. Having an overabundance of markers on each segment, it can lead to difficulties in tracking and labelling all of them. In addition, care must be taken in the marker placement to avoid that the marker are not located in a symmetric manner: actually, in case of symmetric distribution of markers, the calculation of the principal axes can be indeterminate.

Using a set of activity-dependent deformation models, a new technique to reduce the STA errors in the optoelectronic measurement of *in vivo* skeletal motion is proposed by Alexander and Andriacchi, 2001: interval deformation technique. This technique was built on the above-mentioned one and it consists in minimizing the segment deformation with a new optimization criterion based on functional forms of trajectories of the markers in the bone-embedded frame. Fifty simulated trials for an eight-marker cluster set, and experimental data from a patient wearing an Ilizarov external fixation device on the shank, were used for the model validation. The method employs an interval deformation technique which can substantially reduce the amount of error associated with skin marker motion. This technique reduced the errors in limb (shank) segment pose estimate by 33% and 25% compared to the least-square approach used to define position and orientation, respectively. This newly developed method has demonstrated that by accounting for the changing shape of the limb segment, a substantial improvement in the estimates of *in-vivo* skeletal movement can be achieved. These techniques cannot cope with the rigid displacement of the array with respect to the underlying bone, and are also limited by the critical knowledge of the skin deformation models. It has also been suggested (Tashman and Anderst, 2002) that these techniques should be applied with caution for motion studies involving rapid movement and substantial impact.

#### 2.4.6 Global optimization

Traditional methods treat each body segment separately without imposing joint constraints, resulting in apparent dislocation of the joints predominantly caused by the relative movement between the skin markers and the underlying bone.

Lu and O'Connor, 1999, proposed an optimization method for the determination of the positions and orientations of multi-link musculoskeletal models from marker coordinates. The model imposes joint constraints. The hypothesis was that, with joint constraints and a global error compensation scheme, the effects of measurement errors on the reconstruction of the musculoskeletal system and subsequent mechanical analyses can be reduced globally. This method is called Global optimization (GO). The proposed method can significantly reduce the effects of STA on segment pose

estimation, particularly on the critical joint IER and AA. The optimization method is based on the minimization of the weighted sum of squared distances between measured and model-determined marker positions. The model arranged with to a  $n$ -link chain model is customized to individual subjects by using subject specific parameters based on measurements on subject in a standing position (subject calibration). The position of the skin markers in the standing position are taken as reference. Joint constraints were taken as all perfect ball-and-sockets. A weighting matrix accounted for different segmental residual errors but assumed that all markers of a segment are equally affected by STA. A different weighting factor reflecting its average degree of STA was given to each segment. For the model validation, 20 simulated gait trials were used. Artificial noise was added into each marker nominal trajectories as in Chèze et al., 1995. The positions of joint angles and joint centre were evaluated. The average amount of hip and knee joint dislocations were 3.88 cm and 3.24 cm, respectively, when the non-optimized technique based on simple definition of vectors by direct linking of external markers was used. Using standard optimization techniques, which estimate the segment pose in terms of its transformation matrix by minimising marker array deformation from its reference shape in a least-squares sense, these displacements were 1.33 cm and 0.69 cm. When the global optimization was used, no joint dislocations were observed, as prescribed by the priori model. Errors in joint rotations were significantly reduced when the proposed method was used with respect to the traditional one. Moreover, the inclusion of the weighting matrix in the optimization provides a more effective STA compensation: the selection of different weighting factors according to the expected magnitude of STA at different body segments enables better estimation of relevant poses by stronger consideration of the more reliable of these segments.

In 2010, Andersen et al., constrained the knee joint as Lu and O'Connor, 1999, using the *in-vivo* gait data described by Benoit et al., 2006; which includes simultaneously recorded skin and bone-mounted pin markers for the thigh and shank for six healthy male subjects measured during gait. The purpose this study was to evaluate the effects of including idealized knee joint constraints on skin marker-based motions of the femur and the tibia during gait in order to determine if these constraints improve the validity of the skin marker data. To determine if constrains could improve skin marker-derived kinematics, four different analyses were used to reconstruct the motion of the femur and tibia: 1) Pin marker data were used to obtained reference knee motion; 2) Skin marker data with no knee joint constraints were used to obtain the bone motions that should be improved upon by the inclusion of joint constraints; 3) Skin marker data with spherical knee joint constraints and optimised joint centre; 4) Skin marker data with a revolute knee joint constraint and optimised joint centre and joint axes of rotation. Results showed that in the majority of subjects, constraining

the knee joint using both type of constraints resulted in larger errors than when no joint constraints were included, contrary to what was expected. Therefore, the results obtained in this study indicated that no overall improvement in the validity of skin marker-derived kinematics is achieved by including optimised idealized joint constraints for the knee: such knee joint constraints did not eliminate or reduce the effects of STA. This indicates that a rigid-body assumption for the skin markers and an idealized joint constraint for the knee is not an ideal approach to reduce STA and improve measurement validity: more advanced knee joint and STA models must be developed in order to reduce the errors associated with skin marker-based kinematic measurements of tibio-femoral motion.

Duprey et al., in 2010, developed a GO method that allows to easily implement different sets of joint constraints in order to assess their influence on the lower limb kinematics during gait. The segment definition was based on generalized coordinates giving only linear or quadratic joint constraints. Seven sets of joint constraints were assessed, corresponding to different kinematic models at the ankle, knee and hip: SSS, USS, PSS, SHS, SPS, UHS and PPS (where S, U and H stand for spherical, universal and hinge joints and P for parallel mechanism). GO was applied to gait data from five healthy males (age:  $28.8 \pm 4.8$  years; height:  $1.74 \pm 0.09$  m; mass:  $76.5 \pm 13.5$  kg). Results showed that the lower limb kinematics, except hip kinematics, knee and ankle FE, significantly depend on the chosen ankle and knee constraints. The knee parallel mechanism generated some typical knee rotation patterns previously observed in lower limb kinematic studies. Furthermore, only the parallel mechanisms produced joint displacements. Thus, GO using parallel mechanism seems promising. It also offers some perspectives of subject-specific joint constraints consideration.

The following tables (Tables 2.6-2.8) synthetize the main features and conclusions of the studies aimed at the STA minimization and compensation for the different methods described.

<b>Study</b>	<b>Method</b>	<b>Description</b>	<b>Validation of the method</b>	<b>Impact of STA on bone pose or joint kinematics</b>
Chèze et al., 1995	<i>Solidification procedure</i>	Identify the subset of three markers which defines the least-perturbed triangle throughout the entire motion. An iterative procedure identify the ‘solid’ shape which best fits this time-varying triangle: the mean value for each vertex angle are measured for the triangles during the movement and the most deformed frames are eliminated step-by-step, until 75% of the frames are retained.	Simulated data: Nominal trajectories of markers rigidly moved in two cluster (thigh and shank) during the swing phase of gait and perturbed by STA using artificial noise	The results showed that this compensation works just as using an existing least-squares method in reducing kinematic errors: not substantial numerical improvements obtained.
Cappello et al., 1997	<i>Multiple anatomical landmark calibration</i>	A double calibration of the anatomical landmarks, at the two extremes of the expected range of joint motion, has to be performed.	A cycling exercise was used, using reference data obtained from a femoral external fixator	Error in the reconstruction of the GT position was reduced from more than 15 mm (obtained a single calibration, CAST) to less than 10 mm. Error for the femur orientation decreased from 5 deg to 4 deg, and for the position from 7 mm to 4.5 mm.
Ball and Pierrynowski, 1998	<i>Pliant surface modeling</i>	The ‘pliant’ (scales and shears) motion is quantified accounting for deformation of the marker cluster associated with skin stretching, muscle activity and inertial phenomena in addition to rigid rotations and translations.	Walking trials of three volunteers with both pin inserted in the femur and tibia and skin markers glued on the segments.	Errors, with respect to rigid body modelling, reduced of the 45% and 56% for the definition of the position of femur and tibia, respectively.
Lucchetti et al., 1998	<i>Dynamic calibration</i>	Using the postures with knee-locked leg as a reference, the displacement of thigh ALs in the thigh cluster technical frame and the relevant relation to hip FE, AA and IER were computed and stored in the “artefact table”. First approximate hip rotations were estimated using the traditional joint kinematics methods. For each of these rotations, the corresponding least distant values in the “artefact table” were sought. The AL final local positions were corrected by subtracting the corresponding artefact component. The new ALs were used to define the corrected AF. From this AF, compensated knee translations and rotations were computed.	Performed on the patient with a single dof knee prosthesis, which performed different tasks.	Error for knee joint translations decreased from 14 mm to less than 4 mm, while error for knee rotations decreased from 6 deg to 3 deg. This procedure allows extraction of information even from those joint movement components which undergo small variations.

- Table 2.6 -

<i>Study</i>	<i>Method</i>	<i>Description</i>	<i>Validation of the method</i>	<i>Impact of STA on bone pose or joint kinematics</i>
Andriacchi et al., 1998	<i>Point cluster technique</i>	It's based on a cluster of markers uniformly distributed on the segment. Each marker has an assigned arbitrary mass. The eigenvalues and eigenvectors of the inertia tensor are the principal moments of inertia and the principal axes of the 'point cluster'. In order to minimize the changes of the eigenvalues (rigid body assumption), the mass of each marker is adjustable at each frame: the cluster has a time-invariant distribution matrix like that for rigid bodies. The eigenvectors establish a transformation between the segment and the global coordinate system.	Simulation data: systematic and random errors introduced into a fixed cluster of points  10 subjects with intracortical pins	Error due to the non-rigid body movement could be substantially reduced  Technique produces a reasonable approximation to in-vivo knee joint movement. Limitation: overabundance of markers on each segment, (difficulties in tracking and labelling); care must be taken in the marker placement to avoid that the marker are not located in a symmetric manner
Alexander and Andriacchi, 2001	<i>Interval deformation technique</i> (based on <i>PCT</i> )	Segment deformation is minimized with a new optimization criterion based on functional forms of trajectories of the markers in the bone-embedded frame.	Fifty simulated trials for an eight-marker cluster set  A patient wearing an Ilizarov external fixation device on the shank	After processing by the interval deformation algorithm the average centre of mass error was reduced to 29% and the average orientation error was reduced to 19% of the rigid-body model error  This technique reduced the errors in shank segment pose estimate by 33% and 25% compared to the least-square approach used to define position and orientation, respectively.

- Table 2.7 -

<b>Study</b>	<b>Method</b>	<b>Description</b>	<b>Validation of the method</b>	<b>Impact of STA on bone pose or joint kinematics</b>
Lu and O'Connor, 1999	<i>Global optimization</i>	Optimization method for the determination of the positions and orientations of multi-link musculoskeletal models from marker coordinates. The model imposes joint constraints (perfect ball-and-sockets). The weighted sum of squared distances between measured and model-determined marker positions is minimized. A n-link chain model is customized to individual subjects by using subject specific parameters based on measurements on subject (subject calibration). The position of the skin markers in the standing position are taken as reference.	Twenty simulated gait trials were used. Artificial noise was added into each marker nominal trajectories as in Chèze et al., 1995.	The average amount of hip and knee joint dislocations were reduced from 3.88 cm to 1.33 cm and from 3.24 cm to 0.69, respectively.
Andersen et al., 2010	<i>Global optimization</i>	Evaluate the effects of including idealized knee joint constraints on skin marker-based motions of the femur and the tibia during gait in order to determine if these constraints improve the validity of the skin marker data.	<i>In-vivo</i> gait data described by which includes simultaneously recorded skin and pin markers for the thigh and shank of six subjects (Benoit et al., 2006)	No overall improvement in the validity of skin marker-derived kinematics is achieved by including optimised idealized joint constraints for the knee.
Duprey et al., 2010	<i>Global optimization</i>	Method to easily implement different sets of joint constraints in order to assess their influence on the lower limb kinematics during gait. Different sets of constraints were assessed.	Applied to gait data from 5 subjects	Lower limb kinematics, except hip kinematics, knee and ankle FE, significantly depend on the chosen ankle and knee constraints. The knee parallel mechanism generated some typical knee rotation patterns previously observed in lower limb kinematic studies.

- Table 2.8 -

## 2.5 Conclusions

It has been recognized that STA is the most significant source of error in human movement analysis (Andriacchi and Alexander, 2000). Any future investigation aimed at reliably estimating *in-vivo* human joint motion on a six-DOF-base certainly requires sophisticated techniques to compensate for STA. The inaccuracies resulting from this source of error are definitely critical not only in joint mechanics investigations and in virtual reality applications, but also in routine clinical movement analysis. The interpretation of relevant results and the associated clinical decision-making process should therefore include awareness of this critical phenomenon and its effects.

The studies reported in the section 2.2 provide a large quantity of data for describing the amount and the effects of STA at the lower limbs. The different results obtained by different authors may be justified by the different techniques used, by the different locations of the skin-mounted markers, by the large variability in the subjects analysed and, mainly by in the tasks performed.

Despite that, the following general conclusions can be drawn:

- I. errors introduced by the STA are much larger than stereophotogrammetric errors;
- II. the pattern of the artefact is task dependent;
- III. STA is reproducible within, but not among, subjects;
- IV. STA introduces systematic as well as random errors;
- V. STA associated with the thigh is larger than any other lower limb segment;
- VI. Very few data are available on the pelvis, which could also be a perturbed segment.

The knee was the joint most studied in the reported works and the literature suggest that skin marker trajectories can be used to determine only reliably joint FE, while for the other two knee DOF (AA and IER), STA causes error with the same magnitude of the signal that we would like to measure.

Intracortical pins, external fixators and percutaneous trackers used to directly measure STA suffered of the same limitation: STA measurements are altered in case of the presence of external devices, in particular limiting the skin sliding. Several complications can be verified using bone anchored pins, and the likely critical deformation of these has been pointed out by looking at data collected in tests simulating *in-vivo* experiments of direct skeletal motion (Ramsey et al., 2003). In addition, the use of intracortical and percutaneous pins on normal volunteers should be limited also for ethical reasons: the invasive procedure for the pin insertion is complex, the need of a local anaesthesia and a surgery. Besides ethically-related concerns, this approach is limited by the fact imaging

techniques are less invasive, and may be exploited further in the future to simultaneously track both external markers and internal bony landmarks.

The techniques based on fluoroscopy are minimally invasive, providing a complete 3D measurement of the STA, and enable analyses of a larger number of skin markers, although this is limited to a single joint at a time and extensive image data processing is necessary.

Two studies were performed to assess STA on a body segment using a non-invasive statistical approach: Camomilla et al. (2009) and Hara et al. (2014). The first mentioned study quantified the thigh STA using “multiple local independent observers” and it gave results reasonably comparable to those obtained with the fluoroscopic method (Stagni et al., 2005) which analyses the same unrestricted movements based on a completely different approach. In the study performed by Hara et al. (2014), pelvic STA is quantified pelvic STA using a multiple static calibration. Using this method, STA due to dynamic muscle contraction, inertial effects, or wobbling of markers was not quantified. However, both these non-invasive methods do not show a large diffusion in the biomechanics community for the complexity of the calibration procedure or for the lack of a provided definite proof of the validity of the method and a generalization of the results to a population and to motor tasks with higher accelerations.

To solve the STA issue, several other studies attempted to compensate the STA by using different methods as described in section 2.4. Although all these methods reduced more or less the effect of the STA on the estimated tibio-femoral joint kinematics, they did not obtained a satisfying STA compensation. Two general approaches seem to represent well what has been proposed in the literature for STA minimization and compensation in bone pose estimation. These techniques can be distinguished between those modelling the external segment surface (Chèze et al. 1995; Ball and Pierrynowski, 1998; Lucchetti et al., 1998; Andriacchi et al., 1998; Alexander and Andriacchi, 2001) and those addressing also segment relative motion (Cappello et al., 1997; Lucchetti et al., 1998; Lu and O’Connor, 1999). The former, enhancing the traditional methods of segment pose optimal estimation (Söderkvist and Wedin, 1993; Spoor and Veldpaus, 1980) by explicitly addressing the random and systematic effects of STA, consider absolute and relative motion of the skin markers in a purely geometric view, irrespective of the physiological event generating the STA and irrespective of joint motion and constraints. The latter include in the analysis considerations about physiological joint motion, though very simple, for a more reliable final association between CTF and AF. However, two techniques of this latter category (Cappello et al., 1997; Lucchetti et al., 1998) required the performance of an additional task necessary for subject-specific STA calibration.

These two categories have both advantages and disadvantages, and should be chosen according to the specific application. It is the recommendation of the authors here that no *a priori* selection should be pursued among these different techniques, unless a general validation process is carried out based on a single set of consistent and realistic data.

It should also be concluded that the overall reliability obtained by addressing explicitly STA effects exceeds that obtained using traditional filtering and smoothing algorithms on position data and other optimization techniques as reported in Chapter 2.4.6. One of the studies mentioned here (Lucchetti et al., 1998) is exemplary in this respect, reporting the root mean square of the estimates of five DOFs at the knee joint, known to be zero. These values presented in Lucchetti et al. (1998), which represent errors for the corresponding DOFs, were found to decrease very differently when non-optimal, optimal and STA compensation techniques were applied: in AA these were 5.5, 2.4 and 2.5 degrees respectively, in IER 5.5, 4.1 and 2.4 degrees, in antero-posterior displacement 12.5, 11.9 and 3.6 mm, in vertical displacement 7.0, 6.7 and 4.5 mm, in medio-lateral displacement 13.5, 13.0 and 2.9 mm.

GO with joint constraints is one of the methods developed for minimizing STA. Its reliability is under controversy (Stagni et al., 2009; Andersen et al., 2010). Nevertheless, defining a kinematic model is becoming usual in gait analysis (e.g., inverse–forward dynamics, musculoskeletal models, etc.) and the constraint choice is essential. In Duprey et al., (2010) the knee parallel mechanism generated some typical knee rotation patterns previously observed in lower limb kinematic studies, producing also joint displacements. For this reason, it seems the most promising type of constraint.

Despite the numerous solutions proposed, the objective of a reliable estimation of bone pose in *in-vivo* experiments of human movement has not yet been achieved satisfactorily. Theoretically, for an effective compensation of the STA, either *ad-hoc* exercises must be carried out in order to collect relevant subject-specific information, or a systematic general characterization of the artefact must be available. It would be desirable to identify structural models of the STA and to devise experiments that would allow for their calibration, *i.e.* model parameter determination, to be applicable to the specific subject and motor act under analysis.

### 3. Chapter 3

The content of this chapter is referred to the article

#### **“A SOFT TISSUE ARTEFACT MODEL DRIVEN BY PROXIMAL AND DISTAL JOINT KINEMATICS”**

Published in Journal of Biomechanics, 2014, 47 (10), 2354–2361.

Additional information are also presented.

#### Symbols and nomenclature

	$c$	axes component (x, y, z)
	$j$	frames ( $j = 1, \dots, n$ )
	$h_c^\alpha, h_c^\beta, h_c^\gamma, h_c^\delta, h_c^0$	model parameters
	$a_c$	measured STA $c$ component
	$\tilde{a}_c$	estimated STA $c$ component
	$rmsm_c$	root mean square value over time of a measured artefact $c$ component
	$rmsr_c$	root mean square value over time of the difference (residual) between the measured and estimated artefact $c$ component as resulting from the calibration procedure
Symbols	$r_c$	coefficient of correlation between the measured and estimated artefact $c$ component as resulting from the calibration procedure
	$rmse_c$	root mean square value over time of the difference (error) between the measured and estimated artefact $c$ component when the test movement is different from the calibration movement
	$r_{ec}$	correlation coefficient between the measured and estimated artefact $c$ component when the test movement is different from the calibration movement
	%	indicates normalization with respect to $rmsm_c$
	$\Delta_a$	the percentage ratio between the peak to peak values of the two joint kinematics time series
	$r_a$	correlation coefficient between two joint kinematics time series
Joint angles	$\alpha_j$	hip flexion/extension time histories
	$\beta_j$	hip abduction/adduction time histories
	$\gamma_j$	hip internal/external rotation time histories
	$\delta_j$	knee flexion/extension time histories

Nomenclature	STA	soft tissue artefact
	$SSR_c$	sum of the squared residuals
	IQR	inter-quartile range
	$FE_{HK}$	hip and knee flexion-extension
	$FE_H$	hip flexion
	$FE_K$	knee flexion
	$Cir_H$	hip circumduction
	RN	running trial, stance phase

### 3.1 Introduction

When analysing human skeletal movement using non-invasive techniques, the movement of skin points is tracked and not that of the underlying bone. The measurement of skin movement thus obtained can be considered as the sum of the global bone movement plus the local movement of the skin relative to the bone. Since only the former movement is the objective of analysis, the latter is regarded as an artefact (soft tissue artefact: STA). Although during the last decade human movement analysts have reiterated that this artefact is the greatest obstacle to an accurate reconstruction of the skeleton in motion (Leardini et al., 2005; Peters et al., 2010), no effective solution to this problem has yet been found.

When using stereophotogrammetry and skin-markers, because of the STAs, an algorithm for the optimal estimation of bone pose or of a joint centre or axis of rotation is required (skeletal kinematics estimator). This estimator should embed a mathematical model of the artefact. Ample literature on this topic shows that each STA is unique to its specific marker, the specific body segment area of a specific subject executing a specific motor act (Akbarshahi et al., 2010; Leardini et al., 2005; Peters et al., 2010). These circumstances make the *a priori* determination of STAs difficult, although attempts along these lines have been made. Studies have been published that used discrete STA models consisting of tables associating the STA value with that of the joint angle at which it occurred, and determined through *ad hoc* non-invasive experiments (Cappello et al., 1997; Lucchetti et al., 1998). As a potentially more effective alternative, having defined the architecture of an STA analytical model, relevant parameters may be estimated while solving the optimization problem inherent in the skeletal kinematics estimator applied to a specific motor task. To our knowledge, the only study using this approach is that of Alexander and Andriacchi (2001). These authors modelled STAs using parameterized analytical time functions, albeit chosen in a rather arbitrary fashion. None of these methods were well received by the human movement community of analysts, either because cumbersome to implement or because they did not furnish the required improvement.

Another area that requires STA mathematical models is simulation aimed at the comparative assessment of skeletal kinematics estimators (Camomilla et al., 2009; Camomilla et al., 2013; Cereatti et al., 2006). In this case, calibrated models able to provide realistic STA time histories, as generated during any selected motor task, are needed.

The present study aims to devise and assess a mathematical model to co-adjuvate the reconstruction of subject- and marker-specific STA time histories during a given motor task. As mentioned previously, an STA model that could be applied across marker locations or subjects is highly improbable (Akbarshahi et al., 2010; Leardini et al., 2005; Peters et al., 2010) and was hence not explored in this study, which dealt only with the paradigmatic case of artefacts that affect markers located on the thigh.

Based on experimental observations of the STA during functional activity reported in previous studies (Akbarshahi et al., 2010; Cappozzo et al., 1996) and on results obtained by modelling the STA engendered during an open-chain hip movement with stationary knee (Camomilla et al., 2013), we hypothesized that, during a two joint movement, as occurring during locomotion, the STA affecting a given marker located on the thigh of a given non-obese subject, mostly depends on the angles of both the hip and the knee, and that this relationship is linear.

The study addressed the following questions:

- **Architecture feasibility:** can the hypothesised linear model be calibrated with acceptable residuals? The residuals are deemed acceptable under specific circumstances which depend on the added value brought by the model to the selected application when compared to the relevant state of the art.
- **Generalizability:** when and with what limitations can a model calibrated using a given movement be utilized to estimate the STA generated during any other movement of interest? The answer assumes importance when the model is used to generate realistic artefact time histories as required in the above-mentioned simulation exercises.

In general, an STA is caused by: 1) skin sliding associated with joint movement, 2) soft tissue volumetric deformation due to muscular contraction and gravity, 3) inertial effects on soft tissue masses (wobbling). The STA model proposed in this study accounts only for the first cause. We thus assessed the relative weight of the above STA causes and their impact on our model estimates, which allowed us to test whether the proposed model architecture would apply *in-vivo*. To this end,

we used data from experiments carried out both *ex-vivo*, embedding only the STA elicited by skin sliding, and *in-vivo*, embedding STAs elicited by all possible causes.

## 3.2 Methods

### 3.2.1 Model architecture and calibration

Our model applies to a selected subject and skin-marker. The inputs of the model are the joint kinematics time histories of the body segment proximal and distal joints, and the outputs are the time histories of the selected marker artefact represented in the underlying bone anatomical reference frame:

$$\tilde{a}_{cj} = h_c^\alpha \alpha_j + h_c^\beta \beta_j + h_c^\gamma \gamma_j + h_c^\delta \delta_j + h_c^0; \quad j = 1, \dots, n \quad (\text{Eq. 3.1})$$

where  $c = x, y, z$  are the axes of the anatomical frame;  $(\alpha_j, \beta_j, \gamma_j)$  are the hip joint angles time histories (flexion/extension, abduction/adduction, and internal/external rotation, respectively), and  $\delta_j$  is the flexion/extension time history of the knee;  $h_c^\alpha, h_c^\beta, h_c^\gamma, h_c^\delta, h_c^0$  are the fifteen model parameters to be determined through a calibration procedure. The parameters  $h_c^0$  are determined so that the STA vector has a zero value when the subject assumes a reference posture.

Calibration of the model entails the simultaneous knowledge of the time histories of hip and knee angles as specified above, and of the STA measured during a selected calibration movement. For each marker and coordinate  $c$ , the model parameters are determined by minimizing a cost function based on the sum of the squared residuals ( $SSR_c$ ) between measured ( $a_c$ ) and estimated ( $\tilde{a}_c$ ) STA:

$$SSR_c = \begin{cases} \frac{1}{n} \sum_{j=1}^n [a_{cj} - \tilde{a}_{cj}(\alpha_j, \beta_j, \gamma_j, \delta_j)]^2 & r_c > 0 \\ \infty & r_c < 0 \end{cases} \quad (\text{Eq. 3.2})$$

where the Pearson's correlation coefficient between  $a_c$  and  $\tilde{a}_c$  ( $r_c$ ) acts as a penalty factor to exclude solutions that result in STA components in an opposite direction to that of the real artefact.

This calibration problem is non-linear and its solution was obtained using a Matlab® least-squares minimization method (trust-region-reflective).

Model validation was carried out in two steps using both *ex-vivo* and *in-vivo* experimental datasets with two objectives: 1) assessment of model architecture feasibility, and 2) assessment of model generalizability.

### 3.2.2 *Experimental data*

#### *Ex-vivo dataset*

Experimental data from three intact fresh non-obese adult cadavers (S1, S2, S3; stature and largest thigh diameter (Fig. 3.1a): 1.62 m, 0.16 m; 1.48 m, 0.13 m; 1.55 m, 0.19 m, respectively) were used (details may be found in Cereatti et al., 2009). Intracortical bone pins (6 mm diameter) equipped with four-marker clusters were implanted into the right tibia, femur and hip-bone. In addition, twelve skin-markers were glued on the thigh in three rows, medial, frontal, and lateral (Fig. 3.1a). The instantaneous marker positions were reconstructed in a global frame using a 9-camera stereophotogrammetric system (VICON MX - 120 frames/s). The anatomical landmark calibration for the pelvic-bone, femur, and tibia was carried out using the pointer technique (Cappozzo et al., 1995) (Fig. 3.1a). The hip joint centre was determined using a functional approach and pin markers, as described in Cereatti et al. (2009). The relevant anatomical frames were defined using the convention proposed in Cappozzo et al. (1995).

An operator moved the right lower limb in four different patterns, during which the position of both pin and skin markers were monitored. One movement pattern was characterized by a wide flexion-extension cycle of both the hip and knee, associated with relatively small abduction-adduction and internal-external rotations of the former joint ( $FE_{HK}$ ), approximately as would occur during a locomotor act. The second and third movement patterns were a hip flexion ( $FE_H$ ) with the knee virtually stationary, and a knee flexion ( $FE_K$ ) with a virtually stationary hip. The fourth movement pattern was a hip circumduction associated with virtually no knee movement ( $Cir_H$ ). For each specimen, three trials for each movement pattern were carried out.

#### *In-vivo dataset*

The data obtained in the experiments described in Reinschmidt et al. (1997) were used. Pins were inserted into the postero-lateral aspect of the right calcaneus, lateral tibial condyle and lateral femoral condyle of three non-obese male volunteers (V1, V2, V3; age  $27.7 \pm 2.1$ yr, mass  $85.5 \pm 9.6$  kg, stature  $1.88 \pm 0.10$  m). Each pin carried three markers. Five skin-markers were positioned on the thigh (Fig. 3.1b). Markers were tracked using a three video-camera system (sampling frequency: 200 frames/s). For each volunteer, one static trial and five running trials (RN; only stance phase) were captured. During the static trial, volunteers were asked to assume an upright posture where the pelvic-bone and lower limb anatomical frames were assumed to be parallel to the global frame, and the rigid transformations between the former frames and the marker cluster frames were determined

(anatomical calibration). Since no pin-markers on the pelvic-bones were available, the orientation of the pelvis anatomical frame could not be tracked and was thus assumed constant during movement.

### 3.1.1 STAs and reconstructing hip and knee joint kinematics

For both *ex-vivo* and *in-vivo* datasets, the pose of each pin-marker cluster local frame was estimated using the singular value decomposition approach (Grimpampi et al., 2014; Söderkvist et al., 1993). Using anatomical calibration parameters, a rigid transformation of the latter frames into the relevant anatomical frames was carried out (Fig. 3.1).

Hip and knee joint angles were estimated using the relevant anatomical frames and the Cardan convention (Grood and Suntay, 1983). As mentioned previously, pelvic rotations were not available for the *in-vivo* data, thus the hip joint kinematics was represented as the orientation of the thigh anatomical frame with respect to a translating pelvic anatomical frame. Considering pelvic rotations in the global frame during running within a range of 10 deg (Novacheck, 1998; Schache et al., 2002), the latter figure may be considered to be the error engendered by the above-mentioned limitation.

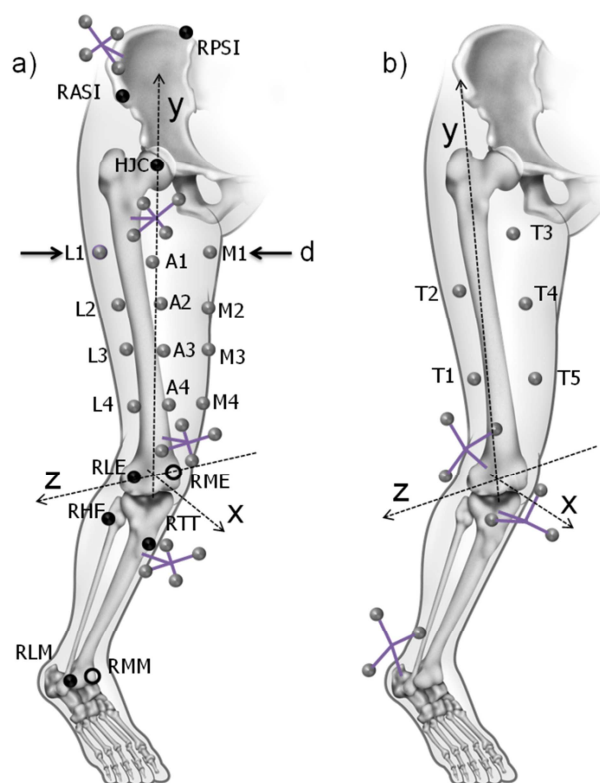


**Figure 3.1** - *Ex-vivo* (a) and *in-vivo* (b) experimental set-ups. The pin-marker clusters, the skin-markers and the calibrated anatomical landmarks (black dots) are indicated. The specimens' maximum thigh diameter (d in Fig. a) and the thigh anatomical frames are also indicated.

The position vector of each skin-marker was represented in a frame with the same orientation as the femoral anatomical frame, and the origin of which was the position of the marker during upright posture. The time series of the components of these position vectors represented the measured STA ( $a_c$ ). The root mean square value over time of the measured artefact components ( $\text{rmsm}_c$ ) was calculated for each trial.

### 3.1.2 Model calibration and model feasibility assessment

The model was calibrated using the data provided by each of the three  $\text{FE}_{\text{HK}}$ ,  $\text{FE}_{\text{H}}$ ,  $\text{FE}_{\text{K}}$ , and  $\text{Cir}_{\text{H}}$  trials for each specimen, and by each of the five RN trials for each volunteer.

In order to assess the feasibility of the model architecture, the similarity between the estimated and the measured STA time histories was determined. This was done using the root of the  $\text{SSR}_c$  ( $\text{rmsr}_c$ ), expressed as a percentage of the  $\text{rmsm}_c$  ( $\text{rmsr}_c\%$ ) and Pearson's correlation coefficient ( $r_c$ ) at the end of the calibration process.

In order to ascertain the impact of the artefact caused by soft tissue mass wobbling and taking into account the typical oscillating nature of this STA component, the time histories of the measured and estimated *in-vivo* STAs, resulting from the calibration procedure, were represented in the frequency domain. After removing the mean value and having zero padded the data series to 512 samples, the relevant power spectrum density functions, the total mean power and the mean powers in the frequency bands 0-5 and 5-10 Hz were estimated by applying a fast Fourier transform to the relevant autocorrelation function. It should be emphasised that, since data collected were positional, it was unlikely for any significant frequencies to be detected beyond 10Hz.

### 3.1.3 Generalizability of the STA estimate

In order to assess the generalizability of a given subject- and marker-specific calibrated model, the STAs generated by movements (test trials) that differed from the calibration movement (calibration trials) were estimated. This assessment could only be done using the *ex-vivo* data. The joint kinematics observed during the *in-vivo* running experiments showed considerable similarities and were hence unsuitable to test model generalizability.

Two trials, one  $\text{FE}_{\text{HK}}$  trial and one  $\text{Cir}_{\text{H}}$  trial, were selected as calibration trials because they involved most of the available degrees of freedom and/or wide movements both at hip and knee and thus were able to accommodate a large variety of motor tasks. Amongst the trials of each group, we chose the trial displaying rotation ranges closest to relevant median values. For each specimen and

marker, both calibrated models were used to estimate the STA generated during the remaining  $FE_{HK}$  and  $Cir_H$  test trials and during the three  $FE_H$  and  $FE_K$  trials.

The similarity between the above-mentioned estimated and measured STA component time histories was assessed using the rms value of their difference expressed as percent of the  $rms_m$  (root mean square error:  $rmse_c\%$ ), and the associated correlation coefficient ( $r_{cc}$ ).

In order to provide quantitative information on the difference between the calibration joint kinematics and test trial joint kinematics, the percentage ratio between the peak to peak values of the two joint kinematics time series ( $\Delta_a$ ) and the relevant correlation coefficient ( $r_a$ ) were calculated for each joint angle.

#### 3.1.4 Statistical analysis

Descriptive statistics of the eligible quantities were obtained using the five-number summary technique (minimum, lower quartile, median, upper quartile, and maximum). Lower and upper quartiles were used to calculate the inter-quartile range (IQR).

### 3.2 Results

#### 3.2.1 Range of joint movement

The overall characteristics of the movements analysed in both the specimens and the volunteers are provided in Table 3.1. Table 3.2, which deals with *ex-vivo* experiments only, displays the ranges of parameters used to quantify the difference between the joint rotations occurring during the two selected calibration trials, and those occurring during the test trials. This data reveals differences in angle time histories during test trials with not only the expected differences in both amplitude and shape compared to calibration trials of a different pattern, but also exhibiting remarkable differences within each pattern. This information is fundamental when assessing model parameter generalizability.

Angle [deg]	$FE_{HK}$	$FE_H$	$FE_K$	$Cir_H$	RN
$\alpha$	54.1 (20.5)	45.3 (9.4)	6.2 (3.0)	45.5(10.6)	47.4 (8.0)
$\beta$	7.6 (1.8)	3.7 (4.2)	2.8 (1.4)	28.1 (9.5)	8.4 (0.5)
$\gamma$	15.3 (7.1)	9.0 (3.3)	2.4 (5.3)	14.3 (8.6)	6.4 (1.9)
$\delta$	101.8 (34.5)	2.4 (5.0)	28.3 (20.8)	2.5 (4.7)	30.6 (14.7)

**Table 3.1** - Median and IQR (in brackets) values of the hip and knee angle ranges for the different movement patterns analysed. Descriptive statistics was performed over all trials and specimens/volunteers.

### 3.1.1 *Amplitude of the soft tissue artefacts*

The statistics of the STA components measured during the trials of the four movement patterns of specimens and the running trials of volunteers are shown in Figs. 3.2 and 3.3 respectively.

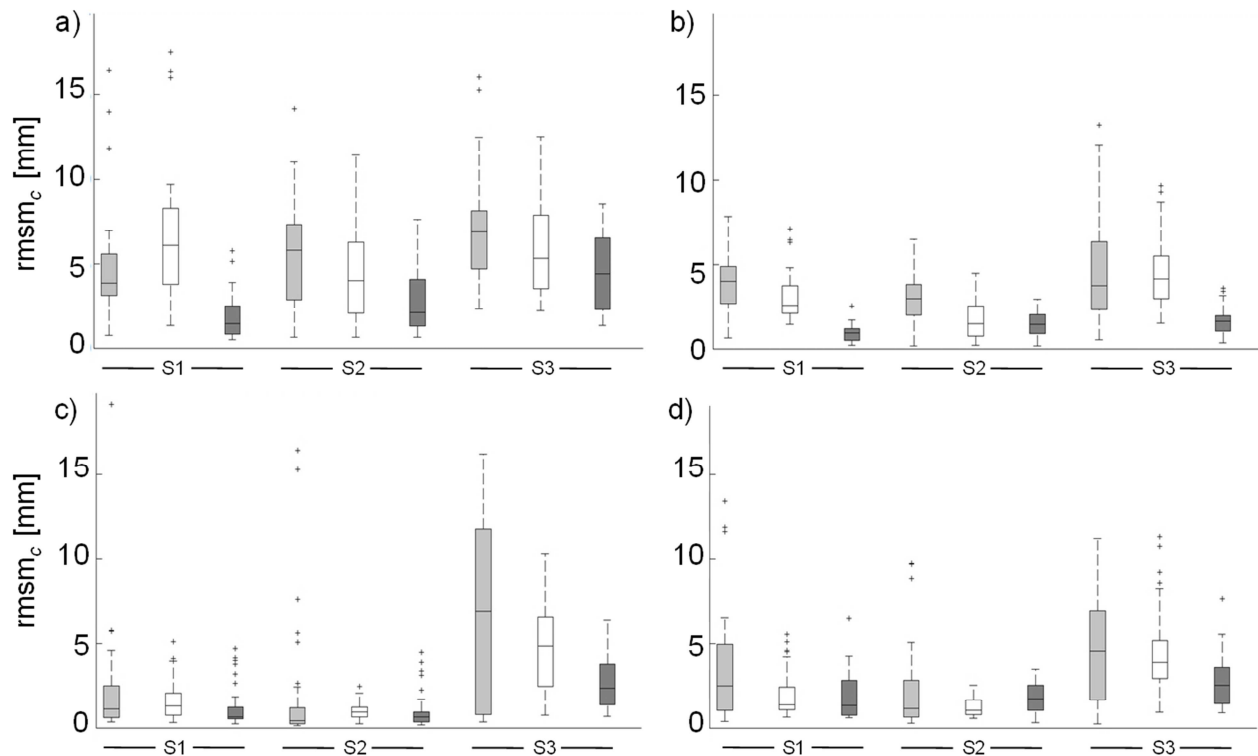
The general characteristics of artefact component amplitudes were consistent amongst specimens and volunteers. The artefact time histories exhibiting  $rmsm_c$  values lower than 0.5 mm were considered too small to allow their reliable measurement and estimate. The parameters derived from these time histories were therefore excluded from all statistics reported below.

Calibration trial: FE <sub>HK</sub>								
Angle	FE <sub>HK</sub>		FE <sub>H</sub>		FE <sub>K</sub>		Cir <sub>H</sub>	
	$r_a$	$\Delta_a$ [%]	$r_a$	$\Delta_a$ [%]	$r_a$	$\Delta_a$ [%]	$r_a$	$\Delta_a$ [%]
$\alpha$	0.74 – 0.99	95 – 109	0.13 – 0.99	65 – 97	0.06 – 0.94	7 – 18	0.56 – 0.83	69 – 87
$\beta$	-0.06 – 0.49	31 – 151	-0.73 – 0.74	12 – 122	-0.69 – 0.37	25 – 73	-0.52 – 0.67	306 – 530
$\gamma$	0.24 – 0.83	58 – 107	-0.28 – 0.81	33 – 63	-0.45 – 0.88	4 – 45	-0.46 – 0.82	68 – 118
$\delta$	0.75 – 0.99	98 – 104	-0.73 – -0.06	1 – 5	0.09 – 0.95	20 – 45	-0.52 – 0.25	1 – 6

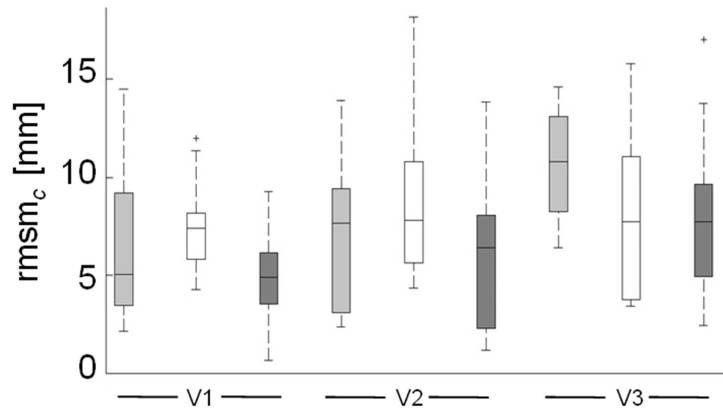
  

Calibration trial: Cir <sub>H</sub>								
Angle	FE <sub>HK</sub>		FE <sub>H</sub>		FE <sub>K</sub>		Cir <sub>H</sub>	
	$r_a$	$\Delta_a$ [%]	$r_a$	$\Delta_a$ [%]	$r_a$	$\Delta_a$ [%]	$r_a$	$\Delta_a$ [%]
$\alpha$	0.45 – 0.87	118 – 151	-0.41 – 0.87	81 – 116	-0.27 – 0.69	9 – 22	0.19 – 0.99	85 – 107
$\beta$	-0.87 – 0.59	8 – 34	-0.79 – 0.77	3 – 29	-0.76 – 0.48	6 – 16	-0.06 – 0.99	89 – 116
$\gamma$	-0.79 – 0.82	65 – 148	-0.76 – 0.02	37 – 87	-0.65 – 0.35	5 – 43	0.29 – 0.97	82 – 128
$\delta$	-0.52 – 0.55	1717 – 5779	-0.46 – 0.78	32 – 92	-0.48 – 0.56	565 – 1351	-0.36 – 0.93	54 – 140

**Table 3.2** - Ranges of the correlation coefficient ( $r_a$ ) between rotations during a given test trial and during the indicated calibration trial, and percentage value ranges of the former in relation to the latter rotation peak-to-peak values ( $\Delta_a$ ). These ranges were calculated over all specimens and test trials, for the four ex-vivo movement patterns analysed.



**Figure 3.2** - Box-plots (minimum, lower quartile, median, upper quartile, and maximum) of the root mean square values of the measured STA components (rmsmc; x component in light grey, y in white, and z in dark grey) for each specimen (S), as determined over all skin-markers and the three FEHK (a), FEH (b), FEK (c), CirH (d) trials, respectively. Outliers are also shown.



**Figure 3.3** - Same as in Fig. 3.2 but with reference to the volunteers (V) and the five RN trials.

### 3.1.2 Model calibration and architecture feasibility assessment

The model parameters resulting from the calibrations that used the three  $FE_{HK}$ ,  $FE_H$ ,  $FE_K$ , and  $Cir_H$  trials for each specimen and the five RN trials for each volunteer were calculated. These values for one trial of the  $FE_{HK}$  and the  $Cir_H$  movement patterns for each specimen and an RN trial of each volunteer are shown in Tables 3.3, 3.4, 3.5, respectively, together with the characteristics of the relevant movements (Figures 3.4, 3.5, 3.6).

markers	S1				S2				S3				
	$h^\alpha$	$h^\beta$	$h^\gamma$	$h^\delta$	$h^\alpha$	$h^\beta$	$h^\gamma$	$h^\delta$	$h^\alpha$	$h^\beta$	$h^\gamma$	$h^\delta$	
L1	x	-0.19	0.12	-0.28	0.14	1.04	-1.98	-1.40	-0.11	-0.01	0.08	-0.45	0.12
	y	-0.05	0.30	0.28	-0.18	0.19	-0.44	-0.26	-0.08	0.38	-0.61	-0.05	-0.29
	z	-0.19	0.38	0.11	0.07	0.01	-0.08	-0.54	0.08	0.14	-0.05	-0.26	-0.08
L2	x	-0.32	-0.21	-0.27	0.27	1.10	-2.16	-1.20	-0.14	-0.06	0.49	-0.22	0.13
	y	-0.17	-0.04	0.27	-0.08	0.26	-0.44	-0.02	-0.12	0.09	-0.40	0.12	-0.14
	z	-0.05	0.32	0.11	-0.04	-0.06	-0.10	-0.39	0.09	0.10	0.14	-0.20	-0.06
L3	x	-0.38	0.13	-0.27	0.32	0.87	-1.90	-0.87	-0.09	-0.57	0.33	-0.38	0.48
	y	-0.03	-0.03	0.24	-0.13	0.46	-0.48	0.32	-0.24	0.28	-0.21	0.25	-0.24
	z	-0.22	0.20	-0.11	0.11	0.07	-0.18	-0.38	0.05	-0.06	-0.02	-0.13	0.04
L4	x	0.00	-0.22	-0.24	0.09	0.11	-1.14	-0.37	0.09	-0.95	0.35	-0.52	0.69
	y	-0.02	0.11	0.23	-0.12	0.08	-0.30	0.31	-0.07	0.20	-0.74	0.03	-0.18
	z	-0.08	-0.15	0.00	0.07	0.09	-0.60	-0.15	0.04	0.04	-0.01	0.06	-0.05
A1	x	-0.49	-0.40	0.02	0.32	0.47	-1.07	-0.50	-0.06	-0.24	0.25	-0.09	0.20
	y	-0.44	0.55	0.38	0.07	0.10	-0.44	-0.29	-0.05	0.15	0.01	0.13	-0.25
	z	-0.05	-0.36	0.08	0.02	-0.63	1.19	0.70	0.03	-0.33	-0.21	0.25	0.09
A2	x	-0.46	-0.36	0.00	0.34	0.39	-1.30	-0.44	0.01	-0.31	0.29	-0.02	0.24
	y	-0.02	0.46	0.40	-0.17	-0.35	0.45	0.25	0.04	0.07	-0.01	0.13	-0.17
	z	-0.20	-0.06	0.14	0.06	-0.50	0.69	0.87	0.05	-0.15	-0.39	0.17	-0.01
A3	x	-0.29	-0.25	0.09	0.22	0.24	-0.46	-0.20	-0.05	-0.37	0.25	-0.16	0.30
	y	0.05	0.57	0.28	-0.22	-0.38	0.45	0.41	0.00	0.16	-0.10	0.05	-0.18
	z	-0.12	-0.08	0.15	0.01	-0.05	-0.24	0.51	0.01	0.18	-0.10	0.26	-0.20
A4	x	-0.13	-0.24	0.02	0.08	0.00	-0.36	-0.18	0.00	-0.42	0.10	-0.22	0.29
	y	0.05	0.25	0.09	-0.32	-0.46	0.81	0.34	-0.06	0.22	-0.31	-0.10	-0.24
	z	-0.22	-0.56	0.13	0.16	0.08	-0.15	0.24	-0.01	0.40	-0.56	0.31	-0.32
M1	x	-1.69	-0.86	0.60	0.72	-0.98	-0.26	2.15	0.08	-2.13	-0.34	0.42	1.17
	y	-0.15	0.84	0.34	-0.01	-0.76	1.42	0.66	0.17	0.51	0.21	0.00	-0.23
	z	-0.31	0.14	0.03	0.15	0.56	-1.10	-0.52	-0.13	0.12	0.24	0.07	-0.11
M2	x	-1.05	-0.43	0.04	0.64	-1.05	0.02	1.58	0.33	-1.45	-0.36	0.21	0.88
	y	-0.01	0.41	0.22	-0.09	-0.63	1.23	0.25	0.14	0.43	-0.02	-0.06	-0.24
	z	0.24	0.00	0.06	-0.14	0.04	-0.38	0.05	0.01	0.12	0.02	0.05	-0.10
M3	x	-0.89	-0.81	-0.24	0.63	-0.66	-0.71	0.94	0.35	-1.18	-0.71	-0.03	0.78
	y	0.20	0.35	0.15	-0.21	-0.51	1.12	0.29	0.05	0.58	0.04	-0.03	-0.35
	z	0.19	0.16	0.19	-0.14	-0.09	-0.31	0.19	0.07	0.32	-0.10	0.06	-0.22
M4	x	-0.58	-0.89	-0.11	0.42	0.00	-1.15	0.32	0.16	-0.76	-0.86	-0.06	0.47
	y	0.20	0.44	0.14	-0.25	-0.54	1.43	0.29	-0.01	0.51	0.15	-0.12	-0.37
	z	0.10	0.00	0.13	-0.07	-0.25	-0.09	0.32	0.15	0.33	-0.49	-0.07	-0.21

**Table 3.3** – *Ex-vivo* experimental data. Subject- and trial- specific model parameters  $h_c^\alpha, h_c^\beta, h_c^\gamma, h_c^\delta$  [mm/deg],  $c = x, y, z$  (anatomical axes: Fig. 1a) for the three specimens S1, S2, and S3. The calibration trials were selected among the  $FE_{HK}$  trials available for each specimen (joint kinematics is depicted in Fig. 3.4). The locations of the twelve skin markers are shown in Fig. 3.1a.

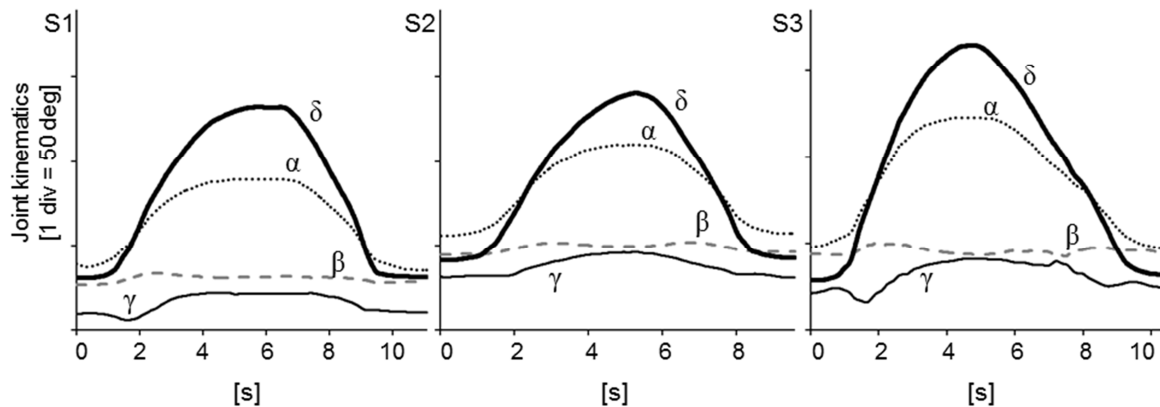


**Figure 3.4** – Joint kinematics time histories (hip: flexion/extension,  $\alpha$ , abduction/adduction,  $\beta$ , internal/external rotation,  $\gamma$ ; knee: flexion/extension,  $\delta$ ) during the selected  $FE_{HK}$  trial for each specimen (S1, S2, S3).

markers		S1				S2				S3			
		$h^\alpha$	$h^\beta$	$h^\gamma$	$h^\delta$	$h^\alpha$	$h^\beta$	$h^\gamma$	$h^\delta$	$h^\alpha$	$h^\beta$	$h^\gamma$	$h^\delta$
L1	x	0.30	-0.56	-0.87	3.30	0.26	-0.60	-0.77	3.47	-0.17	-0.21	-0.82	1.13
	y	-0.05	-0.65	-0.62	1.47	0.17	-0.34	-0.21	2.44	-0.15	0.00	1.15	1.24
	z	-0.05	0.29	0.34	-1.27	0.12	-0.35	-0.61	1.65	-0.16	0.03	0.02	0.59
L2	x	0.17	-0.77	-0.64	2.71	0.12	-0.26	-0.35	0.70	-0.37	0.13	0.68	2.34
	y	0.05	-0.43	-0.66	2.23	0.16	-0.16	-0.14	1.14	-0.03	0.10	0.53	0.47
	z	-0.03	0.12	0.22	-0.90	0.07	-0.20	-0.40	0.78	-0.14	0.05	0.20	0.85
L3	x	0.13	-0.58	-0.55	1.56	0.05	-0.10	-0.15	0.42	-0.28	0.17	0.84	2.34
	y	0.06	-0.21	-0.43	1.47	0.10	-0.06	-0.07	0.86	0.10	0.07	0.18	-0.01
	z	0.02	0.00	0.17	-0.10	0.08	-0.14	-0.26	0.90	-0.10	0.04	0.30	0.65
L4	x	0.05	-0.16	-0.06	0.23	0.01	-0.10	-0.01	-0.32	-0.17	0.11	0.54	1.34
	y	0.03	-0.05	-0.15	0.76	0.05	0.00	-0.03	0.44	0.19	0.01	-0.14	-0.50
	z	-0.01	0.06	0.18	0.53	-0.08	0.10	0.28	0.06	-0.12	0.13	0.35	1.04
A1	x	-0.02	-0.12	-0.18	1.31	0.11	-0.15	-0.26	1.37	0.01	0.03	0.04	0.29
	y	0.05	-0.25	-0.55	1.93	0.02	-0.16	-0.01	1.38	-0.15	-0.01	0.12	0.62
	z	-0.18	0.60	0.72	-1.88	-0.25	0.15	0.23	-0.14	-0.10	-0.04	0.21	-0.27
A2	x	0.00	-0.05	-0.05	0.50	0.01	-0.04	-0.04	0.18	0.00	0.06	0.08	0.22
	y	0.07	-0.27	-0.49	1.56	0.07	-0.10	-0.05	0.94	-0.04	0.02	0.15	0.32
	z	-0.13	0.55	0.60	-1.15	-0.10	0.23	0.09	0.52	-0.07	0.08	0.11	0.13
A3	x	0.01	-0.10	-0.14	0.41	0.03	-0.09	-0.02	0.39	-0.02	0.04	0.20	0.32
	y	0.07	-0.23	-0.45	1.34	0.07	-0.08	-0.07	0.56	0.06	0.00	0.05	0.03
	z	-0.09	0.43	0.49	-0.55	-0.06	0.15	0.15	1.20	-0.03	0.07	-0.04	0.14
A4	x	-0.02	0.04	0.06	-0.06	0.01	0.00	-0.18	-1.84	-0.02	0.04	0.13	0.00
	y	0.06	-0.13	-0.24	0.62	0.06	-0.04	-0.10	0.23	0.14	0.00	-0.11	-0.20
	z	-0.05	0.18	0.21	0.24	-0.02	0.14	-0.01	-0.10	0.01	0.11	-0.05	0.43
M1	x	-0.42	-0.38	-0.32	4.45	-0.49	0.28	0.32	9.25	-0.24	0.38	0.53	2.24
	y	0.04	0.37	-0.05	0.33	0.06	0.12	-0.04	-0.29	0.35	0.04	-0.29	-0.33
	z	-0.13	0.11	0.03	0.55	0.06	-0.27	-0.08	-0.69	-0.12	0.10	0.05	-0.54
M2	x	-0.18	0.67	0.98	1.52	-0.24	0.47	0.28	3.65	-0.09	0.30	0.45	2.28
	y	0.08	-0.12	-0.32	0.11	0.12	-0.09	-0.14	-0.18	0.21	0.00	-0.24	-0.38
	z	0.02	0.03	0.04	-0.56	0.01	0.03	-0.03	-0.77	-0.01	0.09	0.03	-0.19
M3	x	-0.10	0.57	0.81	0.25	-0.12	0.31	0.15	1.65	-0.01	0.16	0.25	2.00
	y	0.07	-0.19	-0.35	0.42	0.09	-0.11	-0.12	0.05	0.20	-0.04	-0.31	-0.71
	z	0.03	-0.13	-0.18	0.00	0.00	0.08	-0.01	-0.46	0.03	0.03	-0.06	-0.16
M4	x	-0.04	0.16	0.16	0.18	-0.05	0.15	0.03	0.45	-0.03	0.10	0.12	1.15
	y	0.05	-0.11	-0.18	0.22	0.08	-0.06	-0.09	0.29	0.22	-0.05	-0.35	-1.02
	z	0.00	0.09	0.19	0.58	0.00	0.06	-0.01	0.24	0.02	0.05	-0.03	0.27

**Table 3.4** – *Ex-vivo* experimental data. Subject- and trial- specific model parameters  $h_c^\alpha, h_c^\beta, h_c^\gamma, h_c^\delta$  [mm/deg],  $c = x, y, z$  (anatomical axes: Fig. 3.1a) for the three specimens S1, S2, and S3. The calibration trials were selected among the  $\text{Cir}_H$  trials available for each specimen (joint kinematics is depicted in Fig. 3.2s). The locations of the twelve skin markers are shown in Fig. 3.1a.

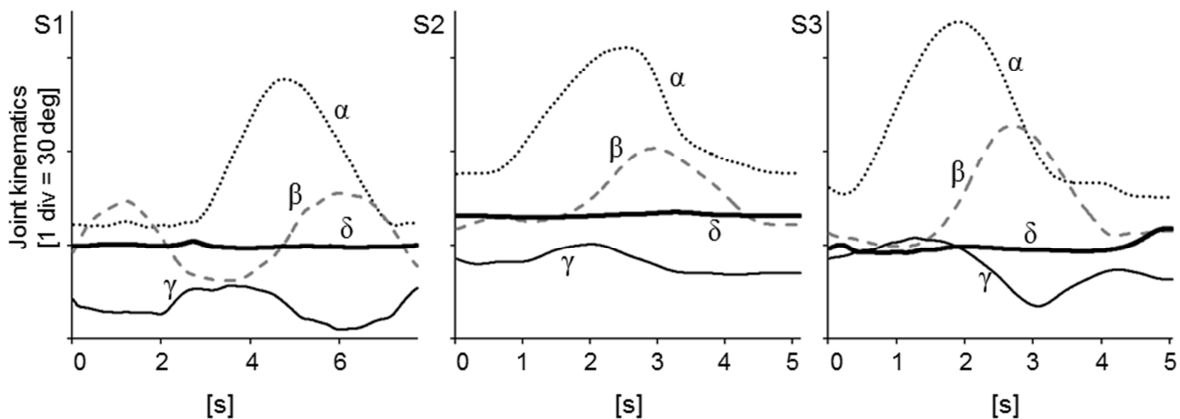


**Figure 3.5** – Joint kinematics time histories (hip: flexion/extension,  $\alpha$ , abduction/adduction,  $\beta$ , internal/external rotation,  $\gamma$ ; knee: flexion/extension,  $\delta$ ) during the selected  $\text{Cir}_H$  trial for each specimen (S1, S2, S3).

markers	V1				V2				V3				
	$h^\alpha$	$h^\beta$	$h^\gamma$	$h^\delta$	$h^\alpha$	$h^\beta$	$h^\gamma$	$h^\delta$	$h^\alpha$	$h^\beta$	$h^\gamma$	$h^\delta$	
T1	x	-0.61	5.14	-1.18	0.60	-0.29	3.30	-0.42	-0.21	-0.22	1.46	-1.03	0.61
	y	0.32	-1.51	0.40	0.05	-0.25	-0.36	-1.06	-0.06	-0.14	-0.93	-0.97	0.06
	z	0.13	-1.92	0.48	-0.17	0.21	-0.77	0.46	0.49	-0.20	-0.37	-0.88	-0.01
T2	x	-0.49	2.78	0.25	-0.01	0.03	0.51	0.15	-0.16	0.04	-0.53	-0.52	0.04
	y	0.17	-1.56	0.68	0.04	-0.13	-0.83	-0.88	0.08	-0.08	-1.38	-0.84	0.06
	z	-0.01	-0.06	-0.11	0.07	-0.02	-0.35	0.10	0.07	-0.15	0.19	-0.82	0.04
T3	x	0.72	-2.30	-1.96	0.34	-0.11	1.62	-0.50	-0.17	0.20	-1.16	2.35	-0.02
	y	-0.24	-1.93	1.34	-0.43	-0.19	-3.47	-0.02	-0.05	-0.62	-1.88	-2.21	-0.05
	z	1.11	-6.72	-0.25	-0.48	0.43	-4.11	0.63	0.23	0.06	-3.33	2.04	-0.81
T4	x	0.42	-2.55	-0.64	-0.30	-0.11	0.19	-0.70	-0.15	0.30	-2.17	2.20	-0.37
	y	-0.31	-1.14	1.87	-0.21	0.10	-3.24	-0.11	0.17	-0.29	-2.45	-2.04	0.01
	z	0.33	-2.20	0.68	-0.39	0.29	-2.76	-0.14	0.11	0.22	-3.42	1.47	-0.89
T5	x	-0.14	-0.40	0.91	-0.30	0.03	-0.21	0.32	-0.11	0.14	-2.05	0.74	-0.30
	y	-0.52	1.35	1.94	0.34	0.14	-1.92	-0.09	0.45	-0.14	-2.45	-1.63	0.04
	z	-0.05	-0.59	0.68	-0.36	-0.05	-1.07	-0.56	-0.04	0.02	-1.94	-0.02	-0.56

**Table 3.5** – *In-vivo* experimental data. Subject- and trial- specific model parameters  $h_c^\alpha, h_c^\beta, h_c^\gamma, h_c^\delta$  [mm/deg],  $c = x, y, z$  (anatomical axes: Fig. 3.1b) for the three volunteers V1, V2, and V3. The calibration trials were selected among the RN trials available for each volunteer (joint kinematics is depicted in Fig. 3.6). The locations of the five skin markers are shown in Fig. 3.1b.

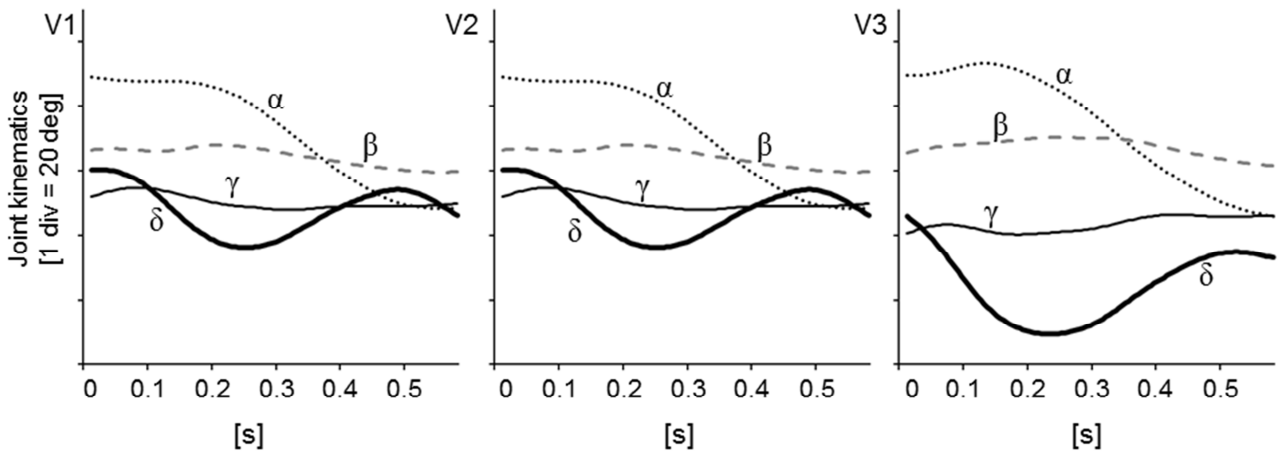


**Figure 3.6** – Joint kinematics time histories (hip: extension/flexion,  $\alpha$ , abduction/adduction,  $\beta$ , internal/external rotation,  $\gamma$ ; knee: flexion/extension,  $\delta$ ) during the selected RN trial for each volunteer (V1, V2, V3).

The time histories of the measured artefact components and of the relevant estimates of a marker, as provided by the calibration problem solution, are shown in Fig. 3.7 for a FE<sub>HK</sub> trial of a specimen and an RN trial of a volunteer. This figure shows the oscillating components present in the curves obtained *in-vivo*, as opposed to those obtained *ex-vivo*, that may be associated with the soft tissue wobbling occurring during running. In addition, it can be seen that the estimated *in-vivo* STA does not exhibit these oscillations. Quantitative aspects of both issues are reported below.

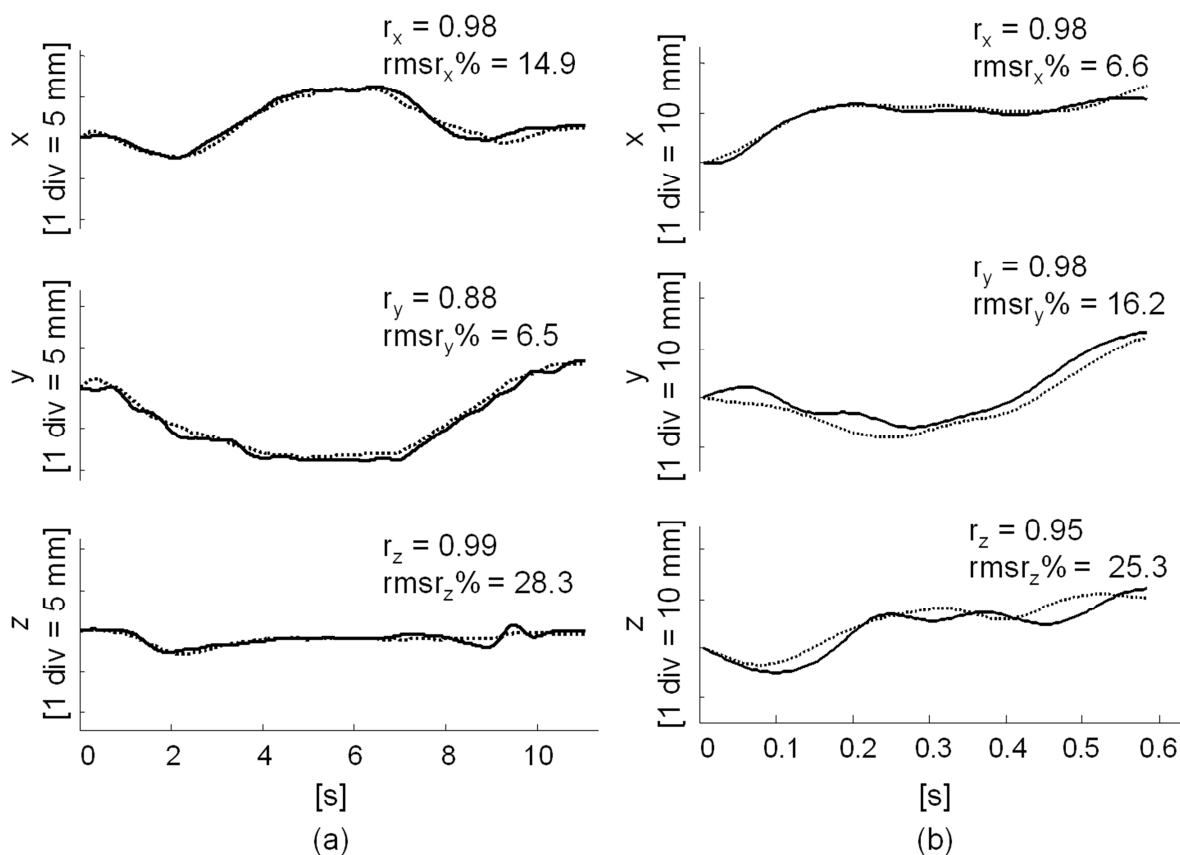


Figure 3.7 - Measured (thick line) and estimated (dotted line) STA components in the femur anatomical frame (x, y, z in Fig. 3.1) of marker A1 of S1 and of marker T5 of V3 during a trial of FE<sub>HK</sub> (a) and a trial of RN (b), respectively. The relevant correlation coefficients ( $r_c$ ) and the  $rmsr_c\%$  values are also shown.

The statistics for all *ex-vivo* and *in-vivo* trials of the residual values of  $rmsr_c\%$  and of  $r_c$  after calibration are reported in Table 3.6.

	FE <sub>HK</sub>		FE <sub>H</sub>		FE <sub>K</sub>		Cir <sub>H</sub>		RN	
	$rmsr_c\%$	$r_c$	$rmsr_c\%$	$r_c$	$rmsr_c\%$	$r_c$	$rmsr_c\%$	$r_c$	$rmsr_c\%$	$r_c$
x	17 (11)	0.97 (0.04)	5 (7)	0.99 (0.02)	6 (7)	0.99 (0.03)	24 (14)	0.96 (0.08)	14 (17)	0.95 (0.14)
y	11 (12)	0.98 (0.03)	5 (5)	0.99 (0.02)	5 (6)	0.99 (0.03)	20 (17)	0.96 (0.05)	15 (9)	0.98 (0.03)
z	19 (14)	0.93 (0.08)	9 (7)	0.97 (0.04)	11 (10)	0.96 (0.06)	27 (14)	0.94 (0.07)	20 (24)	0.95 (0.11)

**Table 3.6** - Model calibration residuals. Median and IQR (in brackets) values of the  $rmsr_c\%$  and Pearson's coefficient ( $r_c$ ) for the different anatomical axes (x, y, z: Fig. 3.1), calculated over all markers and all specimens' FE<sub>HK</sub>, FE<sub>H</sub>, FE<sub>K</sub>, and Cir<sub>H</sub> trials and volunteers' RN trials, respectively.

The power density spectra of the measured and estimated STA components affecting a given marker, as observed *ex-vivo*, had very similar profiles. Over 99% of the mean power of both the measured and estimated STAs was consistently located in the frequency range 0-5 Hz.

In the *in-vivo* experiments, the measured artefact exhibited peaks that tended to be higher than those of the estimated artefact, and shifted towards higher frequencies (Fig. 3.8, Table 3.7). On average, 73% of the mean power of the measured STA components was in the frequency range 0-5 Hz, and

21% in the frequency range 5-10 Hz (Table 3.7). The mean power of the estimated STA components was mainly concentrated in the frequency band 0-5 Hz (89% on average). In the latter band, the measured and estimated power spectra tended to be very similar in both shape and mean power. In fact, the median values and inter-quartile ranges (in brackets) of the difference between the mean powers of the measured and estimated STAs, determined across all volunteers, markers and trials, and expressed as a percentage of the mean power of the measured artefact, were found to be equal to 11% (30%), 4% (10%), and 5% (16%), for the x, y, and z component, respectively.

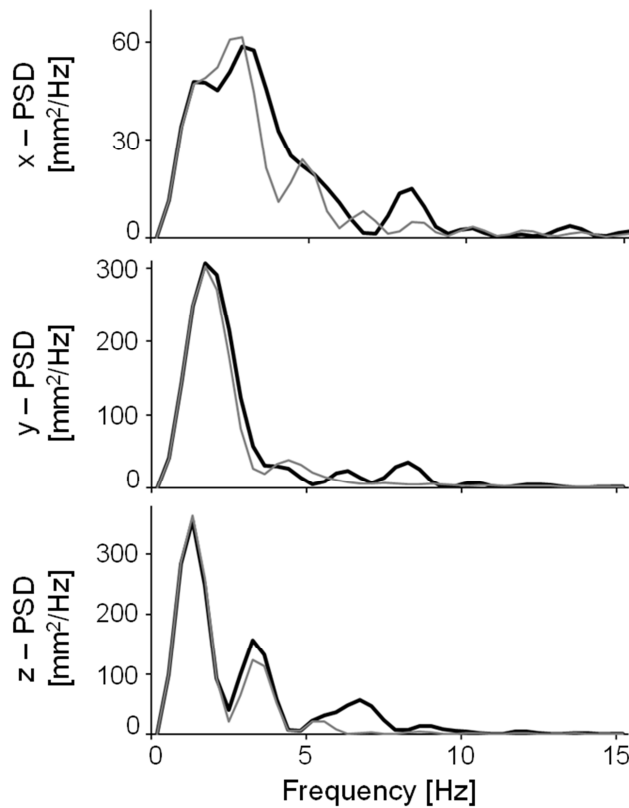


**Figure 3.8** - Power spectral density of the measured (thick lines) and estimated (thin lines) STA components in the femur anatomical frame (x, y, z in Fig. 3.1) of the same volunteer, marker and trial as in Fig. 3.3.

frequency band	estimated STA [%]		measured STA [%]	
	< 5 Hz	5 - 10 Hz	< 5 Hz	5 - 10 Hz
x	87 (20)	10 (13)	58 (26)	31 (26)
y	90 (7)	7 (5)	84 (7)	12 (8)
z	90 (9)	7 (7)	76 (17)	21 (16)

**Table 3.7** - Mean power in the indicated frequency bands, in per cent of the relevant total mean power, of the measured and model estimated STAs using the *in-vivo* dataset. Median and IQR (in brackets) values estimated over all trials of all volunteers and markers for each anatomical axis.

### 3.1.3 Assessment of model generalizability

Results on the similarity between the measured and estimated STAs, obtained through the proposed model calibrated using two different calibration movement patterns, showed that when movement patterns of the test and calibration trials were different, estimates were normally of low to bad quality, thus hindering generalizability. On the contrary, when the test and calibration trials exhibited the same movement pattern, this similarity was high for the shape of the relevant curves (correlation coefficient around 0.9 on average), but nonetheless subject to remarkable variations ( $rmse_c\%$  values that could be as high as 100%) with regard to the absolute values (Table 3.8). This was the case when the two joint movements involved (calibration and test trials) had rather different time histories (i.e a low correlation coefficient) and rotation ranges (Table 3.2).

	$FE_{HK}$		$Cir_H$	
	$rmse_c\%$	$r_{ec}$	$rmse_c\%$	$r_{ec}$
x	51 (39)	0.88 (0.11)	54 (36)	0.93 (0.15)
y	42 (54)	0.97 (0.06)	54 (56)	0.93 (0.10)
z	49 (42)	0.86 (0.21)	50 (34)	0.89 (0.12)

**Table 3.8** - Median and IQR (in brackets) values of the  $rmse_c\%$  and Pearson's coefficient ( $r_{ec}$ ) between the measured and estimated STA components (x, y, z, Fig. 3.1), over the  $FE_{HK}$  and the  $Cir_H$  test trials and all markers and specimens. Estimates were obtained using a model calibrated using a trial of the same movement pattern as the test trial.

## 3.2 Discussion

This study proposes a mathematical model of the STA, for a selected marker location on the thigh of a given subject, which estimates the artefact components in a bone embedded anatomical frame as a function of the hip and knee joint rotations that occur during the execution of a motor task. Based on the outcome of previous studies (Akbarshahi et al., 2010; Cappozzo et al., 1996; Camomilla et al., 2013), a linear relationship between artefact components and the proximal and distal articular angles was hypothesised. The assumption that the STA depends only on joint angles entails that only the portion of the artefact generated by skin sliding was accounted for.

A previously published model estimated the STA, generated during a 3-D movement of the thigh relative to the pelvis with the knee kept stationary (hip joint centre determination using the functional approach), as a function of the hip joint angles (Camomilla et al., 2013). This movement is quasi-static, involving no impacts and few body segment volumetric deformations. Under these circumstances it was deemed acceptable to assume that skin sliding was the major determinant of the STA. The model presented herein aimed to estimate the STA during bi-articular movements, as occurs in locomotion. Under these conditions, the above-mentioned assumption was not a foregone

conclusion. Soft tissue wobbling and deformations due to muscle contraction come into play. Thus, the question was posed whether skin sliding would still be the major determinant of the STA.

### 3.2.1 Model feasibility

It proved possible to calibrate the proposed model both *ex-vivo* and *in-vivo*. Using all calibration movement patterns tested, the rms value of the residual on the artefact estimate was, in most cases, lower than 25% of the measured counterpart. The time histories of the estimated and measured artefacts were also remarkably similar in shape, as indicated by high correlation coefficient values (median value always higher than 0.93; Table 3.6). For each calibration movement involving relatively small and planar joint rotations ( $FE_H$ ,  $FE_K$ ), the above-mentioned figures had better values. During the running experiments, although rotation ranges were similar amongst all trials, the performance of the model was not as good. This could be due to both inaccuracies in the hip kinematics reconstruction and to artefact causes not accounted for by the model, as discussed below. When rotations were very wide and/or out of plane ( $FE_{HK}$ ,  $Cir_H$ ), the  $rmsr_c\%$  and correlation values worsened, but the resulting dissimilarities still did not obscure the major features of the artefact time history (Table 3.6, Fig. 3.3). Thus, the conclusion is that the linear model architecture is feasible, and, more important, this is also the case *in-vivo*.

Based on the good results obtained *in-vivo* with a model that accounts only for the portion of the artefact generated by skin sliding, it may be deduced that this is the major cause of the artefact and that thigh deformation due to muscle contraction and gravity, and soft tissue wobbling (limited to non-obese subjects), have minor roles. This inference was reinforced by the results of frequency analysis, when soft tissue wobbling comes into play. We found that virtually all the estimated artefact's power fell within the 0-5 Hz frequency band (89%; Fig. 3.8, Table 3.7), and that, in the same frequency range, the mean power differed from its measured counterpart by only 7% on average. Joining together the facts that a) the estimated artefact represents only the skin sliding portion, b) the 0-5 Hz frequency range covers virtually the entire estimated artefact and anything correlated with voluntary movement, and c) in this frequency range, the estimated and measured artefacts are very similar, we may conclude that muscle contraction and gravity add very little to the artefact caused by skin sliding. The measured artefact not reconstructed by the model fell within a higher frequency band (5-10 Hz) that could only be ascribed to soft tissue wobbling. This portion accounted for a relatively small part of the total mean power (on average, 13%; Table 3.7) and can thus be regarded as a secondary cause of the artefact. These considerations are based on plausibility, but not on evidence. To the authors' knowledge, no data directly applicable to the present case are

available in the literature. Related studies, in fact, did not investigate thigh tissue wobbling during running and, in addition, used accelerometers attached to the skin, thus detecting higher frequencies than could possibly be the case with stereophotogrammetry (Enders et al., 2012; Wakeling et al., 2003; Wakeling and Nigg, 2001). However, in Wakeling and Nigg (2001), there appear to be clues indicating that the frequency band of soft tissue wobbling consequential to the lower limbs impacting the ground, as in running, may include the 5-10 Hz frequency range as found in the present study.

The above-illustrated conclusions on the feasibility of our model architecture mean that the proposed model can be embedded in a skeletal kinematics estimator. This can be done by representing the marker position vectors as their artefact-affected measured values minus the STA vector analytically represented through the proposed model (Alexander and Andriacchi, 2001). Of course, this adds further parameters to the optimization problem inherent in the estimator, which could pose a convergence problem. For this reason, studies are being carried out to represent the artefact affecting the cluster of markers in a space that exhibits the least number of dimensions possible, in order to minimize the number of parameters in the STA model (Andersen et al., 2012; Dumas et al., 2014a).

### 3.2.2 *Model generalizability*

After excluding the possibility of applying a model calibrated for a given marker location to other locations, or for a given subject to other subjects (Akbarshahi et al., 2010; Leardini et al., 2005; Peters et al., 2010), we investigated the issue of whether a subject- and marker-specific model could be used to produce a realistic artefact engendered during a test movement different from the calibration movement. Results on generalizability showed that our model's estimated STA time histories displayed basic characteristics that, when compared with those of the measured counterpart, make them appear realistic. This was certainly true with the shape of the relevant curves, less true with regard to the absolute values. In addition, this generalizability was valid when the test movement was characterized by joint rotations differing from those used for calibration up to  $\pm 10\%$  or  $\pm 50\%$  in amplitude for the larger and smaller joint rotations, respectively (Table 3.2), provided the two movements involved were characterized by the same pattern (either a prevailing flexion-extension of both hip and knee or hip circumduction with knee flexion).

Thus, within the limits above indicated, the artefact time histories generated by our proposed mathematical model can be used in simulations for the comparative assessment of skeletal kinematics estimators (Cereatti et al., 2006), instead of arbitrary STAs such as those used in

previous studies, (e.g., Andriacchi et al., 1998; Begon et al., 2007; Dumas and Chèze, 2009; Halvorsen, 2003; Lu and O'Connor, 1999; Reinbolt et al., 2005).

#### 4. Chapter 4

The content of this chapter is referred to the article

### **“GENERALIZED MATHEMATICAL REPRESENTATION OF THE SOFT TISSUE ARTEFACT”**

Published in Journal of Biomechanics, 2014, 47 (2), 476–481.

Additional information are also presented.

#### Symbols and Nomenclature

	$i$	body segment ( $i = 1, 2, 3, \dots$ )
	$j$	skin marker ( $j = 1, \dots, m_i$ )
	$k$	sampled instant of time ( $k = 1, \dots, n$ )
	$\mathbf{v}_i^j(k)$	STA vector of the skin marker $j$ glued on the segment $i$
	$\mathbf{V}_i(k)$	STA field of the segment $i$
Symbols	$a_i^l(k)\Phi_i^l$	mode $l$
	$\Phi_i^l$	mode direction
	$a_i^l(k)$	mode amplitude
	$\lambda_i^l$	modal deformation energy
	$p$	energy percentage
	$e_i$	total deformation energy
	$r_i$	number of modes that contributes to represent a given
	$\mathbf{W}$	weighted STA field
	$\tilde{\mathbf{V}}_i(k)$	residual STA field
Knee degrees of freedom	FE	flexion/extension
	AA	abduction/adduction
	IER	internal/external rotation
	LM	medio/lateral
	AP	anterior/posterior
	PD	proximal/distal
Nomenclature	STA	soft tissue artefact
	RMS	root mean square
	AF	anatomical reference frame
	PCA	principal component analysis
	SVD	single value decomposition
	MD	individual marker displacements
	GT	marker-cluster geometrical transformations
	SV	skin envelope shape variations
	RD	row data

Anatomical Landmarks	Pelvic	RASIS	right anterior superior iliac spines
		LASIS	left anterior superior iliac spines
		RPSIS	right posterior superior spines
		LPSIS	left posterior superior spines
		RHJC	right hip joint centre
	Femur	RLE	right lateral femoral epicondyles
		RME	right medial femoral epicondyles
	Tibial	RLM	right lateral malleoli
		RMM	right medial malleoli
		RHF	right head of the fibula
		RTT	right tibial tuberosity

#### 4.1. Introduction

“Soft tissue artefact” (STA) is the term used in the field of movement analysis to designate the relative movement between skin markers, as used with stereophotogrammetry, and the underlying bones. These movements affect the configuration of the ensemble of markers (marker-cluster) associated with each bony segment (Grimpampi et al., 2014) and may jeopardize the estimate of the global pose of the bones involved in the analysis of joint kinematics (Leardini et al., 2005; Peters et al., 2010). To compensate for the STAs engendered during a motor task, many different methods have been proposed (Alexander and Andriacchi, 2001; Andersen et al., 2009; Andriacchi et al., 1998; Ball and Pierrynowski, 1998; Cappello et al., 1997; Challis, 1995; Chèze et al., 1995; Dumas and Cheze, 2009; Duprey et al., 2010; Heller et al., 2011; Lu and O’Connor, 1999; Lucchetti et al., 1998; Söderkvist and Wedin, 1993), but an effective solution still remains an open issue.

Efforts have been made to describe the STA phenomenon with the final objective of defining mathematical models of it that can be embedded in optimal bone pose estimators (Alexander and Andriacchi, 2001; Camomilla et al., 2013) or in algorithms aimed at estimating the location of joint centers using a functional approach (de Rosario et al., 2012). Given the subject and task specificity of STA, these models should be driven by observable biomechanical features of the analyzed task, such as, for instance, joint angles. In addition, for an optimal bone pose estimator to be computationally effective and efficient, the STA model must embed as few parameters as possible.

Prior to tackling the above-mentioned modeling exercise, an appropriate definition of the STA and relevant mathematical representation must be chosen. One issue to consider is whether to represent the STA as individual marker local displacements, as widely done in the literature, or other

definitions. Additional issues concern the level of approximation of the STA mathematical representation and the number of parameters involved in the representation.

The objective of this paper is to propose a generalized mathematical representation of the STA that would accommodate its different possible definitions. To this purpose, a modal approach was used that, most importantly, allows for the splitting of a given STA into additive components, called modes. The modes may be ranked according to the contribution that each of them gives to the reconstruction of the STA. Specifically, this ranking is based on deformation energy and the percentage of this energy associated with each mode. In this way, the STA definition leading to the minimum number of modes, and, therefore, of parameters, that provides an adequate approximation for further purposes can be selected, allowing a trade-off between complexity and effectiveness of the STA model.

For the above purpose, three STA definitions were accounted for: individual marker displacements, marker-cluster geometrical transformations, and skin envelope shape variations. The latter definition falls into continuum mechanics where the STA corresponds to a change of configuration of some material points from their reference position to their current position.

Preliminary quantitative conclusions about the selection and ranking of the corresponding modes were drawn for each STA definition using information available in the literature and experimental data provided by a previous study (Grimpampi et al., 2014). In addition, also running data were used to find the most appropriate STA mathematical representation evaluating the impact of different STA approximation on the accuracy of knee joint kinematics estimates.

#### 4.2. Generalized mathematical formulation

An STA vector,  $\mathbf{v}_i^j(k)$ , is defined to represent the displacement that the skin marker  $j$  ( $j = 1, \dots, m_i$ ) associated with the segment  $i$  ( $i = 1, 2, 3, \dots$ ) undergoes relative to a relevant bone-embedded coordinate system and a reference position at each sampled instant of time  $k$  ( $k = 1, \dots, n$ ) during the analyzed motor task (Fig. 4.1).

The STA of all markers can be represented using the STA field,  $\mathbf{V}_i(k)$ :

$$\mathbf{V}_i(k) = \begin{bmatrix} \mathbf{v}_i^1(k) \\ \vdots \\ \mathbf{v}_i^j(k) \\ \vdots \\ \mathbf{v}_i^{m_i}(k) \end{bmatrix}$$

(Eq. 4.1).

This equation represents the STA field with a dimension (or number of degrees of freedom) of  $3m_i$ . This field can be described by any orthogonal basis of vectors,  $\{\Phi_i^1, \dots, \Phi_i^l, \dots, \Phi_i^{3m_i}\}$ , that represents possible directions in space. Thereafter, the STA field,  $\mathbf{V}_i(k)$ , can be written as

$$\mathbf{V}_i(k) = \sum_{l=1}^{3m_i} a_i^l(k) \Phi_i^l \quad (\text{Eq. 4.2}),$$

where  $a_i^l(k)$  ( $l = 1, \dots, 3m_i$ ) is the amplitude of the projection of  $\mathbf{V}_i(k)$  onto the basis vector,  $\Phi_i^l$ , and can be obtained by the following dot product:

$$a_i^l(k) = (\mathbf{V}_i(k))^T \Phi_i^l \quad (\text{Eq. 4.3}).$$

In the proposed generalized mathematical formulation, mode  $l$  designates  $a_i^l(k) \Phi_i^l$ .

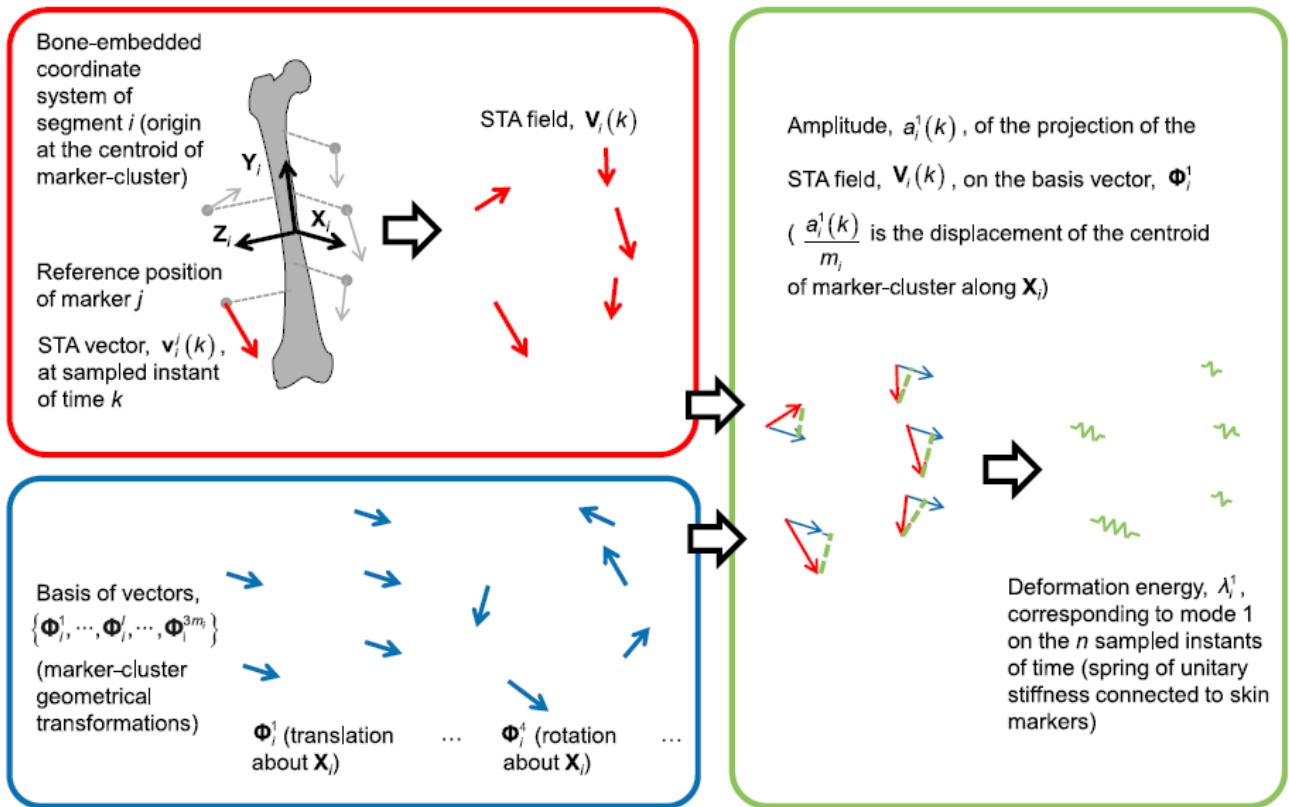


**Figure 4.1** – Framework of the generalized mathematical representation of the STA.

### 4.3. Ranking and selection of modes

The modal representation (Eq. 4.2) is classically used in the field of structure vibrations, where deformation energy is computed for every mode  $l$  and is typically used for data reduction

(Chatterjee, 2000; Kerschen et al., 2005). The deformation energy, corresponding to each mode  $l$ , is computed as the mean square of the amplitudes,  $a_i^l(k)$ , over the  $n$  sampled instants of time (Feeny, 2002)

$$\lambda_i^l = \frac{1}{n} \sum_{k=1}^n (a_i^l(k))^2 \quad (\text{Eq. 4.4}).$$

The modal deformation energies,  $\lambda_i^l$ , are sorted in decreasing order and summed one-by-one (*i.e.*, cumulative representation), until a given percentage  $p$ , of the total sum is obtained

$$\sum_{l=1}^{r_i} \lambda_i^l \geq p \sum_{l=1}^{3m_i} \lambda_i^l \quad (\text{Eq. 4.5}).$$

In Eq. 4.5,  $r_i$  represents the number of modes that contributes to a given percentage,  $p$ , of the total deformation energy,  $e_i$  (*i.e.*, the energy corresponding to all the modes  $l = 1, \dots, 3m_i$ ). With regard to the present application, the total deformation energy normalized with respect to the number of markers (which may be different from one segment to another) is interpreted as the mean over the  $m_i$  markers and the  $n$  sampled instants of time of the square of the STA vectors,  $\mathbf{v}_i^j(k)$ :

$$\frac{e_i}{m_i} = \frac{1}{m_i} \sum_{l=1}^{3m_i} \lambda_i^l = \frac{1}{n} \sum_{k=1}^n \frac{1}{m_i} \sum_{j=1}^{m_i} (\mathbf{v}_i^j(k))^2 \quad (\text{Eq. 4.6}).$$

This energy assumes that a spring of unitary stiffness is connected to every skin marker. The origin of each spring is the reference position of the relevant marker embedded in the segment coordinate system. Its insertion is the current skin marker position as caused by the STA. Based on this definition, any change of configuration in the marker local positions,  $\mathbf{V}_i(k)$ , including the rigid transformation of the marker-cluster, is associated with deformation energy. If required, different weights can be associated with each marker (non-unitary stiffness), by considering a weighted STA field,  $\mathbf{W} \cdot \mathbf{V}_i(k)$ . However, the geometrical meaning of such weighted change of configuration remains unclear. The deformation energy,  $e_i$ , is not representative of the strain in soft tissues. In the present study,  $\sqrt{e_i/m_i}$  is the root mean square (RMS) of the STA vectors, generally reported in the literature (Akbarshahi et al., 2010; Leardini et al., 2005; Peters et al., 2010). Moreover, the sum of

the squares of the STA vectors, at each sampled instant of time, is the typical objective function of bone pose estimation methods (Andersen et al., 2009; Andriacchi et al., 1998; Ball and Pierrynowski, 1998; Challis, 1995; Chèze et al., 1995; Dumas and Cheze, 2009; Duprey et al., 2010; Heller et al., 2011; Lu and O'Connor, 1999; Söderkvist and Wedin, 1993).

#### **4.4. Experimental data**

##### *4.4.1. Ex-vivo dataset*

Dataset produced in a previous study (Grimpampi et al., 2014), and also described in section 3.2.2, were used for a numerical example of the STA generalized mathematical representation and practical considerations that can be drawn using it on *ex-vivo* data.

Data were obtained from skin markers and pin marker-clusters located on the pelvis, thigh, and shank of an intact human specimen as shown in Fig. 4.2. The marker instantaneous positions ( $m_3 = 5$  for the thigh and  $m_2 = 4$  for the shank) were reconstructed in a global frame using a 9-camera stereophotogrammetric system (VICON MX - 120 frames/s) while an operator made the hip undergo a wide flexion-extension movement accompanied by a moderate abduction-adduction and, simultaneously, a knee flexion-extension. Anatomical reference frames were defined after performing the anatomical landmark calibration for the pelvic bone, femur, and tibia (Cappozzo et al., 1995). The STA vectors, of the thigh and shank skin markers, were expressed in the respective anatomical reference frames.

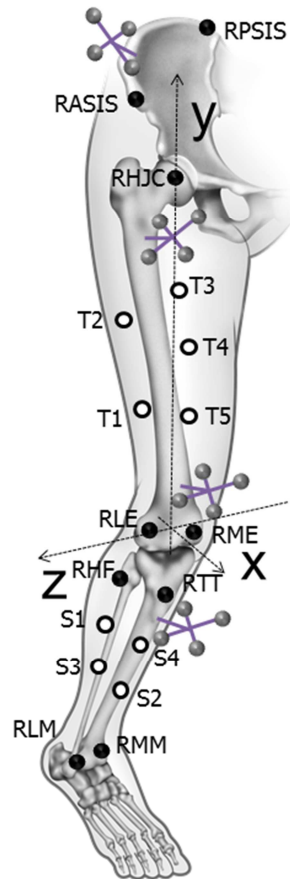


**Figure 4.2** - Five skin markers glued on the thigh (T) and four on the shank (S) (empty circles). The following anatomical landmarks (black circles) were calibrated using a pointer equipped with a cluster of four markers: right and left anterior superior iliac spines (RASIS, LASIS), right and left posterior superior spines (RPSIS, LPSIS), right lateral and medial femoral epicondyles (RLE, RME), lateral and medial malleoli (RLM, RMM), head of the fibula (RHF), and tibial tuberosity (RTT). The right hip joint centre (RHJC) was determined using a functional approach as described in (Cereatti et al., 2009) and the pin markers.

Using the proposed STA generalized mathematical representation, a mode can either stand for the displacement of a marker in one direction, a geometrical transformation of the marker-cluster, or a shape variation of the skin envelope. Results relative to one paradigmatic trial of the above-mentioned dataset were reported.

The STA deformation energy carried by each mode was determined as a percentage of the total energy for the proposed STA definitions and for the two body segment analysed. These energy are represented in Fig. 4.3 in a cumulative fashion. Using the equation 4.6, the total deformation energy normalized by the number of markers glued on the relevant segment were  $e_3/m_3 = 121.4 \text{ mm}^2$  and  $e_2/m_2 = 4.2 \text{ mm}^2$  for the thigh and the shank segment, respectively.

#### 4.4.2. In-vivo dataset

Experimental data provided by Reinschmidt et al., (1997) were used. Three male volunteers (age  $27.7 \pm 2.1$  years, mass  $85.5 \pm 9.6$  kg, stature  $186 \pm 10$  cm) were equipped with intracortical pins

inserted into lateral tibial condyle and lateral femoral condyle with three markers on each pin. Five skin markers were glued on the thigh and four on the shank. A system of three video-cameras was used to track marker trajectories (sampling frequency: 200 frames/s). Five running stance phase trials were acquired for each volunteer and an additional static trial was captured in the upright posture. Intracortical pin marker-clusters and calibrated anatomical landmarks were used to define relevant anatomical reference frames (AFs) (Cappozzo et al., 2005). STA vectors and reference knee kinematics were determined using intracortical pin data during running trials. For each segment  $i$ , a STA field  $\mathbf{V}_i(k)$  was generated.

Knee reference joint angles (flexion/extension, FE; abduction/adduction, AA; internal/external rotation, IER) were calculated at each frame of the trial using the relevant AFs and the Cardan convention (Grood and Suntay, 1983). Reference knee displacement components (lateral/medial, LM; anterior/posterior, AP; proximal/distal, PD) were calculated with a non-orthonormal projection on the joint coordinate system (*i.e.* the axes about which the joint angles were computed) of the vector going from the center of the epicondyles, as calibrated in the reference posture with respect to the femoral AF, to the same point calibrated with respect to the shank AF (Desroches et al., 2010).

#### 4.5. STA definition and interpretation

##### 4.5.1. Individual marker displacements

The first definition of the STA addresses the individual marker displacements relative to a bone-embedded coordinate system (Akbarshahi et al., 2010; Camomilla et al., 2009; Cappozzo et al., 1996; Kuo et al., 2011; Sati et al., 1996; Stagni et al., 2005; Tsai et al., 2011). This definition is used, for instance, in the STA models based on the observation that, during low impact motor tasks, marker displacements are quasi-linearly correlated with adjacent joint angles (Akbarshahi et al., 2010; Camomilla et al., 2013; Cappozzo et al., 1996; Hara et al., 2014).

For this STA definition, in the generalized mathematical formulation, the basis of vectors,  $\{\Phi_i^1, \dots, \Phi_i^l, \dots, \Phi_i^{3m_i}\}$ , is built *a priori*; the basis vectors,  $\Phi_i^l$ , correspond to the columns of a  $m_i$  by-  $3m_i$  identity matrix:

$$[\Phi_i^1, \dots, \Phi_i^l, \dots, \Phi_i^{3m_i}] = \begin{bmatrix} 1 & 0 & \dots & 0 & 0 \\ 0 & \ddots & 0 & 0 & 0 \\ \vdots & 0 & 1 & 0 & \vdots \\ 0 & 0 & 0 & \ddots & 0 \\ 0 & 0 & \dots & 0 & 1 \end{bmatrix}$$

(Eq. 4.7).

In this case, each amplitude,  $a_i^l(k)$ , represents the displacement of one skin marker along one of the axes of the segment coordinate system, and according to Eq. 4.4,  $\sqrt{\lambda_i^l}$  is the RMS of the displacement over time.

From a ranking perspective, the literature has already demonstrated that the skin marker displacements are different depending on marker localization on the segment and anatomical direction (Akbarshahi et al., 2010; Cappozzo et al., 1996; Kuo et al., 2011; Sati et al., 1996; Stagni et al., 2005; Tsai et al., 2011). Generally speaking, for the lower limb, skin marker displacements due to STAs are more pronounced for the thigh than the shank, for markers placed closer to the joints, but are similar in the anterior/posterior, proximal/distal and medial/lateral directions. Nevertheless, the RMS displacements are not very different among markers. Therefore, from a mode selection perspective, every mode may contribute similarly to the total deformation energy, and a large number,  $r_i$ , of these modes would be required to represent a substantial percentage,  $p$ , of the total deformation energy,  $e_i$  (Figs 4.3 and 4.4).

In fact, studies using this STA definition resulted in STA models that required a large number of parameters (Alexander and Andriacchi, 2001; Camomilla et al., 2013). For instance, in a hip joint kinematics driven model (Camomilla et al., 2013), each amplitude was expressed as a four parameter linear combination of the three joint angles ( $\alpha$ ,  $\beta$ , and  $\gamma$ ), resulting in a total of 12 parameters per marker:

$$a_i^l(k) = [\mathbf{h}_i^l] \begin{bmatrix} \alpha(k) \\ \beta(k) \\ \gamma(k) \\ 1 \end{bmatrix}$$

(Eq. 4.8).

In the numerical example obtained on *ex-vivo* data, as shown in Figs. 4.3 and 4.4, it can be seen that individual marker displacement along the superior/inferior direction (*i.e.*,  $y$  or longitudinal axis), in particular for the anterior skin-markers close to the distal joint (T5, S2 and S4), are shown to cause the largest part of the overall STA in both segments (about 55%).

When a paradigmatic energy threshold is chosen (*i.e.*, 95% of the total deformation energy of the STA occurring in a segment), nine and eight modes should be considered to represent such energy using the individual marker displacement definition for the thigh and shank segment, respectively.

In order to model the STA of the thigh ( $m_3 = 5$ ), as a liner combination of three independent variables as done in (Camomilla et al., 2013) using the equation 4.8, the number of parameters to be identified would be thirty-six using this definition.

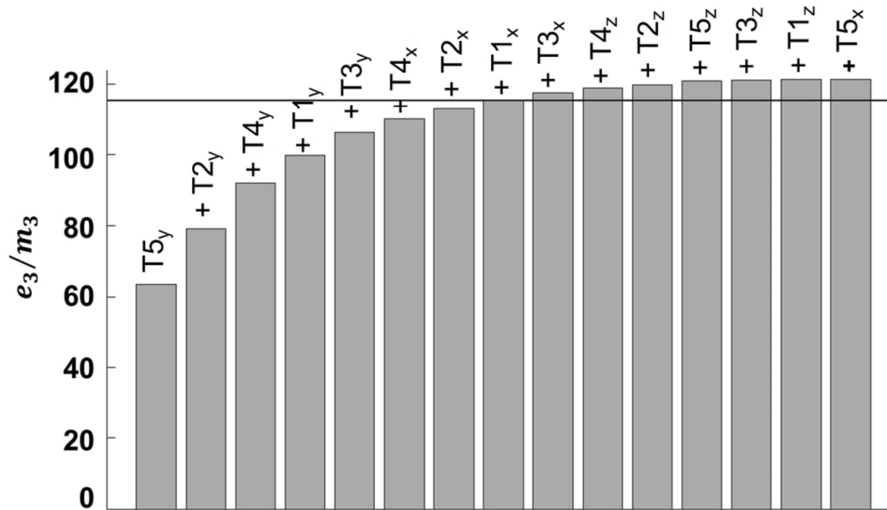


**Figure 4.3** – Cumulative deformation energy of the thigh STA ( $i = 3$ ), calculated using the equation 4.5, expressed in  $\text{mm}^2$  and normalized by the number of markers. The individual marker displacement definition is used. Modes are labelled with marker and, as subscript, axis along which the displacement occurs: anterior/posterior, x; superior/inferior, y; and medial/lateral, z. The energy threshold,  $p$ , is set at 95% and shown with an horizontal line.

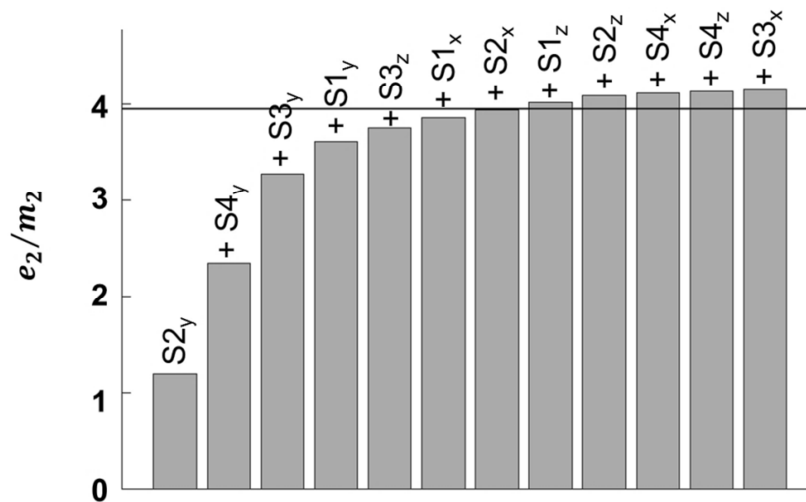


**Figure 4.4** – Cumulative deformation energy of the shank STA ( $i = 2$ ), calculated using the equation 4.5, expressed in  $\text{mm}^2$  and normalized by the number of markers. The individual marker displacement definition is used. Modes are labelled with marker and, as subscript, axis along which the displacement occurs: anterior/posterior, x; superior/inferior, y; and medial/lateral, z. The energy threshold,  $p$ , is set at 95% and shown with an horizontal line.

#### 4.5.2. Marker-cluster geometrical transformations

The second definition of the STA addresses the rigid and non-rigid transformations of the cluster of skin markers. In particular, the following geometrical transformations are accounted for: translation and rotation (De Rosario et al., 2013; Sangeux et al., 2006; Südhoff et al., 2007); translation, rotation and isometric homothety (Challis, 1995; Horn, 1987); translation, rotation, homothety and stretch (Ball and Pierrynowski, 1998; Dumas and Cheze, 2009; Grimpampi et al., 2014). This STA definition is the foundation of most optimal bone pose estimators (Andriacchi et al., 1998; Ball and Pierrynowski, 1998; Challis, 1995; Chèze et al., 1995; Dumas and Cheze, 2009; Söderkvist and Wedin, 1993; Taylor et al., 2005). Rigid transformation alone typically applies to marker-clusters mounted on rigid plates strapped to the body segment (Sangeux et al., 2006; Südhoff et al., 2007) and, in this case, only six transformations (three translations and three rotations) can be considered.

When dealing with the present STA definition, the basis of vectors,  $\{\Phi_i^1, \dots, \Phi_i^l, \dots, \Phi_i^{3m_i}\}$ , is built with a maximum of 12 vectors ( $l = 1, \dots, 12$ , three translations, three rotations, three homotheties and three stretches). Thus, if the number of skin markers is  $m_i > 4$ , the basis is truncated and only defines an STA subspace. One way to obtain the basis vectors,  $\Phi_i^l$ , is to separately apply each of the geometrical transformations (translation, rotation, homothety, or stretch) to the positions of all the skin markers embedded in the segment coordinate system (with the origin at the centroid of the marker-cluster for easier geometrical interpretation). The 12 unitary vectors,  $\Psi_i^l$  ( $l = 1, \dots, 12$ ), are first computed:

$$\Psi_i^l = \left[ \begin{array}{c} (R^l r_i^1 + t^l) - r_i^1 \\ \vdots \\ (R^l r_i^j + t^l) - r_i^j \\ \vdots \\ (R^l r_i^{m_i} + t^l) - r_i^{m_i} \end{array} \right] \left\| \begin{array}{c} (R^l r_i^1 + t^l) - r_i^1 \\ \vdots \\ (R^l r_i^j + t^l) - r_i^j \\ \vdots \\ (R^l r_i^{m_i} + t^l) - r_i^{m_i} \end{array} \right\| \quad (\text{Eq. 4.9}),$$

where

$r_i^j$  is the position of the skin markers  $j$  ( $j = 1, \dots, m_i$ ) embedded in the segment coordinate system, with the origin at the skin marker centroid for easier geometrical transformation;

$$R^l = \begin{bmatrix} 1 & 0 & 0 \\ 0 & 1 & 0 \\ 0 & 0 & 1 \end{bmatrix} \quad (l = 1, \dots, 3);$$

$$\mathbf{R}^4 = \begin{bmatrix} 1 & 0 & 0 \\ 0 & \cos\theta & -\sin\theta \\ 0 & \sin\theta & \cos\theta \end{bmatrix};$$

$$\mathbf{R}^5 = \begin{bmatrix} \cos\theta & 0 & \sin\theta \\ 0 & 1 & 0 \\ -\sin\theta & 0 & \cos\theta \end{bmatrix};$$

$$\mathbf{R}^6 = \begin{bmatrix} \cos\theta & -\sin\theta & 0 \\ \sin\theta & \cos\theta & 0 \\ 0 & 0 & 1 \end{bmatrix};$$

$$\mathbf{R}^7 = \begin{bmatrix} h & 0 & 0 \\ 0 & 1 & 0 \\ 0 & 0 & 1 \end{bmatrix};$$

$$\mathbf{R}^8 = \begin{bmatrix} 1 & 0 & 0 \\ 0 & h & 0 \\ 0 & 0 & 1 \end{bmatrix};$$

$$\mathbf{R}^9 = \begin{bmatrix} 1 & 0 & 0 \\ 0 & 1 & 0 \\ 0 & 0 & h \end{bmatrix};$$

$$\mathbf{R}^{10} = \begin{bmatrix} 1 & 0 & 0 \\ s & 1 & 0 \\ s & 0 & 1 \end{bmatrix};$$

$$\mathbf{R}^{11} = \begin{bmatrix} 1 & s & 0 \\ 0 & 1 & 0 \\ 0 & s & 1 \end{bmatrix};$$

$$\mathbf{R}^{12} = \begin{bmatrix} 1 & 0 & s \\ 0 & 1 & s \\ 0 & 0 & 1 \end{bmatrix};$$

$$\mathbf{t}^1 = \begin{bmatrix} t \\ 0 \\ 0 \end{bmatrix}, \mathbf{t}^2 = \begin{bmatrix} 0 \\ t \\ 0 \end{bmatrix}, \mathbf{t}^3 = \begin{bmatrix} 0 \\ 0 \\ t \end{bmatrix}, \text{ and } \mathbf{t}^l = \mathbf{0} \ (l = 4, \dots, 12);$$

$\theta = 0.2 \text{ rad}, h = 0.8, s = 0.2$  and  $t = 1$  (chosen arbitrarily).

Then, not all vectors obtained are orthogonal, and the basis  $\Phi_i^l, (l = 1, \dots, 12)$ , is finally obtained using a Gram–Schmidt procedure:

$$\Phi_i^l = \frac{\Psi_i^l - \sum_{p=1}^{l-1} \left( (\Psi_i^l)^T (\Psi_i^p) \right) (\Psi_i^p)}{\left\| \Psi_i^l - \sum_{p=1}^{l-1} \left( (\Psi_i^l)^T (\Psi_i^p) \right) (\Psi_i^p) \right\|}$$

(Eq. 4.10).

In the case of rigid transformation of the marker-cluster, the amplitudes divided by the number of markers ( $a_i^l(k)/m_i$ ) are associated with the components of translation (displacement of the centroid of the marker-cluster) and attitude vectors (Woltring, 1994).

From a ranking perspective, the literature has already demonstrated that, for a number of physical activities (Andersen et al., 2012; Barré et al., 2013; de Rosario et al., 2012; Grimpampi et al., 2014), rigid transformations (both translation and rotation) of the marker-cluster normally represent a greater portion of STAs than non-rigid transformations. Moreover, the anterior/posterior and medial/lateral translations (Südhoff et al., 2007), and axial rotations (Sangeux et al., 2006; Südhoff et al., 2007) seem more important than the other marker-cluster rigid transformations. Compensating only for marker-cluster translation has been shown to improve the estimation of joint centers using a functional approach (De Rosario et al., 2013). However, only compensating for the rigid transformations still yields a residual skin marker displacement ( $a_i^l(k)$  in the proposed generalized formulation) of considerable magnitude during gait, hopping, and cutting (Andersen et al., 2012). Therefore, it may be necessary to account for both rigid and non-rigid transformations, proceeding, however, to the selection of a moderate number of modes,  $r_i$  (eleven and six for the thigh and shank segment, respectively; Figs. 4.5 and 4.6). Despite a trend for the shank and thigh marker-clusters to undergo transformations as a function of knee flexion (Barré et al., 2013; Sangeux et al., 2006), it is not clear whether the amplitudes,  $a_i^l(k)$ , of the rigid and non-rigid transformations can be simply correlated with joint angles, as in Eq. 4.8, or with other biomechanical quantities as well.

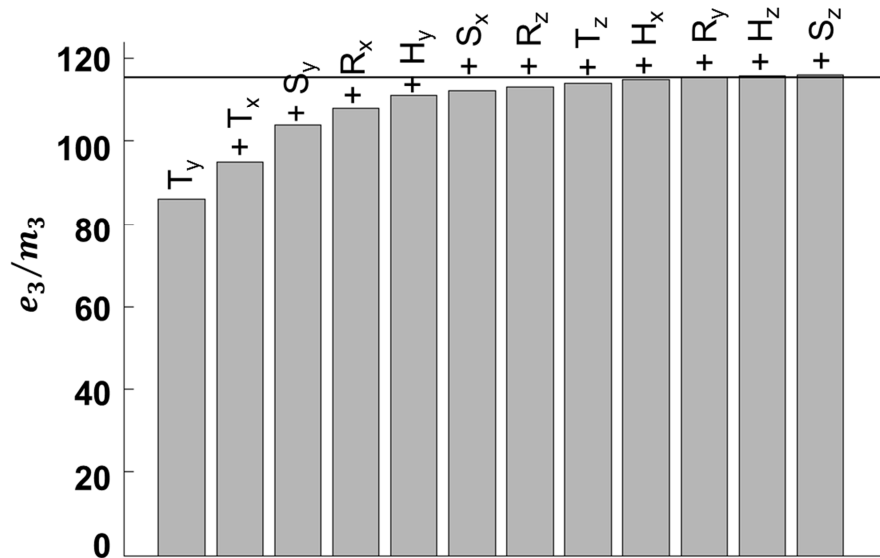


**Figure 4.5** – Cumulative deformation energy of the thigh STA ( $i = 3$ ), calculated using the equation 4.5, expressed in  $\text{mm}^2$  and normalized by the number of markers. The marker-cluster geometric transformation definition is used. Modes are labelled with the relevant transformation (translation, T; rotation, R; homothety, H; and stretching, S) and, as subscript, axis along which the displacement occurs: anterior/posterior, x; superior/inferior, y; and medial/lateral, z. The energy threshold,  $p$ , is set at 95% and shown with an horizontal line.

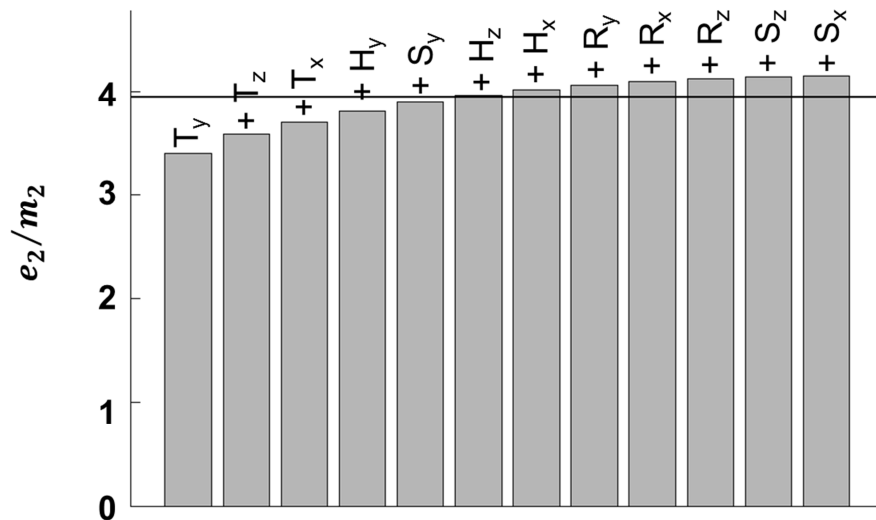


**Figure 4.6** – Cumulative deformation energy of the shank STA ( $i = 2$ ), calculated using the equation 4.5, expressed in  $\text{mm}^2$  and normalized by the number of markers. The marker-cluster geometric transformation definition is used. Modes are labelled with the relevant transformation (translation, T; rotation, R; homothety, H; and stretching, S) and, as subscript, axis along which the displacement occurs: anterior/posterior, x; superior/inferior, y; and medial/lateral, z. The energy threshold,  $p$ , is set at 95% and shown with an horizontal line.

### 4.5.3. Skin envelope shape variations

The third definition of the STA addresses the ensemble of markers associated with a bony segment and assumes that the STA field represents the change of configuration of a continuum (*i.e.*, the skin markers are considered Lagrangian material points). The modes representing the shape variations have been previously identified using either eigen decomposition (Dumas et al., 2009) or principal component analysis (PCA) (Andersen et al., 2012).

In the proposed generalized mathematical formulation, the sample covariance matrix,  $\mathbf{S}_i$ , is first calculated as:

$$\mathbf{S}_i = \frac{1}{n} [\mathbf{V}_i(1) \quad \cdots \quad \mathbf{V}_i(k) \quad \cdots \quad \mathbf{V}_i(n)] [\mathbf{V}_i(1) \quad \cdots \quad \mathbf{V}_i(k) \quad \cdots \quad \mathbf{V}_i(n)]^T \quad (\text{Eq. 4.11}),$$

and the basis of vectors,  $\{\Phi_i^1, \dots, \Phi_i^l, \dots, \Phi_i^{3m_i}\}$ , is computed by a proper orthogonal decomposition (Chatterjee, 2000; Kerschen et al., 2005) of  $\mathbf{S}_i$ ; the basis vectors,  $\Phi_i^l$ , are the eigenvectors of:

$$\mathbf{S}_i = [\Phi_i^1, \dots, \Phi_i^l, \dots, \Phi_i^{3m_i}] \begin{bmatrix} \lambda_i^1 & 0 & \cdots & 0 & 0 \\ 0 & \ddots & 0 & 0 & 0 \\ \vdots & 0 & \lambda_i^l & 0 & \vdots \\ 0 & 0 & 0 & \ddots & 0 \\ 0 & 0 & \cdots & 0 & \lambda_i^{3m_i} \end{bmatrix} [\Phi_i^1, \dots, \Phi_i^l, \dots, \Phi_i^{3m_i}]^T \quad (\text{Eq. 4.11}).$$

Building  $\mathbf{S}_i$  directly from  $\mathbf{V}_i(k)$  allows the direct association of the total deformation energy  $e_i$  with the mean over time of the square of the STA vectors,  $\mathbf{v}_i^j(k)$ . The deformation energy,  $\lambda_i^l$ , of each mode  $l$  is the eigenvalue corresponding to the eigenvector,  $\Phi_i^l$ , but Eq. 4.4 can alternatively be used to determine it.

From a ranking perspective, the literature has already proposed examples in which an exponential decrease in the contribution of the ordered modes to the representation of the STA occurs. More specifically, this exponential decrease was observed in the principal components rather than in the modes (Andersen et al., 2012), but PCA and proper orthogonal decomposition are equivalent methods for feature extraction and data reduction (Chatterjee, 2000; Kerschen et al., 2005). In addition, it has been shown that four principal components may represent 95% of the STA vector,  $\mathbf{v}_i^j(k)$ , variability during walking (Andersen et al., 2012). In other words, a few  $r_i$  modes can

represent a substantial percentage,  $p$ , of the total deformation energy,  $e_i$  (one and two modes for the thigh and shank segment, respectively). Based on this definition, it is likely that an STA model with a very limited number of parameters can be developed. However, such a model requires the assumption that the basis of vectors,  $\{\Phi_i^1, \dots, \Phi_i^l, \dots, \Phi_i^{3m_i}\}$ , can be identified for each subject and motor task. Indeed, especially in this third class of STA definitions, the computation of the basis relies on the covariance matrix,  $\mathbf{S}_i$ , and cannot be built without knowing the STA field (Eq. 4.11).

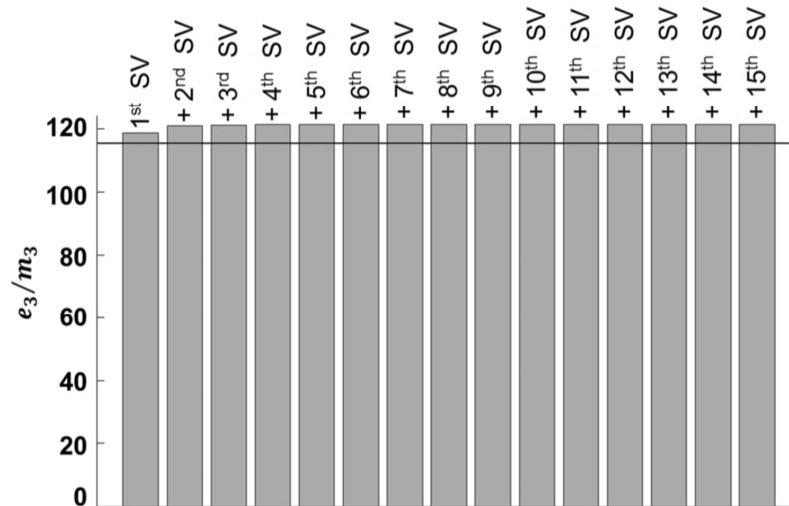


**Figure 4.7** – Cumulative deformation energy of the thigh STA ( $i = 3$ ), calculated using the equation 4.5, expressed in  $\text{mm}^2$  and normalized by the number of markers. The skin envelope shape variation definition is used. Modes are labelled with their rank. The energy threshold,  $p$ , is set at 95% and shown with an horizontal line.

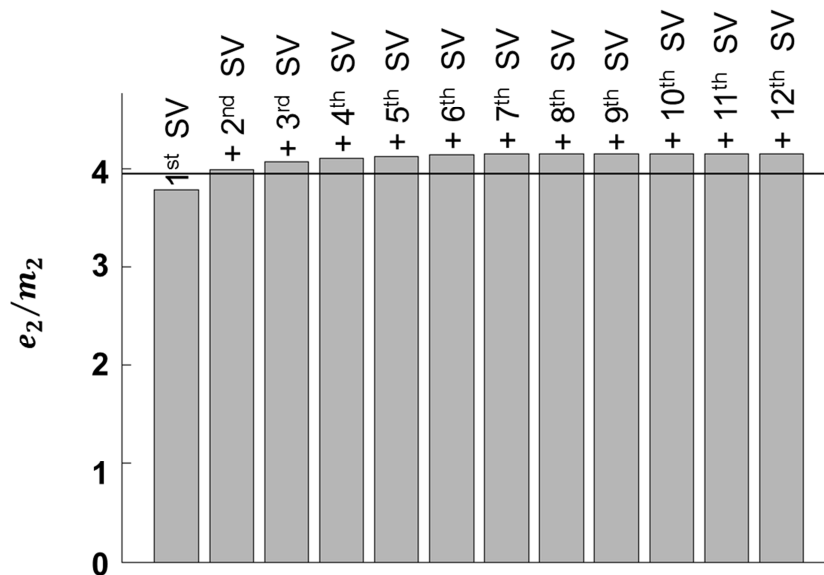


**Figure 4.7** – Cumulative deformation energy of the shank STA ( $i = 2$ ), calculated using the equation 4.5, expressed in  $\text{mm}^2$  and normalized by the number of markers. The skin envelope shape variation definition is used. Modes are labelled with their rank. The energy threshold,  $p$ , is set at 95% and shown with an horizontal line.

#### 4.6. STA mathematical representations: impact on knee kinematics

For each STA definition,  $V_i(k)$  was split into additive modes,  $a_i^l(k)\Phi_i^l$ , that were ranked. As a paradigmatic case, for each definition, a number of modes ( $r_i$ ) was selected that represented the 95% of the STA deformation energy (Table 4.1) and the residual STA (5%) fields computed  $\tilde{V}_i(k)$ .

Knee kinematics was calculated, through an SVD approach, using skin marker positions embedding  $V_i(k)$  (raw data: RD) or  $\tilde{V}_i(k)$  (STA virtually compensated data) associated with each STA definition (MD, GT, SV). For each of the four kinematics estimates thus obtained, the rms difference with respect to the reference kinematics was calculated (rmse), as shown in Figure 4.8.

Segment	STA definitions		
	MD	GT	SV
Thigh	11	10	3
Shank	9	6	2

**Table 4.1** – Median  $r_i$  values of modes for each STA definition that represent the 95% of the phenomenon. Statistics performed over five trials and three volunteers.

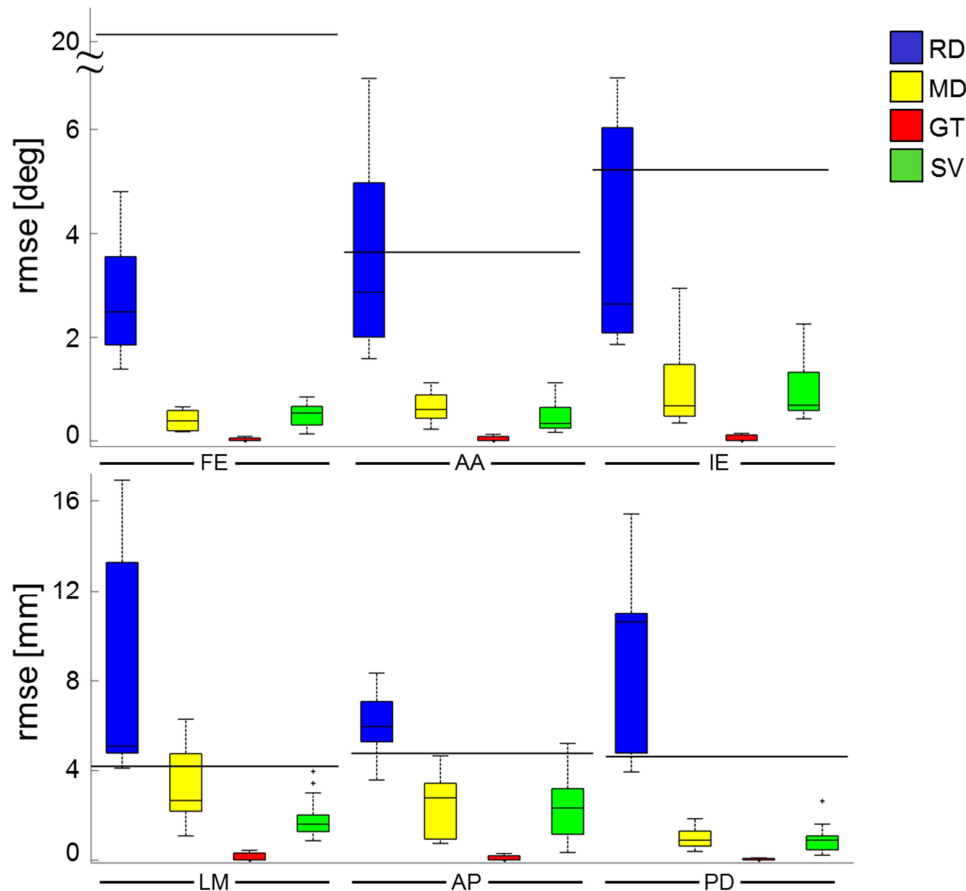


**Figure 4.8** – Box-plots (minimum, lower quartile, median, upper quartile, and maximum) of rmse values for knee kinematics (flexion/extension, **FE**; ab/adduction, **AA**; internal/external rotation, **IE**; lateral/medial, **LM**; anterior/posterior, **AP**; proximal/distal, **PD**) obtained with **RD** (*i.e.*,  $V_i(k)$ ) and each STA definition. With thick black lines, median reference rms kinematic values are shown. Statistics performed over five trials and three volunteers. Outliers are also shown.

#### 4.1. Single ranking of thigh and shank modes: impact on knee kinematics

For each STA definition, the contribution of each STA mode was evaluated. The modes were ranked according to their relative contribution (*i.e.*, deformation energy) to the whole phenomenon. For each segment  $i$ , the deformation energy of each mode  $l$  was calculated using the equation 4.4. The total deformation energy (*i.e.*, the energy due to all  $3*m_i$  modes) of each segment  $i$ , was normalized by the relative number of markers,  $m_i$ . This normalization allowed to perform a single ranking in a decreasing order of both thigh and shank modes and the normalized deformation energies ( $\lambda_i^l/m_i$ ) were summed one by one (*i.e.*, cumulative representation). Ranked modes were sequentially removed from the respective thigh or shank STA field, mode by mode, according to the relative contribution to the whole phenomenon. Cumulative deformation energy values of the ranked thigh and shank modes for the mentioned STA definitions are shown in Fig. 4.9.

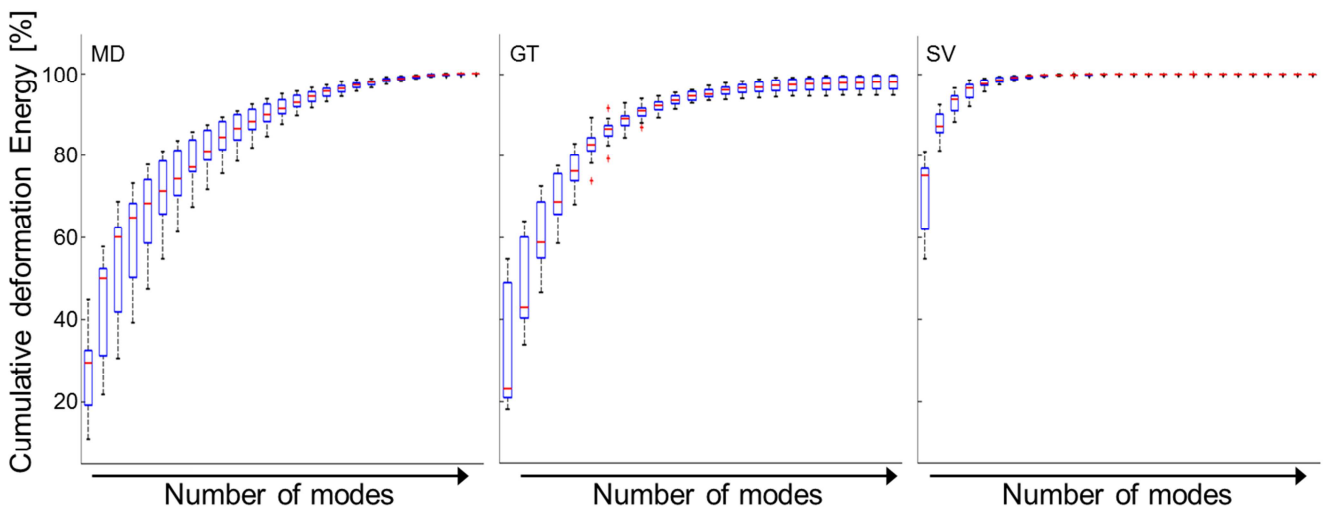


**Figure 4.9** – Box-plots (minimum, lower quartile, median, upper quartile, and maximum) of cumulative deformation energy, in percentage, normalized by the number of markers and the total deformation energy, for the thigh and shank segments, for the ranked modes (for each trial and volunteer) using the MD, GT and SV definition.

For each definition, residual STA fields were obtained in an iterative way

$$\begin{aligned}
 \tilde{\mathbf{V}}_i^1(k) &= \mathbf{V}_i(k) - a_i^1(k) \Phi_i^1 \\
 \tilde{\mathbf{V}}_i^2(k) &= \tilde{\mathbf{V}}_i^1(k) - a_i^2(k) \Phi_i^2 \\
 &\vdots \\
 \tilde{\mathbf{V}}_i^{3*m_i}(k) &= \tilde{\mathbf{V}}_i^{(3*m_i)-1}(k) - a_i^{3*m_i}(k) \Phi_i^{3*m_i}
 \end{aligned}$$

(Eq. 4.12)

thus representing an STA residual field with decreasing energy content.

Knee kinematics were computed from raw data (*i.e.* from  $\mathbf{V}_i(k)$ ) and for each STA definition (MD, GT, SV) for STA models with increasing level of approximation, *i.e.* for residual STA field with a decreased energy content, as obtained with Eq. 4.12. Using an SVD approach, technical reference frames were obtained from skin marker-clusters ( $\mathbf{V}_i(k)$  or  $\tilde{\mathbf{V}}_i(k)$ ). To define AFs affected by residual STA fields, calibrated anatomical landmarks and technical reference frames were used to calculate knee kinematics (Cappozzo et al., 2005). For each of the kinematics estimates thus obtained, the rms distance from the reference kinematics was calculated. The effect of the STA field reduction was represented normalizing the rms distance of the STA propagation to knee kinematics with the rms value of the reference one (RMSE%).

Median RMSE% values, for knee kinematics calculated using raw data (*i.e.*, from  $\mathbf{V}_i(k)$ ), were 11% (IQR: 7%), 79% (IQR: 60%), 51% (IQR: 14%), for FE, AA, IER knee angles, respectively; for the same angles, reference median rms values were 22, 4 and 5 deg, respectively. Concerning LM, AP, PD knee displacements, RMSE% median values were 114% (IQR: 347%), 118% (IQR: 124%), 238% (IQR: 567%), and reference median rms values were 4, 5 and 5mm, respectively.

RMSE% values obtained for the knee kinematics using the proposed STA definitions and increasing levels of STA approximation are shown in Fig. 4.10-4.12. Results are shown only in the range from 0% to 100%, assuming that higher RMSE% values would in any case lead to totally unreliable kinematic estimates.

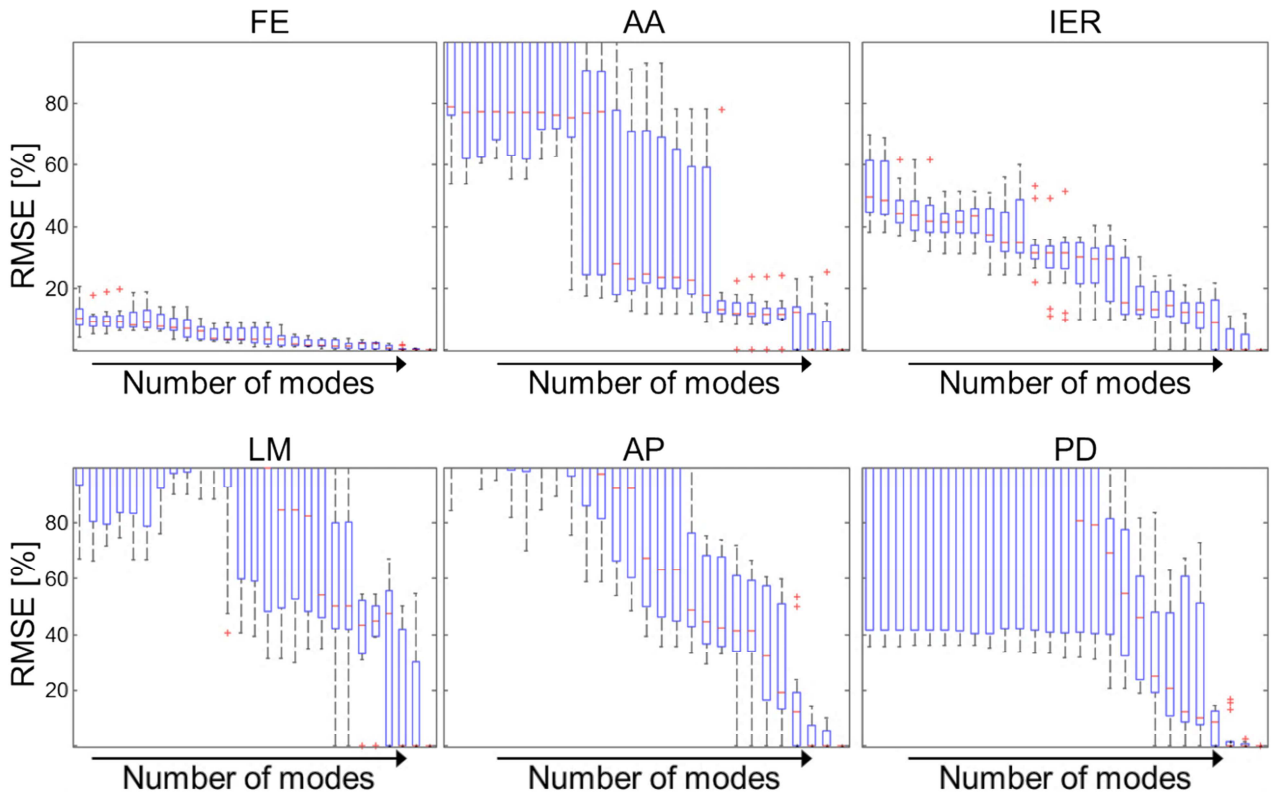


**Figure 4.10** – Box-plots of RMSE% values for the knee kinematics using the MD definition, removing from  $V_i(k)$  the ranked thigh and shank modes.

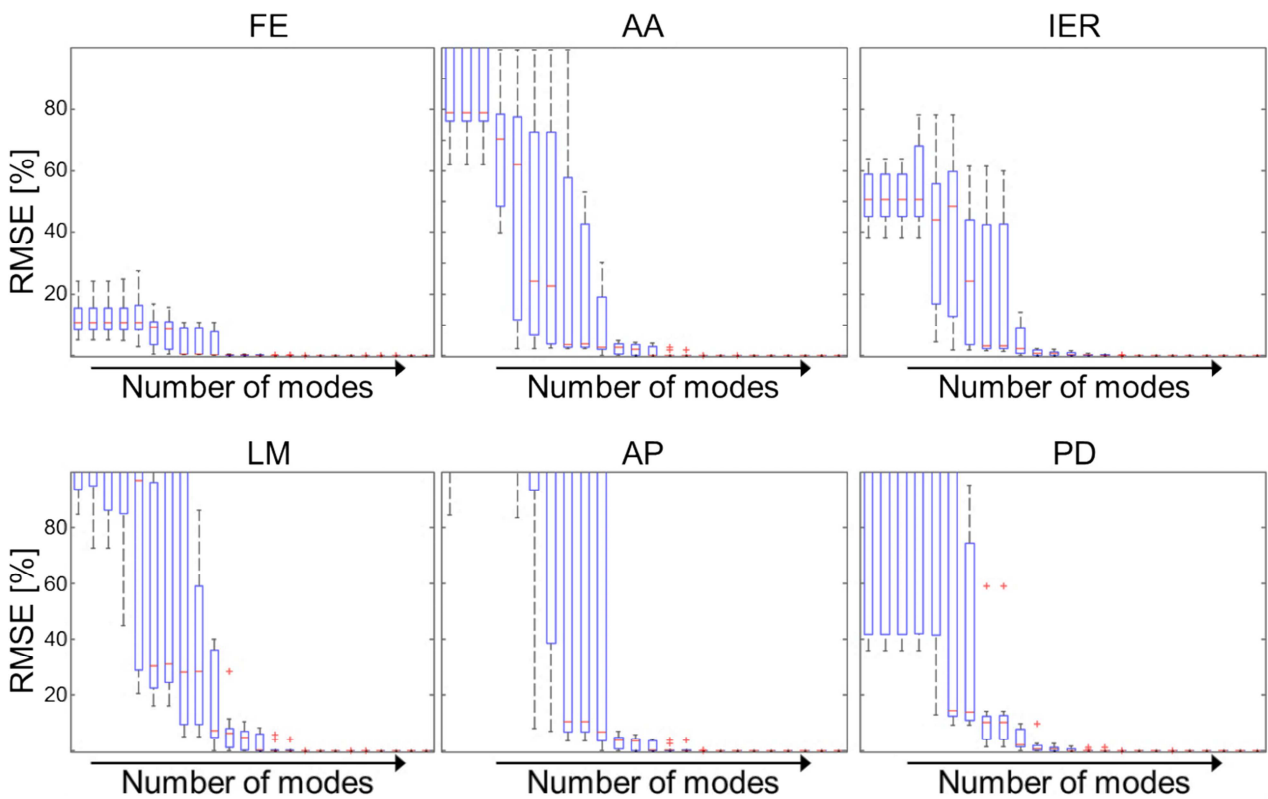


**Figure 4.11** – Box-plots of RMSE% values for the knee kinematics using the GT definition, removing from  $V_i(k)$  the ranked thigh and shank modes.

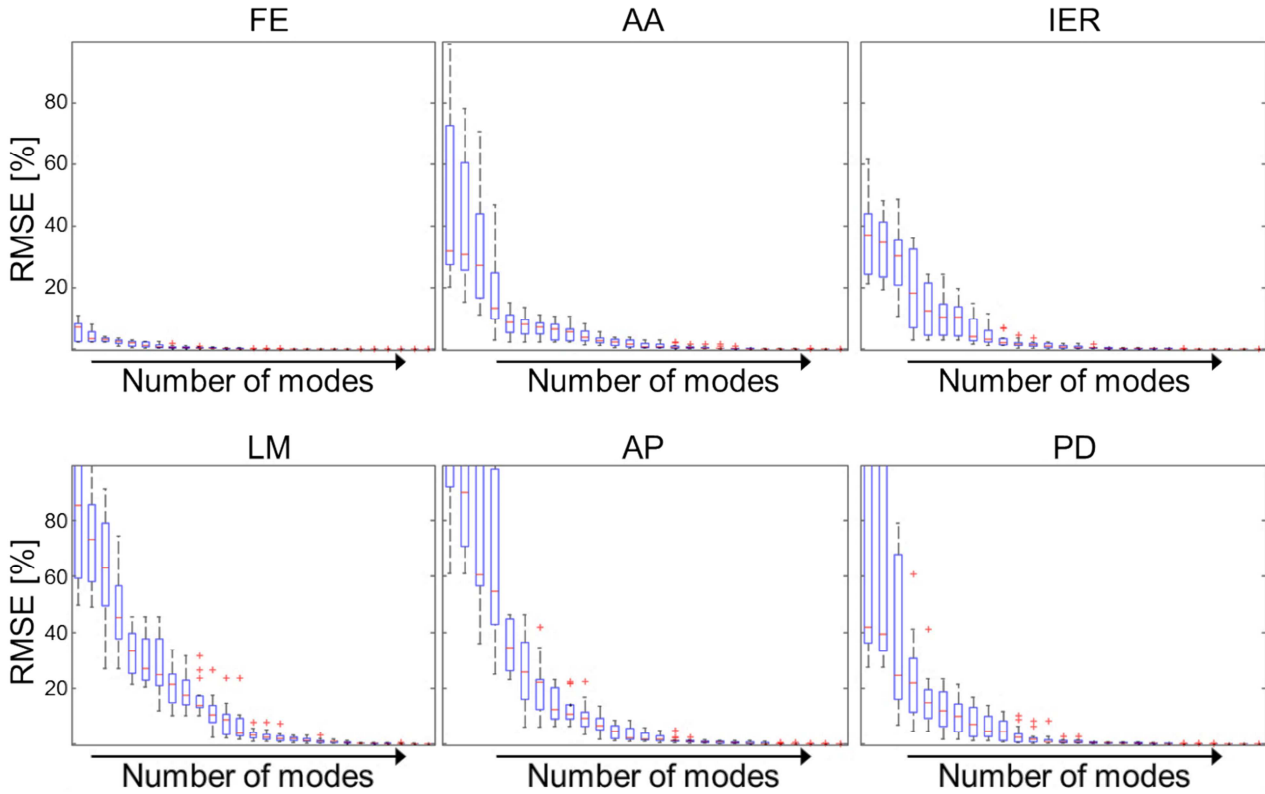


**Figure 4.10** – Box-plots of RMSE% values for the knee kinematics using the SV definition, removing from  $V_i(k)$  the ranked thigh and shank modes.

## 4.2. Discussion

### 4.2.1. STA definitions

The present study categorized the definition of the STA into three classes: individual marker displacements, marker-cluster geometrical transformations, and skin envelope shape variations. The decomposition of the STA vector on a basis of orthogonal vectors allowed these three classes to be embedded in a generalized mathematical formulation. The choice of the basis of vectors can be an arbitrary combination of the previous decompositions or any other basis, on the condition that the vectors are orthogonal. For instance, some authors have proposed to describe STAs with a marker-cluster rigid transformation plus some relative individual marker displacements (Barré et al., 2013; de Rosario et al., 2012). Furthermore, the basis of vectors,  $\{\Phi_i^1, \dots, \Phi_i^l, \dots, \Phi_i^{3m_i}\}$ , for the second class of STAs aims at representing translation, rotation, homothety, and stretch although these transformations are not independent and require a vector orthogonalization (Gram–Schmidt) procedure. Nevertheless, the proposed classes (and corresponding modes) match different possible

views of an STA that were found in the literature: point kinematics, linear algebra for mapping, and continuum mechanics. All definitions are linear.

#### 4.2.2. Ranking and selection of modes

The representation of an STA by modes,  $a_i^l(k)\Phi_i^l$ , directly elicits ranking and selection procedures based on the evaluation of deformation energy. Although, in the general case, the physical meaning of the total deformation energy remains unclear (Chatterjee, 2000; Kerschen et al., 2005), in the present study,  $e_i/m_i$  represents the mean over time of the square of the STA vectors,  $v_i^j(k)$ . Therefore, the ranking and selection procedure allows understanding of what are the main contributors to this mean square value ( $\sqrt{e_i/m_i}$  is the RMS of the STA vectors generally reported in the literature). The contribution is quite easy to assess when considering the individual marker displacements, but becomes not trivial for marker-cluster geometrical transformations and skin envelope shape variations. In the proposed generalized formulation,  $e_i$  can be computed in the same way for any STA definition. For the sake of interpretation, this deformation energy,  $e_i$ , may be more convenient than variability as provided by a PCA (Andersen et al., 2012). Unlike with PCA, the basis of vectors,  $\{\Phi_i^1, \dots, \Phi_i^l, \dots, \Phi_i^{3m_i}\}$ , for the first and second class of STA definition can be built *a priori* or using arbitrary geometrical transformations (Eq. 4.7, 4.9 and 4.10).

Finally, as the three classes are embedded in the same formulation, the modal representation allows simple interclass ranking (individual marker displacements vs. marker-cluster geometrical transformations vs. skin envelope shape variations) based on the use of deformation energy. Therefore, the choice of the STA definition to be used can be based on the number of modes required to represent a given percentage,  $p$ , of the deformation energy,  $e_i$ . This may translate into a limited number of parameters involved in the STA model. When thigh STA ( $m_3 = 5$ ) are modelled as a linear combination of three independent variables using the equation 4.8 (Camomilla et al., 2013), the number of parameters to be identified with a calibration procedure would be thirty-six using the individual marker displacements, twenty-four using the marker-cluster geometrical transformation, and four using the skin envelope shape variations. Of course, the number of parameters indicated above depends on the amount and on the position of skin markers located on each segment, since this define the STA field and could also influence how the deformation energy is distributed.

Concerning the ranking and selection of modes, several considerations can be made based on published information and the numerical example provided here.

First, the RMS skin marker displacements are not highly ordered (Akbarshahi et al., 2010; Peters et al., 2010). Therefore, a large number of displacements may have to be selected to build a representative STA model, as is the case with the models already proposed using this STA definition (Alexander and Andriacchi, 2001; Camomilla et al., 2013) that involves  $3m_i$  modes.

Second, the rigid transformations of the marker-cluster represent a greater portion of the STA (Andersen et al., 2012; Barré et al., 2013; Grimpampi et al., 2014). One of the implications of this greater rigid contribution to the STA is that the classical least squares bone pose estimators cannot fully compensate for it (Andriacchi et al., 1998; Ball and Pierrynowski, 1998; Challis, 1995; Chèze et al., 1995; Dumas and Cheze, 2009; Heller et al., 2011; Söderkvist and Wedin, 1993). In addition, the non-rigid transformations of the STA cannot be neglected (Andersen et al., 2012; Grimpampi et al., 2014). Therefore, the geometrical transformations of the marker-cluster may have to include, beside the three translations and three rotations, also homothety and/or stretch. These results shown a number of parameters which is lower than those obtained using the individual marker displacements definition (eleven and six modes for the thigh and shank segment, respectively). A model based on this STA definition has been recently proposed in the literature (De Rosario et al., 2013).

Third, after skin envelope shape variations have been properly ordered (Andersen et al., 2012), a low number of them may need to be selected to build a representative STA model (one and two modes for the thigh and shank segment, respectively). However, currently, no model based on this STA definition has been proposed in the literature.

Presently, the number and position of skin marker displacements, the number and type of marker-cluster transformations, and the number and form of skin envelope shape variations representative of a given percentage,  $p$ , of  $e_i$  are not fully established and are worth being determined in further studies.

#### 4.2.3. Towards STA mathematical modelling

The interpretation, in the framework of the generalized formulation, of the STA definitions reported in the literature opens the way for new STA models. For instance, the joint kinematics driven STA model recently proposed for individual marker displacements (Camomilla et al., 2013), which uses an exceedingly high number of parameters, may now be extended to marker-cluster transformations or skin envelope shape variations. Moreover, the modal representation (Eq. 4.2) may be incorporated in single-body (Alexander and Andriacchi, 2001) and multi-body optimization

(Richard et al., 2012), where the amplitudes,  $a_i^l(k)$ , (or some parameters,  $h_i^l$ , as in Eq. 4.8) can be estimated together with the bone pose. For that, to build the selected basis of vectors,  $\{\Phi_i^1, \dots, \Phi_i^l, \dots, \Phi_i^{3m_i}\}$ , without knowing the STA vectors,  $v_i^j(k)$ , the positions of the skin markers embedded in the segment coordinate systems must be obtained by calibration in a reference posture (Cappozzo et al., 1995; Donati et al., 2007) and by the application of selected arbitrary geometrical transformations to these positions. Similarly, multiple calibrations (Cappello et al., 1997; Lucchetti et al., 1998) can be used to estimate the STA vectors,  $v_i^j(k)$ , as a function of the joint angles. Furthermore, the estimation of the STA vectors,  $v_i^j(k)$ , from the uncorrelated local inter-marker movements (Camomilla et al., 2009) can be considered a promising alternative approach.

#### 4.2.4. STA reduction and knee kinematics

Identify a STA definition and approximation able to grant reasonable joint kinematics accuracy while using a feasible number of parameters, is one of the aim of this chapter. The selection of a STA definition and its modal representation allows for a trade-off between virtual STA compensation effectiveness and number of modes, that is number of parameters involved, and, therefore, mathematical tractability of the bone-pose estimator. The GT definition grants for the best knee kinematics estimate accuracy, but uses 6-10 modes; while the SV definition allows for a slightly worst accuracy, but uses only 2-3 modes.

In addition, the propagation to knee kinematics of STA residual fields with decreasing energy content was also evaluated for three STA definitions. The RMSE% values of the knee kinematics have been shown to improve, when removing an increasing number of modes from  $V_i(k)$ , for all the proposed definitions, but with different decreasing patterns. The results shown in the section 4.1 suggest that an appropriate number and type of modes could be selected by setting a threshold for the knee kinematics error reduction. To obtain a RMSE% value lower than 10%, all modes (27) are necessary for the MD definition (Fig. 4.10), whereas eleven modes for GT (Fig. 4.11) and fourteen modes for SV (Fig. 4.12) are sufficient. These modes represent 100%, 94% and 99% of the total STA deformation energy, for MD, GT and SV definition, respectively (Fig. 4.9). Therefore, MD definition does not seem to be the most appropriate modal approach to be embedded in bone pose estimators, exhibiting slower trend and moderate RMSE% value reduction as the number of modes increases, as compared to the other two definitions. The latters, instead, allow for an acceptable trade-off between STA compensation effectiveness and number of modes, relative to knee kinematics accuracy and the number of parameters. This opens an interesting scenario for further

work to be performed by using these latter STA definitions in STA models for bone-pose estimators.

## 5. Chapter 5

# “GEOMETRICAL TRANSFORMATION OF A MARKER-CLUSTER AND ITS IMPACT ON BONE POSE ESTIMATION”

### Symbols and Nomenclature

Symbols	$j$	skin marker ( $j = 1, \dots, m$ )
	$k$	sampled instant of time ( $k = 1, \dots, n$ )
	$\mathbf{p}$	reference bone position
	$\theta$	attitude angle (modulus of the attitude vector $\boldsymbol{\theta}=\theta\mathbf{n}$ )
	$\mathbf{v}^j(k)$	STA vector of the skin marker $j$ glued on the segment
	$\mathbf{V}(k)$	STA field of the segment
	$a^l(k)\boldsymbol{\Phi}^l$	mode $l$
	$\boldsymbol{\Phi}^l$	mode direction
	$a^l(k)$	mode amplitude
	$e$	error in the skin marker trajectories reconstruction
	$E_{RM}$	STA energy of the cluster rigid motion
	$E_{NRM}$	STA energy of the cluster non-rigid motion
	$R_{NRM}$	amplification factor
	$\text{rmse}_\theta$	root mean square difference between the artefact-affected and reference AF
	$\text{rmse}_{\text{px}}$	root mean square difference between the artefact-affected and reference AF
	$\text{rmse}_{\text{py}}$	root mean square difference between the artefact-affected and reference AF
$\text{rmse}_{\text{pz}}$	root mean square difference between the artefact-affected and reference AF	
Nomenclature	STA	soft tissue artefact
	PS	procrustes superimposition
	GT	marker-cluster geometrical transformations
	RM	rigid motion
	NRM	non-rigid motion
	BPE	bone pose estimation
	AF	anatomical reference frame
	dof	degrees of freedom
MCS	Monte Carlo simulation	

## 5.1. Introduction

When the bone pose is estimated using skin markers and a stereophotogrammetric system during the execution of a motor task, a number of crucial problems arise, among which the soft tissue artefact (STA) movement with respect to the underlying bone is regarded as the major one. Effective countermeasures are still to be made available (Leardini et al., 2005; Peters et al., 2010).

The pose of a bone is typically reconstructed using the instantaneous position of at least three non-aligned skin markers (cluster), glued on the segment of interest, and their trajectories are used as input for a bone pose estimator. A typical pose estimator is based on simple least squares minimization, between a cluster model and the instantaneous position of the cluster, such as used in the Procrustes superimposition (PS) approach (Dryden and Mardia, 2002), which is based on the use of the shape analysis (Bookstein, 1991). The obtained pose is affected by the real motion between the skin markers and the underlying bone: during the execution of a motor task, each skin marker glued on the body segment undergoes a displacement with respect to the underlying bone for the interposition of soft tissue between them. This motion is position-, task- and subject-dependent: a generalization of this phenomenon is difficult (Leardini et al., 2005; Peters et al., 2010). A sequence of independent geometrical transformations can be used to describe the movement of the cluster with respect to the underlying bone: a translation, a rotation, a change of size and shape of the cluster. Recently, Dumas et al., 2014a, using the modal approach marker-cluster geometrical transformations (GT), describe this movement with twelve additive and independent modes. In particular, there are three modes which define each geometrical transformation: translation, rotation, homothety (*i.e.*, change of size) and stretch (*i.e.*, change in shape). Therefore, the cluster rigid motion (RM) can be described by the composition of translation and rotation modes, while the composition of the other modes describe the cluster non-rigid motion (NRM).

Pose estimators are typically based on a PS approach (Cappozzo et al., 1997; Söderkvist and Wedin, 1993), which address only the cluster NRM. In the perspective to compensate for STA, several other approaches were developed which, similarly, neglect the cluster RM (Alexander and Andriacchi, 2001; Andriacchi et al., 1998; Challis, 1995; Chèze et al., 1995; Heller et al., 2011; Taylor et al., 2005) and produce no significant improvement in the pose estimation (Cereatti et al., 2006). The NRM has been extensively investigated, using different metrics: the variation in the inertia tensor in the Point Cluster Technique (Alexander and Andriacchi, 2001; Andriacchi et al., 1998; Camomilla et al., 2009), or the variation of the inter-marker distances (Gao and Zheng, 2008).

Moreover, Stagni and Fantozzi, 2009 showed that the NRM was not a good indicator of the RM components for the thigh and shank segments, as was hypothesized by Peters et al., 2009.

In a compensation perspective, the RM component can be taken into consideration through a multiple or a double calibration procedure. Such compensation can be achieved interpolating the position of the anatomical landmarks in the relevant frame minimizing the relative displacement between the skin markers and the underlying bone (Cappello et al., 2005, 1997). Recent studies quantified these cluster STA components in different motor tasks (Andersen et al., 2012; Barré et al., 2013; Benoit et al., 2015; de Rosario et al., 2012; Grimpampi et al.), showing that the cluster RM is predominant with respect to the cluster NRM. The results obtained in these studies suggest that the cluster RM is the main component which affect the estimation of the bone pose.

Based on this observation, it is concluded, either explicitly or implicitly, that cluster NRM has a limited impact on bone pose estimation (BPE) and that STA compensation should concentrate on the cluster RM. This chapter disputes the message carried by this statement and demonstrates that the cluster NRM does not have a limited effect on BPE accuracy, but, rather, it has no effect whatsoever and that this is the case independently from its magnitude relative to the cluster RM. For this reason, the only STA component to be compensated for is the cluster RM.

Simulated and *in-vivo* data were used to empirically demonstrate that the cluster RM is the only component that affect the bone pose estimation when the PS approach is used, independently to its amplitude with respect to the cluster NRM component. To assess the impact that cluster NRM has on BPE, a Monte Carlo Simulation framework was used to generate STA fields that have the same cluster RM and amplified cluster NRM. Moreover, artefact-free skin marker trajectories during gait were simulated (Dumas and Cheze, 2009). Realistic thigh artefacts were generated as linear combination of proximal and distal kinematics (as presented in the *Chapter 3*) and were added to the above-mentioned marker trajectories. The above-mentioned GT modal approach was used to assess the cluster RM (translation and rotation modes) and its counterpart (*i.e.*, cluster NRM: homothety and stretch modes) of the simulated STA. The amplitude of the NRM component was randomly amplified, unchanging the RM component, and the variations in thigh pose, as estimated using the PS approach, were evaluated. Therefore, the following question will be answered: bone pose estimator should address the cluster RM for its magnitude with respect to its counterpart or is it independent to their relative amplitude? This answer will be a useful information for future studies aiming at optimal bone pose estimators.

## 5.2. Material and Method

### 5.2.1. Gait data

Reference gait data were generated (Dumas and Cheze, 2009): pelvic-bone, femur, and tibia anatomical frames (AFs) were defined (Figure 5.1) and were used to compute hip and knee kinematics (Grood and Suntay, 1983). Femur pose was generated modelling the hip as a spherical hinge and using reference hip joint angular kinematics during gait. The reference position ( $\mathbf{p}$ ) and the modulus of the attitude vector  $\boldsymbol{\theta} = \theta \mathbf{n}$ , *i.e.* the attitude angle  $\theta$ , were used to represent the thigh AF pose. Twelve skin marker reference positions were defined in the thigh AF and their trajectories, not affected by STA (nominal), were generated in the global coordinate system using the thigh reference pose.

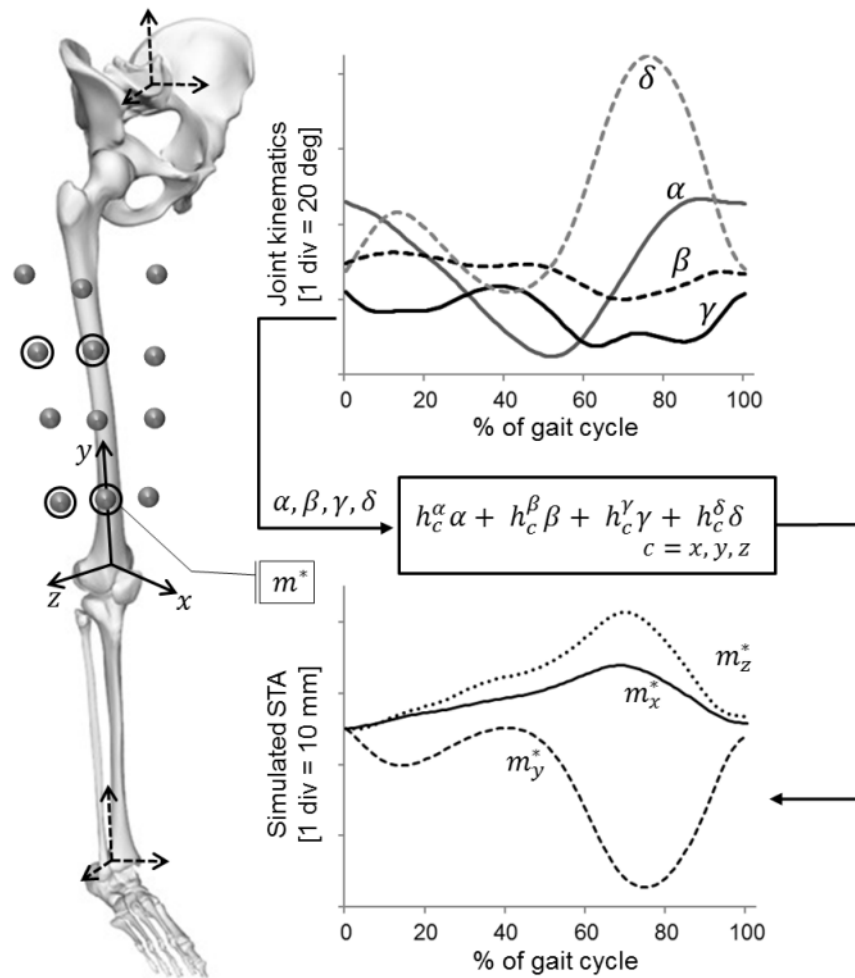


**Figure 5.1** – The location of the skin-marker on the thigh segment is shown. The skin-markers with a double circle are those used in the simulation procedure. Relevant hip ( $\alpha$  – flexion/extension,  $\beta$  – ab/abduction,  $\gamma$  – internal/external rotation) and knee ( $\delta$  – flexion/extension) angles measured during the gait and used as input for the soft tissue artefact modelling during the locomotion are shown. The STA on each skin-marker is defined using the  $h$  model parameters along the  $c$  direction ( $c = x, y, z$ ) as linear combination of the proximal and distal joint kinematics ( $\alpha, \beta, \gamma, \delta$ ). An example of the simulated STA in the femur AF for the skin marker indicated with  $m^*$  and generated with the STA model is also shown. The pelvic-bone, femur, and tibia frames are also indicated.

Artefact affected skin-marker trajectories were simulated, at each sampled instant of time  $k$  ( $k=1, \dots, n$ ), by modelling the STA vectors of the  $j$ -th ( $j=1, \dots, m$ ) skin marker,  $\mathbf{v}^j(k)$ , as a linear combination of the measured proximal and distal joint kinematics (*Chapter 3*, see equation in Figure 5.1). Model parameters were calibrated during an *ex-vivo* bi-articular flexion-extension (shown in Table 3.1, for the specimen S1, in the *Chapter 3*) were used. The hip and knee flexion/extension was chosen as calibrating movement for its range of motion similar to locomotion. The thigh STA field,  $\mathbf{V}(k)$ , was built using the STA vectors  $\mathbf{v}^j(k)$  of all markers (twelve markers depicted in Figure 5.1) as:

$$\mathbf{V}(k) = \begin{bmatrix} \mathbf{v}^1(k) \\ \vdots \\ \mathbf{v}^j(k) \\ \vdots \\ \mathbf{v}^{3*m}(k) \end{bmatrix}$$

These data were used to calculate artefact-affected femur pose, using the PS approach. A cluster model was defined using the position of the skin markers in the first frame ( $k=1$ ) and it was superimposed, in each frame, to the actual cluster by optimally translating and rotating it.

### 5.2.2. Running data

The data obtained in (Reinschmidt et al., 1997c) and relative to the trajectories of both skin and pin thigh markers recorded during 5 trials of each of 3 running subjects (V1, V2, V3) were used. For each trial and subject, a bone anatomical frame (AF) was defined, based on the pin markers, and the movement of four skin-markers reconstructed in the AF. Relevant displacement vectors were represented, in each  $k$ -th sample, as an STA vector field  $\mathbf{V}(k)$ , ( $k=1, \dots, n$ ) (Dumas et al., 2014a).

Skin-marker trajectories were generated from the reference AF pose and the STA fields,  $\mathbf{V}(k)$ , and used to estimate the artefact-affected pose of the AF in the global reference frame with a Procrustes superimposition (PS) approach. The root mean square difference between the artefact-affected and reference AF pose was calculated and considered as an error ( $\text{rmse}_\theta$  for orientation (attitude angle) and  $\text{rmse}_{\text{px}}$ ,  $\text{rmse}_{\text{py}}$ ,  $\text{rmse}_{\text{pz}}$ , for position components).

### 5.2.3. Marker-cluster geometrical transformation

The STA field has  $3*m$  degrees of freedom (dof) and it can be represented with respect to any orthogonal basis with the same dof  $[\Phi^1, \dots, \Phi^{3*m}]$  using a mathematical transformation, as proposed by Dumas et al. (2014a) and described in the previous chapter. For the marker-cluster geometrical transformation (GT), the dof of the basis is fixed, independently to the number of skin markers glued on the segment (dof = 12). A basis of twelve unit vectors representing rotation, translation, homothety, and stretch can be defined, as described in details in Dumas et al. (2014a).

The STA field  $\mathbf{V}(k)$  can be decomposed along the basis of twelve unit vectors, and the change of configuration can be written as a sum of additive and independent components (modes):

$$\mathbf{V}(k) = \sum_{l=1}^{12} a^l(k) \Phi^l$$

(Eq. 5.1).

When the GT definition is used as a mathematical transformation for the STA field and the number of skin markers is  $m > 4$ , only a STA subspace is defined for the truncation of the basis.

For this reason, the energy represented in the twelve modes was calculated when the number of the skin markers goes from 4 to 12 ( $m = 4, \dots, 12$ ). Moreover, it had been measured also the error in the skin marker trajectories between the simulated trajectories and that obtained with the truncated subspace:

$$e = \mathbf{V}(k) - \sum_{l=1}^{12} a^l(k) \Phi^l$$

(Eq. 5.2).

#### 5.2.4. STA components

The first six modes ( $l = 1, \dots, 6$ ) describe the rigid motion of the skin-marker cluster (*i.e.*, its translation and rotation), while the others ( $l = 7, \dots, 12$ ) describe the non-rigid component (*i.e.*, homothety and stretch).

$$\mathbf{V}(k) = \underbrace{\sum_{l=1}^6 a^l(k) \Phi^l}_{\text{rigid}} + \underbrace{\sum_{l=7}^{12} a^l(k) \Phi^l}_{\text{non-rigid}}$$

(Eq. 5.3).

The energy carried by the two STA components was calculated as the sum of the mean square of the relevant amplitude  $a_i^l(k)$  and expressed in percentage to the whole energy of the skin marker cluster. In details, the energy associated with the cluster RM was calculated as

$$E_{RM} = \sum_{l=1}^6 \left( \frac{1}{n} \sum_{k=1}^n (a^l(k))^2 \right)$$

(Eq. 5.4),

and that associated with the cluster NRM

$$E_{NRM} = \sum_{l=7}^{12} \left( \frac{1}{n} \sum_{k=1}^n (a^l(k))^2 \right) \quad (\text{Eq. 5.5}).$$

A factor  $R_{NRM}$  was calculated as the ratio between  $E_{RM}$  and  $E_{NRM}$ , both for the gait and running data.

#### 5.2.5. Impact of RM and NRM on bone pose estimation: reference

The femur pose affected by STA was generated using  $\mathbf{V}(k)$  and with the same procedure as described above. To evaluate the impact of the rigid component of the STA on the pose, the RM were removed from  $\mathbf{V}(k)$ . The root mean square error of the orientation ( $\text{rmse}_\theta$ ) and position components ( $\text{rmse}_{px}$ ,  $\text{rmse}_{py}$ ,  $\text{rmse}_{pz}$ ) were calculated with respect to the reference pose, for both cases, *i.e.*, STA affected and removing its rigid components.

#### 5.2.6. Impact of RM and NRM on bone pose estimation: Monte Carlo Simulation framework

##### Simulated Gait: cluster non-rigid motion amplification

For the gait data, four skin markers affected by STA were selected (skin markers with double circle shown in Figure 5.1, with a similar position in the relevant AF as L2, L4, A2, A4, Figure 3.1 in the *third Chapter* of the thesis) to obtain a STA field with the same dof of the GT basis.

To evaluate the effect on the bone pose of the NRM variability, the amplitude of the six modes that represent the cluster NRM was randomly amplified using a Monte Carlo simulation framework. This technique is widely used in the probabilistic analysis of engineering systems (Mahadevan, 1997). The amplitudes of the simulated NRM were randomly amplified up to the factor  $R_{NRM}$  for the first Monte Carlo simulation (MCS1) and up to the redoubled factor ( $2R_{NRM}$ ) for the second one (MCS2). The Monte Carlo simulations were performed over 1000 possible NRM amplifications, approximating the probability of certain outcomes, using the two maximum amplification factors ( $R_{NRM}$ ,  $2R_{NRM}$ ). For the gait data, the first set of one thousand STA fields,  $\mathbf{V}_{MCS1}(k)$ , that have the same cluster RM and amplified cluster NRM was generated multiplying each mode that describe the latter motion with different factors ( $R_1, \dots, R_6$ ) as:

$$\mathbf{V}_{MCS1}(k) = \sum_{l=1}^6 a^l(k) \Phi^l + R_1(a^7(k) \Phi^7) + \dots + R_6(a^{12}(k) \Phi^{12})$$

(Eq. 5.6),

with  $(R_1, \dots, R_6)$  randomly generated in the range from 1 to  $R_{NRM}$ , *i.e.*  $1 < R_1, \dots, R_6 < R_{NRM}$ ; while in the second set of one thousand STA fields,  $\mathbf{V}_{MCS2}(k)$ , each mode of the cluster NRM was multiplied with different factors  $(R_7, \dots, R_{12})$  as:

$$\mathbf{V}_{MCS2}(k) = \sum_{l=1}^6 a^l(k) \Phi^l + R_7(a^7(k) \Phi^7) + \dots + R_{12}(a^{12}(k) \Phi^{12})$$

(Eq. 5.7),

with  $(R_7, \dots, R_{12})$  randomly generated in the range from 1 to  $2R_{NRM}$ , *i.e.*  $1 < R_7, \dots, R_{12} < 2R_{NRM}$ .

Therefore, during each gait simulation, new skin marker trajectories were obtained, and therefore new STA fields:  $\mathbf{V}_{MCS1}(k)$  and  $\mathbf{V}_{MCS2}(k)$ . For both STA field, the energy of the NRM was higher with respect to its counterpart.

#### Running data: cluster non-rigid motion amplification

For the running data, a set of one thousand STA fields was generated with the same cluster RM and amplified cluster NRM with the same factor,  $r$ :

$$\mathbf{V}_{MCSrun}(k) = \sum_{l=1}^6 a^l(k) \Phi^l + r \sum_{l=7}^{12} a^l(k) \Phi^l$$

(Eq. 5.8).

The amplification factor  $r$  was randomly generated in the range from 1 to  $2\sqrt{R_{NRM}}$ : the mean cluster NRM energy of this set was equal to the cluster RM counterpart.

#### Femur poses

The energy carried by the two STA components and expressed in percentage with respect to the new, and intensified, STA energy of the simulated fields ( $\mathbf{V}_{MCS1}(k)$ ,  $\mathbf{V}_{MCS2}(k)$ ,  $\mathbf{V}_{MCSrun}(k)$ ) was calculated as described above in the section 5.2.4.

The femur pose affected by the simulated STA was generated using all the available STA fields ( $\mathbf{V}_{MCS1}(k)$ ,  $\mathbf{V}_{MCS2}(k)$ , and  $\mathbf{V}_{MCSrun}(k)$ ) and with the same procedure as described above. To

evaluate the impact of the rigid component of the STA on the pose of the femur, the unchanged RM were removed from the above-mentioned STA fields. The femur pose was evaluated in terms of rmse with respect to the reference one (orientation,  $rmse_{\theta}$ ; and position components,  $rmse_{px}$ ,  $rmse_{py}$ ,  $rmse_{pz}$ ), before and after the removal of the unchanged RM component for the different STA fields, for both gait and running data.

### 5.3. Results

#### 5.3.1. Marker-cluster geometrical transformation and number of markers

When the number of the skin markers used in the cluster goes from 4 to 12 the STA energy represented with the 12 GT modes decreases for 100% to 91%, while the error in the reconstruction of the skin markers trajectories increases from 0 mm to 3.7 mm (Figure 5.2).

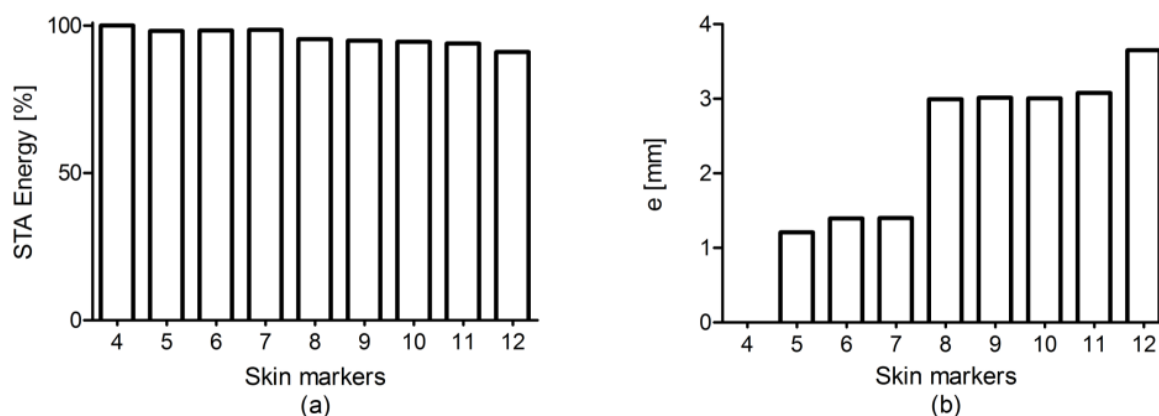


**Figure 5.2** – STA energy (a) carried by the 12 modes of the GT representation, calculated in percentage with respect to the whole phenomenon, and the error (b),  $e$  expressed in mm (Equation 2), when the skin markers trajectories were reconstructed using these modes as function of the number of the skin markers used in the cluster.

The error in the bone pose estimation using the Procrustes superimposition did not change as function of the number of the skin markers used in the cluster, but among all the skin-marker cluster used, when the rigid modes were removed from the skin marker trajectories, the mean error on the bone pose estimation improved from 2.80 deg (std = 1.43 deg) to 0.03 deg (std = 0.01 deg) for the orientation, while for the position vector the following mean improvements were achieved: from 22.82 mm (std = 7.80 mm) to 0.03 mm (std = 0.01 mm), from 6.62 mm (std = 1.75 mm) to 0.05 mm (std = 0.00 mm), from 8.47 mm (std = 4.94 mm) to 0.15 mm (std = 0.02 mm), along the x, y, z directions.

5.3.2. Monte Carlo Simulation: gait data

The amplitudes along each mode,  $a_i^l(k)$ , were measured in mm. The rigid and non-rigid mode amplitudes were obtained first estimating the thigh STA using the model described in the *Chapter 3* and then using the GT representation (Figure 5.3 and 5.4).

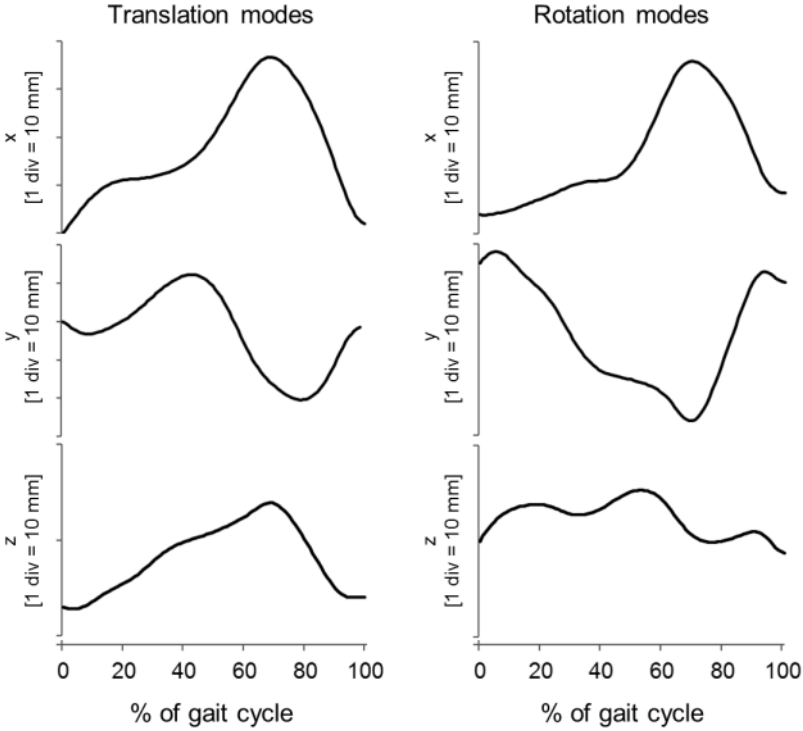


**Figure 5.3** – Measured amplitudes of the rigid modes for the thigh segment during the gait cycle.

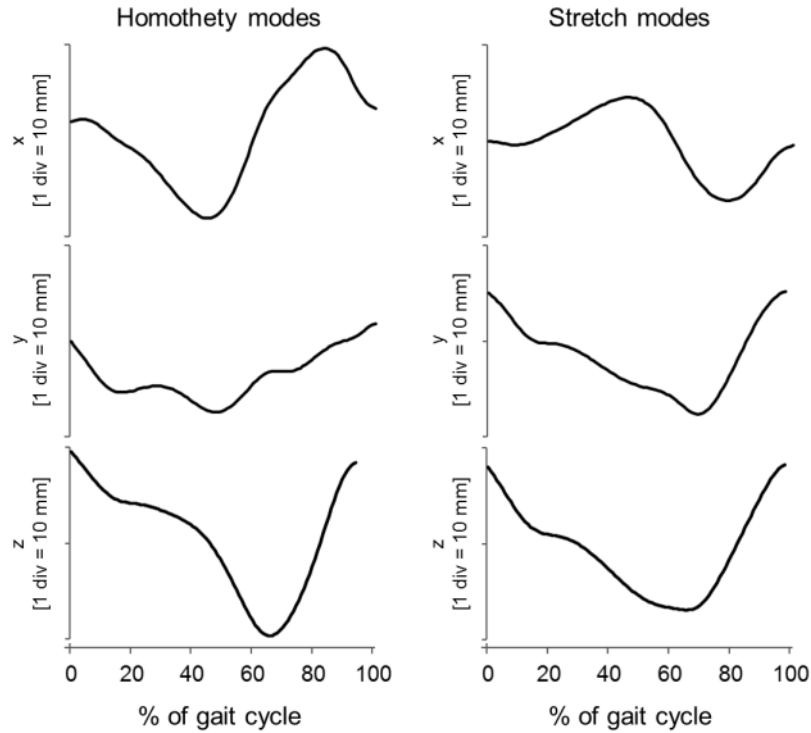


**Figure 5.4** – Measured amplitudes of the non-rigid modes for the thigh segment during the gait cycle.

The factor  $R_{NRM}$  (*i.e.*, the ratio between the cluster RM and NRM energies) during the gait simulation was 2.2. During the two Monte Carlo simulations (*i.e.*, MCS1 and MCS2), the NRM, showed in Figure 5.4, were amplified up to 2.2 and 4.4. The STA energy split between the RM and NRM, expressed in percentage with respect to the whole phenomenon was 69% and 31% during the simulated gait, respectively. During the MCS1, the mean energy for the RM was 45% and 55% for the NRM, while during the MCS2 these values become 24% and 76%, respectively (Figure 5.5).

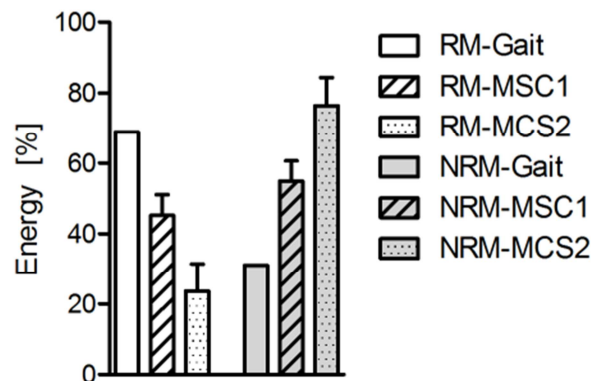


**Figure 5.5** – Mean and standard deviation of the rigid and non-rigid STA component energies expressed in percentage of to the whole STA energy during gait (RM-Gait and NRM-Gait), the MCS1 (RM- MCS1 and NRM- MCS1) and MCS2 (RM- MCS2 and NRM- MCS2). Statistics performed over all the Monte Carlo simulations using the two amplification factors for the NRM components, without affecting the RM components.

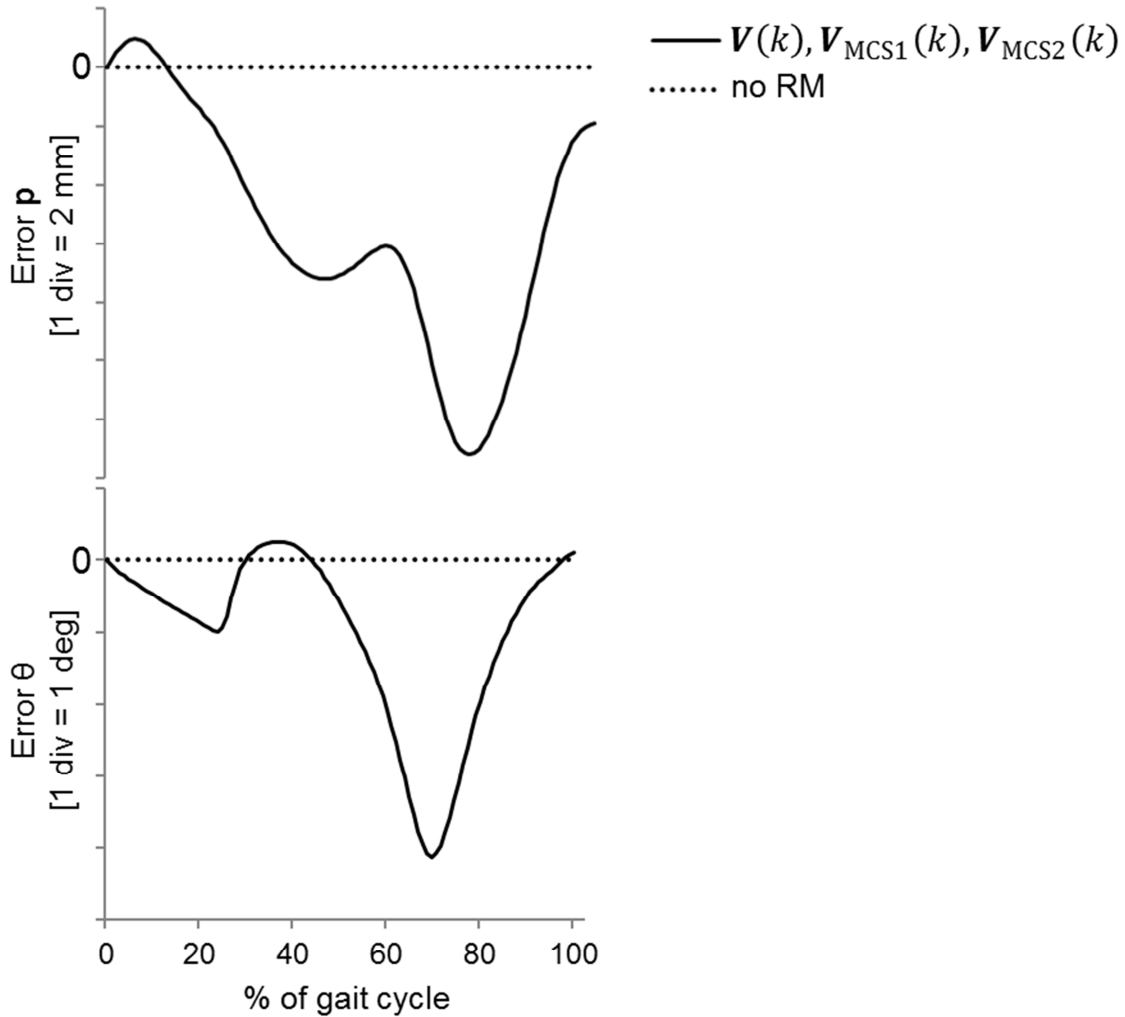


**Figure 5.6** – Femur pose position ( $\mathbf{p}$ ) and orientation ( $\theta$ ) error using skin-marker trajectories affected by STA  $V(k), V_{MCS1}(k), V_{MCS2}(k)$ , and removing the cluster RM component (no RM) from the different STA fields, during the simulated gait. Errors calculated with respect to the reference pose of the femur.

Median orientation error value of the thigh due to the STA during simulated gait was 1.61 deg, the error for the position vector was 10.81 mm, 3.39 mm and 6.18, for the x, y, z direction, respectively. The maximum error for  $\theta$  was 4.12 deg, while for the reference position components, the error values were 19.40 mm, 7.68 mm and 12.54 mm for the x, y, z direction, respectively. The error values for  $rmse_{\theta}$ ,  $rmse_{px}$ ,  $rmse_{py}$ ,  $rmse_{pz}$ , or their maximum, did not change when the NRM was amplified during the MCS1 and MCS2. The direct removal of the cluster RM from  $V(k)$ , or when the cluster NRM was amplified, *i.e.*,  $V_{MCS1}(k)$  and  $V_{MCS2}(k)$ , eliminates the error in the bone-pose estimation introduced by the STA (Figure 5.6).

## 5.3.3. Monte Carlo Simulation: running data

The  $R_{NRM}$  factors were different among trials and subjects. The median (inter-quartile range) values of the  $R_{NRM}$  factors were 7(1), 18(4), and 14(15), for V1, V2 and V3, respectively. Obviously, the cluster NRM amplification caused an increase in the energy percentage of this component with respect to the total energy: mean ( $\pm$ standard deviation) values went from  $8\pm 3\%$  ( $V(k)$ ) to  $52\pm 22\%$  ( $V_{MCSrun}(k)$ ) (Figure 5.7).

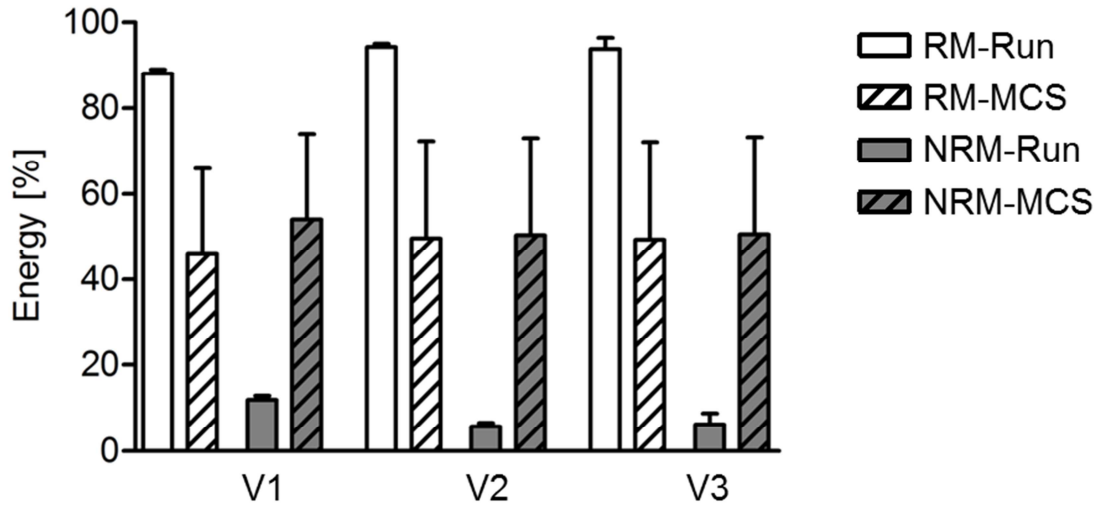


**Figure 5.7** – Mean values of  $E_{RM}$  and  $E_{NRM}$  expressed in percentage with respect to the total STA energy, for the measured (RM-Run and NRM-Run) and simulated STA (RM-MCS and NRM-MCS). Statistics performed over all trials and subjects (V1, V2, V3).

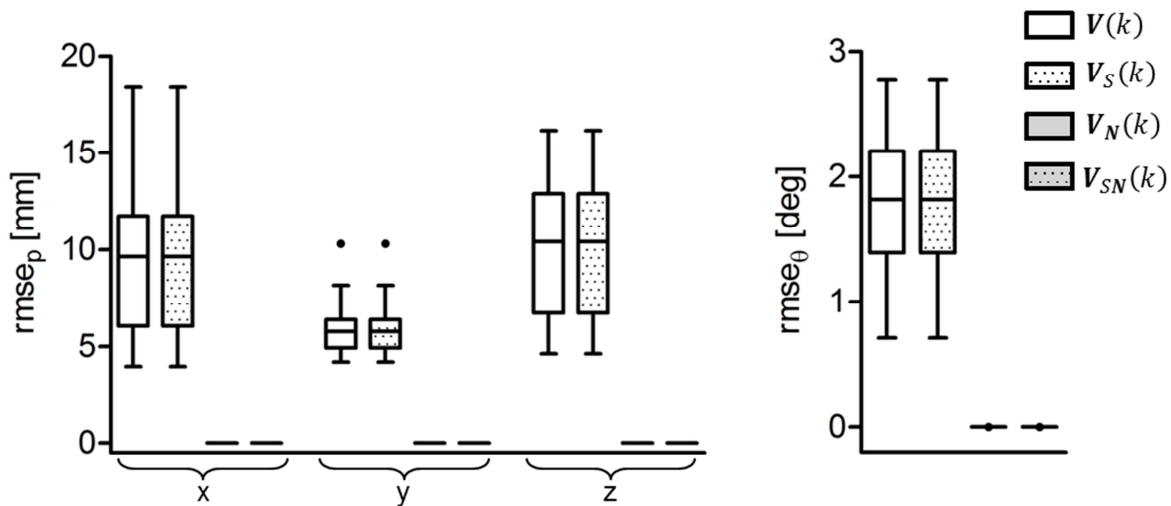


**Figure 5.8** – Box-plots (minimum, lower quartile, median, upper quartile, and maximum) of the BPE errors, for position and orientation, relative to all the STA fields available (measured STA,  $V(k)$ , amplified STA,  $V_S(k)$ , and these fields when the cluster NRM were removed:  $V_N(k)$ , and  $V_{SN}(k)$  respectively).

Before and after the amplification of cluster NRM, errors in pose estimation were exactly the same (although the total STA energy increased) (Figure 5.8). In all cases, after removing RM, not altered throughout the simulation, the error was null.

#### 5.4. Discussion

When the optimal basis is defined and the GT definition is used, the maximum error in the skin marker trajectory reconstruction was less than 4 mm. Such error caused a small impact on the bone pose estimation also when the cluster RM was removed: 0.03 deg and 0.07 mm. This error can increase if the cluster RNM is amplified. For this reason, and since it is a common practise and it seems to be a good practical solution (Cappozzo et al., 1997), a cluster composed by a number of markers equal to four was selected. This skin cluster was used for both data (simulated gait and running data) to determine the effect of the cluster rigid and non-rigid movement due to soft tissue interposition on the bone pose estimation when a stereophotogrammetric system and skin markers are used. This study has shown that the RM of the skin-marker cluster is the only component which affects the pose estimation of the underlying bone. It has been empirically demonstrated that this component affects the pose estimation independently to the relative energy associated with the RM or the NRM. Moreover, the removal of the cluster RM leads to the real bone pose estimation, also when the rigid motion of the cluster represents only the 24% of the total energy of the phenomenon. In effect, all the possible scenarios were evaluated: for the running data, the energy of the NRM was amplified to the same energy of its counterpart, while for the simulation performed for the gait, paradoxical situations were created with the NRM which showed higher energy with respect to the RM component.

In the compensation perspective, Cappello et al., 2005, using a double calibration procedure, even though this method did not allow separate the effects of deformation from the rigid displacement of the surface marker cluster, declared that the most critical source of error is the RM of the cluster with respect to the underlying bone, rather than the cluster deformation.

Recent studies measured the importance of the RM and NRM on real data during different motor tasks (level walking, cutting, hopping trials, shank movements inducted by vertical vibration, gait treadmill) showing that the rigid-body translation and rotation components were the main cause of the STA phenomenon (Andersen et al., 2012; Barré et al., 2013; Benoit et al., 2015; de Rosario et al., 2012). When the STA was not caused by wobbling or muscle contraction (Grimpampi et al., 2014) the STA RM and NRM components exhibited similar magnitudes and therefore impact on

bone pose estimation. All the mentioned studies concluded that techniques focused on addressing marker cluster deformation (Andriacchi et al., 1998; Chèze et al., 1995; Dumas and Cheze, 2009; Söderkvist and Wedin, 1993; Taylor et al., 2005; Veldpaus et al., 1988) will have limited impact on reducing the STA problem. Moreover, bone pose estimators should account also for cluster RM, which is the most critical source of error, both for the nature of the phenomenon and its importance. de Rosario et al. (2012), instead, assessed that only the rigid component propagates to the joint variables as an error, while the deformation component can be filtered during the kinematic analysis process.

However, to the author knowledge, no evidence that the STA RM would be the only component which affects the bone pose estimation, independently to its magnitude, has been reported in the literature.

The results obtained in the present study showed that separating the cluster RM from the NRM using the GT definition, which allow to define the STA as sum of independent modes, the non-rigid movement of the cluster has no influence on the bone pose estimation when the Procrustes superimposition approach is used. Furthermore, also when the amplitude of the cluster NRM is simulated to be bigger than the RM, it has been even demonstrated that it has no impact on the results, as shown in Figure 5.6.

Therefore, with the results obtain in the present study, we can infer the RM motion is the only movement of the cluster which affects the bone pose estimation.

Future work has to be performed in developing a model for accurately predicting RM, using STA *a priori* information (Camomilla et al., 2013, 2009; Gao and Zheng, 2008; Richard et al., 2012; Chapter 3).

### Appendix Chapter 5

In the *Chapter 4* some parameters of the GT definition were chosen arbitrarily  $(\theta, h, s, t)$ . The effect of  $\theta$  was evaluated changing this parameter for different pure rotations applied to a four skin marker cluster (simulated). Such rotation changed between 5 to 20 deg, increasing this value by steps of 1 deg during the simulation. The choice of the rotation range was based on the observation of the cluster motion in a previous study (Grimpampi et al., 2014). For each cluster-rotation value, the parameter  $\theta$  changed with a step of 0.001 deg in the range from 0.001 deg to 0.1 deg, and with a step of 0.1 deg in the range from 0.2 to 2 deg, and with a step of 1 deg in the range from 3 to 10 deg. The GT definition was applied the different skin-marker configuration obtained as described above. The error in the reconstruction of the position of the skin markers were evaluated changing  $\theta$  and the cluster rotation, before,  $\mathbf{V}(k) = [\mathbf{v}^1(k), \dots, \mathbf{v}^{3*m}(k)]$  (using the equation 5.1), and after the application of the GT definition:

$$\sum_{l=1}^{12} a^l(k) \Phi^l = \hat{\mathbf{V}}(k)$$

(Eq. 5.A1).

This error, expressed in mm, was calculated as the difference between  $\mathbf{V}(k)$  and  $\hat{\mathbf{V}}(k)$ . The mean error value, for all the combinations of the cluster rotation and  $\theta$ , was calculated among all directions and markers (Figure 5.A1.1).

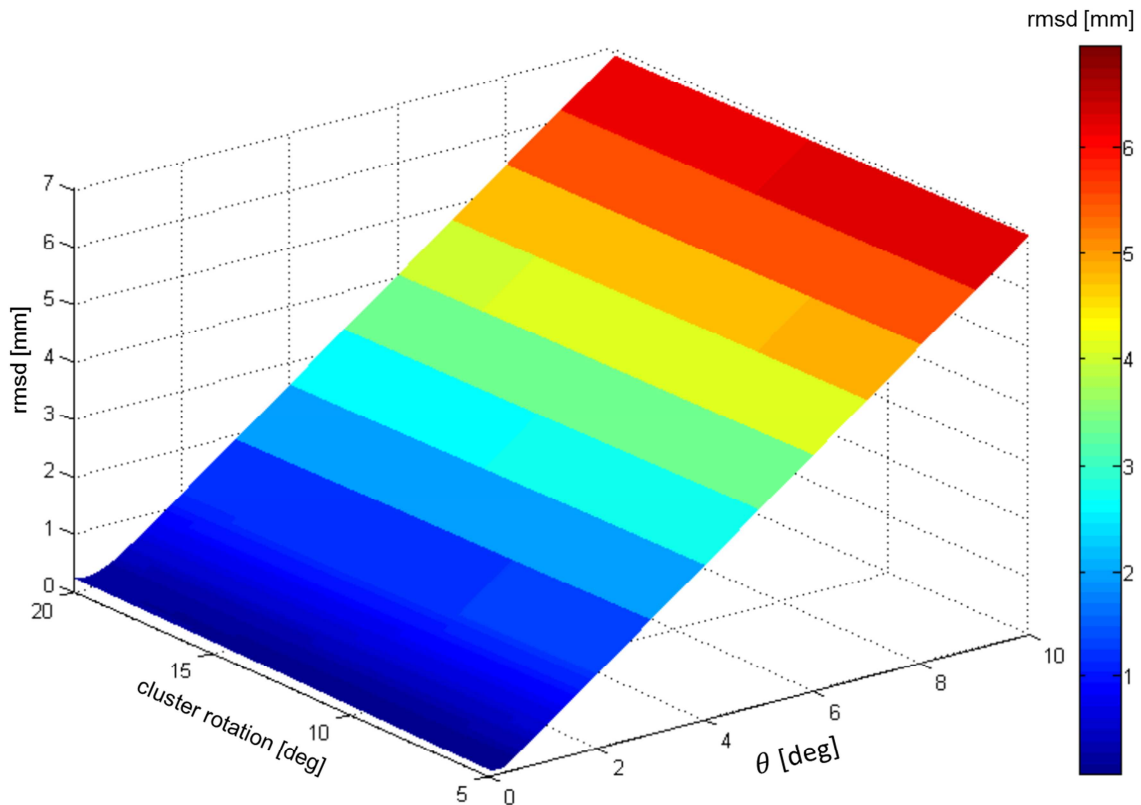


**Figure 5.A1.1** – Root mean square difference (rmsd) between  $V(k)$  and  $\hat{V}(k)$  when the GT definition is applied, changing the cluster pure rotation and the parameter  $\theta$  of this definition.

From the Figure 5.A1.1, it is clear that the choice of the parameter  $\theta$  has a relevant influence on a possible error introduced in the reconstruction of the position of the skin markers: if  $\theta$  is set equal to 10 deg, an error up to 7 mm can be found. This can lead to a wrong interpretation of the result: if the basis is not correctly defined, the rotation of the cluster can be projected onto other modes which describe other movements of the cluster.

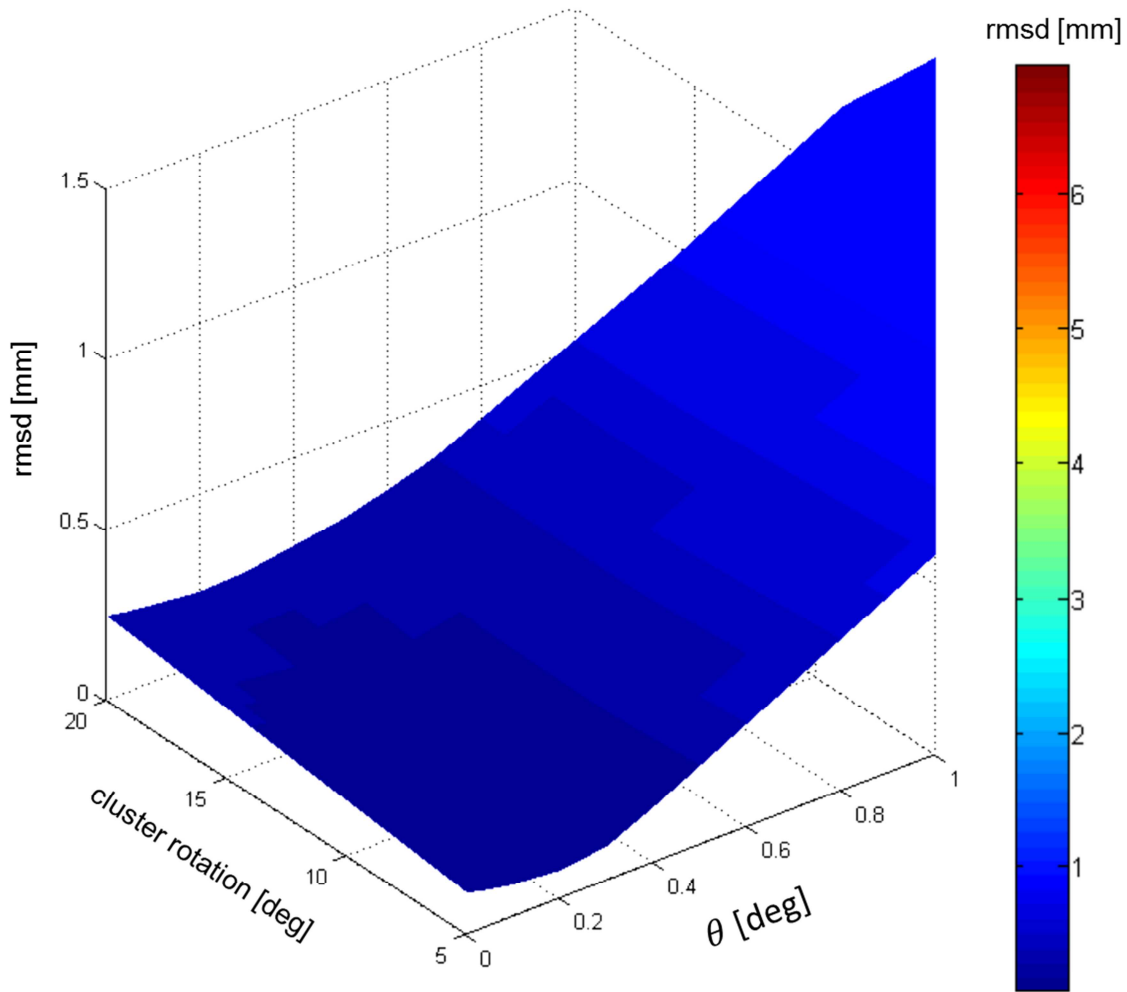


**Figure 5.A1.2** – Zoom of the Figure 5.A1.1. Root mean square difference (rmsd) between  $V(k)$  and  $\hat{V}(k)$  when the GT definition is applied, changing the cluster pure rotation and the parameter  $\theta$  of this definition.

In Table 5.A1.1 are reported the optimal value of  $\theta$  for different cluster rotation:  $\theta_{opt}$ .

Cluster	$\theta_{opt}$
5	0.08
6	0.08
7	0.09
8	0.10
9	0.11
10	0.12
11	0.13
12	0.14
13	0.15
14	0.16
15	0.17
16	0.18
17	0.18
18	0.19
19	0.20
20	0.21

**Table 5.A1.1** – Optimal  $\theta$  value ( $\theta_{opt}$ ) for different cluster rotations.

Based on the results obtained in a previous study which quantified the cluster rotation (Grimpampi et al., 2014), the value of  $\theta$  has been set equal to 0.20 deg (Table 5.A1.1 and Figure 5.A1.2).

## 6. Chapter 6

The content of this chapter is referred to the article

### **“WHAT PORTION OF THE SOFT TISSUE ARTEFACT REQUIRES COMPENSATION WHEN ESTIMATING JOINT KINEMATICS?”**

Submitted for publication (under first review in Journal of Biomechanical Engineering).

Additional information are also presented.

#### Symbols and Nomenclature

Symbols	$i$	body segment ( $i = 1, 2, 3, \dots$ )
	$j$	skin marker ( $j = 1:m_i$ )
	$k$	sampled instant of time ( $k = 1:n$ )
	$\mathbf{R}_i(k)$	rotation matrix of the anatomical calibration for the segment $i$
	$\mathbf{t}_i(k)$	position vector of the anatomical calibration for the segment $i$
	$\mathbf{V}_i^{AF}(k)$	STA field for the segment $i$ in the anatomical reference frame
	$\bar{\mathbf{r}}_{M_i^j}^{AF}$	mean positions of the $m_i$ skin markers in the anatomical reference frame
	$\alpha_i^l(k)\Phi_i^l$	mode $l$
	$\Phi_i^l$	mode direction
	$a_i^l(k)$	mode amplitude
	$\lambda_i^l$	modal energy
	$p_i$	energy percentage
	$p_i^*$	energy percentage relative to the rigid modal energy
	Knee degrees of freedom	FE
AA		abduction/adduction
IER		internal/external rotation
LM		medio/lateral
AP		anterior/posterior
PD		proximal/distal
Nomenclature	STA	soft tissue artefact
	MD	individual marker displacements
	GT	marker-cluster geometrical transformations
	SV	skin envelope shape variations
	GF	global reference frame
	AF	anatomical reference frame
	RMSE	root mean square error
IQR	inter-quartile range	

Kinematic variables as estimated using	SKIN	STA-affected dataset
	GT-rigid	STA-compensated datasets: removing the rigid modes
	MD-90%	STA-compensated datasets: removing MD modes which represent the 90% of the total STA energy
	GT-90%	STA-compensated datasets: removing GT modes which represent the 90% of the total STA energy
	SV-90%	STA-compensated datasets: removing SV modes which represent the 90% of the total STA energy

### 6.1. Introduction

When joint kinematics are analysed using non-invasive stereophotogrammetry, any change of configuration in the skin marker positions relative to the underlying bone is regarded as an artefact (soft tissue artefact: STA) since it noticeably jeopardizes the bone pose estimations. Any action to compensate for this artefact requires designing an STA estimation model that can be embedded in the bone pose estimator. For this purpose, a definition and a mathematical representation of the artefact must be devised which meet the following requirements: the STA relative to each body segment analysed must be represented with a minimum number of time functions, but at the same time provide an adequate approximation of the artefact for further purposes (Alexander and Andriacchi, 2001; Camomilla et al., 2013; De Rosario et al., 2013; *Chapter 3*), thus allowing a trade-off between complexity and effectiveness of the STA model within the bone pose estimator.

The STA may be approximated for only the portion which is assumed to impact most on the end results. This can be achieved using different selection criteria, depending on the definition and mathematical representation of the artefact. Using the individual marker displacement (MD) definition, only the markers expected to locally displace most (Akbarshahi et al., 2010; Stagni et al., 2005; Tsai et al., 2009) can be accounted for. If marker-cluster geometrical transformation (GT) is used to define the STA, it may be seen/considered as principally composed of a rigid component as opposed to a non-rigid component (Andersen et al., 2012; Barré et al., 2013; de Rosario et al., 2012; Dumas et al., 2014b; Grimpampi et al., 2014). When skin envelope shape variation (SV) is used, the main features of the artefact may be extracted through proper orthogonal decomposition (Dumas et al., 2014a) or principal component analysis (Andersen et al., 2012).

The above-mentioned studies suggest that compensating for a portion of the artefact can lead to an appropriate estimation of joint kinematics. However, no evidence that this would be the case has been reported. In addition, which portion should be selected remains an issue. The objective of this

chapter was to analyse the impact of different STA approximations on artefact compensation while estimating joint kinematics.

All the above-listed STA definitions (MD, GT and SV) were represented using the generalized mathematical formulation proposed in (Dumas et al., 2014a). Most importantly, a modal approach was used that allowed for splitting a given STA into additive components (modes) and thus for selecting a subset of these modes. For all three STA definitions, modes were ranked by their contribution to STA energy, and the series truncated at a given threshold of this energy (Dumas et al., 2014a and 2014b). Additionally, when the GT definition was used, only those modes that represented the marker-cluster rigid transformation (*i.e.*, three translation and three rotation modes) were chosen directly.

The different STA approximations were compared using data obtained in volunteers carrying both pin and skin markers during the stance phase of running. Knee joint kinematics, estimated from the skin markers after compensating for the selected (truncated or directly chosen) STA modes, was compared to the reference kinematics obtained using the pin markers.

## 6.2. Material and methods

### 6.2.1. Experimental data

Data recorded by Reinschmidt and colleagues were used (Reinschmidt et al., 1997c). Bone pins were inserted into the tibial and femoral lateral condyles of three non-obese male volunteers (age  $27.7 \pm 2.1$  years, mass  $85.5 \pm 9.6$  kg, height  $1.86 \pm 0.10$  m). Each pin was equipped with three markers while six skin markers were glued on the shank ( $i = 1$ ,  $m_1 = 6$ ) and five on the thigh ( $i = 2$ ,  $m_2 = 5$ ). Marker trajectories were tracked in a global reference frame (GF) using a three cine-film system at 200 frames per second and were low-pass filtered with a cut-off frequency of 8 Hz. For each volunteer, the stance phase of five running trials was recorded.

An anatomical calibration was performed by a radiostereometric analysis (van den Bogert et al., 2008) and the poses (*i.e.*, rotation matrix,  $\mathbf{R}_i(k)$ , and position vector,  $\mathbf{t}_i(k)$ ) of the anatomical reference frames (AFs), assumed to be rigidly associated with the relevant bone (Figure 6.1), were computed in each sampled instant of time  $k$  ( $k = 1:n$ ) using a least squares method (Söderkvist and Wedin, 1993) and the pin marker trajectories.

### 6.2.2. STA approximations and compensation

The running data were used for building an STA field,  $\mathbf{V}_i^{AF}(k)$ , representing the three-dimensional displacements of the  $m_i$  skin markers relative to their mean positions,  $\bar{\mathbf{r}}_{M_i^j}^{AF}$ , in the AF (the apex “AF” denotes the AF and  $M_i^j$  the  $j$ -th skin marker of the  $i$ -th segment,  $j = 1:m_i$  and  $i = 1,2$ ). This STA field was described using three orthogonal bases of vectors,  $\{\Phi_i^1, \dots, \Phi_i^l, \dots, \Phi_i^{3m_i}\}$ , each corresponding to one of the three above-listed STA definitions (MD, GT and SV), thus leading to different modes,  $a_i^l(k)\Phi_i^l$  ( $l = 1: 3m_i$ ), with different STA modal energies,  $\lambda_i^l$ . For each definition, the STA modal energies were sorted in decreasing order and summed one-by-one, until a given percentage,  $p_i$ , of the total energy was obtained:

$$\sum_{l=1}^{r_i} \lambda_i^l \geq p \sum_{l=1}^{3m_i} \lambda_i^l \quad (\text{Eq. 6.1})$$

with

$$\lambda_i^l = \frac{1}{n} \sum_{k=1}^n (a_i^l(k))^2 \quad (\text{Eq. 6.2})$$

and

$$a_i^l(k) = \left( \mathbf{V}_i^{AF}(k) \right)^T \Phi_i^l \quad (\text{Eq. 6.3}).$$

Thus,  $r_i$ , is the number of modes that contributes to the percentage,  $p_i$ , of the STA energy. Details on this generalized mathematical formulation (e.g., the construction of the three orthogonal bases of vectors) can be found in (Dumas et al., 2014a) or in *Chapter 4*. In particular, the construction of the basis of SV vectors was obtained by a proper orthogonal decomposition.

For the GT definition, the modes corresponding to the rigid transformations of the marker-cluster ( $r_i^* = 6$ ) were directly selected and accounted for independently from their modal energies. The corresponding percentage,  $p_i^*$ , of the STA energy was also computed. For all three STA definitions, the modes were selected with a truncation of the series at 90% of STA energy (Dumas et al., 2014a). This threshold was chosen because it is close to the values found for  $p_i^*$ , as illustrated in the next section. This procedure yielded four STA-compensated skin marker position datasets: GT-rigid, MD-90%, GT-90%, and SV-90%. A fifth dataset was the measured, STA-affected, skin marker trajectories (Skin). In addition, two other energy thresholds were chosen: 85% and 95%, as those used in previous studies (Andersen et al., 2012; Dumas et al., 2014a, 2014b). The pose of the

shank and thigh AFs were estimated using the above-listed datasets and a least squares method (Söderkvist and Wedin, 1993) and were compared to the STA-free pose  $(\mathbf{R}_i(k), \mathbf{t}_i(k))$ , obtained using the pin markers (Pin). The skin marker position datasets were represented as (Figure 6.1):

$$\begin{bmatrix} \tilde{\mathbf{r}}_{M_i^1}(k) \\ \vdots \\ \tilde{\mathbf{r}}_{M_i^j}(k) \\ \vdots \\ \tilde{\mathbf{r}}_{M_i^{m_i}}(k) \end{bmatrix} = \begin{bmatrix} \mathbf{R}_i(k) & & & \\ & \ddots & & \\ & & \mathbf{R}_i(k) & \\ & & & \ddots \\ & & & & \mathbf{R}_i(k) \end{bmatrix} \begin{bmatrix} \tilde{\mathbf{r}}_{M_i^1}^{AF} \\ \vdots \\ \tilde{\mathbf{r}}_{M_i^j}^{AF} \\ \vdots \\ \tilde{\mathbf{r}}_{M_i^{m_i}}^{AF} \end{bmatrix} + \mathbf{V}_i^{AF}(k) - \sum_{l=1}^{r_i} a_i^l(k) \Phi_i^l + \begin{bmatrix} \mathbf{t}_i(k) \\ \vdots \\ \mathbf{t}_i(k) \\ \vdots \\ \mathbf{t}_i(k) \end{bmatrix} \quad (\text{Eq. 6.4}).$$

Note that, in equation 6.4, the STA-affected positions of the skin markers in the GF,  $\mathbf{r}_{M_i^j}(k)$ , correspond to  $r_i = 0$ , while the STA-free position of each skin marker is given by  $\mathbf{R}_i(k)\tilde{\mathbf{r}}_{M_i^j}^{AF} + \mathbf{t}_i(k)$ .

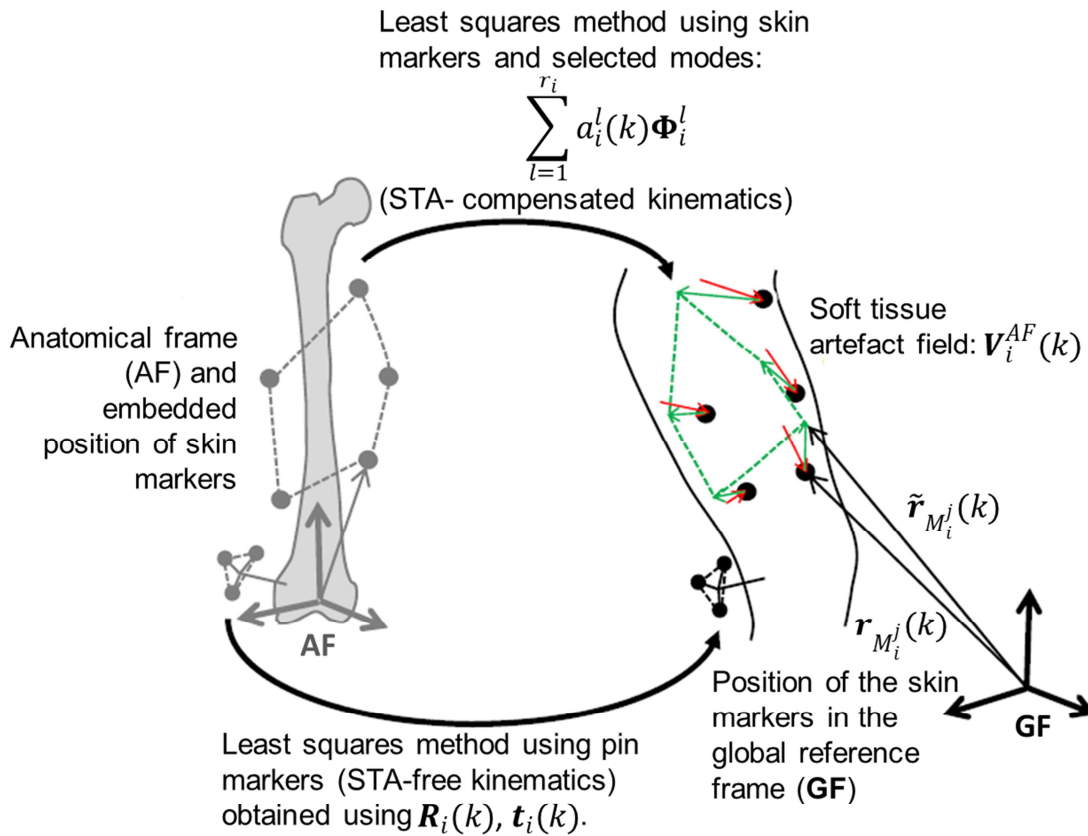


**Figure 6.1** – Principle of computation STA-compensated kinematics.

### 6.2.3. Errors on knee joint kinematics estimate

Knee joint kinematics were estimated from the above-mentioned bone poses (Pin, SKIN, GT-rigid, MD-90%, GT-90%, and SV-90%) and using a joint coordinate system (Wu et al., 2002) (flexion/extension, FE; abduction/adduction, AA; internal/external rotation, IER). The joint displacement components were expressed along the joint axes (Desroches et al., 2010) (lateral/medial, LM; anterior/posterior, AP; and proximal/distal, PD).

The root mean square (RMS) differences between the six kinematic variables as estimated using both the STA-affected (SKIN) and the four STA-compensated datasets (GT-rigid, MD-90%, GT-90%, and SV-90%) and the corresponding STA-free values (Pin) were calculated and regarded as estimation errors (RMSEs).

### 6.2.4. Statistical analysis

Minimum, lower quartile, median, upper quartile, maximum, and inter-quartile range (IQR) were computed over the three volunteers and five trials for the percentage,  $p_i^*$ , of the STA energy corresponding to the rigid GT modes, and for the number of modes,  $r_i$ , in the modal series truncated at 90% of the total STA energy. The same descriptive statistics were computed for the RMSE relative to knee joint kinematics estimated with the STA-affected/compensated skin marker datasets (SKIN, GT-rigid, MD-90%, GT-90%, and SV-90%) as well as for the RMS amplitudes of the STA-free kinematics (Pin).

## 6.3. Results

### 6.3.1. Energy and number of the selected modes

The median (IQR) percentage of the STA energy,  $p_i^*$ , corresponding to the rigid GT modes ( $r_i^* = 6$ ) was 87(16)% for the shank, and 91(11)% for the thigh. These values justify choosing the 90% energy threshold for the modal series truncation. The median (IQR) number of modes,  $r_1$ , representing 90% of the shank STA energy was 11(1), 7(3), and 3(0) for the MD, GT and SV STA definitions, respectively. Correspondingly,  $r_2$  was 10(0), 6(3), and 3(1) for the thigh.

When the other thresholds were used for the STA reduction, the number of modes are reported in Tables 6.1 and 6.2 for the thigh and shank segment, respectively.

	THIGH								
	85%			90%			95%		
	LQ	Median	UQ	LQ	Median	UQ	LQ	Median	UQ
MD	8	8	9	10	10	10	12	12	12
GT	5	5	7	6	6	9	7	8	12
SV	2	2	3	2	3	3	3	3	4

**Table 6.1** – Lower Quartile (LQ), Median, and Upper Quartile (UQ) of the number of modes,  $r_2$ , representing 85%, 90%, and 95% of the thigh STA energy, for the three STA definitions (MD, GT, SV).

	SHANK								
	85%			90%			95%		
	LQ	Median	UQ	LQ	Median	UQ	LQ	Median	UQ
MD	10	10	11	11	11	12	13	14	14
GT	5	5	8	6	7	9	9	12	12
SV	2	2	3	3	3	3	3	4	4

**Table 6.2** – Lower Quartile (LQ), Median, and Upper Quartile (UQ) of the number of modes,  $r_1$ , representing 85%, 90%, and 95% of the shank STA energy, for the three STA definitions (MD, GT, SV).

### 6.3.2. Knee joint kinematics

The statistics of the RMS amplitudes of the STA-free (Pin) kinematics are depicted in Figure 6.2. The RMSEs that affect the knee joint kinematics estimated using the five STA-affected/compensated skin marker datasets (SKIN, GT-rigid, MD-90%, GT-90%, and SV-90%) are shown in Figure 6.3. Using the STA-affected skin marker dataset, the RMSEs resulted as having values close to, and sometimes greater, than those of the RMS amplitudes of the AA and IE angles (median(IQR): 2 (0) deg and 3 (1) deg vs. 1 (2) deg° and 2 (1) deg, respectively) and higher than the RMS amplitudes of the LM, AP and PD displacements (3 (1) mm, 4 (2) mm, and 5 (2) mm vs. 2 (1) mm, 3 (1) mm, and 2 (1) mm, respectively). Conversely, for FE, the RMSE was 2 (1) deg and the RMS 22 (5) deg. The knee kinematics time histories measured with pins and those estimated using the above-mentioned STA affected/compensated skin markers dataset are shown in Figure 6.4.

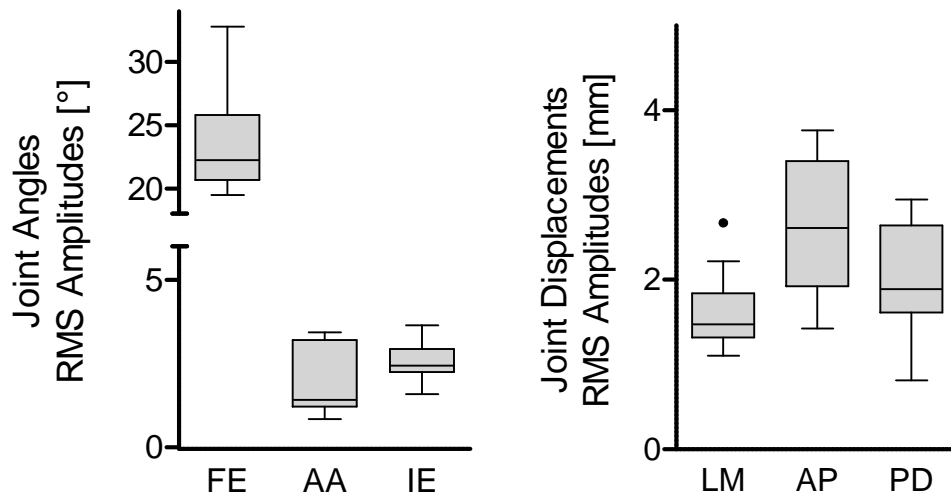


**Figure 6.2** – Box-plots (minimum, lower quartile, median, upper quartile, and maximum) of the root mean square amplitudes of the STA-free (Pin) knee joint kinematics during the running stance phase. Descriptive statistics was performed over all trials and volunteers. Outliers are also shown.

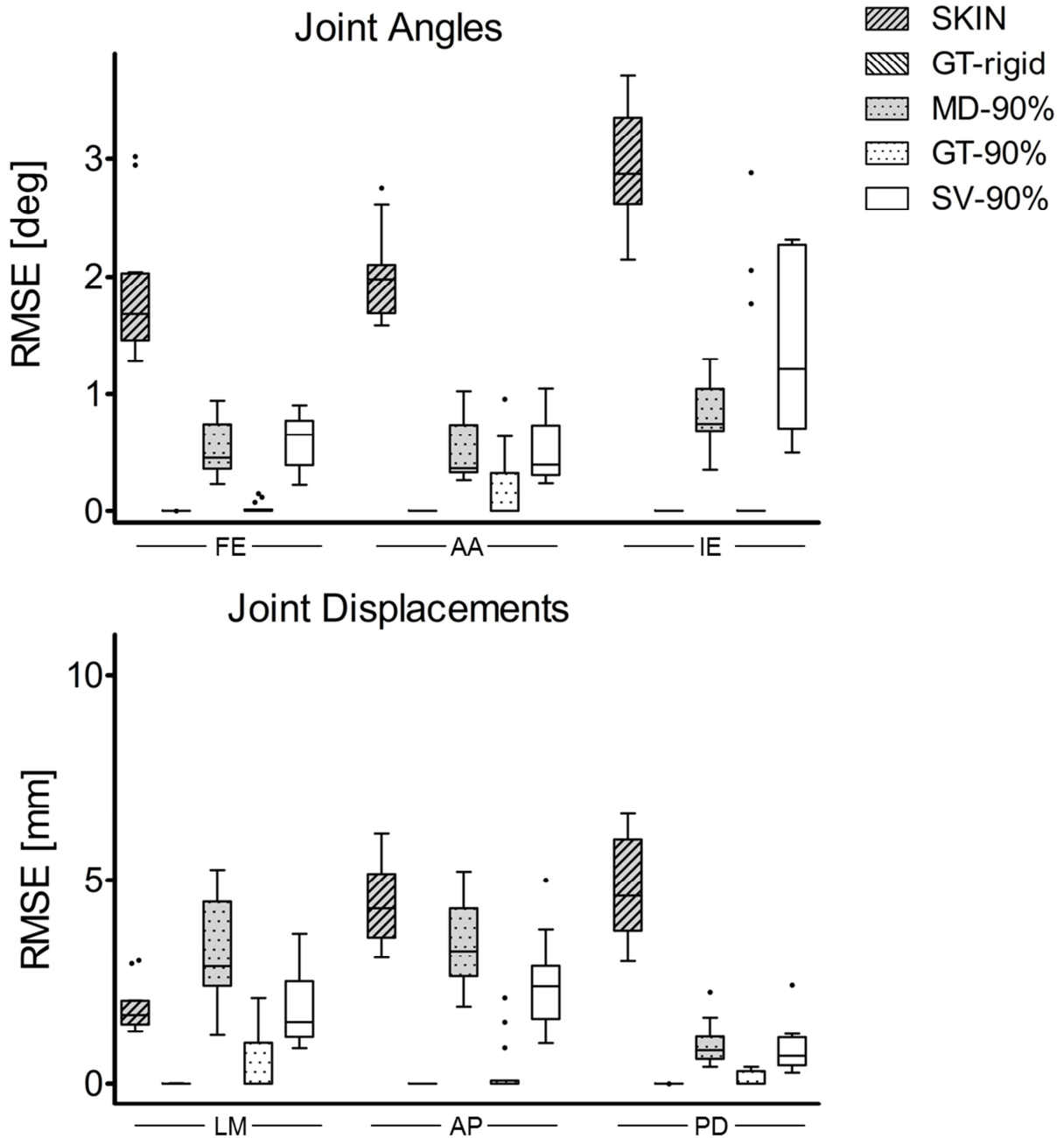


**Figure 6.3** – Box-plots (minimum, lower quartile, median, upper quartile, and maximum) of the root mean square error (RMSE) values which affect knee joint kinematics as obtained with the following datasets: STA-affected, SKIN; or STA-compensated using different STA approximation, GT-rigid, MD-90%, GT-90%, SV-90%. Descriptive statistics was performed over all trials and volunteers. Outliers are also shown.

All the STA-compensated datasets improved estimations of the knee joint kinematics, except for the LM displacement obtained with the MD-90% dataset. Indeed, the latter RMSE (3(2) mm) was greater than the RMSE of the STA-affected (SKIN) kinematics. The improvement in estimation of FE was highly effective with all STA-compensated datasets.

The lowest RMSEs were obtained with the GT-rigid and GT-90% datasets, and the highest were generally obtained with the MD-90% and SV-90% datasets. With all STA-compensated skin marker datasets, the median RMSEs were below 1 deg for AA and below 2 deg for IE angles. For the joint displacements, the compensation efficiency depended on the STA approximation. In particular, the median RMSEs in the AP displacement were in the range of 2-3 mm with the MD-90% and SV-90% datasets, but almost 0 mm with the GT-90% dataset. The compensation with the GT-rigid dataset appeared the most effective. Notably, the RMSEs were virtually null for all joint angles and displacements. An example of the knee kinematic time histories during the running stance phase of a volunteer is shown in Figure 6.4.

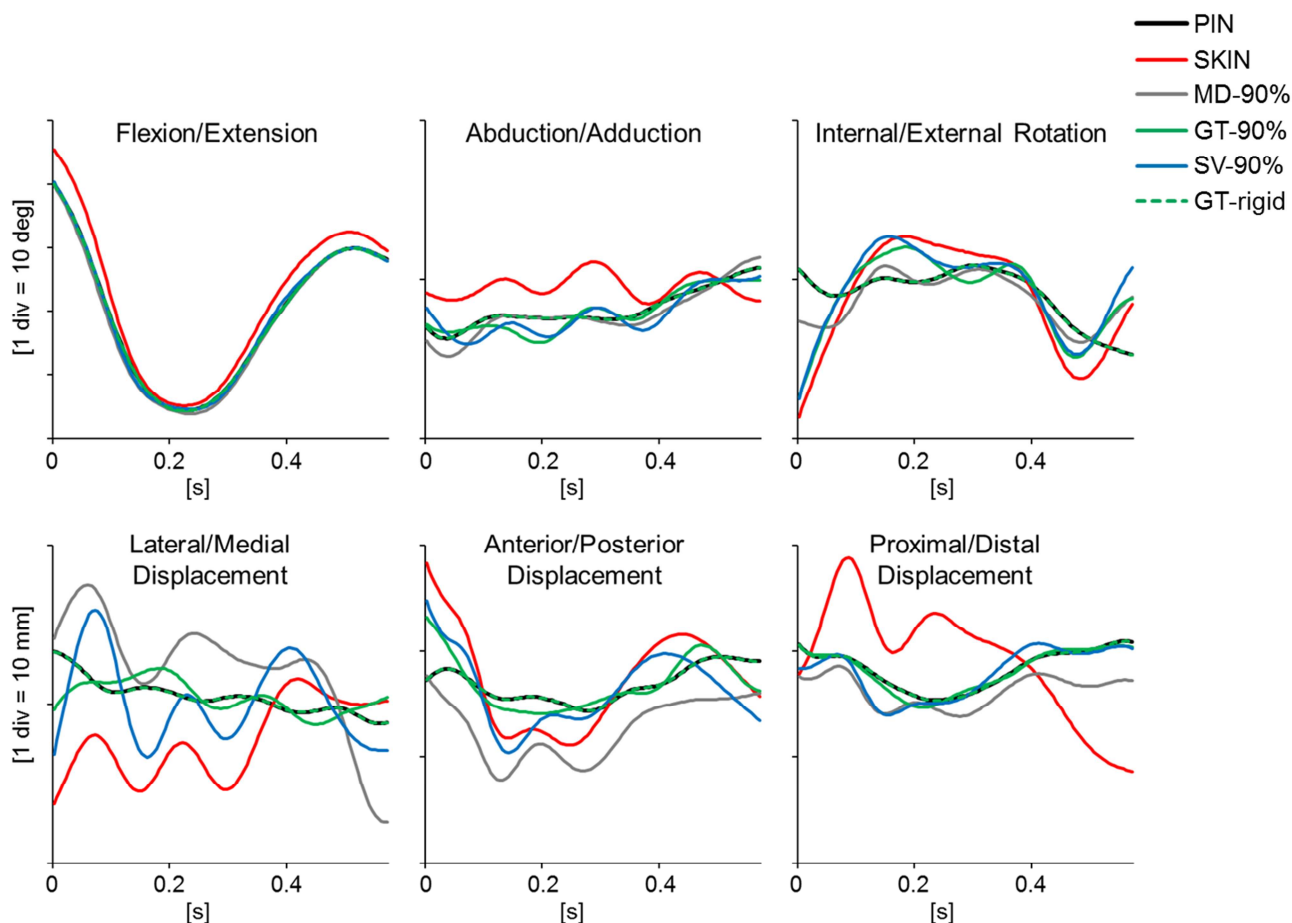


**Figure 6.4** – The six knee joint kinematic components are shown for a trial one volunteer, as obtained using the following marker-cluster data: 1) pin marker trajectories (REF, black solid line), 2) measured skin marker trajectories (SKIN, red solid line), 3) compensated skin marker trajectories using modes that represent the 90% of the total STA energy when the individual marker displacement definition is used (MD-90%, grey solid line); 4) compensated skin marker trajectories using modes that represent the 90% of the total STA energy when the marker-cluster geometrical transformation definition is used (GT-90%, green solid line); 5) compensated skin marker trajectories using modes that represent the 90% of the total STA energy when the skin envelope shape variation definition is used (SV-90%, blue solid line); 6) compensated skin marker trajectories using the rigid modes obtained with the marker-cluster geometrical transformation (GT-rigid, green dotted line).

In addition, when  $p$  was set equal to 85% and 95%, the median (IQR) RMSE values for the knee angle kinematics are shown in Table 6.3 for the proposed STA definitions. An example of the knee kinematics time histories obtained with the different threshold analysed are shown for each definition in the Figures 6.5-6.7.

	$p$	FE [deg]	AA [deg]	IER [deg]	LM [mm]	AP [mm]	PD [mm]
<i>MD</i>	85	0.7(0.3)	0.6(0.3)	1.1(0.7)	4.0(2.1)	4.1(2.2)	1.0(0.7)
	90	0.5(0.3)	0.4(0.4)	0.7(0.3)	2.9(2.1)	3.3(1.6)	0.8(0.5)
	95	0.3(0.3)	0.3(0.2)	0.6(0.2)	2.0(0.9)	2.4(1.0)	0.7(0.5)
<i>SV</i>	85	0.7(0.2)	0.5(0.5)	1.8(0.9)	1.9(0.9)	2.7(1.3)	0.9(0.6)
	90	0.7(0.4)	0.4(0.4)	1.2(1.6)	1.5(1.2)	2.4(1.2)	0.7(0.6)
	95	0.5(0.4)	0.3(0.1)	0.6(0.3)	1.2(0.5)	1.8(1.2)	0.6(0.4)
<i>GT</i>	85	0.1(0.1)	0.7(0.5)	1.9(1.8)	1.9(1.1)	1.0(1.5)	0.4(0.3)
	90	0.0(0.0)	0.0(0.2)	0.0(0.0)	0.0(0.8)	0.0(0.1)	0.0(0.2)
	95	0.0(0.0)	0.0(0.0)	0.0(0.0)	0.0(0.0)	0.0(0.0)	0.0(0.0)

**Table 6.3** – Median and inter-quartile range (IQR) of the root mean square error (RMSE) values which affect knee joint kinematics as obtained compensating the STA using different STA approximations ( $p = 85\%$ ,  $90\%$ , and  $95\%$ ). Descriptive statistics was performed over all trials and volunteers.

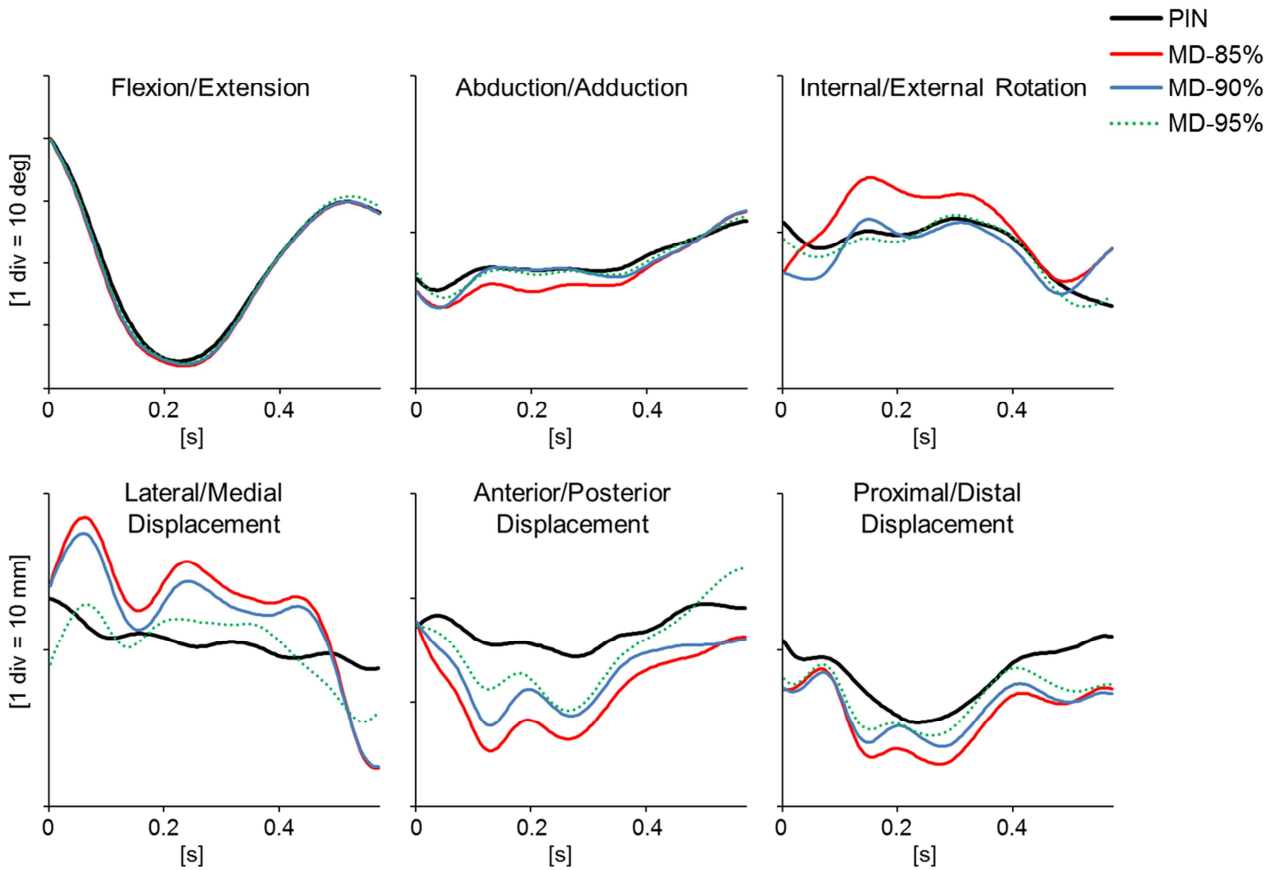


**Figure 6.5** – The six knee joint kinematic components are shown for the same trial and volunteer of the Figure 6.4, as obtained using the following marker–cluster data: pin marker trajectories (REF, black solid line), compensated skin marker trajectories using modes that represent the 85% (MD-85%, red solid line), 90% (MD-90%, blue solid line), and 95% (MD-95%, green dotted line) of the total STA energy when the individual marker displacement definition is used.

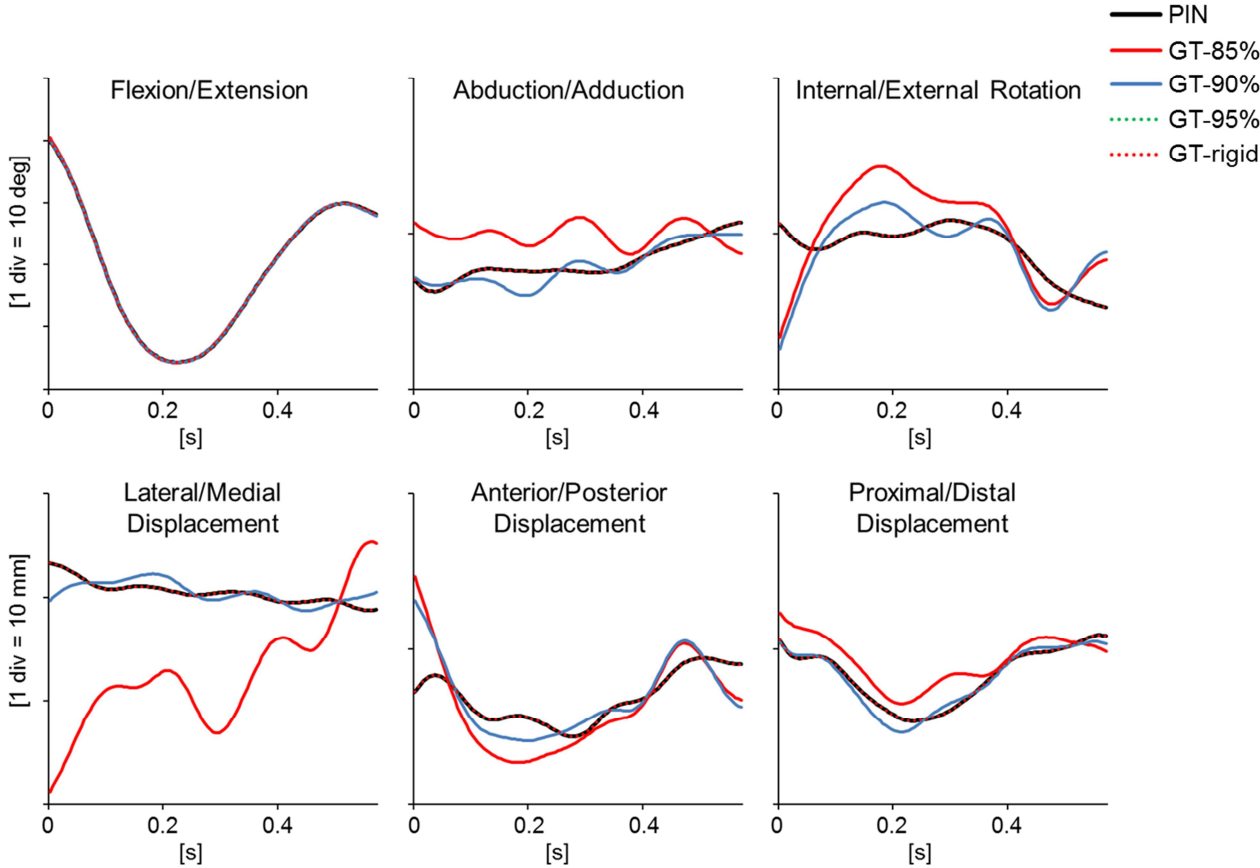


**Figure 6.6** – The six knee joint kinematic components are shown for the same trial and volunteer of the Figure 6.4, as obtained using the following marker-cluster data: pin marker trajectories (REF, black solid line), compensated skin marker trajectories using modes that represent the rigid modes (GT-rigid, red dotted line), the 85% (GT-85%, red solid line), 90% (GT-90%, blue solid line), and 95% (GT-95%, green dotted line) of the total STA energy when the marker-cluster geometrical transformation is used.

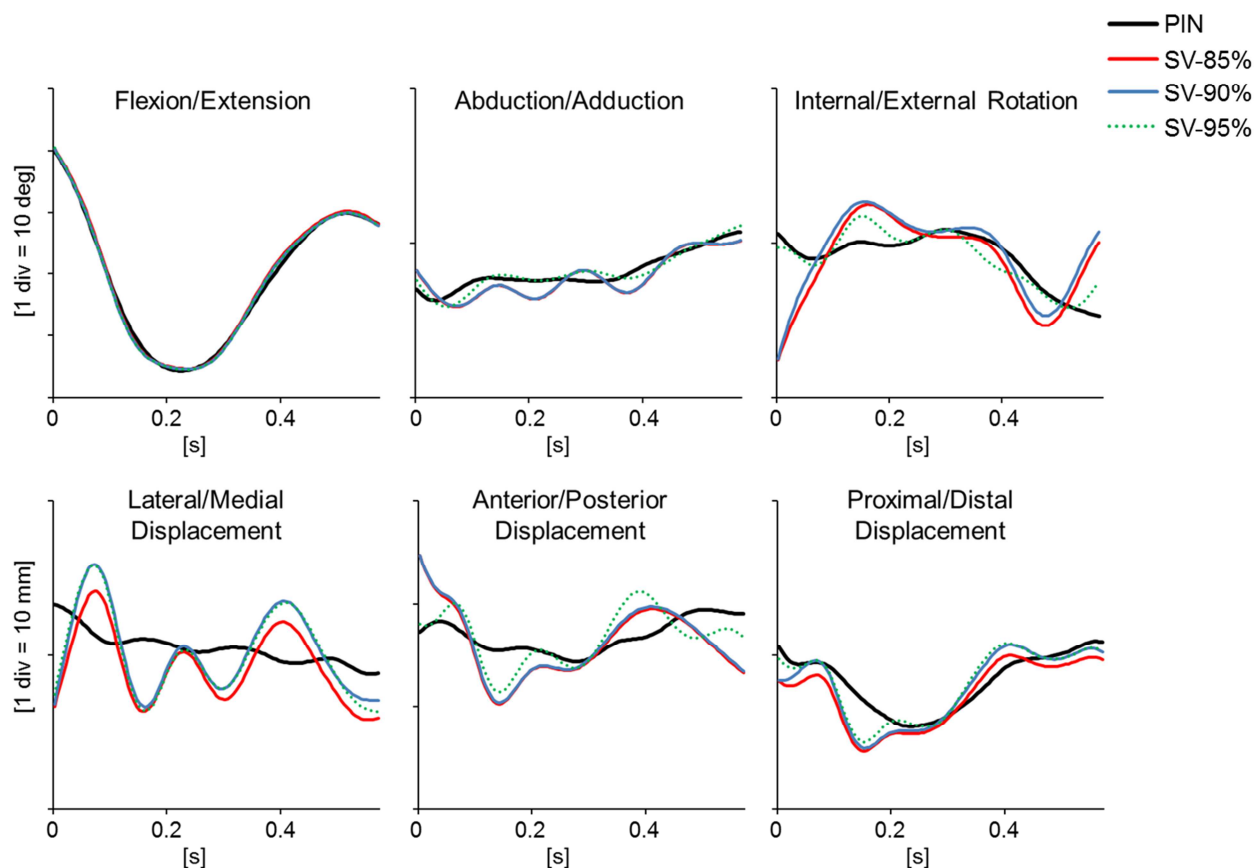


**Figure 6.7** – The six knee joint kinematic components are shown for the same trial and volunteer of the Figure 6.4, as obtained using the following marker–cluster data: pin marker trajectories (REF, black solid line), compensated skin marker trajectories using modes that represent the 85% (SV-85%, red solid line), 90% (SV-90%, blue solid line), and 95% (SV-95%, green dotted line) of the total STA energy when the skin envelope shape variation is used.

#### 6.4. Discussion

Recent literature has suggested that compensating for a selected portion of STAs may be sufficient for an appropriate estimation of joint kinematics (Andersen et al., 2012; Cappello et al., 2005; De Rosario et al., 2013; Dumas et al., 2014b). This hypothesis has been supported both by quantitative analysis of different STA definitions and representations (e.g., amplitude of markers displacements (Peters et al., 2010)), and qualitative considerations (e.g., types of marker-cluster transformation, patterns of skin envelope shape variation (Dumas et al., 2014a)). It has now been well established that an STA is mostly composed of a rigid component (Andersen et al., 2012; Barré et al., 2013; De Rosario et al., 2013; Dumas et al., 2014a; Grimpampi et al., 2014) and can be described by a reduced number of shape variations (Andersen et al., 2012; Dumas et al., 2014b). Thus, we could expect that the efficiency of compensation for a portion of STAs can be notably altered, depending on which of the different STA definitions found in the literature (MD, GT and SV) are utilized.

In this context, the present study assessed the accuracy of knee joint kinematics obtained with compensation using a selection of the modes that represent the STA. This modal approach was proposed as a generalized representation of the STA (Dumas et al., 2014b) and allows for different feature extraction and data reduction techniques. In fact, in the present study, the modes were selected by either truncation, taking those series of modes representing 90% of STA energy, or by direct choice, selecting only those representing the rigid component, *i.e.* translations and rotations of the marker-cluster (independently from their energy). This energy, normally called deformation energy (Dumas et al., 2014a), is associated to the mean square displacement of the skin markers caused by the STA and, therefore, it does not involve only the non-rigid transformation (deformation) but also the rigid transformation of the marker-cluster. For this reason, in this study, the expression STA energy was preferred.

Other arbitrary thresholds have been proposed in the literature 85% (Dumas et al., 2014a) and 95% (Andersen et al., 2012; Dumas et al., 2014b) for the data reduction. In addition to these thresholds, in this study, the choice of  $p_i = 90\%$  was set so that the percentage of STA energy,  $p_i^*$ , corresponding to the rigid GT modes, remains close to this threshold.

Compared to the number of GT modes, when the energy threshold was  $p_i^*$ , the number of truncated MD modes was double, and the number of truncated SV modes half. The number of truncated modes was generally higher for the shank than for the thigh, simply because the number of skin markers, and consequently the number of modes, ( $l = 1: 3m_i$ ) was different.

The selected modes were used to compute four STA-compensated skin marker position datasets (GT-rigid, MD-90%, GT-90%, and SV-90%) and the pose of the shank and thigh AFs were estimated using a least squares method (Söderkvist and Wedin, 1993). The term compensation is somewhat arbitrary in this context because the modes were selected and the STA-compensated skin marker positions computed knowing the reference pose of the segments (*i.e.*, obtained with the pin markers). This constitutes the main limitation of the present study, together with the low number of subjects and movements tested.

The present study confirms that STA compensation is mandatory, as the RMSEs on the knee joint kinematics due to STAs appeared to have the same magnitude as the RMS amplitudes for AA, IE, and were even superior for LM, AP and PD. Compensation utilizing the MD-90% dataset provided minor improvements in joint kinematics, and also had the highest number of selected modes. Therefore, compensating for a portion of the marker displacements does not seem appropriate. Noticeably, all markers have been included in the STA models based on this STA definition

(Alexander and Andriacchi, 2001; Camomilla et al., 2013; *Chapter 3*). Conversely, compensation with the GT-90% and SV-90% datasets provided fair results, and the number of selected modes was also the lowest for the SV definition. This was expected because the basis of vector is constructed with proper orthogonal decomposition that finds the optimal low rank approximation to a dataset, in a least squares sense. No STA models based on the SV definition have been proposed so far in the literature, perhaps because it cannot be used without having the true pose of the segments (*i.e.*, obtained with pin markers) from which the basis of vectors may be derived.

Not surprising, when the STA-compensation is performed with an higher threshold for the STA energy, RMSE values decrease in all the proposed definitions (Table 6.3, Figs. 6.5-6.7), but the number of modes increase in both segments (Table 6.1-6.2). In the perspective to model the STA time histories, a trade-off between STA representation and effectiveness has to be done.

Therefore, the portion of the STA that is the most appropriate for compensation is represented by the rigid GT modes (*i.e.*, three translations and three rotations of the marker-cluster). The improvements in joint kinematics were remarkable, and the number of modes constant:  $r_i^* = 6$ , independently from the subject, the trial and the number of skin markers. The virtually null RMSEs can be explained by the fact that the joint kinematics are obtained through a least squares method (Söderkvist and Wedin, 1993) (*i.e.* affected exclusively by the rigid movement of the marker-cluster).

It was recently stated in the literature (Andersen et al., 2012; Dumas et al., 2014b; Grimpampi et al., 2014) that any least squares method directly applied to the skin marker positions cannot be effective because it does not address the rigid component of the STA, which is of greater amplitude than the non-rigid component. As a consequence, the portion of the STA which should be modelled to correct the skin marker position is this rigid component. Such an STA model has already been applied to estimating the joint centre of a ball-and-socket mechanical analog (De Rosario et al., 2013), but not to the estimation of in vivo joint kinematics.

Further examination of the STA's main portions (e.g., direction and anatomical region of high or low marker displacements, relative proportions between translation, rotation and deformation of the marker-cluster, patterns of the main shape variations) and of how they impact joint kinematics remain of considerable interest to further knowledge of this phenomenon. However, in designing an STA model, it seems clear that such a model must be based on the rigid component of the STA. Whether such a model can be driven by joint angles or other biomechanical parameters, be

calibrated using in vivo data, and finally be embedded in the least squares method are the next issues to be solved in order to obtain an accurate estimation of joint kinematics.

## 7. Chapter 7

The content of this chapter is referred to the article

### “A MODEL OF THE SOFT TISSUE ARTEFACT RIGID COMPONENT”

Submitted for publication (under first review in Journal of Biomechanical Engineering).

Additional information are also presented.

#### Symbols and Nomenclature

	$i$	body segment ( $i = th$ and $sh$ , for thigh and shank respectively)	
	$j$	skin marker ( $j = 1:m_i$ )	
	$k$	sampled instant of time ( $k = 1:n$ )	
	$\mathbf{v}_i^j(k)$	STA vector of the skin marker $j$ glued on the segment $i$	
	$\mathbf{V}_i(k)$	STA field of the segment $i$	
	$a_i^l(k)\Phi_i^l$	mode $l$	
	$\Phi_i^l$	mode direction	
	$a_i^l(k)$	mode amplitude	
	$\tilde{\mathbf{V}}_i(k)$	STA field of the segment $i$ approximated by six rigid modes	
Symbols	$\tilde{a}_i^l$	modelled mode amplitude	
	$\mathbf{h}_i^l$	model parameters vector	
	$\alpha(k)$	hip orientation vector projected along pelvic anterior-posterior axes (FE)	
	$\beta(k)$	hip orientation vector projected along pelvic medial-lateral axes (AA)	
	$\gamma(k)$	hip orientation vector projected along pelvic inferior-superior axes (IE)	
	$\delta(k)$	knee orientation vector amplitude	
	$\zeta(k)$	ankle orientation vector projected along shank medial-lateral axes (Plantar/Flexion)	
	$\eta(k)$	ankle orientation vector projected along foot anterior-posterior axes (Inversion/Eversion)	
	$\tilde{\mathbf{V}}_i(k)$	STA field of the segment $i$ approximated by modelling rigid modes	
	$\hat{\mathbf{V}}_i(k)$	artefact-compensated skin marker data	
	Knee degrees of freedom	FE	flexion/extension
		AA	abduction/adduction
IER		internal/external rotation	
LM		medio/lateral	
AP		anterior/posterior	
PD		proximal/distal	

Nomenclature	STA	soft tissue artefact
	BPE	bone pose estimator
	REF	reference pin data
	MMD	measured skin-marker data
	CMD	artefact-compensated skin marker data
	rmsd	root mean square difference between each measured $a_i^l$ , and modelled $\tilde{a}_i^l$ , amplitudes resulting at the end of the calibration procedure.
	$\rho$	Pearson correlation coefficient
	SD	standard deviation
	IQR	inter-quartile range

### 7.1. Introduction

In professional decision-making based on the analysis of non-invasive human movement, accurately estimating skeletal kinematics, and joint kinematics in particular, is crucial (Andriacchi and Alexander, 2000; Baker, 2006; Cappozzo et al., 2005). When this estimate is based on stereophotogrammetric data, it is subject to errors caused by movement between the skin markers and the underlying bones, *i.e.* the so-called soft tissue artefact (STA) (Leardini et al., 2005; Peters et al., 2010). This source of error is totally disruptive for the joints' degrees of freedom with a limited range of motion, such as knee abduction-adduction, internal–external rotation, and linear displacements (e.g. Benoit et al., 2006, Akbarshahi et al., 2010, Tsai et al., 2009).

The STA of a body segment may be represented, at marker level, as a vector field made up of displacements of the individual markers relative to the underlying bone. Alternatively, it may be described at marker-cluster level by considering the markers as landmark points of a deformable shape undergoing geometric transformation (Bookstein, 1989), *i.e.* a transformation formed by a non-rigid (a change in size and shape), and a rigid component (translation and rotation displacement) (Andersen et al. 2012; Barré et al. 2013; Benoit et al., 2015; de Rosario et al., 2012; Dumas et al. 2014a; Grimpampi et al. 2014). The latter component has been recently proved to be the dominant part (Andersen et al., 2012; Barré et al., 2013; Benoit et al., 2015; Dumas et al., 2014b).

To date, the most commonly used bone pose estimators (BPEs) are based on the Procrustes superimposition approach (Andriacchi et al., 1998; Arun et al., 1987; Ball and Pierrynowski, 1998; Cappello et al., 1996; Cappozzo et al., 1997; Cereatti et al., 2006; Challis, 1995; Chèze et al., 1995; Dryden and Mardia, 2002; Heller et al., 2011; Söderkvist and Wedin, 1993; Veldpaus et al., 1988). These BPEs leave untouched the rigid component of the artefact, which directly maps into the bone pose estimate. Any attempt to improve the bone pose estimate must, therefore, deal with this issue.

One possibility of improving the bone pose estimate and account for the rigid component is to estimate it through embedding a mathematical model of the artefact in the BPE and thus correct the original marker displacement data. The literature has proposed models that were either chosen in a rather arbitrary fashion, or required cumbersome ad hoc experiments for the *a priori* determination of their parameters (Alexander and Andriacchi, 2001; Cappello et al., 1997; Lucchetti et al., 1998). A further option is the multi-body optimization approach, which, however, by embedding constraints at the joints, limits the possibility of assessing their real kinematics (Andersen et al., 2010; Li et al., 2012; Stagni et al., 2009). Hence practical and effective countermeasures for the STA's rigid component are to date still unavailable.

Enhanced mathematical models of the STA, besides dealing with the rigid component of the artefact, must take into account the following critical aspects. First, STAs are subject-, marker-location-, and motor act-specific, thus no *a priori* quantitative or specific knowledge may be expected (Peters et al., 2010). Therefore, although we may assume that a generalizable STA model architecture may be identified (Camomilla et al., 2013; *Chapter 3*), its parameters must be determined (model calibration) using information generated during execution by the subject of the specific motor act under analysis. Second, since the model calibration must be concurrent with the bone pose estimate, the likeliness of finding a solution of the relevant optimization problem is influenced by the number of parameters of the STA rigid component model embedded in the BPE optimization which, therefore, must be kept as low as possible.

This study presented in *this Chapter* is aimed to devise the architecture of a model for the artefact that brings together the priority of accounting for the STA rigid component and minimizing the number of model's parameters.

Dumas et al. (2014a), or presented here in *Chapter 4*, have suggested mathematically representing the STA as a geometrical transformation of the marker-cluster through a modal series. Each mode corresponds to the projection of the STA field onto a basis vector appropriately chosen to represent the rigid and non-rigid components. This series, similarly to that produced by principal component analysis (Andersen et al., 2012), is mostly used for feature extraction and data reduction. However, it can also be used as a mathematical representation of the STA that allows isolating its different components and, in particular, the rigid component of interest. Thus, by considering only the six modes relative to rotation and translation of the marker-cluster (thereafter called rigid modes), the STA rigid component can be represented as consisting of six basis unity vectors multiplied by six time functions (mode amplitudes), whatever the number of markers in the cluster.

Since the cost function of a BPE is based on the distance between measured and modelled marker trajectories, the marker-cluster rotations and translations must be transformed into the latter trajectories to embed the STA model in the BPE. This is normally done using quaternions, attitude vectors, or transformation matrices (de Rosario et al., 2013, Richard et al., 2012) that entail specific algebra and constraints (e.g., unitary quaternions, orthogonal matrices). This procedure, overly complicated from the computational point of view, can be avoided by using the modal representation, which is a more convenient choice for the optimization procedure of the BPE.

Previous studies (Akbarshahi et al, 2010; Cappozzo et al., 1996; Camomilla et al., 2013; *Chapter 3*) have established a linear relationship between marker displacements and the proximal and distal articular angles. Moreover, Barré et al. (2013) and Sangeux et al. (2006) described a linear relationship between marker-cluster rigid movements and joint angles. One of these studies showed that soft tissue wobbling and deformations due to muscle contraction could reasonably be neglected in slow running, a motor task not entailing abrupt accelerations (as presented in the *Chapter 3*). Based on these evidences, it was decided to model the amplitude of the six rigid modes, assuming that, in similar motor tasks, also the rigid component of the artefact mostly depends on joint motion and is linearly correlated with proximal and distal joint angles. The issue as to the possibility of neglecting soft tissue wobbling and deformations due to muscle contraction was also tackled.

The feasibility of the artefact rigid component model was tested for the thigh and shank, and its effectiveness in compensating for the artefact was assessed within the estimation of knee joint kinematics, as a worst case and relevant scenario. To this purpose pin- and skin-marker data of three running subjects were analysed (Reinschmidt et al., 1997c)

## 7.2. Materials and Methods

### 7.2.1. STA rigid component model architecture

An STA vector,  $\mathbf{v}_i^j(k)$ , is defined to represent the displacement from a fixed reference position that the skin marker  $j$  ( $j=1, \dots, m_i$ ), associated with the body segment  $i$ , undergoes relative to a bone-embedded anatomical frame at each sampled instant of time  $k$  ( $k=1, \dots, n$ ). The STA of all markers, vectors  $\mathbf{v}_i^j(k)$ , can be used to build an STA field for each segment:

$$\mathbf{V}_i(k) = \begin{bmatrix} \mathbf{v}_i^1(k) \\ \vdots \\ \mathbf{v}_i^j(k) \\ \vdots \\ \mathbf{v}_i^{m_i}(k) \end{bmatrix}$$

(Eq. 7.1).

To describe the geometrical transformations of a marker-cluster, this STA field can be projected onto the basis vectors,  $\{\Phi_i^l\}$  ( $l = 1, \dots, 12$ ), representing three translations, three rotations, three homotheties, and three stretches. These basis vectors are built *a priori* (see *Paragraph 4.5.2*, for further details), using the reference position of the markers, while the amplitudes,  $a_i^l(k)$ , are the projections of  $V_i(k)$  over them. With this description, the mode  $l$  is indicated as  $a_i^l(k)\Phi_i^l$  and its amplitude,  $a_i^l(k)$ , is homogeneous to a distance. When only the rigid component of the STA is taken into account, the construction of the basis vectors remains the same, but the STA field is approximated by six additive modes:

$$\check{V}_i(k) = \sum_{l=1}^6 a_i^l(k)\Phi_i^l \quad (\text{Eq. 7.2})$$

In the architecture we propose for the STA rigid component, the amplitudes of the rigid modes were modelled as function of the kinematics of the adjacent joints. The model inputs were selected to describe the features of joints kinematics that are assumed to impact most on the artefact,  $\Lambda(k)$ . Joint kinematics was represented using the attitude vector (Woltring, 1994). For the knee we used its amplitude and, for the hip and ankle, its components relative to selected joint axes, since this approach has been proved to be less prone to experimental error propagation (Chèze, 2000). The joint axes were defined as the latero-medial axis of the proximal anatomical frame, the longitudinal axis of the distal one, and the cross-product between the latter axes as described in Wu et al. (2002) for the hip and in (Baker 2003; Cole et al., 1993) for the ankle. Based on the experience reported in Camomilla et al. (2013) and Bonci et al. (2014) with artefact representation at individual marker level, a linear relationship between artefact rigid mode amplitudes and  $\Lambda(k)$  was assumed and the mode amplitudes,  $\tilde{a}_i^l$ , for the thigh and shank segment ( $i = th, sh$ ) were modelled as:

$$\tilde{a}_{th}^l(\Lambda_{th}(k)) = h_{th,\alpha}^l\alpha(k) + h_{th,\beta}^l\beta(k) + h_{th,\gamma}^l\gamma(k) + h_{th,\delta}^l\delta(k) + h_{th,0}^l$$

with  $\Lambda_{th}(k) = [\alpha(k), \beta(k), \gamma(k), \delta(k)]$  (Eq. 7.3),

$$\tilde{a}_{sh}^l(\Lambda_{sh}(k)) = h_{sh,\delta}^l\delta(k) + h_{sh,\zeta}^l\zeta(k) + h_{sh,\eta}^l\eta(k) + h_{sh,0}^l$$

with  $\Lambda_{sh}(k) = [\delta(k), \zeta(k), \eta(k)]$  (Eq. 7.4),

where  $\Lambda_i(k)$  represents the relevant joint kinematics ( $\alpha(k), \beta(k), \gamma(k)$  are the components of the hip attitude vector,  $\delta(k)$  is the knee attitude vector amplitude, and  $\zeta(k), \eta(k)$  are the components of the ankle attitude vector relative to the dorsi/plantar flexion and inversion/eversion axes, while the

pronation-supination component was not accounted for because too small);  $\mathbf{h}_{th}^l, \mathbf{h}_{sh}^l$  are the model parameter vectors to be determined through a calibration procedure. The parameters  $h_{i,0}^l$  are determined so that the modelled vectors have a zero value when the subject assumes a reference posture. Therefore, the STA rigid component was modelled using the same basis vectors as in Eq. 7.2 and the above-mentioned modelled mode amplitudes:

$$\tilde{\mathbf{V}}_i(\boldsymbol{\Lambda}_i(k)) = \sum_{l=1}^6 \tilde{a}_i^l(\boldsymbol{\Lambda}_i(k), \mathbf{h}_i^l) \boldsymbol{\Phi}_i^l$$

(Eq. 7.5).

The choice of the above-mentioned angles to modelled thigh and shank STA was assessed using the described experimental data with different angle time histories combinations for both segments described in Table 7.1 and comparing the obtained results as described in the next sections. At the end, the number of parameters of the model is 30 for the thigh and 24 for the shank.

	<b>Thigh STA modelling</b>	<b>Shank STA modelling</b>
<b>1</b>	<ul style="list-style-type: none"> <li>• Hip FE</li> <li>• Hip AA</li> <li>• Hip IER</li> <li>• Knee Orientation Vector</li> </ul>	<ul style="list-style-type: none"> <li>• Knee Orientation Vector</li> <li>• Ankle Orientation Vector</li> </ul>
<b>2</b>	<ul style="list-style-type: none"> <li>• Hip FE</li> <li>• Hip AA</li> <li>• Hip IER</li> <li>• Knee Orientation Vector</li> </ul>	<ul style="list-style-type: none"> <li>• Knee Orientation Vector</li> <li>• Plantar/Flexion component of the ankle Orientation Vector</li> <li>• Inversion/Eversion component of the ankle orientation vector</li> </ul>
<b>3</b>	<ul style="list-style-type: none"> <li>• Hip FE</li> <li>• Hip AA</li> <li>• Hip IER</li> <li>• FE component of knee Orientation Vector</li> </ul>	<ul style="list-style-type: none"> <li>• FE component of knee Orientation Vector</li> <li>• Plantar/Flexion component of the ankle Orientation Vector</li> <li>• Inversion/Eversion component of the ankle orientation vector</li> </ul>
<b>4</b>	<ul style="list-style-type: none"> <li>• Hip FE</li> <li>• Hip AA</li> <li>• Hip IER</li> <li>• Knee FE</li> </ul>	<ul style="list-style-type: none"> <li>• Knee FE</li> <li>• Ankle Plantar/Flexion</li> <li>• Ankle Inversion/Eversion</li> </ul>
<b>5</b>	<ul style="list-style-type: none"> <li>• Hip Orientation Vector</li> <li>• Knee Orientation Vector</li> </ul>	<ul style="list-style-type: none"> <li>• Knee Orientation Vector</li> <li>• Ankle Orientation Vector</li> </ul>
<b>6</b>	<ul style="list-style-type: none"> <li>• Hip FE</li> <li>• Hip IER</li> <li>• Knee Orientation Vector</li> </ul>	<ul style="list-style-type: none"> <li>• Knee Orientation Vector</li> <li>• Ankle Orientation Vector</li> </ul>
<b>7</b>	<ul style="list-style-type: none"> <li>• FE component of the hip Orientation Vector</li> <li>• AA component of the hip Orientation Vector</li> <li>• IE component of the hip Orientation Vector</li> <li>• Knee Orientation Vector</li> </ul>	<ul style="list-style-type: none"> <li>• Knee Orientation Vector</li> <li>• Ankle Orientation Vector</li> </ul>
<b>8</b>	<ul style="list-style-type: none"> <li>• FE component of the hip Orientation Vector</li> <li>• AA component of the hip Orientation Vector</li> <li>• IE component of the hip Orientation Vector</li> <li>• Knee Orientation Vector</li> </ul>	<ul style="list-style-type: none"> <li>• Knee Orientation Vector</li> <li>• Plantar/Flexion component of the ankle Orientation Vector</li> <li>• Inversion/Eversion component of the ankle orientation vector</li> </ul>

**Table 7.1** – Eight different combinations of joint angles for thigh and shank STA modelling.

7.2.2. *Experimental data*

To assess the model architecture feasibility and its STA compensation effectiveness, the pin- and skin-marker data acquired by Reinschmidt et al. (1997c) were used. Three male volunteers (V1, V2, V3; age  $27.7 \pm 2.1$  years, mass  $85.5 \pm 9.6$  kg, stature  $1.86 \pm 0.10$  m) were analysed while running at slow speed ( $2.9 \pm 0.2$  ms<sup>-1</sup>). Three clusters of three markers each attached to an intracortical pin. These pins were inserted into the postero-lateral aspect of the right calcaneus, lateral tibial condyle and lateral femoral epicondyle. Five skin markers were glued on the thigh ( $m_{th} = 5$ ) and six on the shank ( $m_{sh} = 6$ ) (Figure 7.1). Markers were tracked using a three film-camera system (sampling frequency: 200 frames/s). For each volunteer, the stance phase of five running trials was captured. Reference thigh and shank anatomical frames were defined by an anatomical calibration that used a radiostereometric analysis (van den Bogert et al., 2008). The foot frame was defined as parallel to the global frame while standing. The reference poses of these three anatomical frames were estimated in each instant of time during movement, using pin markers, through a Procrustes superimposition approach (Söderkvist and Wedin, 1993). Due to the lack of pins and markers on the pelvis segment, the relevant anatomical frame was assumed to be always parallel to the global frame.

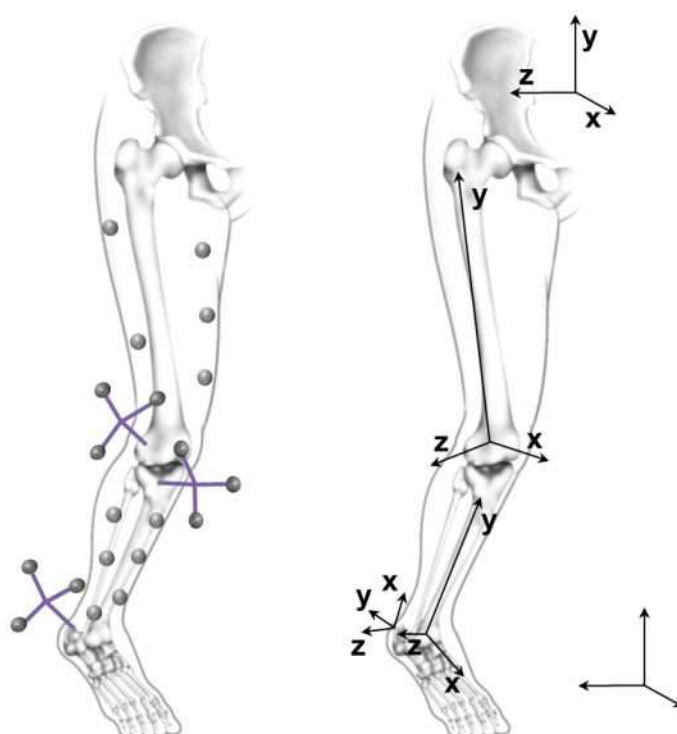


**Figure 7.1** – Positions of the skin markers glued on thigh and shank during the running trials are shown on the left side. The pelvis, thigh, shank, and foot anatomical frames are indicated on the right side.

### 7.2.3. STA model calibration

The hip, knee, and ankle attitude vector components were computed using the four anatomical frames and the conventions defined above. For the thigh and shank segments ( $i = th, sh$ ), the STA vectors,  $\mathbf{v}_i^j(k)$ , were defined as the displacement of the skin markers relative to their mean position in the local frame over the five running trials for each volunteer. These mean positions were considered as a reference also to build subject-specific basis vectors for the rigid modes of each body segment,  $\Phi_i^l$ , ( $l = 1, \dots, 6$ ) (Chapter 4). To obtain the measured amplitudes of the rigid modes,  $a_i^l(k)$ , the STA fields of each trial,  $\mathbf{V}_i(k)$ , were projected on these subject-specific basis vectors.

The rigid STA model,  $\tilde{\mathbf{V}}_i(\Lambda_i(k))$ , was calibrated and the model parameters,  $\mathbf{h}_i^l$ , were identified by minimising the sum of the squared differences between measured,  $a_i^l(k)$ , and modelled amplitudes,  $\tilde{a}_i^l(\Lambda_i(k), \mathbf{h}_i^l)$ . The Pearson correlation coefficient ( $\rho$ ) between these amplitudes was used as a penalty factor to exclude solutions that result in estimated STA components in an opposite direction to the measured STA. The optimization problem was solved using a non-linear least-squares minimization method in Matlab® (trust-region-reflective). For further details on the calibration procedure, see the Chapter 3.

### 7.2.4. STA compensation

Three different datasets were determined to assess the effectiveness of the proposed modelling approach to compensate for the STA:

- a. pin data (reference: REF);
- b. measured skin-marker data that, with the pin data, provide the measured STA field,  $\mathbf{V}_i$  (MMD);
- c. artefact-compensated skin marker data (CMD), as obtained by subtracting the modelled STA rigid component (Eq. 7.3 and Eq. 7.4) from the measured STA field:

$$\hat{\mathbf{V}}_i(\Lambda_i(k)) = \mathbf{V}_i(k) - \tilde{\mathbf{V}}_i(\Lambda_i(k)) \quad (\text{Eq. 7.6}).$$

This residual STA field embeds both the STA non-rigid component ( $\hat{\mathbf{V}}_i(\Lambda_i(k)) = \mathbf{V}_i(k) - \tilde{\mathbf{V}}_i(k)$ ) and the difference between the real and modelled rigid component ( $\tilde{\mathbf{V}}_i(k) - \tilde{\mathbf{V}}_i(\Lambda_i(k))$ ).

### 7.2.5. Evaluation of calibration feasibility and compensation effectiveness

Calibration feasibility was assessed in terms of Pearson correlation coefficient and of the root mean square difference (rmsd) between each measured,  $a_i^l(k)$ , and modelled,  $\tilde{a}_i^l(\Lambda_i(k), \mathbf{h}_i^l)$ , amplitude.

Compensation effectiveness was tested based on the estimates of knee angular and linear displacements computed using the three above-listed datasets (REF, MMD, CMD). Shank and thigh poses were estimated using the Procrustes superimposition approach (Söderkvist and Wedin, 1993) between measured and reference marker positions in the relevant anatomical frame; the knee joint angles (flexion/extension, FE; abduction/adduction, AA; internal/external rotation, IE) were estimated consistently with the Cardanic convention (Grood and Suntay, 1983). The midpoint between the two epicondyles (C) was calibrated using the above-mentioned radiostereometric data. Its position was determined both in the thigh ( $C_1$ ) and shank ( $C_2$ ) anatomical frames. Knee linear displacement was defined as the vector from  $C_1$  to  $C_2$ . Its components (lateral/medial, LM; antero/posterior, AP; proximal/distal, PD) were defined performing non-orthogonal projections onto the joint axes (Desroches et al., 2010).

To assess the similarity between the reference knee kinematics (REF) and the kinematics obtained using measured (MMD) and compensated (CMD) skin-marker trajectories, root mean square difference (rmsd) values, their percentage value with respect to the relevant range (rmsd%), and the Pearson correlation coefficient were calculated. The values of the latter coefficient were classified as follows: low for  $\rho \leq 0.35$ , moderate for  $0.36 < \rho < 0.67$ , high for  $0.68 < \rho < 0.89$ , and very high for  $\rho \geq 0.90$  (Taylor, 1990).

Moreover, the proposed architecture models only the effect of soft tissue deformation produced directly by joint motion. To assess if soft tissue wobbling becomes the dominant source of error after the proposed STA compensation, we analysed the power distribution of the error affecting knee kinematics time histories. This error was obtained subtracting reference kinematics to that obtained using the MMD and CMD datasets. Soft tissue wobbling during running was assumed to be included in the 5-10 Hz frequency range (Wakeling and Nigg, 2001). Therefore, two frequency bands (below 5 Hz, associated to skin sliding, and above 5 Hz, for soft tissue wobbling) were considered. After removing the mean value and having zero padded the data series to 512 samples, since the acquired trials did not last more than 1s (200 samples), the mean powers in these bands were estimated by applying a fast Fourier transform to the relevant autocorrelation function.

Descriptive statistics of selected quantities were obtained after testing for normal distribution, using the Shapiro-Wilk normality test, using the five-number summary technique (minimum, lower quartile, median, upper quartile, and maximum) and representing the data using box-plots. Lower and upper quartiles were used to calculate the inter-quartile range (IQR). Power distribution of the kinematic error obtained with the MMD and CMD datasets were compared using the non-

parametric statistical analysis of Friedman for repeated measures, due to the non-normal distributions of most of the parameters. Statistical significance was set to  $p < 0.05$ . SPSS version 21.0 (IBM SPSS Inc., Chicago, USA).

### 7.3. Results

#### 7.3.1. STA assessment

The statistics of the root mean square (rms) of the twelve STA mode amplitudes which describe marker-cluster motion relative to the bone in terms of geometrical transformation (rigid motion: rotation and translation; non-rigid motion: homothety and stretch) is shown in Figure 7.2; the general characteristics of these components were consistent among volunteers.

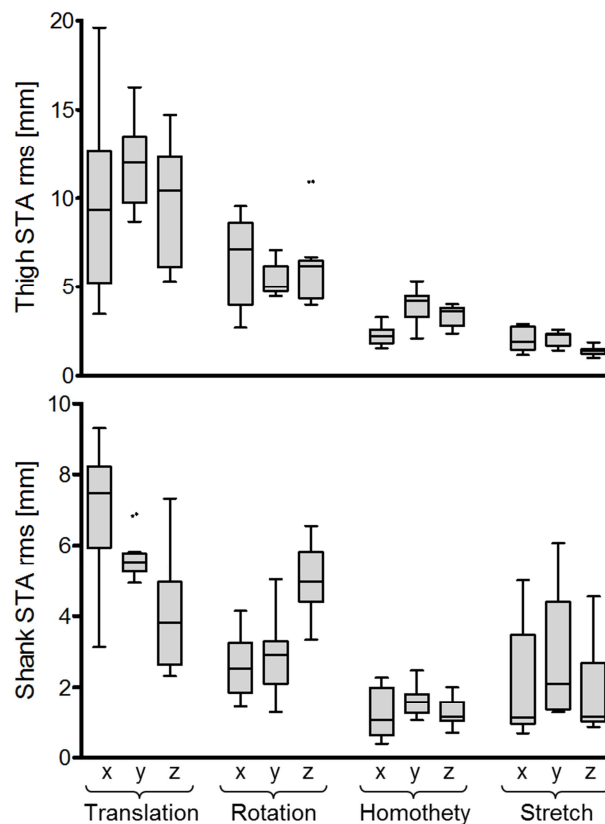


**Figure 7.2** – Box-plots (minimum, lower quartile, median, upper quartile, and maximum) of the root mean square values of the measured amplitudes of the STA modes,  $a_i^l(k)$ , for thigh and shank along the different basis vectors defined using the marker-cluster geometrical transformations. Statistics performed over 15 trials (five trials performed by each of the three volunteers). Outliers are also shown.

## 7.3.2. STA modelling: selection of angle time histories

The results of the thigh and shank modelling with different angle time histories (Table 7.1) are shown in Tables 7.2 and 7.3. In addition, also the impact on the knee joint estimations was evaluated (Table 7.4).

	$\rho$ Thigh								rmsd [mm] Thigh								rmsd% Thigh								
	1	2	3	4	5	6	7	8	1	2	3	4	5	6	7	8	1	2	3	4	5	6	7	8	
Translation	x	0.92 (0.30)	0.92 (0.30)	0.92 (0.31)	0.92 (0.34)	0.59 (0.43)	0.88 (0.31)	0.91 (0.23)	0.91 (0.23)	2.5 (1.2)	2.5 (1.2)	2.5 (1.4)	2.5 (1.6)	4.3 (1.5)	3.7 (1.6)	2.1 (0.7)	2.1 (0.7)	14 (47)	14 (47)	14 (49)	14 (50)	29 (44)	24 (46)	18 (34)	18 (34)
	y	0.98 (0.02)	0.98 (0.02)	0.98 (0.02)	0.98 (0.02)	0.81 (0.07)	0.94 (0.04)	0.97 (0.02)	0.97 (0.02)	2.5 (1.2)	2.5 (1.2)	2.0 (1.4)	2.0 (1.3)	6.3 (2.2)	4.3 (1.6)	2.5 (1.1)	2.5 (1.1)	14 (11)	14 (11)	13 (8)	13 (8)	44 (20)	25 (10)	14 (12)	14 (12)
	z	0.95 (0.17)	0.95 (0.17)	0.95 (0.17)	0.95 (0.16)	0.42 (0.60)	0.90 (0.21)	0.92 (0.20)	0.92 (0.20)	2.3 (1.4)	2.3 (1.4)	2.3 (1.4)	2.3 (1.4)	5.0 (2.9)	3.2 (1.2)	2.7 (1.3)	2.7 (1.3)	13 (46)	13 (46)	12 (46)	13 (44)	40 (64)	19 (45)	16 (49)	16 (49)
Rotation	x	0.95 (0.10)	0.95 (0.10)	0.95 (0.10)	0.95 (0.10)	0.72 (0.26)	0.93 (0.16)	0.94 (0.13)	0.94 (0.13)	1.2 (0.7)	1.2 (0.7)	1.2 (0.7)	1.2 (0.7)	2.9 (1.1)	1.7 (1.0)	1.2 (0.8)	1.2 (0.8)	12 (22)	12 (22)	12 (22)	12 (22)	32 (25)	13 (28)	12 (26)	12 (26)
	y	0.81 (0.40)	0.81 (0.40)	0.81 (0.45)	0.81 (0.40)	0.48 (0.24)	0.62 (0.49)	0.80 (0.29)	0.80 (0.29)	2.9 (2.5)	2.9 (2.5)	2.9 (2.8)	2.9 (2.7)	5.1 (1.1)	3.9 (2.9)	3.2 (2.1)	3.2 (2.1)	32 (56)	32 (56)	32 (66)	32 (63)	53 (41)	39 (61)	38 (53)	38 (53)
	z	0.97 (0.01)	0.97 (0.01)	0.97 (0.02)	0.97 (0.02)	0.39 (0.53)	0.95 (0.04)	0.96 (0.03)	0.96 (0.03)	1.4 (0.7)	1.4 (0.7)	1.1 (0.6)	1.1 (0.6)	4.1 (1.5)	1.7 (0.8)	1.6 (0.7)	1.6 (0.7)	14 (10)	14 (10)	13 (7)	11 (8)	45 (33)	21 (10)	17 (13)	17 (13)
N°Par	4	4	4	4	2	3	4	4	4	4	4	4	2	3	4	4	4	4	4	4	2	3	4	4	

**Table 7.2** – Median and inter-quartile range (IQR) correlation coefficient  $\rho$ , rmsd and rmsd% (expressed as percent of the root mean square value over time of the relevant rigid mode amplitude) values between the measured,  $a_i^l$ , and the modelled,  $\tilde{a}_i^l$ , rigid mode amplitudes for the thigh segment. Statistics performed over all trials and volunteers. Thigh STA modelling were performed using the eight different time history combinations. The number of the angle time histories are also shown (N° Par).

		$\rho$ Shank								rmsd [mm] Shank								rmsd% Shank							
		1	2	3	4	5	6	7	8	1	2	3	4	5	6	7	8	1	2	3	4	5	6	7	8
Translation	x	0.89 (0.06)	0.94 (0.05)	0.94 (0.05)	0.93 (0.06)	0.89 (0.06)	0.89 (0.06)	0.89 (0.06)	0.94 (0.05)	2.5 (1.0)	2.1 (0.7)	2.1 (0.7)	2.4 (1.5)	2.5 (1.0)	2.5 (1.0)	2.5 (1.0)	2.1 (0.7)	25 (8)	22 (7)	23 (7)	24 (12)	25 (8)	25 (8)	25 (8)	22 (7)
	y	0.68 (0.21)	0.78 (0.12)	0.84 (0.16)	0.83 (0.30)	0.68 (0.21)	0.68 (0.21)	0.68 (0.21)	0.78 (0.12)	4.1 (0.6)	3.5 (1.2)	2.8 (1.4)	3.6 (2.1)	4.1 (0.6)	4.1 (0.6)	4.1 (0.6)	3.5 (1.2)	46 (41)	37 (18)	37 (25)	25 (50)	46 (41)	46 (41)	46 (41)	37 (18)
	z	0.78 (0.32)	0.79 (0.29)	0.77 (0.27)	0.85 (0.18)	0.78 (0.32)	0.78 (0.32)	0.78 (0.32)	0.79 (0.29)	2.4 (1.1)	2.1 (1.3)	2.0 (1.3)	2.1 (1.3)	2.4 (1.1)	2.4 (1.1)	2.4 (1.1)	2.1 (1.3)	12 (44)	11 (20)	11 (22)	11 (22)	12 (44)	12 (44)	12 (44)	11 (20)
Rotation	x	0.91 (0.16)	0.91 (0.16)	0.90 (0.16)	0.92 (0.09)	0.91 (0.16)	0.91 (0.16)	0.91 (0.16)	0.91 (0.16)	1.2 (0.9)	1.2 (0.9)	1.2 (0.8)	1.2 (0.7)	1.2 (0.9)	1.2 (0.9)	1.2 (0.9)	1.2 (0.9)	10 (20)	9 (8)	9 (7)	7 (16)	10 (20)	10 (20)	10 (20)	9 (8)
	y	0.68 (0.22)	0.78 (0.08)	0.78 (0.09)	0.86 (0.19)	0.68 (0.22)	0.68 (0.22)	0.68 (0.22)	0.78 (0.08)	1.7 (1.5)	1.5 (1.3)	1.3 (1.2)	1.1 (1.0)	1.7 (1.5)	1.7 (1.5)	1.7 (1.5)	1.5 (1.3)	54 (26)	40 (29)	42 (23)	33 (23)	54 (26)	54 (26)	54 (26)	40 (29)
	z	0.95 (0.07)	0.96 (0.04)	0.96 (0.03)	0.96 (0.07)	0.95 (0.07)	0.95 (0.07)	0.95 (0.07)	0.96 (0.04)	1.3 (0.9)	1.1 (0.6)	1.2 (0.5)	1.1 (0.9)	1.3 (0.9)	1.3 (0.9)	1.3 (0.9)	1.1 (0.6)	15 (12)	13 (10)	13 (9)	13 (7)	15 (12)	15 (12)	15 (12)	13 (10)
<b>N°Par</b>		<b>2</b>	<b>3</b>	<b>3</b>	<b>3</b>	<b>2</b>	<b>2</b>	<b>2</b>	<b>3</b>	<b>2</b>	<b>3</b>	<b>3</b>	<b>3</b>	<b>2</b>	<b>2</b>	<b>2</b>	<b>3</b>	<b>2</b>	<b>3</b>	<b>3</b>	<b>3</b>	<b>2</b>	<b>2</b>	<b>2</b>	<b>3</b>

**Table 7.3** – Median and inter-quartile range (IQR) correlation coefficient  $\rho$ , rmsd and rmsd% (expressed as percent of the root mean square value over time of the relevant rigid mode amplitude) values between the measured,  $a_i^l$ , and the modelled,  $\tilde{a}_i^l$ , rigid mode amplitudes for the shank segment. Statistics performed over all trials and volunteers. Thigh STA modelling were performed using the eight different time history combinations. The number of the angle time histories are also shown (N° Par).

		<b>knee kinematics</b>		<b>rmsd%</b>								
		<i>Range</i>	<i>rms</i>	$V_i$	$\widehat{V}_i$ (1)	$\widehat{V}_i$ (2)	$\widehat{V}_i$ (3)	$\widehat{V}_i$ (4)	$\widehat{V}_i$ (5)	$\widehat{V}_i$ (6)	$\widehat{V}_i$ (7)	$\widehat{V}_i$ (8)
<b>Angle</b>	<i>FE</i>	29 (13)	22 (2)	11 (7)	2 (1)	2 (1)	2 (0)	2 (1)	6 (2)	2(2)	2 (1)	2 (1)
	<i>AA</i>	10 (9)	4 (1)	79 (60)	21 (38)	21 (35)	22 (39)	21 (38)	32 (33)	25 (34)	23 (33)	23 (34)
[deg]	<i>IE</i>	10 (5)	5 (6)	51 (14)	34 (34)	29 (28)	28 (29)	27 (31)	36 (30)	35 (35)	35 (32)	30 (30)
<b>Displacement</b>	<i>LM</i>	5 (2)	4 (3)	114	42 (30)	39 (28)	39 (26)	40 (30)	65 (17)	50 (26)	42 (29)	37 (29)
	<i>AP</i>	8 (7)	5 (2)	118	31 (17)	28 (22)	24 (25)	28 (24)	75 (85)	45 (15)	43 (23)	36 (22)
[mm]	<i>PD</i>	7 (2)	5 (8)	238	49 (65)	35 (53)	32 (54)	45 (43)	94 (185)	46 (83)	52 (65)	33 (55)
<i>Number of angle time histories involved</i>					<b>4 + 2</b>	<b>4 + 3</b>	<b>4 + 3</b>	<b>4 + 3</b>	<b>2 + 2</b>	<b>3 + 2</b>	<b>4 + 2</b>	<b>4 + 3</b>

**Table 7.4** – Median and inter-quartile range (IQR) of the rmsd% (expressed as percent of the root mean square value over time of the relevant knee joint kinematics amplitude) values between the reference kinematics and those obtained with the different STA modelling for the thigh and shank segments. Statistics performed over all trials and volunteers. The number of the angle time histories involved in the STA modelling are shown (Thigh segment + Shank segment). In addition, also the range and the rms values for the knee kinematics are shown.

## 7.3.3. STA model calibration

The results of the comparison between the measured,  $a_i^l(k)$ , and the modelled,  $\tilde{a}_i^l(\Lambda_i(k), h_i^l)$ , amplitudes of the rigid modes of the STA are reported in Figure 7.3.

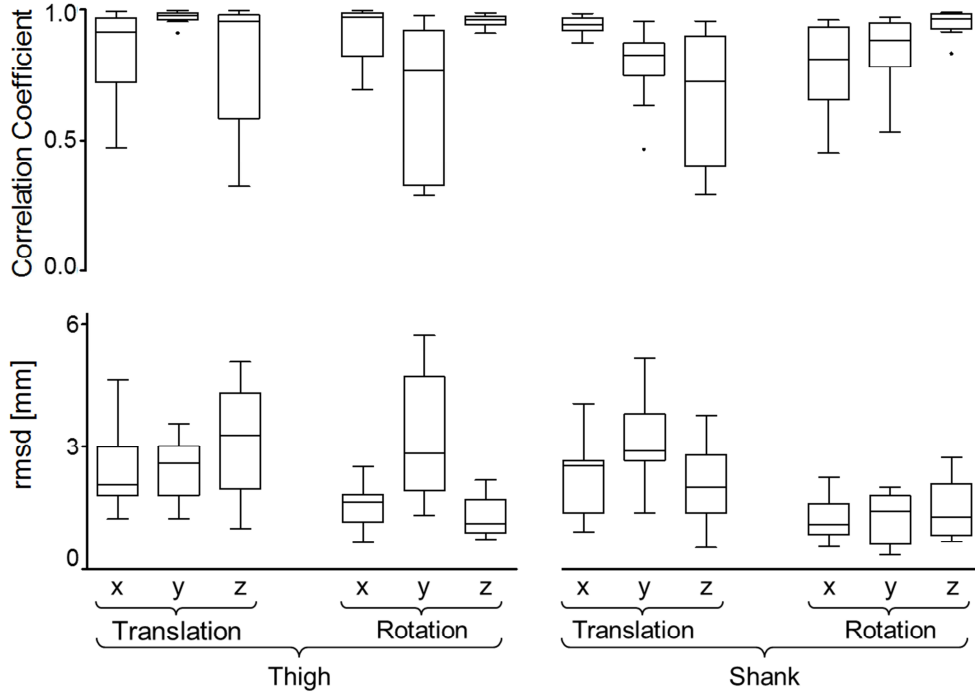


**Figure 7.3** – Box-plots of the correlation coefficient  $\rho$  and of the rmsd values between the measured,  $a_i^l(k)$ , and the modelled,  $\tilde{a}_i^l(\Lambda_i(k), h_i^l)$ , rigid mode amplitudes for the thigh (left panel) and shank segment (right panel). Statistics performed over 15 trials (five trials performed by each of the three volunteers). Outliers are also shown.

The time histories of the amplitudes of the rigid modes obtained from the measured artefact  $a_i^l(k)$ , and those estimated by calibrating the STA rigid component model  $\tilde{a}_i^l(\Lambda_i(k), h_i^l)$ , are shown for a randomly selected trial for the thigh and the shank in Figs. 7.4 and 7.5, respectively.

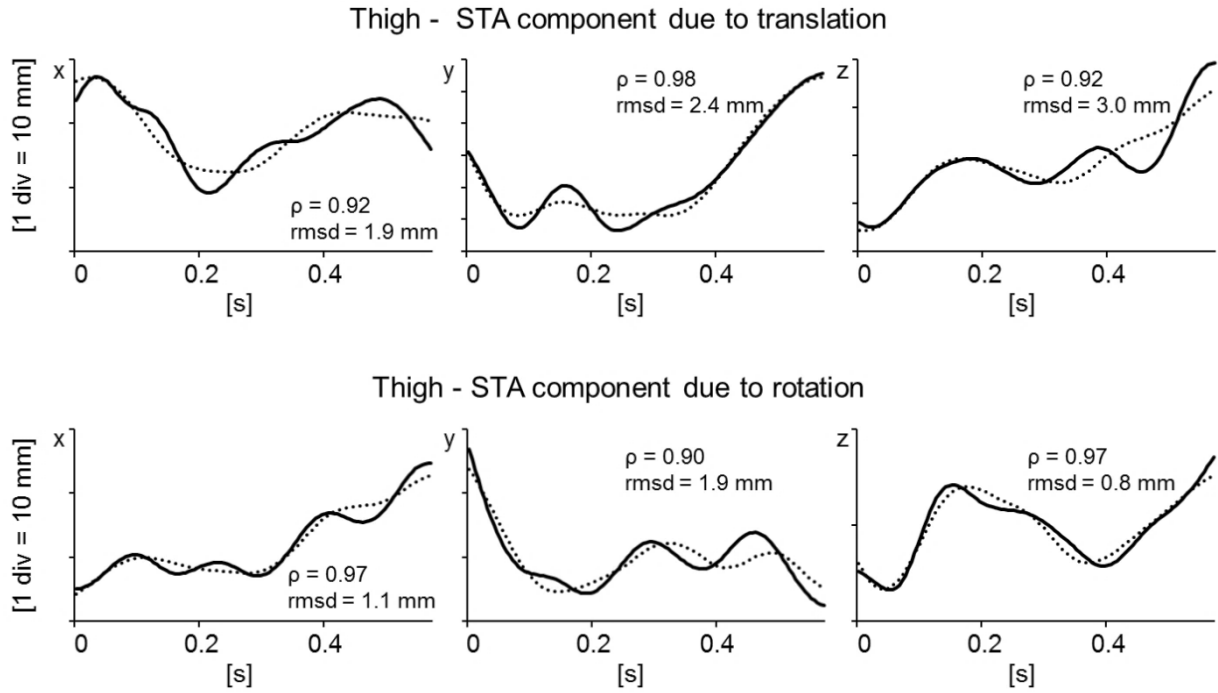


**Figure 7.4** - Measured (solid line) and modelled (dotted line) amplitudes of the rigid modes for the thigh segment relative to a trial of volunteer V3. The relative  $\rho$  and rmsd values are also shown.

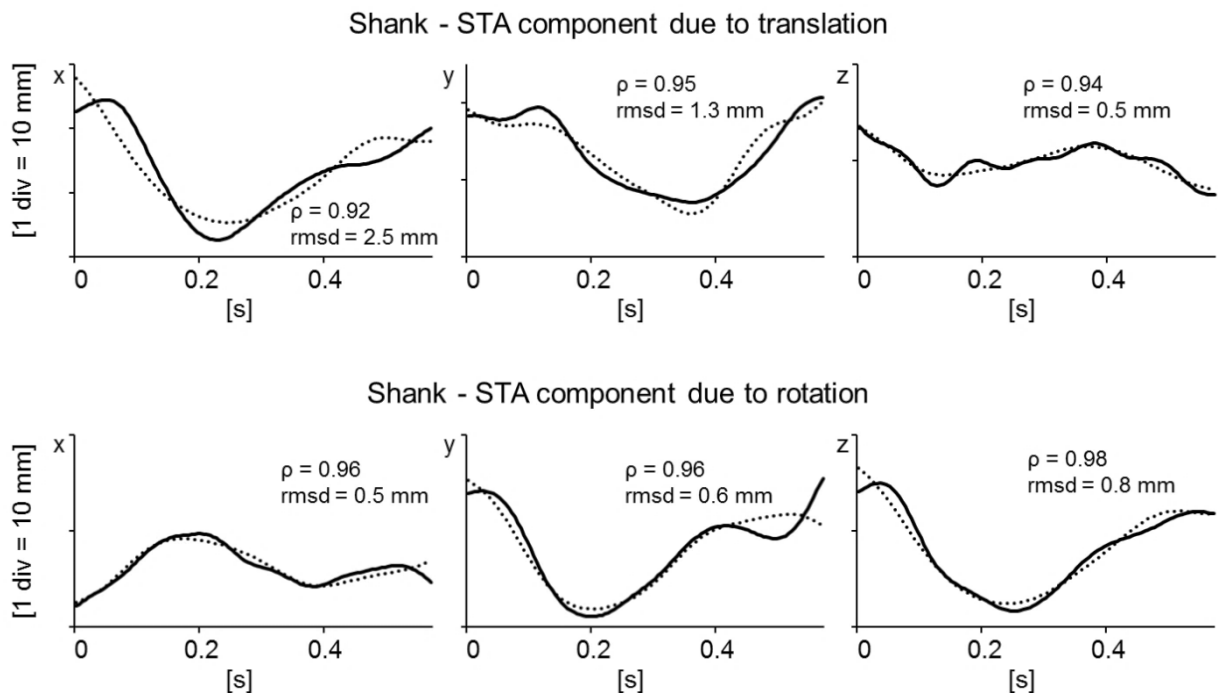


**Figure 7.5** - Measured (solid line) and modelled (dotted line) amplitudes of the rigid modes for the shank segment of the same volunteer and trial as in Figure 7.4. The relative  $\rho$  and rmsd values are also shown.

In Tables 7.5-7.6 are reported the subject- and trial- specific model parameters for thigh ( $h_{th,\alpha}^l, h_{th,\beta}^l, h_{th,\gamma}^l, h_{th,\delta}^l$ ) and shank ( $h_{sh,\delta}^l, h_{sh,\zeta}^l, h_{sh,\eta}^l$ ) segments [mm/deg], for the translation (Table 7.5) and rotation (R) modes (Table 7.6),  $c = x, y, z$  (anatomical axes as in Figure 7.1), and for the three volunteers (V1, V2, and V3). In the Figures 7.6-7.8 the mean and standard deviation of

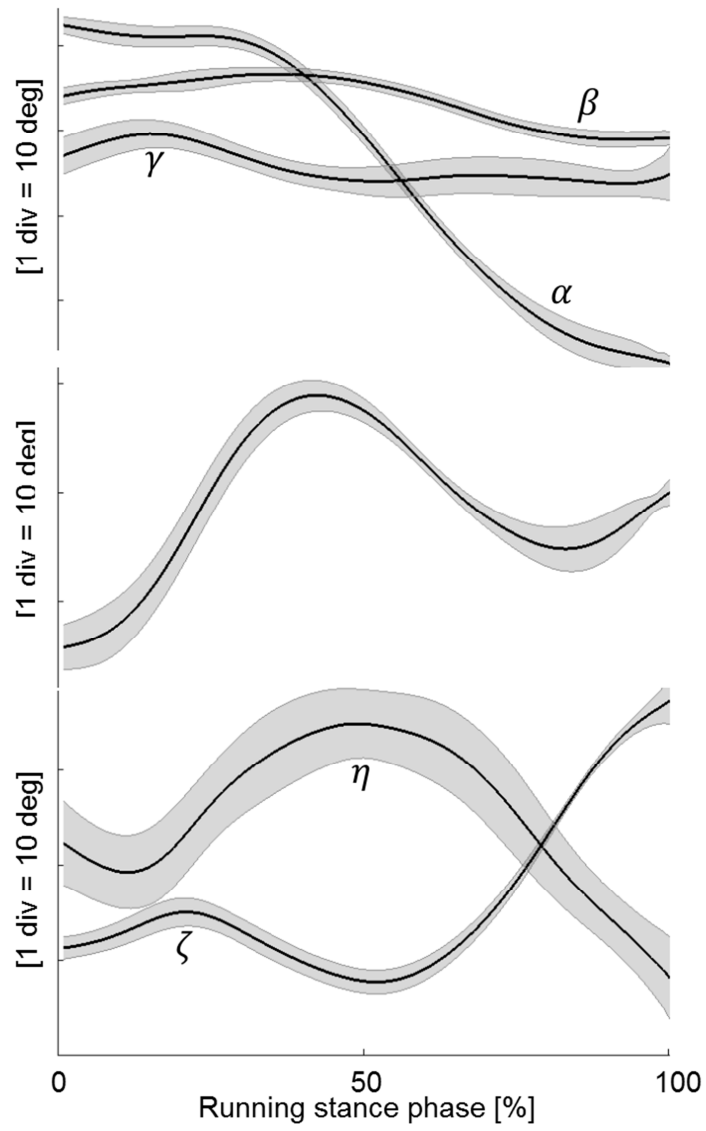
joint kinematics time histories of the attitude vector components (hip: flexion/extension,  $\alpha$ , abduction/adduction,  $\beta$ , internal/external rotation,  $\gamma$ ; knee:  $\delta$ ; ankle: dorsi/plantar flexion,  $\zeta$ , and inversion/eversion  $\eta$ ) estimated during the five running trials performed by the three volunteers (V1, V2, and V3), and used to calibrate the model, are shown.

		Thigh				Shank				
		$h_{th,\alpha}^l$	$h_{th,\beta}^l$	$h_{th,\gamma}^l$	$h_{th,\delta}^l$	$h_{sh,\delta}^l$	$h_{sh,\zeta}^l$	$h_{sh,\eta}^l$		
<b>Translation</b>	x	V1	t1	0.52	-0.25	-2.76	-0.18	-0.45	-1.53	-2.07
			t2	0.43	-2.27	-1.09	0.56	-0.21	-0.62	-1.20
			t3	0.31	-2.52	0.98	0.71	-0.06	-0.86	-1.47
			t4	1.17	-4.48	-2.10	0.17	-0.31	-0.97	-1.45
			t5	0.41	-1.43	-1.58	0.31	-0.94	0.23	0.12
	V2	t1	0.04	1.68	-0.37	0.36	-0.09	-0.64	-0.81	
		t2	0.03	-4.40	-5.41	1.48	-0.18	-0.34	-0.58	
		t3	-0.05	0.95	0.36	0.56	-0.11	-0.54	-0.91	
		t4	0.02	-4.01	-2.42	1.33	-0.01	-0.34	-0.84	
		t5	-0.30	-2.06	-2.52	1.48	0.01	-0.27	-0.85	
	V3	t1	0.23	-0.23	1.52	-0.38	-0.45	-0.01	-0.45	
		t2	0.46	-6.45	0.99	1.03	-0.49	-0.30	-0.56	
		t3	0.13	-3.62	5.01	0.36	-1.06	-0.21	1.70	
		t4	0.68	-5.06	3.93	0.75	-0.13	0.23	-0.71	
		t5	0.34	0.00	3.60	0.12	-0.11	0.24	-0.60	
y	V1	t1	0.12	-5.15	1.51	0.07	0.37	-0.21	-0.93	
		t2	1.55	-11.84	0.25	0.70	0.83	-0.81	-1.75	
		t3	0.78	-8.02	1.03	0.91	0.19	-0.16	-0.84	
		t4	2.40	-12.27	0.52	0.88	0.36	-0.19	-0.97	
		t5	1.38	-10.30	3.39	1.40	1.47	-1.39	-2.42	
V2	t1	-0.48	-3.54	-1.28	-0.29	0.71	-0.36	-1.33		
	t2	-0.12	-6.24	-3.59	0.13	0.92	-0.05	-1.04		
	t3	-0.16	-4.89	-0.04	-0.09	0.88	-0.30	-1.65		
	t4	-0.10	-7.56	0.11	0.01	0.56	-0.14	-0.91		
	t5	-0.25	-5.43	-0.49	-0.09	1.23	-0.08	-1.74		
V3	t1	-0.43	-3.00	-2.90	-0.14	0.30	0.33	-0.98		
	t2	-0.18	-3.39	-3.94	0.02	-0.69	0.56	2.26		
	t3	-0.21	-5.77	2.39	0.21	-0.10	0.19	-0.14		
	t4	0.18	-5.64	0.10	0.23	0.40	0.35	-1.46		
	t5	-0.23	-3.37	1.10	-0.17	0.83	0.81	-2.29		
z	V1	t1	0.07	-2.60	1.09	0.52	0.05	-0.16	0.19	
		t2	0.85	-4.12	-2.47	0.23	-0.02	0.14	0.18	
		t3	-0.11	0.07	-2.70	-0.34	-0.21	0.12	0.30	
		t4	-0.18	1.98	-2.55	-0.90	0.06	-0.22	-0.27	
		t5	1.05	-4.27	-0.75	0.26	-0.85	0.58	1.06	
V2	t1	0.04	-2.85	-0.02	-0.57	0.34	-0.43	-0.39		
	t2	0.18	-0.52	3.20	-1.00	-0.44	-0.19	0.49		
	t3	0.03	-1.90	-0.46	-0.59	-0.02	-0.29	0.03		
	t4	0.02	0.03	3.99	-1.02	-0.01	-0.33	-0.20		
	t5	0.26	-2.16	3.64	-0.86	0.04	-0.60	-0.54		
V3	t1	0.10	-2.57	1.43	0.72	-0.19	-0.24	0.01		
	t2	-0.62	0.10	4.12	0.10	0.87	-0.71	-3.76		
	t3	-0.44	-3.54	1.98	0.83	0.00	-0.15	-0.22		
	t4	-0.55	1.08	-3.66	-0.18	-0.13	-0.09	0.20		
	t5	-0.67	-3.72	-4.18	0.68	-0.66	-0.51	0.93		

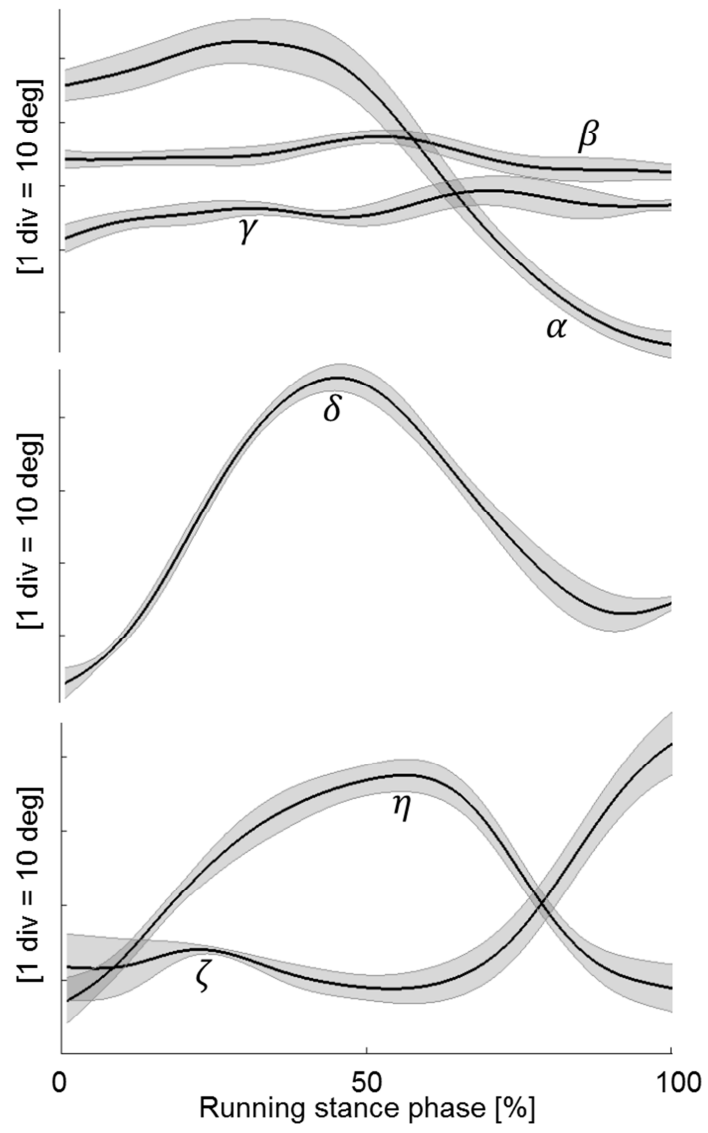
– Table 7.5 –

		Thigh				Shank			
		$h_{th,\alpha}^l$	$h_{th,\beta}^l$	$h_{th,\gamma}^l$	$h_{th,\delta}^l$	$h_{sh,\delta}^l$	$h_{sh,\zeta}^l$	$h_{sh,\eta}^l$	
<b>Rotation</b>	<b>V1</b>	<i>t1</i>	0.07	-2.17	0.41	0.03	0.03	0.23	0.10
		<i>t2</i>	0.20	-2.25	0.33	0.14	0.17	-0.16	-0.09
		<i>t3</i>	0.01	-1.24	-0.23	-0.01	0.16	-0.19	-0.17
		<i>t4</i>	-0.32	1.45	-0.53	-0.57	0.21	0.12	0.12
		<i>t5</i>	0.48	-2.50	-0.14	0.10	0.78	-0.74	-1.11
	<b>V2</b>	<i>t1</i>	0.20	-2.07	1.13	-0.49	0.10	0.16	0.07
		<i>t2</i>	0.28	-2.30	2.22	-0.47	0.38	0.25	-0.11
		<i>t3</i>	0.23	-0.95	1.07	-0.60	0.30	0.12	-0.10
		<i>t4</i>	0.19	0.74	3.75	-0.76	0.20	0.26	0.05
		<i>t5</i>	0.35	-1.49	3.30	-0.63	0.22	0.38	0.17
	<b>V3</b>	<i>t1</i>	0.10	-1.47	2.04	0.28	0.29	0.13	-0.19
		<i>t2</i>	-0.34	-1.58	2.82	0.32	-0.25	0.29	1.35
		<i>t3</i>	-0.40	-1.97	3.16	0.36	0.05	0.09	0.00
		<i>t4</i>	-0.31	-0.40	0.56	0.09	0.07	0.09	-0.11
		<i>t5</i>	-0.38	-0.52	0.93	0.28	0.14	0.17	0.20
<b>x</b>	<b>V1</b>	<i>t1</i>	-0.45	4.52	-0.68	-0.54	0.01	-0.55	-0.53
		<i>t2</i>	-0.50	2.93	-0.41	-0.36	0.17	-0.56	-0.80
		<i>t3</i>	-0.14	0.42	1.12	0.17	0.17	-0.49	-0.62
		<i>t4</i>	-0.03	0.50	-1.66	-0.33	0.20	-0.89	-1.04
		<i>t5</i>	-0.43	3.34	-3.27	-0.84	0.08	-0.39	-0.24
	<b>V2</b>	<i>t1</i>	0.07	1.97	0.66	-0.11	-0.35	0.29	0.38
		<i>t2</i>	-0.08	-0.34	-1.69	0.21	-0.33	0.09	0.16
		<i>t3</i>	0.10	1.06	0.83	-0.05	-0.33	0.20	0.28
		<i>t4</i>	0.07	-2.69	-3.34	0.31	-0.44	0.13	0.46
		<i>t5</i>	-0.21	1.28	-3.38	0.16	-0.18	0.04	0.16
	<b>V3</b>	<i>t1</i>	-0.52	2.29	-3.27	-0.80	-0.24	-0.01	0.13
		<i>t2</i>	0.31	1.09	-3.58	-0.59	-0.08	-0.24	-0.74
		<i>t3</i>	0.62	-0.79	-5.44	-0.31	-0.48	-0.14	0.80
		<i>t4</i>	0.38	-1.38	0.07	-0.23	-0.17	0.00	0.00
		<i>t5</i>	0.33	1.03	1.81	-0.64	-0.17	-0.07	0.00
<b>y</b>	<b>V1</b>	<i>t1</i>	-0.83	0.91	2.75	0.69	-0.47	-0.27	-0.50
		<i>t2</i>	-0.83	1.23	3.41	0.43	-0.57	0.20	-0.04
		<i>t3</i>	-0.26	-0.89	2.31	0.59	-0.29	-0.24	-0.55
		<i>t4</i>	-0.06	-2.40	4.11	1.60	-0.52	-0.11	-0.35
		<i>t5</i>	-0.74	1.13	2.57	0.35	-1.01	0.59	0.61
	<b>V2</b>	<i>t1</i>	-0.08	-1.48	0.62	-0.05	-0.07	-0.34	-0.51
		<i>t2</i>	-0.14	-0.05	2.06	-0.28	-0.26	-0.07	-0.20
		<i>t3</i>	0.03	-2.21	0.72	0.01	-0.09	-0.35	-0.59
		<i>t4</i>	-0.12	-0.77	1.82	-0.20	-0.12	-0.06	-0.40
		<i>t5</i>	-0.03	-1.10	1.77	-0.28	-0.20	-0.02	-0.38
	<b>V3</b>	<i>t1</i>	-0.05	-1.15	-1.10	0.36	-0.34	0.04	-0.14
		<i>t2</i>	-0.06	-0.48	-4.47	0.33	-0.27	-0.22	-0.85
		<i>t3</i>	-0.15	-0.62	-0.63	0.28	-0.80	-0.15	0.93
		<i>t4</i>	-0.06	-2.14	-0.34	0.57	-0.31	0.11	-0.28
		<i>t5</i>	-0.23	-0.61	1.52	0.38	-0.31	0.05	-0.21

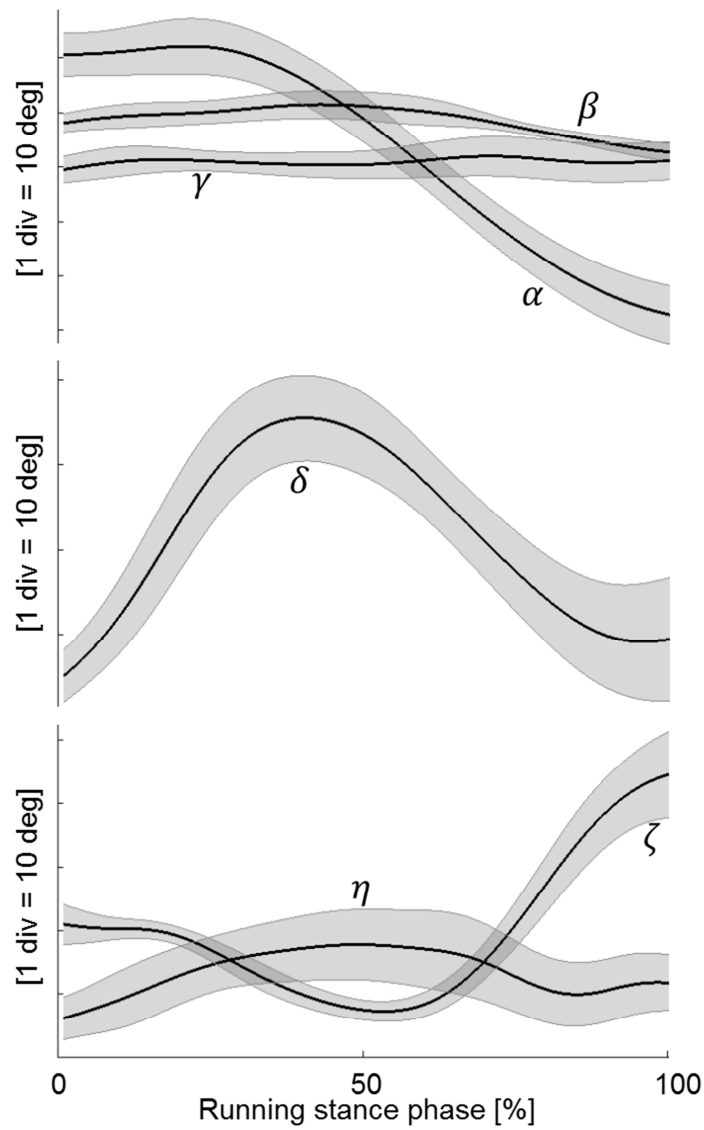
– Table 7.6 –



– Figure 7.6 –



– Figure 7.7 –



– Figure 7.8 –

Their inter- and intra-subject variability can be inferred by Figure 7.9.

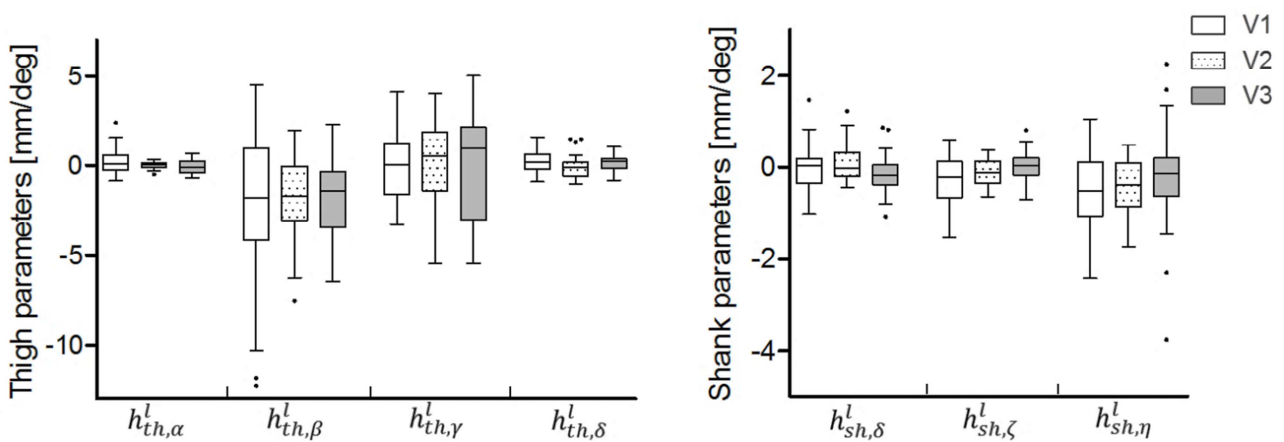


**Figure 7.9** - Box-plots of the model parameters for the thigh,  $h_{th}^l$  (left panel), and shank segment,  $h_{sh}^l$  (right panel). Statistics performed for each volunteer, V, over 5 trials. Outliers are also depicted.

7.3.4. STA compensation

Reference knee kinematics were characterized in terms of rms values (median(IQR), FE: 22(5) deg, AA: 1(2) deg, IE: 3(1) deg, LM: 1(0) mm, AP: 1(3) mm, PD: 2(1) mm) and ranges (median(IQR), FE: 30(16) deg, AA: 4(1) deg, IE: 9(4) deg, LM: 5(1) mm, AP: 8(3) mm, PD: 6(3) mm).

The effectiveness of STA compensation on knee kinematics is depicted using paradigmatic time histories for a running stance phase, in Fig. 7.10. Statistical results are reported in Fig. 7.11, for rmsd and  $\rho$  values, and in Table 7.7, for rmsd%.

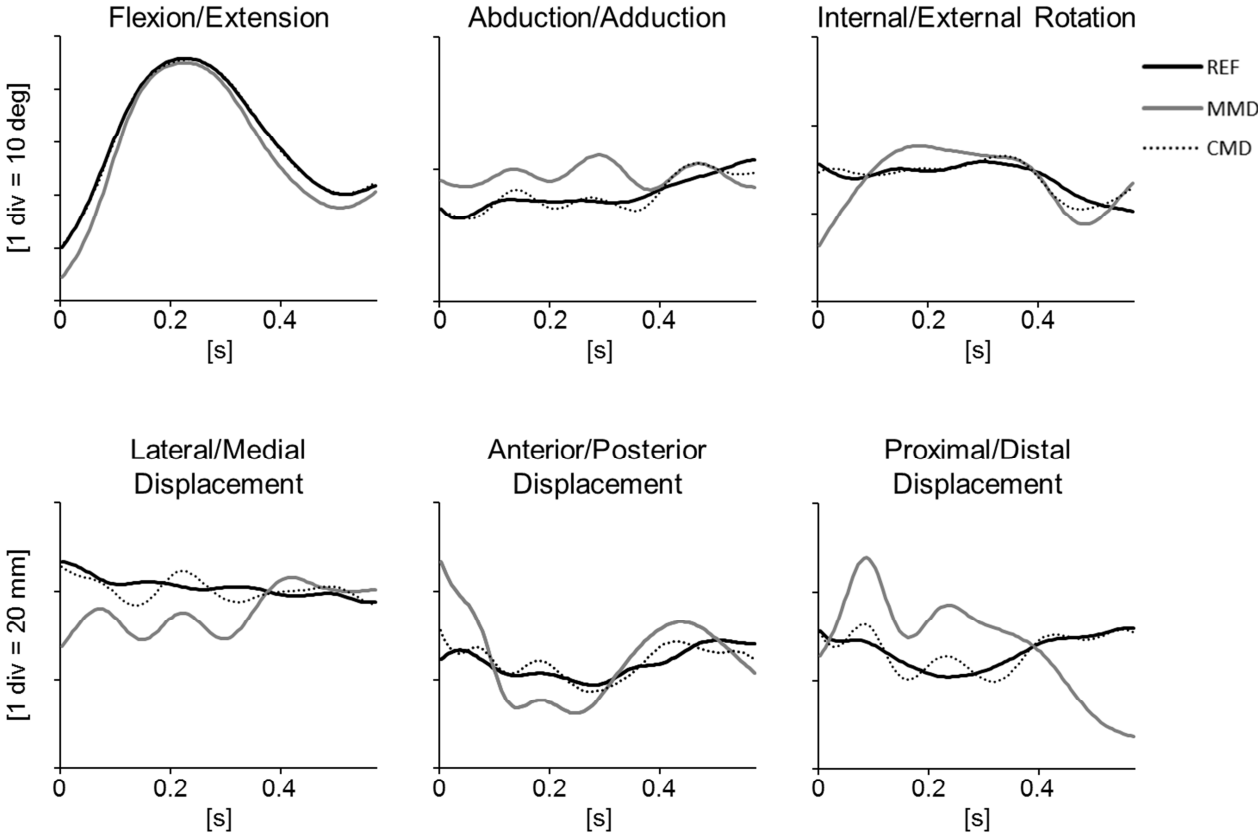


**Figure 7.10** - The six knee joint kinematics components are shown for the same volunteer and trial as in Figure 7.3, obtained using the following marker-cluster data: a) pin marker trajectories (REF, black solid line), b) measured skin marker trajectories (MMD, grey solid line), c) compensated skin marker trajectories (CMD, black dotted line). For the flexion-extension angle the dotted line is superimposed with the solid line.

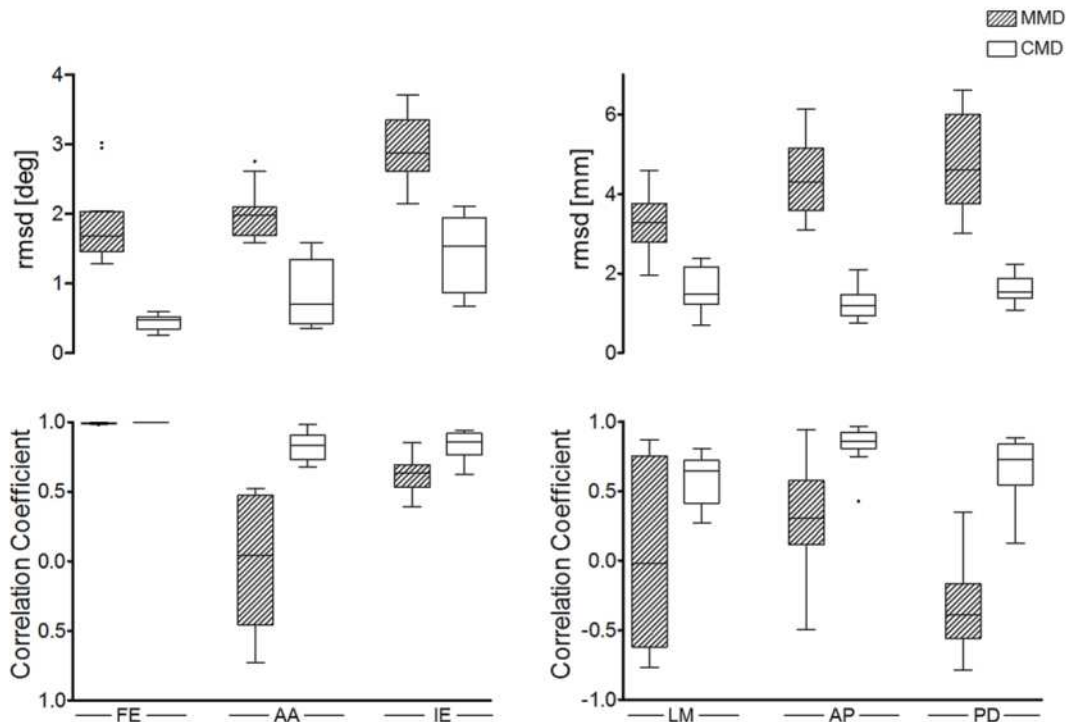


**Figure 7.11** – Box-plots for angular and linear knee kinematics. Upper panel: rmsd between reference kinematics and the kinematics obtained using measured (MMD) and compensated (CMD) skin marker trajectories. Lower panel:  $\rho$  values comparing reference kinematics with those obtained using MMD and CMD data. Statistics performed over 15 trials (five trials performed by each of the three volunteers). Flexion/extension, FE; abduction/adduction, AA; internal/external rotation, IE; lateral/medial displacement, LM; antero/posterior displacement, AP; proximal/distal displacement PD. Outliers are also shown.

rmsd%		MMD		CMD	
		median (IQR)		median (IQR)	
<i>Angles</i>	<i>FE</i>	6 (3)	1 (1)		
	<i>AA</i>	45 (17)	17 (13)		
	<i>IE</i>	32 (19)	15 (7)		
<i>Displacement</i>	<i>LM</i>	70 (31)	33 (21)		
	<i>AP</i>	56 (27)	16 (8)		
	<i>PD</i>	79 (66)	25 (11)		

**Table 7.7** – Median and IQR rmsd% values, calculated for the relevant range of knee kinematics calculated using measured (MMD) and compensated (CMD) skin marker trajectories. Flexion/extension, FE; abduction/adduction, AA; internal/external rotation, IE; lateral/medial displacement, LM; antero/posterior displacement, AP; proximal/distal displacement PD.

The mean power densities, below and above 5 Hz, of the knee joint kinematic errors as obtained using measured (MMD) and compensated (CMD) skin-marker trajectories are reported in Table 7.8. For the STA-affected dataset, the median (IQR) power was 84% (14%), in the range below 5 Hz, and 11% (11%), above 5 Hz. After removing the modelled rigid modes, the median value of the power below 5 Hz became significantly lower (56% (25%),  $\chi^2(1) = 60.8$ ,  $p < 0.001$ ), and significantly higher (34%, (23%),  $\chi^2(1) = 71.1$ ,  $p < 0.001$ ) in the other frequency band. These

changes were due to a shift towards the band above 5 Hz of the power spectrum of all the knee degrees of freedom (DOFs).

frequency band	FE [%]		AA [%]		IE [%]		LM [%]		AP [%]		PD [%]	
	MMD	CMD										
< 5 Hz	83(6)	59(33)	88(8)	55(22)	89(35)	60(22)	81(12)	53(28)	74(14)	47(29)	91(7)	63(22)
> 5 Hz	12(9)	34(33)	8(7)	38(20)	7(22)	31(9)	13(9)	37(28)	18(6)	39(26)	7(4)	31(16)

**Table 7.8** – Mean power in the indicated frequency bands, as percentage of the total power, of knee kinematics errors obtained using measured (MMD) and compensated (CMD) skin marker trajectories. Statistics (median values (IQR)) estimated over 15 trials (five trials performed by each of the three volunteers) for all the degrees of freedom of the knee (flexion/extension, FE; abduction/adduction, AA; internal/external rotation, IE; lateral/medial displacement, LM; antero/posterior displacements, AP; proximal/distal displacements, PD). All degrees of freedom had a significantly different power content after removal of the STA rigid component model.

#### 7.4. Discussion

This study described in this *Chapter* proposes and tests a modelling architecture for the STA rigid component that is appropriate to being embedded in BPEs. Additive translation and rotation components (modes) of the STA were obtained using a modal approach. A model of these rigid modes was developed and calibrated for the thigh and shank of each trial analysed, which estimates the amplitudes of the rigid modes in a bone embedded frame as a function of the proximal and distal joint rotations that occur during the execution of a motor task.

This STA rigid component model was proved effective on knee joint linear and angular kinematics: removing the modelled rigid modes from the STA-affected data remarkably improved joint kinematics, particularly those degrees of freedom subject to relatively small variations, considered to have diagnostic significance in the clinical examination for ligament injuries, *i.e.* abduction-adduction, internal-external rotation and antero-posterior displacement of the knee (Lubowitz et al., 2008).

##### 7.4.1. STA assessment

Current results confirmed the known properties of the STA phenomenon: in general it was higher on the thigh segment with respect to the shank and it presented a large variability to be ascribed to subject-specificity of the data (Leardini et al., 2005, Peters et al., 2010). Moreover, knee kinematics calculated using skin marker data presented errors up to two times higher with respect to the reference kinematics amplitude, for all DOFs except flexion-extension. Paradoxical translations of the tibia with respect to the femur were observed in all directions, as evidenced by some counter-phase (negative) moderate or high correlations for knee translations (Figure 7.11), and reinforcing

previous evidence observed in the antero-posterior direction during the knee extension phase of a step-up motor task (Garling et al., 2007). The necessity of STA compensation for the clinical use or for other applications of knee kinematics is thus confirmed.

The rigid motion of the skin marker cluster was confirmed to be the main STA component (Figure 7.2). The rigid component presented similar characteristics, although with higher values, as those obtained in other *in vivo* studies: during walking (Andersen et al., 2012; Barré et al., 2013), cutting and hopping (Andersen et al., 2012), Table 7.9. This discrepancy can possibly be ascribed to different causes: in Barré et al., 2013, the subjects had a total knee prosthesis that could limit the performed movement; in Andersen et al., 2012, the healthy volunteers jumped from a single leg standing position to standing on the other leg, which may entail a lower change in the linear momentum with respect to the running stance phase analyzed here. *Ex vivo* results relative to the thigh segment during hip and knee flexion-extension movements (Grimpampi et al., 2014), not surprisingly, presented lower translation ranges with respect to current results (Table 7.10), since there was no contribution of muscle contraction. On the other hand, in the same study, wider orientation ranges of motion were evidenced, to be ascribed to a larger joints range of motion, intentionally reached by the operator flexing the lower limb.

		Present study	Barré et al., 2013	Andersen et al., 2012
Task		Running stance	Walking stance	Hopping
Thigh [mm]	10 <sup>th</sup> percentile	9.0	5.4	–
	median	12.9	7.1	–
	90 <sup>th</sup> percentile	22.0	10.2	–
	max	29.0	–	11.8
Shank [mm]	10 <sup>th</sup> percentile	5.3	2.0	–
	median	11.5	2.7	–
	90 <sup>th</sup> percentile	13.9	3.8	–
	max	23.5	–	11.5

**Table 7.9** - The amplitude of the rigid components (in mm) as obtained in different studies are compared. For the current study, the module of the sum of all rotational and translational modes is computed for each marker and the statistics is performed over all segments' markers, 5 trials, and 3 volunteers. Data from Barré et al. 2013, are calculated as the difference between the position of the marker represented in the AF of the bone and the relative position reconstructed using a least squares pose estimator during the walking stance. Data from Andersen et al. 2012, are obtained assuming that, for the hopping task, only the rigid component was the cause of the maximum residual artifact for the first four PCA components: reported numbers were, thus, obtained as difference between 4<sup>th</sup> and 0<sup>th</sup> DOF of Figure 2 in Andersen et al., 2012.

		Present study	Grimpampi et al., 2014	
Task		Running stance	<i>Ex-vivo</i> hip and knee flexion- extension	
Translation [mm]	Thigh	median	22.1	13.9
		IQR	11.2	2.6
		max	30.0	20.9
	Shank	median	11.6	–
		IQR	2.8	–
		max	18.3	–
Rotation [deg]	Thigh	median	10.2	9.7
		IQR	2.8	4.4
		max	14.0	23.6
	Shank	median	4.9	–
		IQR	2.2	–
		max	6.7	–

**Table 7.10** - The orientation and the linear range of motion relative to current results was computed as in Grimpampi et al., 2014, over all 5 trials and 3 volunteers, and compared with the results obtained in Grimpampi et al., 2014, over all 3 trials and 3 specimens.

#### 7.4.2. STA model calibration

The functional relationship between proximal and distal joint kinematics and individual marker STA displacements (as shown in *Chapter 3*) was confirmed as applicable also to rigid mode amplitudes (Figure 7.3). Using the modal approach eased translating the previously proposed architecture (Camomilla et al. 2013, and in *Chapter 3*) to describing the marker-cluster geometrical transformations. The rigid mode amplitude model preserved the major features of the artefact time histories (Figs. 7.4 and 7.5). For the thigh, the modelled and measured modes most often showed very high correlations (only rotations about the inferior-superior axis presented a median correlation value as low as 0.65, Figure 7.3). These same curves always presented median correlation values above 0.68 for the shank. For both segments, the rmsd values were lower than 3 mm in 81% of the cases. The variability of some of the model parameters was quite high (Figure 7.9), preventing the possibility of using them to estimate the STA for trials different from those used for their calibration. This result forces to calibrate the model at a trial level, which can be done within the optimization procedure used to estimate the bone pose. Therefore, the mathematical model here calibrated for both segments (reported in the supplementary material), can be used in simulations aiming at assessing the effects of STA on related estimates, such as bone pose estimation (Cereatti et al., 2006).

#### 7.4.3. STA compensation

Current results confirmed some of the known properties of the STA phenomenon: knee kinematics calculated using skin-marker data presented errors up to two times higher than the reference kinematics amplitude for all DOFs except flexion-extension. Opposite movement with respect to the real ones were observed for all knee translations, as evidenced by some counter-phase (negative) moderate or high correlations (Figure 7.11), confirming the need for STA compensation to correctly estimate and interpret knee kinematics.

When compensating for STAs by removing the modelled rigid components from the skin-marker trajectories, all DOFs noticeably improved, both in terms of the error amplitude (which was reduced to 1%, 17%, 16% of the kinematic range for FE, AA and IE, respectively and to 33%, 16%, and 25%, for LM, AP, and PD displacements, respectively, Table 7.7) and increased in correlation to reference kinematics which reached a median value of 0.84 (Figure 7.11). These improvements are similar to those obtained using the methods proposed by Cappello et al., (2005) and Lucchetti et al., (1998), both requiring the acquisition of supplementary experiments. However, the effectiveness of our compensation was evaluated by calibrating the model with both input and output data obtained from pins. Current results should be considered as the best possible improvement that could be

obtained with this STA compensation approach performed calibrating the model without a direct measure of STA, *i.e.* in the real human movement analysis setting.

The analysis of the power distribution of knee kinematics errors showed that, for all knee DOFs, STA compensation significantly increased the percentage of power above 5 Hz (median power in this band: 11% and 34% for MMD and CMD, respectively). This power shift can be attributed to a higher ratio between the wobbling and skin sliding components of the phenomenon in the compensated condition. Nevertheless, what the model is not able to reproduce, including mainly the wobbling component, is moderate enough to allow for a notable reduction of the error amplitude. Contrary to the dominant negative effect of wobbling masses on joint dynamics (Pain and Challis, 2006), the joint kinematics has here been confirmed to be mainly affected by skin sliding (as in *Chapter 3*). These results support the hypothesis that embedding a model of the artefact caused by skin sliding in a BPE may compensate for most of the artefact propagation.

### 7.5. Conclusion

Since the mode amplitudes,  $a_i^l(k)$ , can in principle be estimated together with bone pose, the proposed model architecture is appropriate for incorporation in various kinds of BPEs: single-body BPEs (Alexander and Andriacchi, 2001), multi-body BPEs (Richard et al., 2012), and algorithms based on a functional approach (de Rosario et al., 2013).

The choice to embed in a BPE only the model of STA rigid components is supported by the following considerations:

- The modelled STA amplitudes present a high or very high degree of similarity to the real phenomenon, and their removal from the original dataset reduce the joint kinematics error amplitude and increase the correlation between compensated and reference kinematics;
- The basis vectors along which the amplitudes of the rigid modes are to be estimated can be determined through subject-specific calibration in a reference posture of the positions of the skin-markers in the anatomical frames (Cappozzo et al., 1995; Donati et al., 2007). For other methods, such as principal component analysis (Andersen et al., 2012) or proper orthogonal decomposition (*Chapter 4*), the basis vectors are trial-specific and must be estimated along with the amplitudes within the BPE problem;
- Modelling the rigid mode amplitudes entails estimating a reduced number of parameters than representing all individual marker displacements (Alexander and Andriacchi, 2001; Camomilla et al., 2009; Camomilla et al., 2013; *Chapter 3*). For example, modelling the thigh rigid modes during a multi-articular movement requires calibrating 24 parameters, and

this is true for any number of markers; while the number of parameters increases to 48 when modelling the individual displacements of four skin-markers (as shown in *Chapter 3*).

The improvements obtained for joint kinematics are very promising and justify dedicating further efforts to properly designing such a pose estimator. However, it must be kept in mind that the model was here calibrated using reference joint kinematics as input and reference artefact as output. In routine experimental conditions, however, only skin-marker data are available; the joint kinematics used as input must be obtained based on quantities that are the output of the BPE. Thus, the model parameters can only be obtained in parallel with estimating the bone pose, as the result of an iterative optimization problem. The reduction of the parameters number entailed in this optimization could potentially increase the possibility to solve it.

### Soft tissue artefact: from cluster-level to marker-level

An approximation of the displacement of each marker in the relevant anatomical frames can be defined by defining the appropriate basis vectors and using the calibration parameters reported for the three volunteers in the Tables 7.5 and 7.6, performing the following steps:

#### 1. Construction of the basis vectors

When the position of the skin markers  $j$  ( $j = 1, \dots, m_i$ ) in the relevant anatomical reference frame,  $\mathbf{r}_i^j$ , is known (e.g. Table 7.11 and shown in Figure 7.12 for the presented data), the 6 basis vectors  $\Phi_i^l$ , ( $l = 1, \dots, 6$ ) which describe translation and rotation of the cluster are computed as:

$$\left[ \begin{array}{c} (\mathbf{R}^l \mathbf{r}_i^1 + \mathbf{t}^l) - \mathbf{r}_i^1 \\ \vdots \\ (\mathbf{R}^l \mathbf{r}_i^j + \mathbf{t}^l) - \mathbf{r}_i^j \\ \vdots \\ (\mathbf{R}^l \mathbf{r}_i^{m_i} + \mathbf{t}^l) - \mathbf{r}_i^{m_i} \end{array} \right] \left/ \left\| \left( \begin{array}{c} (\mathbf{R}^l \mathbf{r}_i^1 + \mathbf{t}^l) - \mathbf{r}_i^1 \\ \vdots \\ (\mathbf{R}^l \mathbf{r}_i^j + \mathbf{t}^l) - \mathbf{r}_i^j \\ \vdots \\ (\mathbf{R}^l \mathbf{r}_i^{m_i} + \mathbf{t}^l) - \mathbf{r}_i^{m_i} \end{array} \right) \right\| \right.$$

where

$$\mathbf{R}^l = \begin{bmatrix} 1 & 0 & 0 \\ 0 & 1 & 0 \\ 0 & 0 & 1 \end{bmatrix} \quad (l = 1:3);$$

$$\mathbf{R}^4 = \begin{bmatrix} 1 & 0 & 0 \\ 0 & \cos\theta & -\sin\theta \\ 0 & \sin\theta & \cos\theta \end{bmatrix};$$

$$\mathbf{R}^5 = \begin{bmatrix} \cos\theta & 0 & \sin\theta \\ 0 & 1 & 0 \\ -\sin\theta & 0 & \cos\theta \end{bmatrix};$$

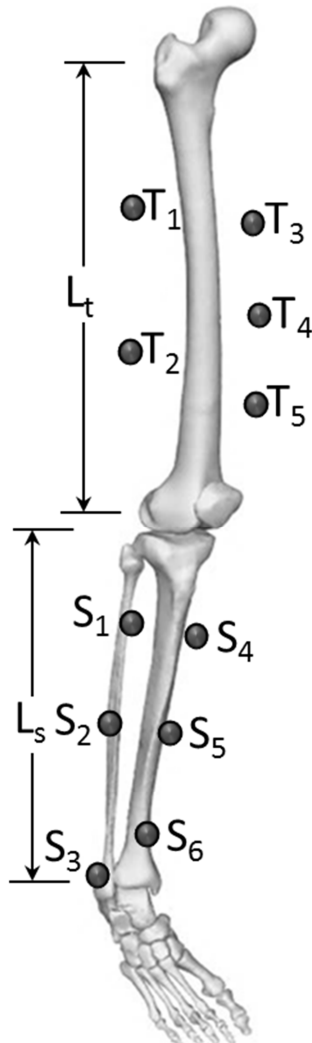
$$\mathbf{R}^6 = \begin{bmatrix} \cos\theta & -\sin\theta & 0 \\ \sin\theta & \cos\theta & 0 \\ 0 & 0 & 1 \end{bmatrix};$$

$$\mathbf{t}^1 = \begin{bmatrix} t \\ 0 \\ 0 \end{bmatrix}, \mathbf{t}^2 = \begin{bmatrix} 0 \\ t \\ 0 \end{bmatrix}, \mathbf{t}^3 = \begin{bmatrix} 0 \\ 0 \\ t \end{bmatrix}, \text{ and } \mathbf{t}^l = \mathbf{0} \quad (l = 4:6);$$

$\theta = 0.2$  deg and  $t = 1$  (chosen arbitrarily).

The origin of the basis vectors is located at the skin marker centroid. Note that an orthogonalization (*i.e.*, Gram–Schmidt) procedure is not required to obtain the basis, because translation and rotation modes are orthogonal by construction, *i.e.*,  $(\Phi_i^l)^T (\Phi_i^p) = 0$ ,  $l \neq p$ .

**Figure 4s** – The position of the skin markers glued on thigh and shank segments during the running trials are depicted. Thigh and shank lengths are also shown ( $L_t$  and  $L_s$ , respectively).



	V1	V2	V3	
	$L_t = 480$	$L_t = 456$	$L_t = 467$	
T <sub>1</sub>	x	-36	5	-8
	y	290	288	277
	z	87	86	87
T <sub>2</sub>	x	-11	16	10
	y	124	122	100
	z	63	59	64
T <sub>3</sub>	x	78	102	103
	y	301	328	364
	z	1	-3	17
T <sub>4</sub>	x	80	100	107
	y	191	202	260
	z	4	-5	23
T <sub>5</sub>	x	83	86	98
	y	70	71	151
	z	-15	-6	20
	$L_s = 461$	$L_s = 461$	$L_s = 432$	
S <sub>1</sub>	x	-2	-11	17
	y	337	361	337
	z	86	82	71
S <sub>2</sub>	x	-16	-25	-4
	y	176	194	175
	z	77	84	76
S <sub>3</sub>	x	-41	-21	-30
	y	19	32	22
	z	66	88	86
S <sub>4</sub>	x	44	62	59
	y	400	430	371
	z	-1	1	3
S <sub>5</sub>	x	33	35	47
	y	262	274	243
	z	151	-1	24
S <sub>6</sub>	x	16	21	32
	y	113	125	108
	z	14	9	45

**Table 7.12** – Position of the skin markers depicted in the Figure 4s represented in the relevant anatomical frame. Thigh and shank lengths, indicated in Figure 4s, are also shown ( $L_t$  and  $L_s$ , respectively). Data are in mm.

### 2. Reconstruction of the mode amplitudes

The amplitude of each rigid mode along the respective unit vector can be estimated using the parameters reported in the Tables 7.5 and 7.6,  $\mathbf{h}_i^l$ , for different trials and volunteers and selected joint kinematics time histories,  $\mathbf{\Lambda}_i(k)$ , relative to the movement under analysis,  $\tilde{\mathbf{a}}_i^l(\mathbf{\Lambda}_i(k), \mathbf{h}_i^l)$ , (Equations 7.3 and 7.4).

### 3. Approximated STA field at marker-level

The artefact for the thigh and shank skin markers can be approximated using Equation 5 in the original article:

$$\tilde{\mathbf{V}}_i(\Lambda_i(k)) = \sum_{l=1}^6 \tilde{\alpha}_i^l(\Lambda_i(k), \mathbf{h}_i^l) \Phi_i^l.$$

where the rows of the vector field  $\tilde{\mathbf{V}}_i$  represent the marker coordinates (expressed in the relevant anatomical reference frame) in the same order as described in the vectors  $\Phi_i^l$ .

## **8. Chapter 8**

### **“CONCLUSION”**

In human movement analysis, bone pose estimate can be carried out in an indirect and non-invasive fashion using markers located on the skin and stereophotogrammetry, as widely described in the thesis. This method, however, has two main sources of error: one introduced by the system itself, which can be dealt with using filtering or smoothing techniques, and a second source of error is a real movement occurring between skin markers and the underlying bone, the so called soft tissue artefact, for which the acronym STA is largely used and it is the topic of this thesis. Moreover, also of the mislocation of anatomical landmarks, used to build segment joint coordinate systems and then joint coordinate systems contribute to experimental errors.

The artefact has a devastating effect on bone pose estimation and effective countermeasures are still to be made available. First of all, it is important to recognize the limitations inherent in estimating joint kinematics, as evidence suggests that with skin markers knee joint kinematics estimates may, in effect, be opposite to actual tibio-femoral motions, as shown in Garling et al. (2007). The lower limb kinematics is an integral part of the research performed in many studies, and, in particular, for those researches designed to lead to clinical intervention. For these reasons, it is crucial to gain the ability to estimate joint kinematics with high accuracy using non-invasive *in-vivo* methods. This step is necessary to develop evidence-based clinical intervention strategies. This thesis is only a part of efforts to find the best solution for the STA problem.

A multi-disciplinary work including different scientific domains (biomechanics, data analysis, signal processing, image processing, and motion capture) has allowed the development of the research described in the thesis. The main results and contributions of this work are summarized in the following sections. In addition, also the main limitations and the future perspectives are pointed out.

#### **8.1. A possible model of thigh STA**

A mathematical model of the thigh STA, for a selected marker location of a given subject, which estimates the artefact components in a bone embedded anatomical frame (AF) as a function of the

hip and knee joint rotations that occur during the execution of a motor task was proposed. A linear relationship between artefact components and the proximal and distal articular angles was hypothesised, based on the outcome of previous studies (Akbarshahi et al., 2010; Camomilla et al., 2013; Cappozzo et al., 1996). The previously published thigh STA model proposed by Camomilla et al. (2013) estimated the STA, during a mono-articular movement, as a function of the hip joint angles. Seeing as this movement is quasi-static and no impacts were involved in the movement, it was deemed acceptable to assume that skin sliding was the major determinant of the STA. The model presented in *Chapter 3*, otherwise, aimed to estimate the STA during bi-articular movements, as occurs in locomotion. Under these conditions, the above-mentioned assumption was not a predictable conclusion. Moreover, the model was calibrated during both *ex-vivo* and *in-vivo* motor task. It was shown that residual artefact estimates were, in most cases, lower than 25% of the measured counterpart. These estimations were also remarkably similar in shape (median correlation value always higher than 0.93). Therefore, the linear model architecture is feasible, and, more important, this is also the case *in-vivo*. Based on the good results obtained *in-vivo* with the proposed model and the results obtained from the frequency analysis, it may be deduced that skin sliding is the major cause of the artefact and that thigh deformation due to muscle contraction and gravity, and soft tissue wobbling (limited to non-obese subjects), have minor roles. These considerations are based on plausibility, but not on evidence.

Regarding the model generalizability, it is excluded the possibility of applying a model calibrated for a given marker location to other locations, or for a given subject to other subjects (Akbarshahi et al., 2010; Leardini et al., 2005; Peters et al., 2010). For the same subject, the generalizability was valid when the test movement was characterized by joint rotations differing from those used for calibration up to  $\pm 10\%$  or  $\pm 50\%$  in amplitude for the larger and smaller joint rotations, respectively.

Therefore this model could be used for simulation purposes, but for the inclusion in a bone pose estimator, this adds further parameters to the optimization problem, which could pose a convergence problem. For this reason, the research was then focused on the artefact affecting the cluster of markers in a space that exhibits the least number of dimensions possible, in order to minimize the number of parameters in the STA model (Andersen et al., 2012; Dumas et al., 2014a).

## 8.2. STA degrees of freedom reduction

STA were categorized into three definitions: individual marker displacements (MD), marker-cluster geometrical transformations (GT), and skin envelope shape variations (SV). A modal approach let the representation of STA by modes. Each mode,  $a_i^l(k)\Phi_i^l$ , is characterized by a time-dependent amplitude,  $a_i^l(k)$ , and a direction  $\Phi_i^l$ , which is constant during the performed task. Such representation allows the ranking and selection procedures of the modes based on the evaluation of deformation energy. In the perspective to include one of the proposed STA definition in a bone pose estimator, the choice can be based on the number of modes required to represent a given percentage,  $p$ , of the total STA energy. This may translate into a limited number of parameters involved in the STA model. When thigh STA (using a five skin marker cluster) are modelled as a linear combination of three independent variables using the equation 4.8 (Camomilla et al., 2013) the number of parameters to be identified with a calibration procedure would be thirty-six using the individual marker displacements, twenty-four using the marker-cluster geometrical transformation, and four using the skin envelope shape variations (values relative to the number of modes relative to the *ex-vivo* experimental data used in *Chapter 4* and a paradigmatic energy threshold). Of course, this number of parameters depends on the amount and on the position of skin markers located on each segment, since this defines the STA field and could also influence how the deformation energy is distributed. The following consideration on the ranking and selection of modes can be made based on the results shown in *Chapter 4* and based on the literature:

- root mean square of skin marker displacements, relative to the underlying bone, are not highly ordered (Akbarshahi et al., 2010; Peters et al., 2010): a large number of displacements may have to be selected to build a representative STA model, as those proposed by Alexander and Andriacchi, (2001) and Camomilla et al. (2013) that involves 3 times skin marker number modes;
- the rigid transformations of the marker-cluster represent a greater portion of the STA (Andersen et al., 2012; Barré et al., 2013; Grimpampi et al., 2014);
- When skin envelope shape variations have been properly ordered (Andersen et al., 2012), a low number of them may need to be selected to build a representative STA model. However, currently, no model based on this STA definition has been proposed in the literature. A proof of concept of the use of this definition is described in *Appendix 1*.

Identify a STA definition and approximation able to grant reasonable joint kinematics accuracy while using a feasible number of parameters, is a crucial issue. From the numerical results obtained

in the *Chapter 4*, an appropriate number and type of modes could be selected by setting a threshold for the knee kinematics error reduction. To obtain a root mean square error expressed in percentage to the relevant angle amplitude value (RMSE%) lower than 10%, all modes (27) are necessary for the MD definition (Fig. 4.10), whereas eleven modes for GT (Fig. 4.11) and fourteen modes for SV (Fig. 4.12) are sufficient. These modes represent 100%, 94% and 99% of the total STA deformation energy, for MD, GT and SV definition, respectively (Fig. 4.9). Therefore, MD definition does not seem to be the most appropriate modal approach to be embedded in bone pose estimators, exhibiting slower trend and moderate RMSE% value reduction as the number of modes increases, as compared to the other two definitions. The latter, instead, allow for an acceptable trade-off between STA compensation effectiveness and number of modes, relative to knee kinematics accuracy and the number of parameters.

### 8.3. STA characterization

When the GT definition (one of the above-mentioned promising STA definition) is used, the STA can be described at marker-cluster level by a series of geometrical transformations, such as rotations and translations (cluster rigid motion: RM), homotheties and stretches (cluster non-rigid motion: NRM). Recent study quantified these components (Andersen et al., 2012; Barré et al., 2013; de Rosario et al., 2012; Grimpampi et al., 2014) showing that RM is normally predominant with respect to NRM. Based on this observation, it is concluded, either explicitly or implicitly, that NRM has a limited impact on bone pose estimation (BPE) and that STA compensation should concentrate on RM. Otherwise, in the *Chapter 5*, it has been empirically demonstrated that NRM does not have a limited effect on BPE accuracy, but, rather, it has no effect whatsoever and that this is the case independently from its magnitude relative to RM. For this reason, the only STA component to be compensated for is RM. The results empirically showed that, using a Procrustes superimposition approach, only RM has an impact on the accuracy of the BPE, independently of the amplitude of NRM. In addition, when the RM was removed, the real bone pose was obtained. It must be acknowledged that a reference pose obtained with pin markers was used to compute the modes and to remove RM from skin-marker trajectories. In the present context, this choice does not constitute a limitation, but does simply show that the NRM has no effect on BPE.

#### 8.4. Mode selection criteria

An appropriate selection of whole STA phenomenon and its removal from skin marker trajectories may be sufficient for an appropriate estimation of joint kinematics (Andersen et al., 2012; Cappello et al., 2005; De Rosario et al., 2013; Dumas et al., 2014a). A different efficiency of compensation for a portion of STAs can be notably altered, depending on which of the different STA definitions found in the literature (MD, GT and SV) are utilized. Analysing the impact that different possible selection criteria used to approximate the STA have when utilized for compensation on the accuracy of knee joint kinematics, the following conclusions were pointed out:

- for joint angles, the compensation efficiency was almost equivalent across the STA approximations based on an energy threshold (median root mean square errors (RMSEs) were below 1 deg for flexion/extension and 2 deg for abduction/adduction and internal/external rotation);
- for the joint displacements, the compensation efficiency depended on the STA approximation (Median RMSEs for antero/posterior displacement was 1- 4 mm using either MD, GT or SV truncated series);
- RMSEs were virtually null when the STA was approximated using only the GT rigid modes.

Therefore, the portion of the STA that is the most appropriate for compensation is represented by the rigid GT modes (*i.e.*, three translations and three rotations of the marker-cluster). The improvements in joint kinematics were remarkable, and the number of modes constant (6), independently from the subject, the trial and the number of skin markers. The virtually null RMSEs can be explained by the fact that the joint kinematics are obtained through a least squares method (Söderkvist and Wedin, 1993) (*i.e.* affected exclusively by the rigid movement of the marker-cluster). Whether such a model can be driven by trial specific variables, such as joint angles or other biomechanical parameters, can be calibrated using *in-vivo* data, and finally be embedded in the least squares method are the next issues to be solved in order to obtain an accurate estimation of joint kinematics.

#### 8.5. STA rigid modelling

The rigid component of STA was decomposed into additive translation and rotation components (modes) using a modal approach and the GT definition. A model of these rigid modes was developed and calibrated for the thigh and shank of different subjects. The latter estimates the

amplitudes of the rigid modes in a bone embedded AF as a function of the proximal and distal joint rotations that occur during the execution of a task. The hypothesis of a linear relationship between these amplitudes and the proximal and distal articular angles was confirmed also in this case. Removing the modelled rigid modes from the STA-affected data remarkably improved knee joint kinematics, particularly those degrees of freedom subject to relatively small variations, considered to have diagnostic significance in the clinical examination for ligament injuries, *i.e.* abduction-adduction, internal-external rotation and antero-posterior displacement of the knee (Lubowitz et al., 2008). Therefore, the model was proved effective in knee joint estimation. In particular, when compensating for rigid modelled STA, all knee degrees of freedom (DOFs) noticeably improved, both in terms of the reduction of error amplitude and increase in correlation to reference kinematics. Abduction-adduction and internal-external rotation angles and the antero-posterior translation presented high or very high correlations to reference kinematics, and the median residual errors for these DOFs were 17%, 15% and 16% of the range of the respective measured quantity. These improvements are similar to those obtained using the methods proposed by Cappello et al., 2005; and Lucchetti et al., 1998; both requiring the acquisition of supplementary experiments. The results shown in the *Chapter 7*, however, demonstrate the effectiveness of compensation obtained with the rigid mode modelling evaluated by calibrating the model with data obtained from pins. These results represent the best possible improvement that can be obtained with the proposed STA compensation approach when the model is calibrated without reference data.

### 8.6. Future work and perspective

The main characteristic of the STA has been defined and also those which affect the bone pose estimation: using the GT definition to represent the STA phenomenon, the rigid motion of the cluster, which is the only movement that affect BPE, can be extrapolated. Therefore, the component of the STA that should be compensated for has been defined.

The variability of some of the parameters obtained with the available experimental data was quite high, preventing the possibility of using them for trials different from those used for their calibration. This result does not weaken the method, since the future prospective is to calibrate the model at a trial-level, *i.e.* simultaneously with the estimate of the bone pose using an optimization approach. The modelling of rigid STA components using trial specific variables, as described on this thesis, but without using data obtained by pins is what should be focused in future work. Of

course, this STA modelling adds further parameters in the optimisation process inherent in the BPE. This can cause problems in the convergence of the optimization procedure. Nevertheless, the marked improvements obtained for joint kinematics shown in *Chapter 7* are very promising, and justify dedicating further efforts to properly designing such a pose.

Future work can be focused on the following aspects:

1. Since the rigid component of the artefact is the main cause of joint kinematics errors, the proposed method, in particular the one proposed in the *Chapter 7*, can be extended to experimental data without restriction on the STA phenomenon;
2. Further validation of the predictive capacity of the model should be performed in different conditions than those explained (the generalizability of the model calibrated on *ex-vivo* experimental data, in *Chapter 3*, was valid when the test movement was characterized by joint rotations differing from those used for calibration up to  $\pm 10\%$  or  $\pm 50\%$  in amplitude for the larger and smaller joint rotations, respectively): this condition is crucial to validate the model with its descriptive and interpretative features;
3. The modes which describe the non-rigid and rigid components of the artefact can be associated with the different causes of the phenomenon (skin sliding associated with joint movement, soft tissue volumetric deformation due to muscular contraction and gravity, and wobbling due to the inertial effects on soft tissue masses);
4. The method proposed in the thesis, is a step towards the STA compensation and future studies should be performed for its applicability in a clinical context and in routine experimental conditions.

In particular, an enhanced BPE can be defined. The calibration of the model presented in the thesis was performed using joint kinematics time histories obtained by pins, while an enhanced BPE should perform both model calibration and pose estimation, at the same time, using at the first step, joint kinematics time histories of first approximation. In routine experimental conditions, indeed, only skin-marker data are available; the joint kinematics used as input must be obtained based on quantities that are the output of the BPE. Thus, the model parameters can only be obtained in parallel with estimating the bone pose, as the result of an iterative optimization problem. The reduction of the parameters number entailed in this optimization could potentially increase the possibility to solve it.

**References**

- Akbarshahi, M., Schache, A.G., Fernandez, J.W., Baker, R., Banks, S., Pandy, M.G., 2010. Non-invasive assessment of soft-tissue artifact and its effect on knee joint kinematics during functional activity. *Journal of Biomechanics*, 43(7), 1292–301.
- Alexander, E.J., Andriacchi, T.P., 2001. Correcting for deformation in skin-based marker systems. *Journal of Biomechanics*, 34(3), 355–61.
- Andersen, M.S., Benoit, D.L., Damsgaard, M., Ramsey, D.K., Rasmussen, J., 2010. Do kinematic models reduce the effects of soft tissue artefacts in skin marker-based motion analysis? An in vivo study of knee kinematics. *Journal of Biomechanics*, 43(2), 268–73.
- Andersen, M.S., Damsgaard, M., Rasmussen, J., 2009. Kinematic analysis of over-determinate biomechanical systems. *Computer Methods in Biomechanics and Biomedical Engineering*, 12(4), 371–384.
- Andersen, M.S., Damsgaard, M., Rasmussen, J., Ramsey, D.K., Benoit, D.L., 2012. A linear soft tissue artefact model for human movement analysis: proof of concept using in vivo data. *Gait & Posture*, 35(4), 606–11.
- Andriacchi, T.P., Alexander, E.J., 2000. Studies of human locomotion : past , present and future. *Journal of Biomechanics*, 33(10), 1217–1224.
- Andriacchi, T.P., Alexander, E.J., Toney, M.K., Dyrby, C., Sum, J., 1998. A point cluster method for in vivo motion analysis: applied to a study of knee kinematics. *Journal of Biomechanical Engineering*, 120(6), 743 – 749.
- Angeloni, C., Cappozzo, A., Catani, F., Leardini, A., 1992. Quantification of relative displacement between bones and skin-and plate-mounted markers. In: *Proceedings of the VIII Meeting on European Society of Biomechanics*, Rome, Italy (Vol. 20, p. 279).
- Baker, R., 2003. Letter to the editor regarding ISB recommendation on definition of joint coordinate systems for the reporting of human joint motion—part I: ankle, hip and spine. *Journal of Biomechanics*, 36(2), 300–302.
- Baker R., 2006. Gait analysis methods in rehabilitation. *Journal of NeuroEngineering and Rehabilitation*, 3(4).
- Ball, K., Pierrynowski, M., 1998. Modeling of the pliant surfaces of the thigh and leg during gait. In: *BiOS'98 International Biomedical Optics Symposium*. International Society for Optics and Photonics. pp. 435–446.
- Barré, A., Thiran, J.-P., Jolles, B.M., Theumann, N., Aminian, K., 2013. Soft tissue artifact assessment during treadmill walking in subjects with total knee arthroplasty. *Biomedical Engineering, IEEE Transactions on*, 60(11), 3131–3140.
- Begon, M., Monnet, T., Lacouture, P., 2007. Effects of movement for estimating the hip joint centre. *Gait & Posture* 25(3), 353–359.
- Benoit, D.L., Ramsey, D.K., Lamontagne, M., Xu, L., Wretenberg, P., Renström, P., 2006. Effect of skin movement artifact on knee kinematics during gait and cutting motions measured in vivo. *Gait & Posture*, 24(2), 152–164.
- Benoit, D.L., Ramsey, D.K., Andersen, M.S., 2015. Translation, rotation, scaling and deformation of surface marker clusters: how do they contribute to soft tissue artefact about the knee? *Journal of Biomechanics*, accepted for publication.

- Bookstein, F. L., 1989. Principal warps: Thin-plate splines and the decomposition of deformations. *IEEE Transactions on pattern analysis and machine intelligence*, 11(6), 567-585.
- Bookstein, F. L., 1991. *Morphometric tools for landmark data: geometry and biology*. Cambridge University Press.
- Camomilla, V., Cereatti, A., Cheze, L., Cappozzo, A., 2013. A hip joint kinematics driven model for the generation of realistic thigh soft tissue artefacts. *Journal of Biomechanics*, 46(3), 625–630.
- Camomilla, V., Cereatti, A., Vannozzi, G., Cappozzo, A., 2006. An optimized protocol for hip joint centre determination using the functional method. *Journal of Biomechanics*, 39(6), 1096–1106.
- Camomilla, V., Donati, M., Stagni, R., Cappozzo, A., 2009. Non-invasive assessment of superficial soft tissue local displacements during movement: a feasibility study. *Journal of Biomechanics*, 42(7), 931–937.
- Cappello, A., Cappozzo, A., La Palombara, P.F., Lucchetti, L., Leardini, A., 1997. Multiple anatomical landmark calibration for optimal bone pose estimation. *Human Movement Science*, 16(2), 259–274.
- Cappello, A., La Palombara, P.F., Leardini, A., 1996. Optimization and smoothing techniques in movement analysis. *International Journal of Biomedical Computing*, 41(3), 137–151.
- Cappello, A., Stagni, R., Fantozzi, S., Leardini, A., 2005. Soft tissue artifact compensation in knee kinematics by double anatomical landmark calibration: performance of a novel method during selected motor tasks. *Biomedical Engineering, IEEE Transactions on*, 52(6), 992–998.
- Cappozzo, A., 1984. Gait analysis methodology. *Human Movement Science*, 3(1), 27–50.
- Cappozzo, A., Cappello, A., Della Croce, U., Pensalfini, F., 1997. Surface-marker cluster design criteria for 3-D bone movement reconstruction. *Biomedical Engineering, IEEE Transactions on*, 44(12), 1165–1174.
- Cappozzo, A., Catani, F., Della Croce, U., Leardini, A., 1995. Position and orientation in space of bones during movement: anatomical frame definition and determination. *Clinical Biomechanics*, 10(4), 171–178.
- Cappozzo, A., Catani, F., Leardini, A., Benedetti, M.G., Della Croce, U., 1996. Position and orientation in space of bones during movement: experimental artefacts. *Clinical Biomechanics*, 11(2), 90–100.
- Cappozzo, A., Della Croce, U., Della Croce, U., Leardini, A., Chiari, L., 2005. Human movement analysis using stereophotogrammetry Part 1: theoretical background. *Gait & Posture* 21(2), 186–196.
- Cereatti, A., Della Croce, U., Cappozzo, A., 2006. Reconstruction of skeletal movement using skin markers: comparative assessment of bone pose estimators. *Journal of NeuroEngineering and Rehabilitation*, 3(7).
- Cereatti, A., Donati, M., Camomilla, V., Margheritini, F., Cappozzo, A., 2009. Hip joint centre location: an ex vivo study. *Journal of Biomechanics*, 42(7), 818–823.
- Challis, J., 1995. A procedure for determining rigid body transformation parameters. *Journal of Biomechanics*, 28(6), 733–737.
- Chatterjee, A., 2000. An introduction to the proper orthogonal decomposition. *Current Science*, 78(7), 808–817.
- Chéze, L., 2000. Comparison of different calculations of three-dimensional joint kinematics from video-based system data. *Journal of Biomechanics*, 33(12), 1695–1699.

- Chèze, L., Fregly, B.J., Dimnet, J., 1995. A solidification procedure to facilitate kinematic analyses based on video system data. *Journal of Biomechanics*, 28(7), 879–884.
- Chiari, L., Della Croce, U., Leardini, A., Cappozzo, A., 2005. Human movement analysis using stereophotogrammetry. Part 2: instrumental errors. *Gait & Posture* 21(2), 197–211.
- Cole, G.K., Nigg, B.M., Ronsky, J.L., Yeadon, M.R., 1993. Application of the Joint Coordinate System to Three-Dimensional Joint Attitude and Movement Representation: A Standardization Proposal. *Journal of Biomechanical Engineering*, 115(4A), 344–349.
- De Rosario, H., Page, A., Besa, A., 2012. Kinematic description of soft tissue artifacts : quantifying rigid versus deformation components and their relation with bone motion. *Medical & Biological Engineering & Computing*, 50(11), 1173–1181.
- De Rosario, H., Page, Á., Besa, A., Valera, Á., 2013. Propagation of soft tissue artifacts to the center of rotation: a model for the correction of functional calibration techniques. *Journal of Biomechanics*, 46(15), 2619–2625.
- Della Croce, U., Cappozzo, A., Kerrigan, D.C., 1999. Pelvis and lower limb anatomical landmark calibration precision and its propagation to bone geometry and joint angles. *Medical & Biological Engineering & Computing*, 37(2), 155–161.
- Della Croce, U., Leardini, A., Chiari, L., Cappozzo, A., 2005. Human movement analysis using stereophotogrammetry: Part 4: assessment of anatomical landmark misplacement and its effects on joint kinematics. *Gait & Posture* 21(2), 226–237.
- Desroches, G., Chèze, L., Dumas, R., 2010. Expression of joint moment in the joint coordinate system. *Journal of Biomechanical Engineering*, 132(11), 114503.
- Donati, M., Camomilla, V., Vannozzi, G., Cappozzo, A., 2007. Enhanced anatomical calibration in human movement analysis. *Gait & Posture* 26(2), 179–185.
- Donati, M., Camomilla, V., Vannozzi, G., Cappozzo, A., 2008. Anatomical frame identification and reconstruction for repeatable lower limb joint kinematics estimates. *Journal of Biomechanics*, 41(10), 2219–2226.
- Dryden, I., Mardia, K., 2002. *Statistical shape analysis*. New York.
- Dumas, R., Camomilla, V., Bonci, T., Cheze, L., Cappozzo, A., 2014a. Generalized mathematical representation of the soft tissue artefact. *Journal of Biomechanics*, 47(2), 476–481.
- Dumas, R., Camomilla, V., Bonci, T., Cheze, L., Cappozzo, a, 2014b. A qualitative analysis of soft tissue artefact during running. *Computer Methods in Biomechanics and Biomedical Engineering*, 17 Suppl 1, 124–125.
- Dumas, R., Cheze, L., 2009. Soft tissue artifact compensation by linear 3D interpolation and approximation methods. *Journal of Biomechanics*, 42(13), 2214–2217.
- Dumas, R., Lafon, Y., Jacquelin, E., Chèze, L., 2009. Soft tissue artefacts: compensation and modelling. *Computer Methods in Biomechanics and Biomedical Engineering*, 12(S1), 103–104.
- Duprey, S., Cheze, L., Dumas, R., 2010. Influence of joint constraints on lower limb kinematics estimation from skin markers using global optimization. *Journal of Biomechanics*, 43(14), 2858–2862.
- Ehrig, R.M., Taylor, W.R., Duda, G.N., Heller, M.O., 2006. A survey of formal methods for determining the centre of rotation of ball joints. *Journal of Biomechanics*, 39(15), 2798–2809.

- Enders, H., von Tscharnar, V., Nigg, B.M., 2012. Analysis of damped tissue vibrations in time-frequency space: a wavelet-based approach. *Journal of Biomechanics*, 45 (16), 2855-2859.
- Feeny, B., 2002. On proper orthogonal co-ordinates as indicators of modal activity. *Journal of Sound and Vibration*, 255(5), 805–817.
- Fuller, J., Liu, L., Murphy, M., Mann, R., 1997. A comparison of lower-extremity skeletal kinematics measured using skin-and pin-mounted markers. *Human Movement Science*, 16(2), 219–242.
- Gamage, S., Lasenby, J., 2002. New least squares solutions for estimating the average centre of rotation and the axis of rotation. *Journal of Biomechanics*, 35(1), 87–93.
- Gao, B., Zheng, N.N., 2008. Investigation of soft tissue movement during level walking: translations and rotations of skin markers. *Journal of Biomechanics*, 41(15), 3189–3195.
- Garling, E.H., Kaptein, B.L., Mertens, B., Barendregt, W., Veeger, H.E.J., Nelissen, R.G.H.H., Valstar, E.R., 2007. Soft-tissue artefact assessment during step-up using fluoroscopy and skin-mounted markers. *Journal of Biomechanics*, 40 Suppl 1, S18–24.
- Grimpampi, E., Camomilla, V., Cereatti, A., 2014. Metrics for Describing Soft-Tissue Artefact and Its Effect on Pose, Size, and Shape of Marker Clusters. *Biomedical Engineering, IEEE Transactions on*, 61(2), 362–367.
- Grood, E.S., Suntay, W.J., 1983. A joint coordinate system for the clinical description of the three-dimensional motions: application to the knee. *Journal of Biomechanical Engineering*, 105(2), 136–144.
- Halvorsen, K., 2003. Bias compensated least squares estimate of the center of rotation. *Journal of Biomechanics*, 36(7), 999–1008.
- Hara, R., Sangeux, M., Baker, R., McGinley, J., 2014. Quantification of pelvic soft tissue artifact in multiple static positions. *Gait & Posture* 39(2), 712–717.
- Heller, M.O., Kratzstein, S., Ehrig, R.M., Wassilew, G., Duda, G.N., Taylor, W.R., 2011. The Weighted Optimal Common Shape Technique Improves Identification of the Hip Joint Center of Rotation In Vivo. *Journal of Orthopaedic Research*, 29(10), 1470–1475.
- Holden, J.P., Orsinibt, J.A., Siegelctd, K.L., Keppled, T.M., Gerberc, L.H., Stanhopecvd, S.J., 1997. Surface movement errors in shank kinematics and knee kinetics during gait. *Gait & Posture*, 5(3), 217–227.
- Horn, B.K.P., 1987. Closed-form solution of absolute orientation using unit quaternions. *JOSA A*, 4(4), 629–642.
- Houck, J., Yack, H.J., Cuddeford, T., 2004. Validity and comparisons of tibiofemoral orientations and displacement using a femoral tracking device during early to mid stance of walking. *Gait Posture*, 19(1), 76–84.
- Karlsson, D., Lundberg, A., 1994. Accuracy estimation of kinematic data derived from bone anchored external markers. In *Proceedings of the 3rd International Symposium on 3-D Anal Hum Mov*, Stockholm. pp. 27–30.
- Kerschen, G., Golinval, J., Vakakis, A.F., 2005. The method of proper orthogonal decomposition for dynamical characterization and order reduction of mechanical systems: an overview. *Nonlinear dynamics*, 41(1-3), 147-169.

- Kuo, M.-Y., Tsai, T.-Y., Lin, C.-C., Lu, T.-W., Hsu, H.-C., Shen, W.-C., 2011. Influence of soft tissue artifacts on the calculated kinematics and kinetics of total knee replacements during sit-to-stand. *Gait & Posture*, 33(3), 379–84.
- Lafortune, M.A., 1984. The use of intra-cortical pins to measure the motion of the knee joint during walking. The Pennsylvania State University. PhD Thesis.
- Lafortune, M.A., Cavanagh, P.R., Sommer, H.J., Kalenak, A., 1992. Three-dimensional kinematics of the human knee during walking. *Journal of Biomechanics*, 25(4), 347–357.
- Lafortune, M.A., Lake, M.J., 1991. Errors in 3-D analysis of human movement. In *Proceedings of the 1st Int. Symp. on 3-D Anal Hum Mov (Montreal)*. pp. 55–56.
- Leardini, A., Chiari, L., Della Croce, U., Cappozzo, A., 2005. Human movement analysis using stereophotogrammetry. Part 3. Soft tissue artifact assessment and compensation. *Gait & Posture*, 21(2), 212–225.
- Levens, A.S., Verne T. Inman, Blosser., J.A., 1948. Transverse rotation of the segments of the lower extremity in locomotion. *The Journal of Bone & Joint Surgery*, 30(4), 859–872.
- Li, K., Zheng, L., Tashman, S., Zhang, X., 2012. The inaccuracy of surface-measured model-derived tibiofemoral kinematics. *Journal of Biomechanics*, 45(15), 2719–2723.
- Lu, T.W., O'Connor, J.J., 1999. Bone position estimation from skin marker co-ordinates using global optimisation with joint constraints. *Journal of Biomechanics*, 32(2), 129–134.
- Lubowitz, J.H., Bernardini, B.J., Reid, J.B., 2008. Current Concepts Review Comprehensive Physical Examination for Instability of the Knee. *The American Journal of Sports Medicine*, 36(3), 577-594
- Lucchetti, L., Cappozzo, A., Cappello, A., Della Croce, U. Della, 1998. Skin movement artefact assessment and compensation in the estimation of knee-joint kinematics. *Journal of Biomechanics*, 31(11), 977–984.
- Mahadevan, S., 1997. Monte Carlo Simulation, MECHANICAL. ed. New York.
- Manal, K., Davis, I.M., Galinat, B., Stanhope, S., 2003. The accuracy of estimating proximal tibial translation during natural cadence walking: bone vs. skin mounted targets. *Clinical Biomechanics*, 18(2), 126–131.
- Manal, K., McClay, I., Richards, J., Galinat, B., Stanhope, S., 2002. Knee moment profiles during walking : errors due to soft tissue movement of the shank and the influence of the reference coordinate system. *Gait & Posture*, 15(1), 10-17.
- Manal, K., McClay, I., Stanhope, S., Richards, J., Galinat, B., 2000. Comparison of surface mounted markers and attachment methods in estimating tibial rotations during walking: an in vivo study. *Gait & Posture* 11(1), 38–45.
- Maslen, B. a, Ackland, T.R., 1994. Radiographic study of skin displacement errors in the foot and ankle during standing. *Clinical Biomechanics*, 9(5), 291–296.
- Novacheck, T. F., 1998. The biomechanics of running. *Gait & Posture*, 7(1), 77–95.
- Pain, M., Challis, J., 2006. The influence of soft tissue movement on ground reaction forces, joint torques and joint reaction forces in drop landings. *Journal of Biomechanics*, 39(1), 119–124.
- Peters, A., Galna, B., Sangeux, M., Morris, M., Baker, R., 2010. Quantification of soft tissue artifact in lower limb human motion analysis: a systematic review. *Gait & Posture* 31(1), 1–8.

- Peters, A., Sangeux, M., Morris, M.E., Baker, R., 2009. Determination of the optimal locations of surface-mounted markers on the tibial segment. *Gait & Posture* 29(1), 42–48.
- Ramakrishnan, H.K., Kadaba, M.P., 1991. On the estimation of joint kinematics during gait. *Journal of Biomechanics*, 24(10), 969–977.
- Ramsey, D., Wretenberg, P., 1999. Biomechanics of the knee: methodological considerations in the in vivo kinematic analysis of the tibiofemoral and patellofemoral joint. *Clinical Biomechanics*, 14(9), 595–611.
- Ramsey, D.K., Wretenberg, P.F., Benoit, D.L., Lamontagne, M., Németh, G., 2003. Methodological concerns using intra-cortical pins to measure tibiofemoral kinematics. *Knee Surgery, Sports Traumatology, Arthroscopy*, 11(5), 344–349.
- Reinbolt, J.A., Schutte, J.F., Fregly, B.J., Koh, B.I., Haftka, R.T., George, A.D., Mitchell, K.H., 2005. Determination of patient-specific multi-joint kinematic models through two-level optimization. *Journal of Biomechanics* 38(3), 621–626.
- Reinschmidt, C., van den Bogert, A.J., Lundberg, A., Nigg, B.M., Murphy, N., Stacoff, A., Stano, A., 1997a. Tibiofemoral and tibiocalcaneal motion during walking: external vs . skeletal markers. *Gait & Posture* 6(2), 98–109.
- Reinschmidt, C., van den Bogert, A.J., Murphy, N., Lundberg, A., Nigg, B.M., 1997b. Tibiocalcaneal motion during running, measured with external and bone markers. *Clinical Biomechanics*, 12(1), 8–16.
- Reinschmidt, C., Van Den Bogert, A.J., Nigg, B.M., Lundberg, A., Murphy, N., 1997c. Effect of skin movement on the analysis of skeletal knee joint motion during running. *Journal of Biomechanics*, 30(7), 729–732.
- Richard, V., Camomilla, V., Cheze, L., Cappozzo, A., Dumas, R., 2012. Feasibility of incorporating a soft tissue artefact model in multi-body optimisation. *Computer Methods in Biomechanics and Biomedical Engineering*, 15(Sup1), 194–196.
- Rozumalski, A., Schwartz, M., Novacheck, T., Wervey, R., Swanson, A., Dykes, D., 2008. Quantification of pelvic soft tissue artifact. In *Proceedings of the Gait and Clinical Movement Analysis Society*.
- Ryu, T., Soon, H., Chung, M.K., 2009. Soft tissue artifact compensation using displacement dependency between anatomical landmarks and skin markers – a preliminary study. *International Journal of Industrial Ergonomics*, 39(1), 152–158.
- Sangeux, M., Marin, F., Tho, M.C.H.B., 2006. Quantification of the 3D relative movement of external marker sets vs . bones based on magnetic resonance imaging. *Clinical Biomechanics*, 21(9), 984–991.
- Sati, M., Guise, J. De, Larouche, S., Drouin, G., 1996. Quantitative assessment of skin-bone movement at the knee. *The Knee* 3(3), 121–138.
- Schache, A. G., Blanch, P., Rath, D., Wrigley, T., & Bennell, K., 2002. Three-dimensional angular kinematics of the lumbar spine and pelvis during running. *Human Movement Science*, 21(2), 273-293.
- Söderkvist, I., Wedin, P.-Å., 1993. Determining the movements of the skeleton using well-configured markers. *Journal of Biomechanics*, 26(12), 1473–1477.
- Stagni, R., Fantozzi, S., 2009. Can cluster deformation be an indicator of soft tissue artefact? *Gait & Posture*, 30, S55.

- Stagni, R., Fantozzi, S., Cappello, A., 2006. Propagation of anatomical landmark misplacement to knee kinematics : Performance of single and double calibration. *Gait & Posture*, 24(2), 137–141.
- Stagni, R., Fantozzi, S., Cappello, A., 2009. Double calibration vs . global optimisation : Performance and effectiveness for clinical application. *Gait & Posture* 29(1), 119–122.
- Stagni, R., Fantozzi, S., Cappello, A., Leardini, A., 2003. Validation of the interval deformation technique for compensating soft tissue artefact in human motion analysis. In: *Surgery Simulation and Soft Tissue Modeling*. Springer Berlin Heidelberg, 293–301.
- Stagni, R., Fantozzi, S., Cappello, A., Leardini, A., 2005. Quantification of soft tissue artefact in motion analysis by combining 3D fluoroscopy and stereophotogrammetry : a study on two subjects. *Clinical Biomechanics*, 20(3), 320–329.
- Stagni, R., Leardini, A., Cappozzo, A., Benedetti, M.G., Cappello, A., 2000. Effects of hip joint centre mislocation on gait analysis results. *Journal of Biomechanics*, 33(11), 1479–1487.
- Südhoff, I., Driessche, S. Van, Laporte, S., 2007. Comparing three attachment systems used to determine knee kinematics during gait. *Gait & Posture* 25(4), 533–543.
- Tashman, S., Anderst, W., 2002. Skin motion artifacts at the knee during impact movements. In: *Proceedings of the 7th Annual Meeting of Gait and Clinical Movement Analysis Society*.
- Taylor, W.R., Ehrig, R.M., Duda, G.N., Schell, H., Seebeck, P., Heller, M.O., 2005. On the influence of soft tissue coverage in the determination of bone kinematics using skin markers. *Journal of Orthopaedic Research*, 23(4), 726 – 734.
- Tranberg, R., Karlsson, D., 1998. The relative skin movement of the foot: a 2-D roentgen photogrammetry study. *Clinical Biomechanics*, 13(1), 71–76.
- Tsai, T.-Y., Lu, T.-W., Kuo, M.-Y., Hsu, H.-C., 2009. Quantification of Three-Dimensional Movement of Skin Markers Relative To the Underlying Bones During Functional Activities. *Biomedical Engineering: Applications, Basis and Communications*, 21(03), 223–232.
- Tsai, T.-Y., Lu, T.-W., Kuo, M.-Y., Lin, C.-C., 2011. Effects of soft tissue artifacts on the calculated kinematics and kinetics of the knee during stair-ascent. *Journal of Biomechanics*, 44(6), 1182–1188.
- Van den Bogert, a J., Reinschmidt, C., Lundberg, A., 2008. Helical axes of skeletal knee joint motion during running *Journal of Biomechanics*, 41(8), 1632–1638.
- Van Sint Jan, S., 2007. *Color atlas of skeletal landmark definitions: guidelines for reproducible manual and virtual palpations*, Churchill. ed.
- Veldpaus, F., Woltring, H., Dortmans, L., 1988. A least-squares algorithm for the equiform transformation from spatial marker. *Journal of Biomechanics*, 21(1), 45–54.
- Wakeling, J.M., Liphardt, A.M., Nigg, B.N., 2003. Muscle activity reduces soft-tissue resonance at heel-strike during walking. *Journal of Biomechanics*, 36(12), 1761–1769.
- Wakeling, J.M., Nigg, B.M., 2001. Soft-tissue vibrations in the quadriceps measured with skin mounted transducers. *Journal of Biomechanics*, 34(4), 539–543.
- Westblad, P., Halvorsen, K., Hashimoto, T., Winson, I., Lundberg, A., 2000. Ankle-joint complex motion during stance phase of walking as measured. In: *Proceedings of the 6th International Symposium on 3D Analysis of Human Movement*. pp. 49–51.
- Woltring, H.J., 1994. 3-D attitude representation of human joints: A standardization proposal. *Journal of Biomechanics*, 27(12), 1399–1414.

Wu, G., Siegler, S., Allard, P., Kirtley, C., Leardini, A., Rosenbaum, D., Whittle, M., D'Lima, D., Cristofolini, L., Witte, H., Schmid, O., Stokes, I., 2002. ISB recommendation on definitions of joint coordinate system of various joints for the reporting of human joint motion-part I: ankle, hip, and spine. *Journal of Biomechanics*, 35(4), 543–548.

## *Appendix A1.*

# **“SOFT TISSUE ARTEFACT MODELLING USING THE SKIN ENVELOPE SHAPE VARIATION DEFINITION: IMPACT ON HIP JOINT CENTRE ESTIMATION DURING THE STAR-ARC MOVEMENT”**

### **Introduction**

The localization of the hip joint centre (HJC) position is required in lower limb movement analysis protocols. This point is considered as the centre of rotation of the human hip joint, which is normally represented as a spherical hinge: a pure rotation is supposed to occur between the femur and the pelvis. The HJC position is used to define the femoral anatomical axes (Cappozzo, 1984). Erroneous HJC estimations causes inaccuracy with which this axis definition is performed. An effective solution to this problem has yet been found (Della Croce et al., 1999; Stagni et al., 2000).

In the laboratory, the subject-specific location of the HJC can be determined with a functional approach (Camomilla et al., 2006; Della Croce et al., 2005; Ehrig et al., 2006) which entails moving the femur, passively or actively, relative to the pelvis. The movement of these body segments is reconstructed using a stereophotogrammetric system with reflective skin markers glued over them. The estimation of the HJC position is affected by the relative movement between the skin markers and the underling bone, *i.e.* the soft tissue artefact (STA).

Cereatti et al. (2009) evaluated the HJC determination on *ex-vivo* data, using a proximal and a distal thigh skin marker cluster and two analytical methods: the quartic sphere fit (QSF) method (Gamage and Lasenby, 2002) with the correction term introduced by Halvorsen (2003) and the symmetrical centre of rotation estimation (SCoRE) method (Ehrig et al., 2006). The obtained results showed that, in presence of STA, HJC position errors highly varied among subjects, methods, and skin marker clusters (between 1.4 and 38.5mm), with larger errors observed in the subject with larger STA. In addition, better results were shown when the method proposed by Gamage and Lasenby (2002) was applied and the distal cluster was used to determine the HJC location (mean HJC location accuracy better than 10mm over all subjects). Nevertheless, the results are still affected by STA.

Recently, Camomilla et al. (2013) modelled thigh STA during a hip joint movement as function of the involved joint kinematics. Such modelling has a high number of model parameters which are subject- and trial-specific. These parameters weight joint kinematic time histories to estimate STA during the task. To reduce this number, the skin envelope shape variations (SV) definition (described in *Chapter 4*) was used for the STA modal representation and to select a subspace of the thigh STA field. Modes, composed by an amplitude and a direction, which represent the main part of the whole phenomenon of the skin marker cluster were selected and removed from skin marker trajectories, as described in *Chapter 4*. The aim of this appendix was to assess the improvement of the HJC estimation when the main part of the STA is removed from the thigh skin markers trajectories. Moreover, the selected mode amplitudes, which are time dependent, were also modelled as linear combination of the hip joint kinematics, as proposed by Camomilla et al. (2013), to estimate these parameters with trial-specific variables. The estimations were done using a distal and a proximal skin markers cluster.

### Material and Methods

Experimental data of four *ex-vivo* subjects were used. Intracortical pin were implanted into pelvis, femur and tibia. Twelve skin markers ( $j=12$ ) were glued on the thigh segment ( $i$ ) as shown in Figure A1.1.

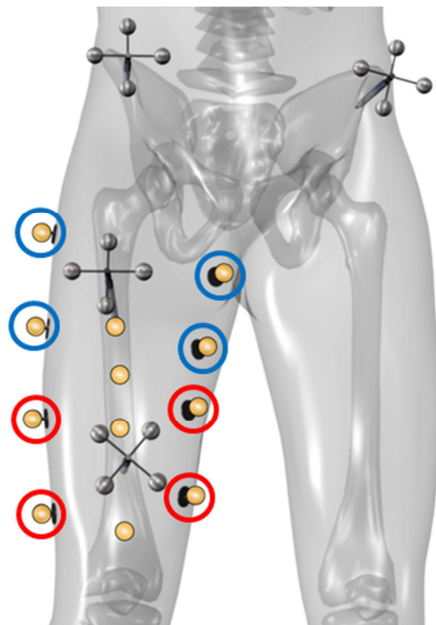


**Figure A1.1** – Intracortical pin equipped with four-marker clusters were implanted into femur and hip-bone (grey) and the skin-markers (yellow) glued on the thigh, are indicated. Skin markers selected for the proximal skin-marker cluster are highlighted with a blue circle, while with a red one those selected for the distal skin-marker cluster.

The instantaneous position of markers was recorded using a 9-camera stereophotogrammetric system. Three trials were recorded for each specimen. The movement for the HJC estimation (“Star-Arc” movement, depicted in Figure A1.2) was made by an operator maintaining the leg straight.

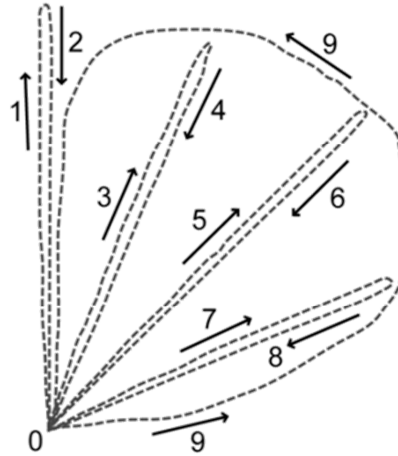


**Figure A1.2** – Star-Arc movement in the transverse plane

Pin markers were used to define bone poses. The hip joint kinematics and STA vectors,  $\mathbf{v}_i^j(k)$ , of the skin markers were reconstructed in the femoral anatomical frame (AF), as described in *Chapter 3* (paragraph 1.1), at each sampled instant of time  $k$  ( $k = 1:n$ ) during the “Star-arc” movement. The STA of all markers can be represented using the STA field,  $\mathbf{V}_i(k)$ :

$$\mathbf{V}_i(k) = \begin{bmatrix} \mathbf{v}_i^1(k) \\ \vdots \\ \mathbf{v}_i^j(k) \\ \vdots \\ \mathbf{v}_i^{m_i}(k) \end{bmatrix}$$

as described in *Chapter 4* (paragraph 2).

From the twelve skin markers, two subsets of skin-marker clusters were selected to represent a proximal (composed by  $m_{i_P}$  markers) and a distal skin-marker cluster (composed by  $m_{i_D}$  markers) as shown in Figure A1.1. Therefore, two different STA fields were defined using the pin data:

$$\mathbf{V}_{i_P}(k) = \sum_{l=1}^{3m_{i_P}} a_{i_P}^l(k) \Phi_i^l$$

and

$$\mathbf{V}_{i_D}(k) = \sum_{l=1}^{3m_{i_D}} a_{i_D}^l(k) \Phi_i^l,$$

for the proximal and distal skin-marker cluster, respectively.

For the STA modal representation, the SV definition was used, as described in details in the Paragraph 4.5.3. To estimate the HJC position, the QSF method was applied to the proximal and the distal thigh skin cluster trajectories. For both the STA fields, *i.e.*,  $\mathbf{V}_{i_P}(k)$  and  $\mathbf{V}_{i_D}(k)$ , the modes were ranked as described in Paragraph 4.3 and were selected those modes that summed one-by-one (*i.e.*, cumulative representation), represent a given percentage  $p$  ( $p = 85\%$ ,  $90\%$  and  $95\%$ ) of the relative STA field.

STA were removed, mode by mode, from the relevant STA fields, *i.e.*,  $\mathbf{V}_{i_P}(k)$  or  $\mathbf{V}_{i_D}(k)$ , and the position of the HJC was estimated for each mode removal. The error in mm of the HJC position during the above-mentioned estimation was evaluated with respect the real HJC location defined using pin data. Therefore, briefly, the HJC estimation was performed using:

- the skin marker trajectories ( $\mathbf{V}_{i_P}(k)$  or  $\mathbf{V}_{i_D}(k)$ ) represented in the AF (row data, RD);
- the skin marker trajectories removing progressively the measured ranked STA modes;
- the skin marker trajectories without STA, providing the reference position for the HJC in the pelvic AF or, in other words, using the pin markers (skin markers trajectories minus all the modes give the pin markers trajectories).

The error in the HJC estimation was calculated as the norm of the difference between the reference HJC position obtained with pin data (case c) and the HJC position in the same reference frame using the a and b cases, for each trial of each specimen.

The correlation coefficient between  $a_{i_P}^l(k)$  and  $a_{i_D}^l(k)$  with all the hip joint angles time histories were also defined. Then, the mode amplitude were modelled as:

$$\tilde{\alpha}_{i_P}^l(k) = h_{i_P,\alpha}^l \alpha(k) + h_{i_P,\beta}^l \beta(k) + h_{i_P,\gamma}^l \gamma(k) + h_{i_P,0}^l$$

$$\tilde{\alpha}_{i_D}^l(k) = h_{i_D,\alpha}^l \alpha(k) + h_{i_D,\beta}^l \beta(k) + h_{i_D,\gamma}^l \gamma(k) + h_{i_D,0}^l$$

where  $\alpha(k), \beta(k), \gamma(k)$  are the hip joint angles time histories (flexion/extension, abduction/adduction, and internal/external rotation, respectively);  $\mathbf{h}_{i_P}^l, \mathbf{h}_{i_D}^l$  are the model parameter vectors to be determined through a calibration procedure for the proximal and distal skin-marker cluster, respectively. The parameters  $h_{i_P,0}^l$  and  $h_{i_D,0}^l$  are determined so that the modelled vectors

have a zero value when the specimen assumes a reference posture. Therefore, the STA field for the two skin-marker clusters can be modelled as follows:

$$\tilde{\mathbf{V}}_{i_P}(k) = \sum_{l=1}^{3m_{i_P}} \tilde{a}_{i_P}^l(k) \Phi_i^l$$

and

$$\tilde{\mathbf{V}}_{i_D}(k) = \sum_{l=1}^{3m_{i_D}} \tilde{a}_{i_D}^l(k) \Phi_i^l$$

for the proximal and distal skin-marker cluster, respectively.

The rigid STA models,  $\tilde{\mathbf{V}}_{i_P}(k)$  and  $\tilde{\mathbf{V}}_{i_D}(k)$ , were calibrated and the model parameters,  $\mathbf{h}_{i_P}^l$  and  $\mathbf{h}_{i_D}^l$ , were identified by minimising the sum of the squared differences between measured,  $a_{i_P}^l(k)$  or  $a_{i_D}^l(k)$ , and modelled amplitudes,  $\tilde{a}_{i_P}^l(k)$  or  $\tilde{a}_{i_D}^l(k)$ . The Pearson correlation coefficient ( $\rho$ ) between these amplitudes was used as a penalty factor to exclude solutions that result in estimated STA components in an opposite direction to the measured STA. The optimization problem was solved using a least-squares minimization method in Matlab® (trust-region-reflective). For further details on the calibration procedure, see the *Chapter 3* of the thesis.

These modelled fields were used for the HJC position estimation, and then, modelled STA were removed, mode by mode, from the relevant STA fields, *i.e.*,  $\tilde{\mathbf{V}}_{i_P}(k)$  or  $\tilde{\mathbf{V}}_{i_D}(k)$ , and the position of the HJC was estimated for each mode removal. The error in mm of the HJC position during the above-mentioned estimation was evaluated as described above.

## Results

### *Analysis of modes in terms of STA energy*

It was important to assess the number of modes that are necessary to represent more than a selected threshold of the total energy of the relevant STA field, to define the minimum number of modes that are necessary to reconstruct the phenomenon under analysis. The modes of the STA were calculated for both the distal and the proximal marker clusters. The analysis in terms of energy distribution was done for all the trials for each specimen.

		Specimen 1			Specimen 2			Specimen 3			Specimen 4		
		Trial			Trial			Trial			Trial		
		1	2	3	1	2	3	1	2	3	1	2	3
Energy	85	2	2	2	2	2	2	3	2	3	3	2	2
	90	2	2	2	2	2	2	3	3	3	3	3	3
	95	3	3	2	3	3	3	4	4	4	4	4	4

**Table A1.1** - Number of modes necessary to represent the threshold of energy selected (85%, 90% and 95%) in all the trials for each specimen, in the **proximal** cluster, *i.e.* using  $V_{i_p}(k)$ .

		Specimen 1			Specimen 2			Specimen 3			Specimen 4		
		Trial			Trial			Trial			Trial		
		1	2	3	1	2	3	1	2	3	1	2	3
Energy	85	2	2	2	2	2	2	3	3	3	3	2	2
	90	2	3	2	2	2	3	3	4	4	3	3	3
	95	3	3	3	3	3	3	4	5	5	3	3	3

**Table A1.2** - Number of modes necessary to represent the threshold of energy selected (85%, 90% and 95%) in all the trials for each specimen, in the **distal** cluster, *i.e.* using  $V_{i_D}(k)$ .

#### *Hip joint centre position estimation*

When raw data were used, *i.e.*  $V_{i_p}(k)$ , blue, and  $V_{i_D}(k)$ , red, error values for the HJC estimations, expressed in mm, for all specimens, are shown in Figure A1.3 (on the top). The same values are shown in the same Figure when the first (in the middle of the Figure) and second ranked modes (on the bottom) are removed from  $V_{i_p}(k)$  and  $V_{i_D}(k)$ , respectively.

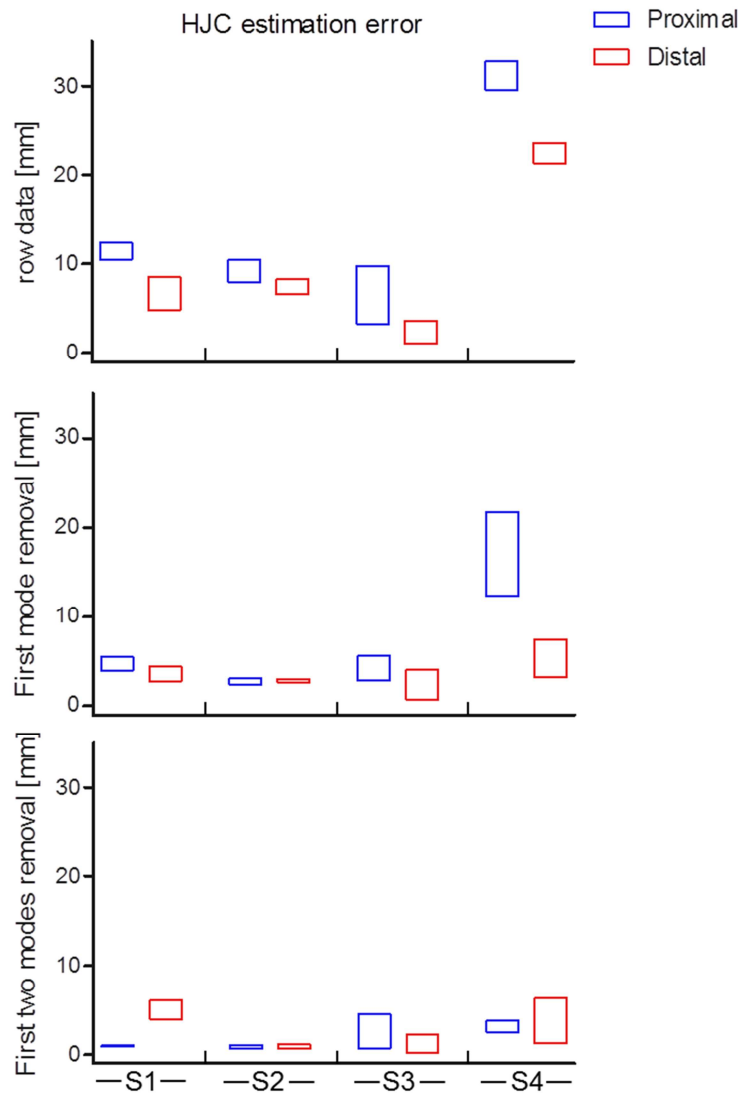


**Figure A1.3** - Range (minimum, and maximum) of the amplitude of the error [mm] in the HJC estimation calculated as the norm of the difference between the HJC position in the pelvic AF using raw data (top panel), removing the amplitude of the STA along the first mode (central panel), and the STA along the first two ranked modes (bottom panel) with respect to the reference position (pin). Statistics performed over all trials and specimens (S1, S2, S3, S4), for both skin marker clusters (distal in red and proximal in blue).

The trend of the error values for the HJC estimation when the removal of modes increases in number is shown in the Figures A1.4 for the all the trials performed by each specimen using the distal and the proximal marker cluster.

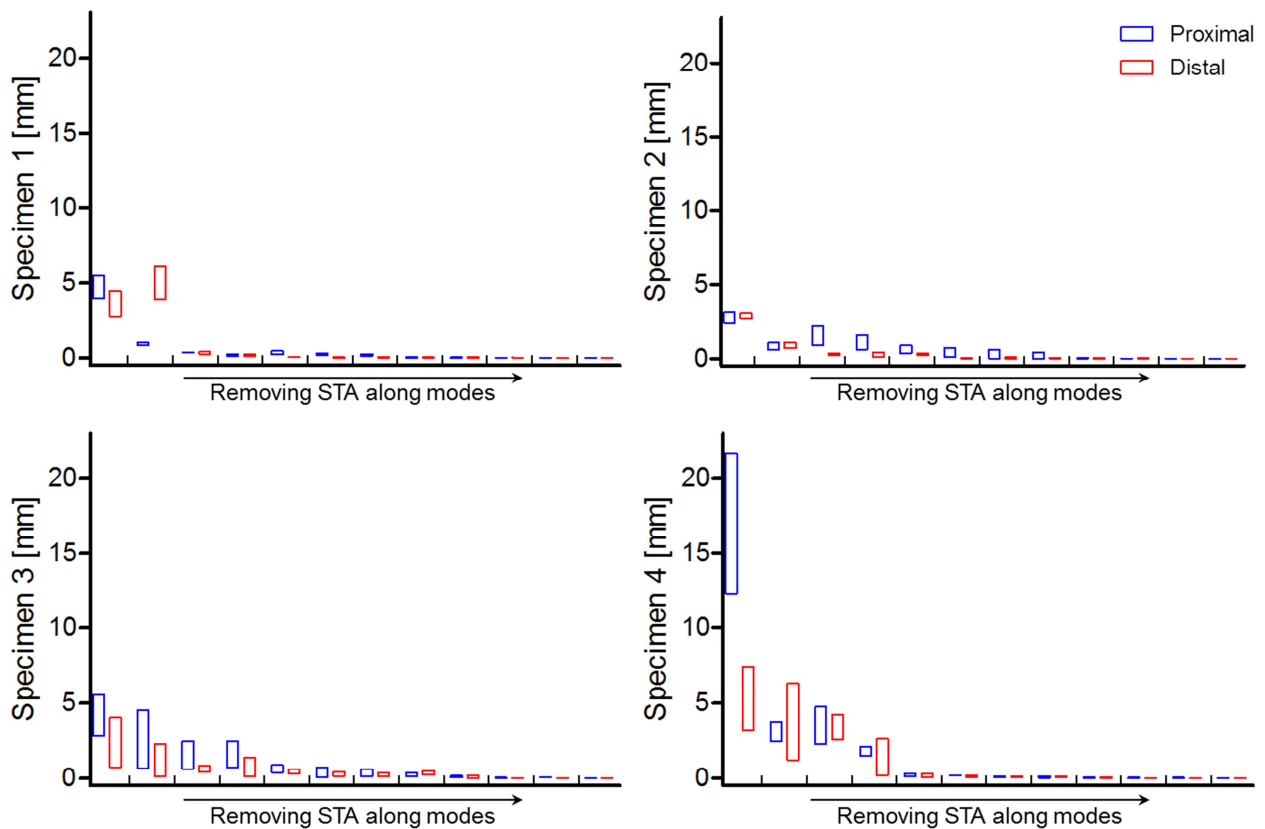


**Figure A1.4** - Range (minimum, and maximum) of the amplitude of the error [mm] in the HJC estimation calculated as the norm of the difference between the HJC position in the pelvic AF using reference data (pin), and progressively removing the amplitude of the STA along the ranked modes. Statistics shown for the different specimens and performed over all trials, for both skin marker clusters (distal in red and proximal in blue).

The trend of the error values for the HJC estimation when the removal of modes increases in number is shown in the Figures A1.5 for all specimens and trials, using the distal and the proximal marker cluster.

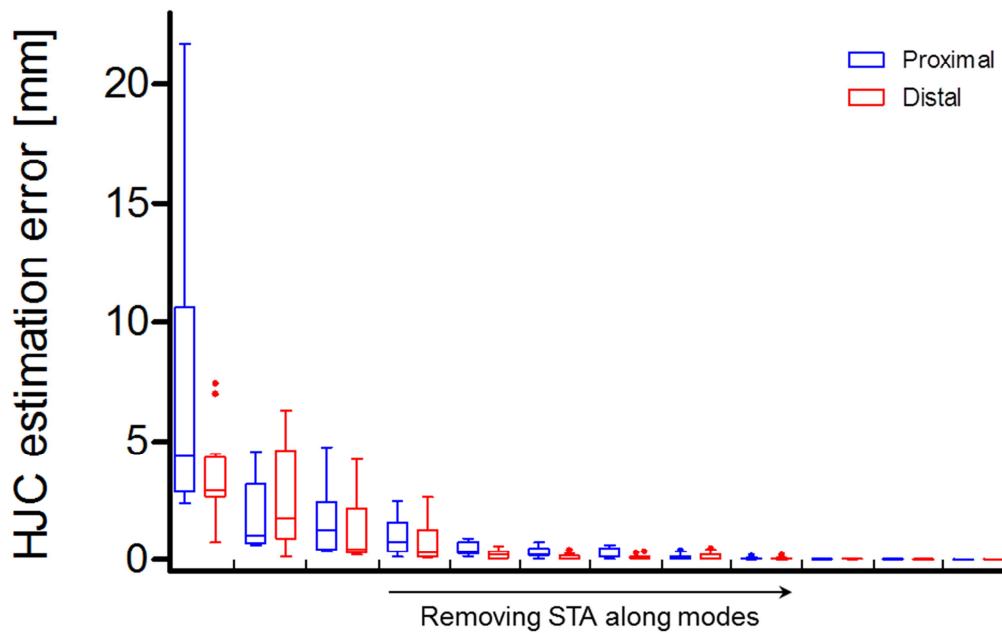


**Figure A1.5** - Box plot (minimum, lower quartile, median, upper quartile and maximum) of the amplitude of the error [mm] in the HJC estimation calculated as the norm of the difference between the reference HJC position (pin) in the pelvic AF using and the HJC position estimated in the same reference frame progressively removing the amplitude of the STA along the ranked modes. Statistics performed over all trials and specimens, for both skin marker clusters (distal in red and proximal in blue).

#### *Model architecture to link hip joint kinematics to modes*

The correlation between the measured ( $a_{i_p}^l(k)$  and  $a_{i_D}^l(k)$ ) and the three hip joint angles time histories (FE: flexion/extension, AA: abduction/adduction, IE: internal/external rotation) measured during the “Star-Arc” movement, as shown for example in Figure A1.6, are reported in Table A1.3 for the proximal skin-marker cluster and Table A1.4 for the distal skin-marker cluster.

As shown in Figures A1.7-8 for example, mode amplitudes, when the SV representation was used, changed among the different trials performed by the same specimen for the two skin marker clusters.

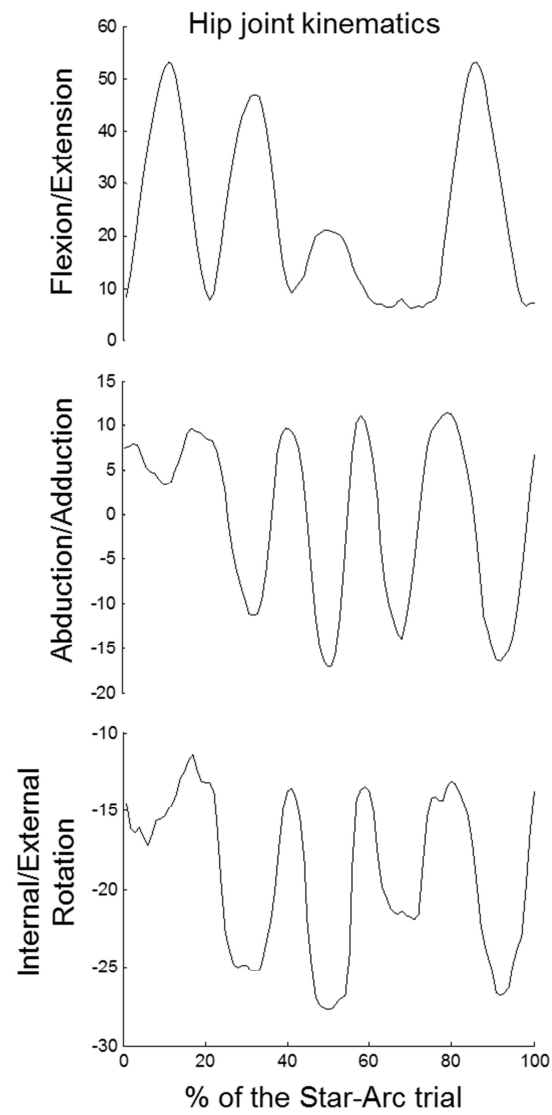


**Figure A1.6** – Reference hip joint kinematics time histories [deg] measured using pin data for a trial of a specimen (S1) during the Star-Arc movement.

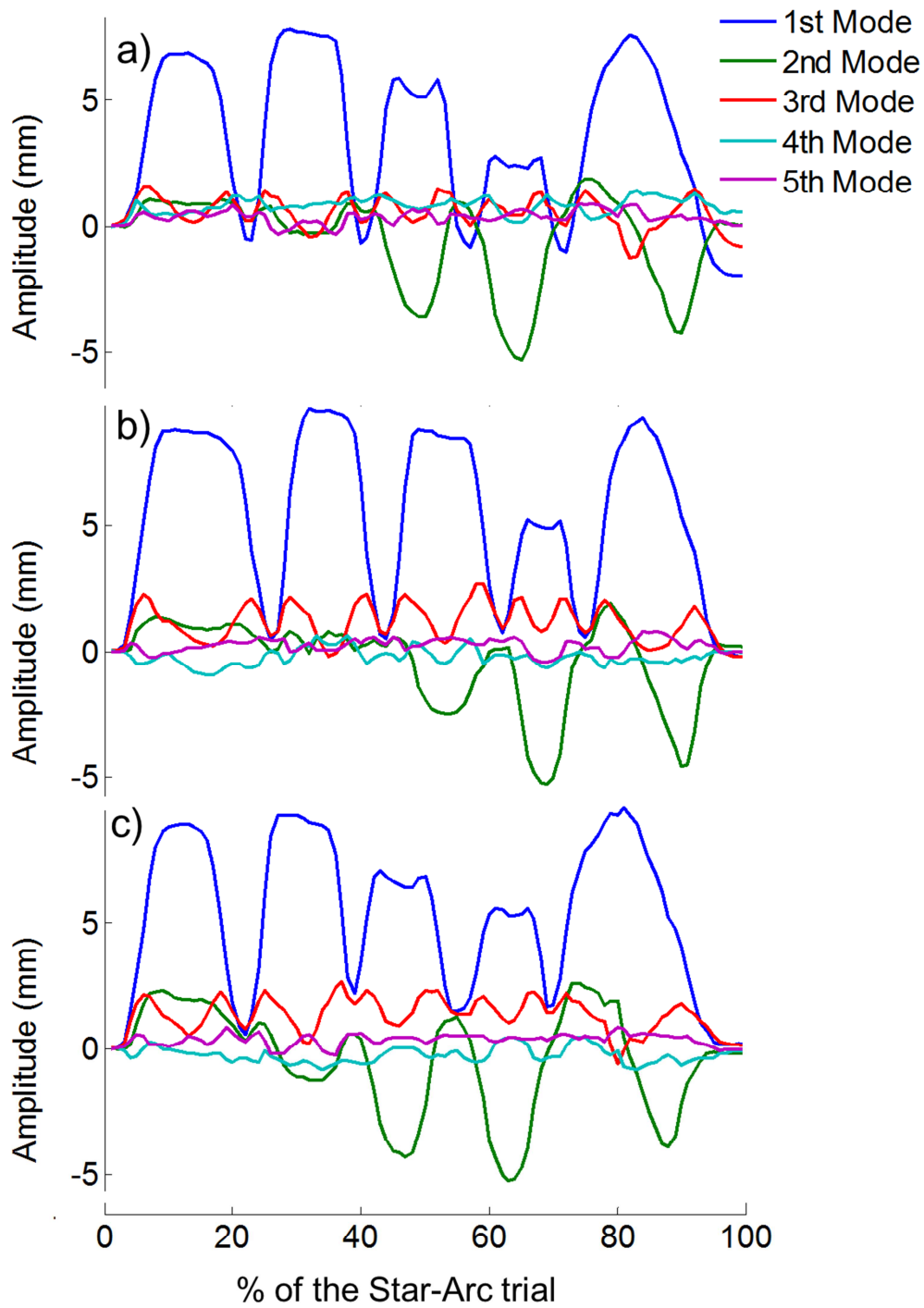


**Figure A1.7** – Amplitudes of the first five modes measured during the three trials (indicated here as a, b, and c trial) performed by a specimen (S1) for the proximal skin-marker cluster.

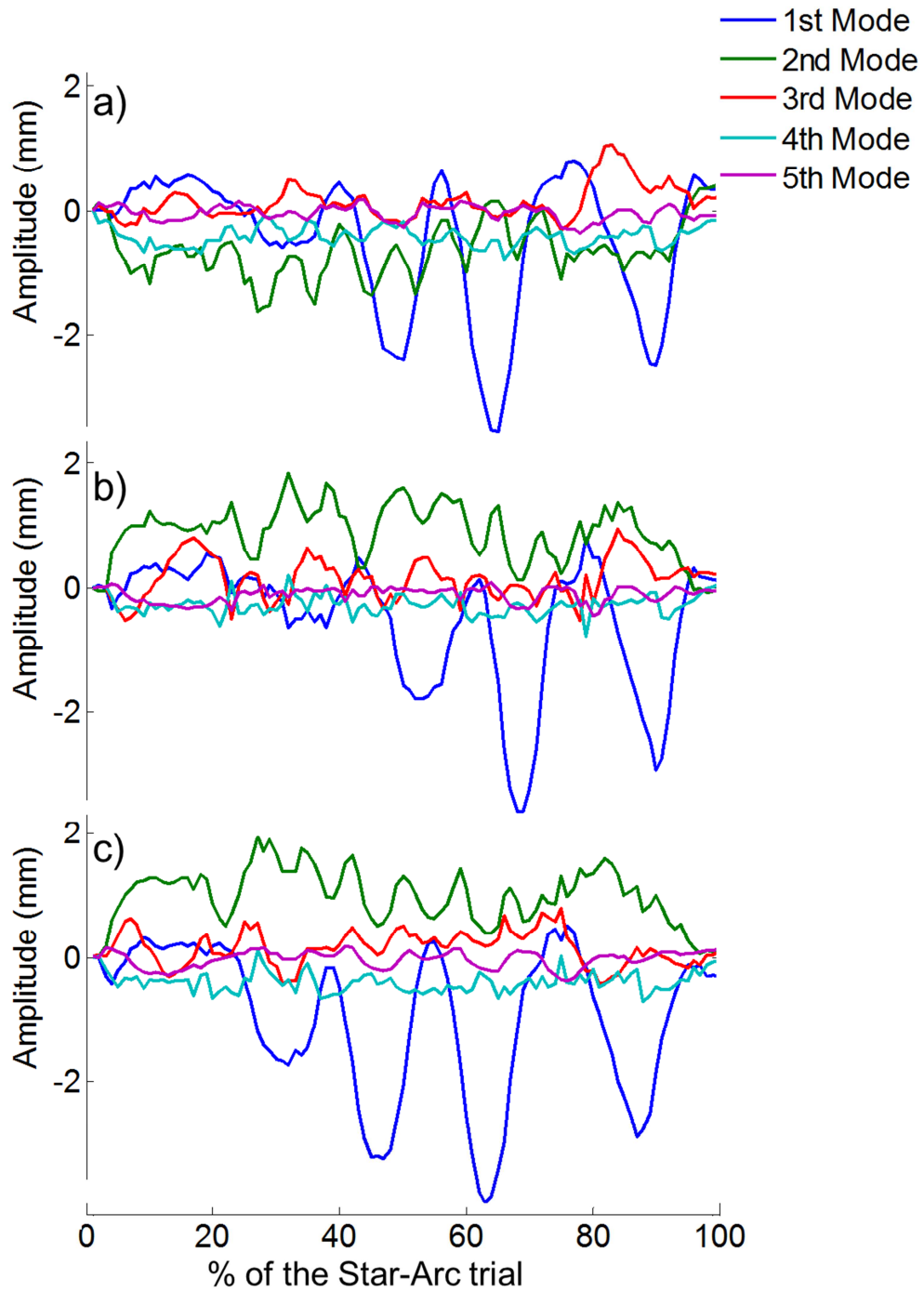


**Figure A1.8** – Amplitudes of the first five modes measured during the three trials (indicated here as a, b, and c trial) performed by a specimen (S1) for the distal skin-marker cluster.

	Trial	Mode 1			Mode 2			Mode 3			Mode 4			Mode 5			
		FE	AA	IE	FE	AA	IE	FE	AA	IE	FE	AA	IE	FE	AA	IE	
Specimen	1	0,27	<b>0,83</b>	<b>0,72</b>	0,45	0,23	0,46	0,39	0,31	0,24	0,22	0,09	0,16	<b>0,55</b>	0,21	0,10	
	1	2	0,19	<b>0,83</b>	<b>0,70</b>	<b>0,62</b>	0,28	0,35	<b>0,52</b>	0,35	0,22	0,09	0,12	0,16	0,41	0,01	0,08
	1	3	0,26	<b>0,86</b>	<b>0,71</b>	<b>0,64</b>	0,30	0,45	0,35	0,31	0,24	0,15	0,11	0,10	<b>0,53</b>	0,10	0,03
	2	1	0,06	<b>0,90</b>	<b>0,70</b>	<b>0,82</b>	0,31	0,41	0,29	0,19	0,14	0,03	0,05	0,30	0,04	0,16	0,07
	2	2	0,17	<b>0,86</b>	<b>0,59</b>	<b>0,84</b>	0,38	0,27	0,37	0,25	0,21	0,12	0,00	0,43	0,08	0,15	0,07
	2	3	0,04	<b>0,84</b>	0,49	<b>0,91</b>	0,37	0,35	0,13	0,25	0,27	0,13	0,01	0,34	0,03	0,19	0,08
	3	1	0,33	<b>0,82</b>	<b>0,60</b>	0,21	0,28	0,23	0,47	0,12	0,10	0,04	0,07	0,10	0,29	0,02	0,04
	3	2	0,40	<b>0,92</b>	<b>0,71</b>	0,14	0,02	0,10	0,34	0,01	0,13	0,38	0,11	0,09	0,37	0,03	0,32
	3	3	0,32	<b>0,90</b>	<b>0,62</b>	0,01	0,03	0,06	0,07	0,13	0,02	0,39	0,02	0,27	0,09	0,20	0,35
	4	1	<b>0,68</b>	0,41	0,00	0,31	<b>0,61</b>	0,30	<b>0,57</b>	0,24	0,45	0,02	0,49	<b>0,68</b>	0,21	0,01	0,31
	4	2	<b>0,70</b>	0,50	0,11	<b>0,60</b>	0,02	0,19	0,09	0,49	0,20	0,18	0,30	0,08	0,14	<b>0,50</b>	<b>0,79</b>
	4	3	<b>0,64</b>	<b>0,52</b>	0,22	0,35	0,45	0,27	<b>0,60</b>	0,16	0,23	0,16	0,37	0,24	0,09	0,40	<b>0,56</b>

**Table A1.3** – Correlation values between the amplitude of the first five modes and the hip joint kinematics (flexion/extension (FE), abduction/adduction (AA) and internal/external rotation (IE)) in all the trials for each specimen, for the distal skin markers cluster.

	Trial	Mode 1			Mode 2			Mode 3			Mode 4			Mode 5			
		FE	AA	IE	FE	AA	IE	FE	AA	IE	FE	AA	IE	FE	AA	IE	
Specimen	1	<b>0,86</b>	<b>0,53</b>	<b>0,58</b>	0,35	<b>0,78</b>	<b>0,65</b>	0,27	0,23	0,07	0,04	0,14	0,24	0,11	0,02	0,19	
	1	2	<b>0,88</b>	<b>0,54</b>	<b>0,60</b>	0,30	<b>0,76</b>	<b>0,59</b>	0,25	0,28	0,23	0,15	0,05	0,22	0,07	0,10	0,00
	1	3	<b>0,83</b>	<b>0,58</b>	<b>0,68</b>	0,45	<b>0,75</b>	<b>0,56</b>	0,25	0,23	0,16	0,02	0,12	0,19	0,04	0,07	0,04
	2	1	0,50	<b>0,66</b>	<b>0,78</b>	<b>0,79</b>	<b>0,69</b>	0,15	0,26	0,13	0,16	0,00	0,13	0,49	0,14	0,18	0,01
	2	2	<b>0,55</b>	<b>0,60</b>	<b>0,55</b>	<b>0,77</b>	<b>0,71</b>	0,06	0,12	0,22	<b>0,57</b>	0,04	0,10	0,26	0,23	0,10	0,25
	2	3	<b>0,56</b>	0,45	<b>0,54</b>	<b>0,68</b>	<b>0,77</b>	0,04	0,34	0,24	0,19	0,18	0,25	0,09	0,12	0,06	0,46
	3	1	<b>0,51</b>	<b>0,53</b>	<b>0,63</b>	<b>0,67</b>	<b>0,54</b>	0,15	0,12	0,21	0,23	0,08	0,09	0,01	0,18	0,25	0,05
	3	2	0,06	<b>0,73</b>	<b>0,65</b>	<b>0,88</b>	<b>0,56</b>	0,11	0,17	0,08	0,13	0,02	0,00	0,08	0,18	0,13	0,23
	3	3	0,01	<b>0,77</b>	<b>0,60</b>	<b>0,86</b>	0,36	0,09	0,23	0,28	0,16	0,05	0,05	0,01	0,06	0,03	0,14
	4	1	<b>0,78</b>	0,25	0,27	0,17	<b>0,88</b>	<b>0,69</b>	0,28	0,09	<b>0,55</b>	0,48	0,08	0,06	0,06	0,29	0,28
	4	2	<b>0,80</b>	0,42	0,26	0,04	<b>0,71</b>	0,47	0,41	0,10	<b>0,58</b>	0,38	0,37	0,44	0,07	0,24	0,26
	4	3	<b>0,72</b>	<b>0,52</b>	0,28	0,21	<b>0,65</b>	0,35	<b>0,53</b>	0,10	<b>0,56</b>	0,33	0,36	<b>0,52</b>	0,04	0,27	0,24

**Table A1.4** - Correlation values between the amplitude of the first five modes and the hip joint kinematics (flexion/extension (FE), abduction/adduction (AA) and internal/external rotation (IE)) in all the trials for each specimen, for the proximal skin markers cluster.

The results in the improvement in HJC estimation removing the modelled STA modes were compared with those obtained with the measured ones. This improvement was evaluated in terms of error values, expressed in mm, with respect to the reference HJC position, defined with pin data, for the different specimens and skin marker clusters (Figures A1.9).

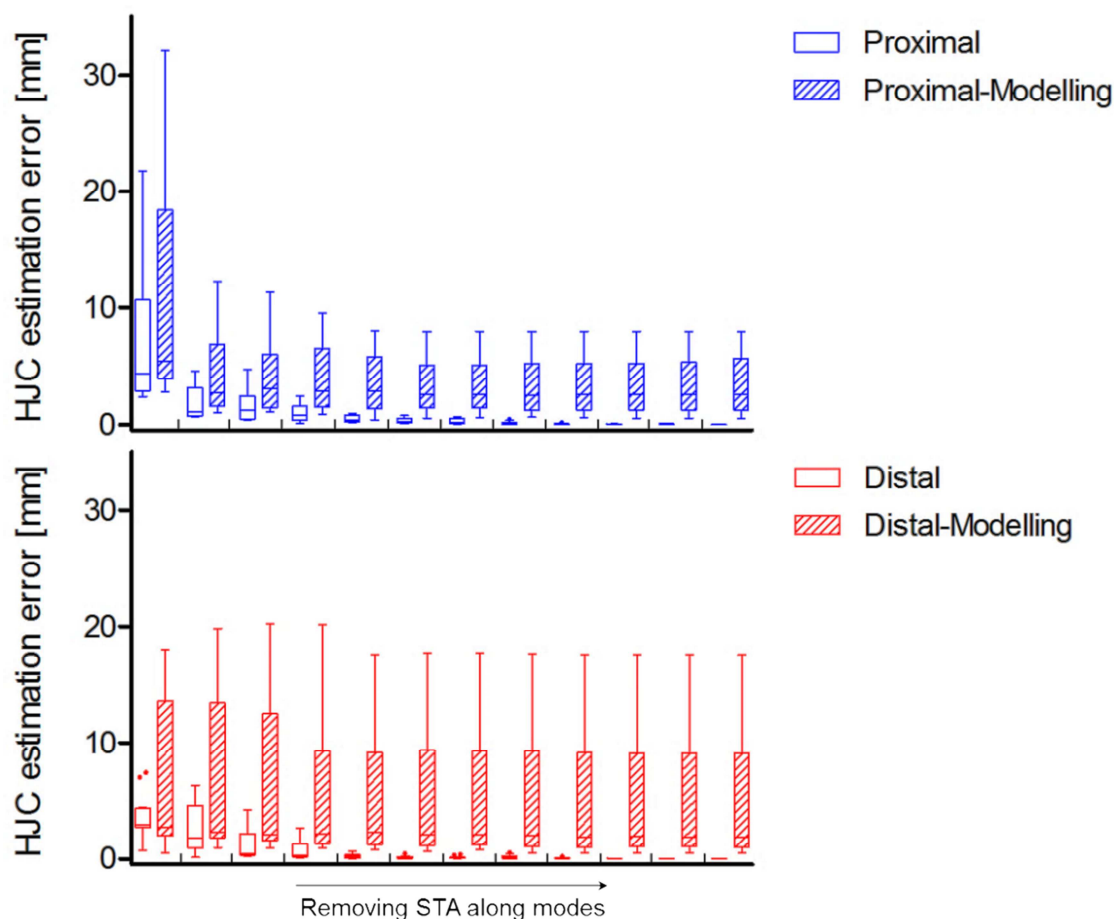


**Figure A1.9** - Box plot (minimum, lower quartile, median, upper quartile and maximum) of error values [mm] for the HJC estimation calculated as the norm of the difference between reference HJC position (pin) in the pelvic AF and those estimated in the same reference frame system modelling STA modes, for both proximal (blue) and distal (red) skin marker cluster. Statistics performed over all trials and specimens.

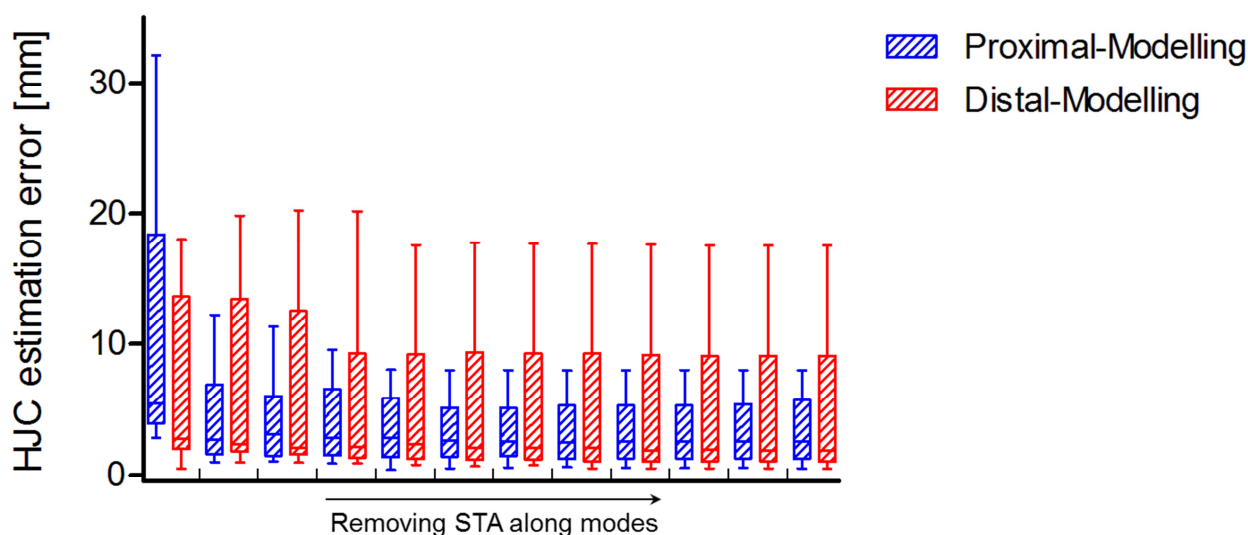


**Figure A1.10** - Box plot (minimum, lower quartile, median, upper quartile and maximum) of the error values [mm] for the HJC estimation calculated as the norm of the difference between the reference HJC position (pin) in the pelvic AF and those estimated in the same reference frame system modelling STA modes, for both proximal (blue) and distal (red) skin marker cluster. Statistics performed over all trials and specimens.

The improvements in the HJC estimation are expressed in percentage. When the improvement is the 100% the real position of the HJC is obtained. These values are shown in Table A1.5 for the proximal marker-cluster and in Table A1.6 for the distal one. These improvement are represented with the mean, median and inter-quartile range of the results obtained in the different trials of the same specimens; in addition these values are reported also for all trials and specimens.

		Specimen 1			Specimen 2			Specimen3			Specimen 4			All Specimens		
		Mean	Median	IQR	Mean	Median	IQR	Mean	Median	IQR	Mean	Median	IQR	Mean	Median	IQR
		[%]	[%]	[%]	[%]	[%]	[%]	[%]	[%]	[%]	[%]	[%]	[%]	[%]	[%]	[%]
<b>Measured Modes</b>	1	58	59	15	71	71	1	29	29	22	50	58	19	52	54	14
	2	92	92	2	91	93	6	64	54	25	90	88	4	84	82	9
	3	97	97	1	82	83	14	79	76	9	88	88	6	87	86	8
	4	98	98	1	89	94	11	78	75	8	94	95	1	90	90	5
	5	97	98	2	93	92	6	88	91	7	99	99	0	94	95	4
	6	98	97	1	96	98	7	92	93	12	99	99	0	96	97	5
	7	98	99	1	97	99	6	91	94	13	100	100	0	96	98	5
	8	99	99	1	98	99	4	97	96	1	100	100	0	98	99	1
	9	100	100	0	100	100	0	98	98	1	100	100	0	99	99	0
	10	100	100	0	100	100	0	100	100	0	100	100	0	100	100	0
	11	100	100	0	100	100	0	99	99	1	100	100	0	100	100	0
	12	100	100	0	100	100	0	100	100	0	100	100	0	100	100	0
<b>Modelled Modes</b>	1	40	35	16	55	60	13	31	32	25	15	15	20	35	36	19
	2	85	88	9	68	73	12	51	49	41	66	63	14	68	68	19
	3	85	88	9	65	66	12	55	47	29	69	65	14	68	67	16
	4	87	90	9	66	62	13	52	48	37	72	69	7	69	67	17
	5	88	91	8	68	66	7	48	38	59	77	74	8	70	67	20
	6	87	90	7	69	66	9	57	48	42	78	75	8	73	70	16
	7	87	90	7	70	66	8	58	50	39	78	75	8	73	70	15
	8	87	90	7	70	68	8	64	58	31	78	75	8	75	73	14
	9	87	89	7	69	67	8	63	56	32	78	75	8	74	72	14
	10	87	89	7	69	67	8	64	57	33	78	75	8	74	72	14
	11	87	89	7	69	67	8	63	57	34	78	75	8	74	72	14
	12	87	89	7	69	67	8	62	56	37	78	75	8	74	72	15

**Table A1.5** – Mean, median and inter-quartile range (IQR) values of the improvements in the HJC estimation, expressed in percentage [%], for the proximal markers cluster.

	Subject 1			Subject 2			Subject 3			Subject 4			All Subjects			
	Mean	Median	IQR	Mean	Median	IQR										
	%	%	%	%	%	%	%	%	%	%	%	%	%	%	%	
<b>Measured Modes</b>	1	47	48	8	60	56	10	17	21	39	74	70	13	49	49	17
	2	14	15	59	87	88	5	46	37	57	83	82	16	58	55	34
	3	95	95	1	96	96	1	46	35	55	86	89	7	81	79	16
	4	96	95	2	96	96	4	31	35	101	93	91	8	79	80	29
	5	99	99	0	96	96	1	74	72	12	99	100	1	92	92	3
	6	99	100	1	100	100	0	83	84	7	99	99	0	95	96	2
	7	99	99	0	99	99	1	79	70	21	100	100	0	94	92	6
	8	100	100	0	100	100	0	74	77	22	100	100	0	93	94	6
	9	99	100	1	100	99	0	92	98	15	100	100	0	98	99	4
	10	100	100	0	100	100	0	99	99	1	100	100	0	100	99	0
	11	100	100	0	100	100	0	99	100	1	100	100	0	100	100	0
	12	100	100	0	100	100	0	100	100	0	100	100	0	100	100	0
<b>Modelled Modes</b>	1	50	52	8	60	59	11	38	51	41	23	23	2	43	46	15
	2	55	53	6	69	71	5	18	6	43	20	21	5	40	38	15
	3	67	68	16	72	70	8	2	8	35	19	15	11	40	40	18
	4	70	70	11	71	71	9	15	25	25	26	17	25	46	46	17
	5	76	78	15	71	72	9	-19	30	120	33	26	16	40	52	40
	6	76	78	15	70	73	12	-5	45	128	32	25	16	43	56	43
	7	76	78	14	71	73	12	-9	39	131	32	25	17	43	54	43
	8	76	78	14	71	74	11	-3	14	144	32	25	17	44	48	47
	9	76	79	14	71	74	11	18	58	109	33	25	17	49	59	38
	10	76	78	14	70	74	12	16	59	113	33	26	17	49	59	39
	11	76	78	14	71	74	11	18	59	109	33	26	17	49	59	38
	12	76	78	14	71	74	11	19	60	110	33	26	17	50	59	38

**Table A1.5** – Mean, median and inter-quartile range (IQR) values of the improvements in the HJC estimation, expressed in percentage [%], for the distal markers cluster.

## Discussion

The aim of this study is to demonstrate the possibility to apply a model of the STA that can be included in a bone pose estimator. Based on the thigh STA modelling proposed by Camomilla et al. (2013) and on the results shown in Cereatti et al. (2009), to reduce the number of the model parameters to be estimated, the degrees of freedom of the STA was reduced using the SV definition, described in *Chapter 4*.

Using this definition, the energy distribution changes among skin marker-clusters, trials and specimens as shown in Table A1.1 and Table A1.2. Two or three modes can represent the 85% of the total STA energy, the same number of modes is sufficient to represent also the 90% of the total energy, but for distal skin-marker cluster of the third specimen four modes are required. For the same specimen and cluster, five modes represent the 95% of the whole STA energy, while for the other clusters and specimens, three or four modes can represent the same amount of energy.

In this study, it has been demonstrated that the progressive elimination of STA modes, represented using the SV definition, for the relevant STA field, the estimation of the HJC position improves:

error values decreased in all specimens, both for the distal and the proximal skin clusters, as shown in Figure A1. 4.

To evaluate the effect of the choice on the skin marker-cluster location, for all trials and specimens, the error values were compared between specimens (Figure A1.5). When the whole STA field is used (*i.e.*, no STA compensation) for the HJC position estimation, the lower errors are obtained for the distal skin marker-cluster (Figure A1.3-upper panel). Moreover, these errors are related to the size of the thigh of the different specimens, as shown in the Table A1.6 (Camomilla et al., 2013): the biggest errors are obtained for fourth specimen and the lower for third one.

	Subj1	Subj2	Subj3	Subj4
$S_p$	161	132	114	190
$S_m$	123	111	96	151
$S_d$	105	106	101	123
$L_t$	396	360	411	364

**Table A1.7-** Diameters of the proximal ( $S_p$ ), median ( $S_m$ ), and distal ( $S_d$ ) sections of the thigh. The length of the thigh ( $L_t$ ) was measured as the distance between the centre of the femoral head (HJC) and the midpoint between the femoral epicondyles. Data in mm.

The removal of the first STA mode does not change the choice of the skin marker cluster: the norm of the error is lower when the estimation of the HJC position is performed using the distal skin cluster instead using the proximal one for all specimens (Figure A1.3-central panel). When also the second mode is removed from the relevant STA field (Figure A1.3-bottom panel), the choice of the cluster is irrelevant. The latter result does not change when progressively all the STA modes are removed for the skin marker trajectories in all the specimens, as shown in Figure A1.5.

Before applying the STA linear model for the mode amplitude estimation, the correlation coefficient between the measured mode amplitudes and the hip joint kinematics time histories showed high values of correlation (more than 0.5) mostly between the first two modes and hip joint kinematics. However, there is not a general law for all trials and specimens (for example, there is not a high value of correlation in all the cases analyzed between the flexion/extension of the hip and the variation of the amplitude along the first mode), therefore all the hip joint angles were used to estimate the variation of the amplitude in the model used.

When the STA linear model was used to estimate mode amplitudes, the error values in the HJC estimation were higher with respect to those obtained when the measured modes were removed from the skin marker trajectories, as shown in the Figures A1.9. As expected, in all the cases examined, the improvement in HJC estimation using the model is less accurate. The enhancement

for the HJC estimation, in percentage, is reported in Table A1.5 for the proximal marker cluster. Removing the measured first mode, an improvement of about 50% was obtained in the HJC estimation, while using two modes, the improvement reached 84%. Instead, removing the modelled modes for the relevant STA field, the improvement using the first mode is reduced to 35% and using the first two, to 68% (mean values over all trials and specimens). The same results are reported for the distal marker cluster in Table A1.6. The improvement in HJC estimation obtained when one mode was removed was 49% and 43% when the same mode was estimated as a linear combination of the hip joint kinematics; using two modes, the enhancement was 57% and 40%, respectively. The percent improvement achieved using the proximal marker cluster is higher than the one obtained using the distal one, but the absolute errors are greater for the proximal marker cluster.

The great variation of the modes amplitudes also between different trials performed by the same specimen is expressed clearly in Table A1.3 and Table A1.4, where different correlation values were observed between these amplitudes and the hip joint kinematics time histories. In addition, an evident example is shown in Figures A1.7-8. This amplitude variability, in addition to the definition of the direction of mode, limits the generalizability of this approach.

Future study has to be focused in the STA modelling without the use of pin data.

**References – A1**

- Camomilla, V., Cereatti, A., Cheze, L., Cappozzo, A., 2013. A hip joint kinematics driven model for the generation of realistic thigh soft tissue artefacts. *Journal of Biomechanics*, 46(3), 625–630.
- Camomilla, V., Cereatti, A., Cheze, L., Cappozzo, A., 2013. A hip joint kinematics driven model for the generation of realistic thigh soft tissue artefacts. *Journal of Biomechanics*, 46(3), 625–630.
- Cappozzo, A., 1984. Gait analysis methodology. *Human Movement Science*, 3(1), 27–50.
- Cereatti, A., Donati, M., Camomilla, V., Margheritini, F., Cappozzo, A., 2009. Hip joint centre location: an ex vivo study. *Journal of Biomechanics*, 42(7), 818–823.
- Della Croce, U., Leardini, A., Chiari, L., Cappozzo, A., 2005. Human movement analysis using stereophotogrammetry: Part 4: assessment of anatomical landmark misplacement and its effects on joint kinematics. *Gait & Posture* 21(2), 226–237.
- Della Croce, U., Cappozzo, A., Kerrigan, D.C., 1999. Pelvis and lower limb anatomical landmark calibration precision and its propagation to bone geometry and joint angles. *Medical & Biological Engineering & Computing*, 37(2), 155–161.
- Ehrig, R.M., Taylor, W.R., Duda, G.N., Heller, M.O., 2006. A survey of formal methods for determining the centre of rotation of ball joints. *Journal of Biomechanics*, 39(15), 2798–2809.
- Gamage, S., Lasenby, J., 2002. New least squares solutions for estimating the average centre of rotation and the axis of rotation. *Journal of Biomechanics*, 35(1), 87–93.
- Halvorsen, K., 2003. Bias compensated least squares estimate of the center of rotation. *Journal of Biomechanics*, 36(7), 999–1008.
- Stagni, R., Leardini, A., Cappozzo, A., Benedetti, M.G., Cappello, A., 2000. Effects of hip joint centre mislocation on gait analysis results. *Journal of Biomechanics*, 33(11), 1479–1487.

---

## *Appendix A2.*

# ***“PELVIS SOFT TISSUE ARTEFACT ASSESSMENT DURING 3-D HIP MOVEMENTS”***

### **Introduction**

The soft tissue artefact (STA), as occurring during human movement analysis using non-invasive stereophotogrammetry, has been investigated with reference to skin markers located on various body segments. The real and relative movement between the surrounding soft tissue leading and the underlying bone leads to inaccurate results of the poses of the underlying bones (Leardini et al., 2005). However, to date only two studies assessed it with reference to markers located on the pelvis.

Rozumalski et al. (2008) quantified STA at the pelvis using an invasive method: bone pins inserted in the S1 vertebrae. The relative displacement between skin marker and the underlying bone was measured over 35 mm and over 25 mm during the sit-to stand task and gait, respectively. Hara et al. (2014), instead, quantified this motion with a multiple calibration technique: it was investigated how skin markers at the pelvis were displaced in relation to anatomical body landmarks in multiple static calibration positions. This was done by determining how the local position of anatomical landmarks (ALs) varied, as determined through manual palpation, while the hip assumed different flexion/extension angles (multiple anatomical calibration). The position and orientation of the anatomical frame (AF) of the relevant bone relative to a marker cluster frame is obtained using the position of anatomical landmarks (AL) in the latter frame and a deterministic or statistical geometric rule (calibrated anatomical system technique (CAST) protocol (Cappozzo, 1984; Cappozzo et al., 1995)). Superficial ALs are identified by palpation; the location of internal ALs is estimated using statistical models (Della Croce et al., 2005) or, as occurs for the hip joint centre identification, using a functional approach (Cappozzo, 1984). In the review article of Della Croce et al. (2005) it was shown that several studies were aimed in quantified the precision of locating both internal and palpable ALs by this anatomical calibration procedure and of estimating the pose of the relevant AFs. Also the impact of these uncertainties were investigated as a propagation to joint kinematics and kinetics (Della Croce et al., 1999; Ramakrishnan and Kadaba, 1991; Stagni et al., 2000). This error source is no less important than the STA movement (Della Croce et al., 1999).

---

Therefore, the scarce repeatability with which palpable ALs are identified may lead to concealing both the intra- and inter-individual differences sought in clinical practice as well as in basic research (Donati et al., 2008).

To try to reduce the ALs identification errors in the this chapter the pelvic STA has been quantified during multiple static calibration positions as done in Hara et al. (2014), but through a different anatomical calibration method which allowed for a better reliability (UP-CAST (Donati et al., 2008)) and for different hip flexion/extension and ad-abduction angles.

### **Materials and methods**

#### *Subjects and digital bone*

Five healthy subjects with different BMI were recruited in this study (Table A2.1). After giving their written consent, they underwent MRI scanning of the pelvis.

Subject	Gender	Age [year]	Height [m]	Mass [kg]	BMI [kg/m <sup>2</sup> ]
1	F	47	1.60	68	26.6
2	M	34	1.90	80	22.2
3	F	40	1.64	60	22.3
4	M	55	1.78	90	28.4
5	M	60	1.71	85	29.1

**Table A2.1** – Anthropometric characteristics of the five subjects involved in the study.

Using the MRI images acquired in the three anatomical plane (sagittal, frontal and medial plane), as shown in Figure A1.1, the digital model of the bone was reconstructed using the AMIRA® software (Figure A1.2).

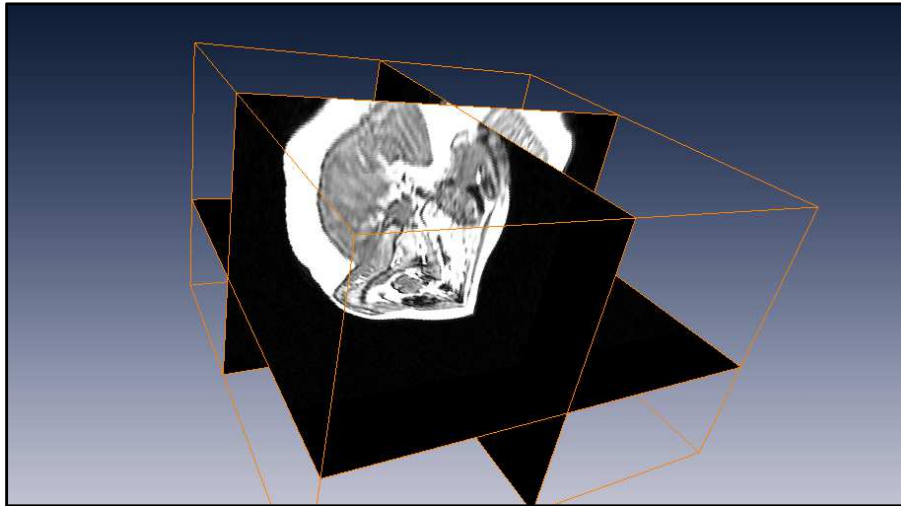


**Figure A2.1** – MRI images of a subject acquired in the three anatomical plane and used to reconstruct the digital model of the bone using the AMIRA® software.

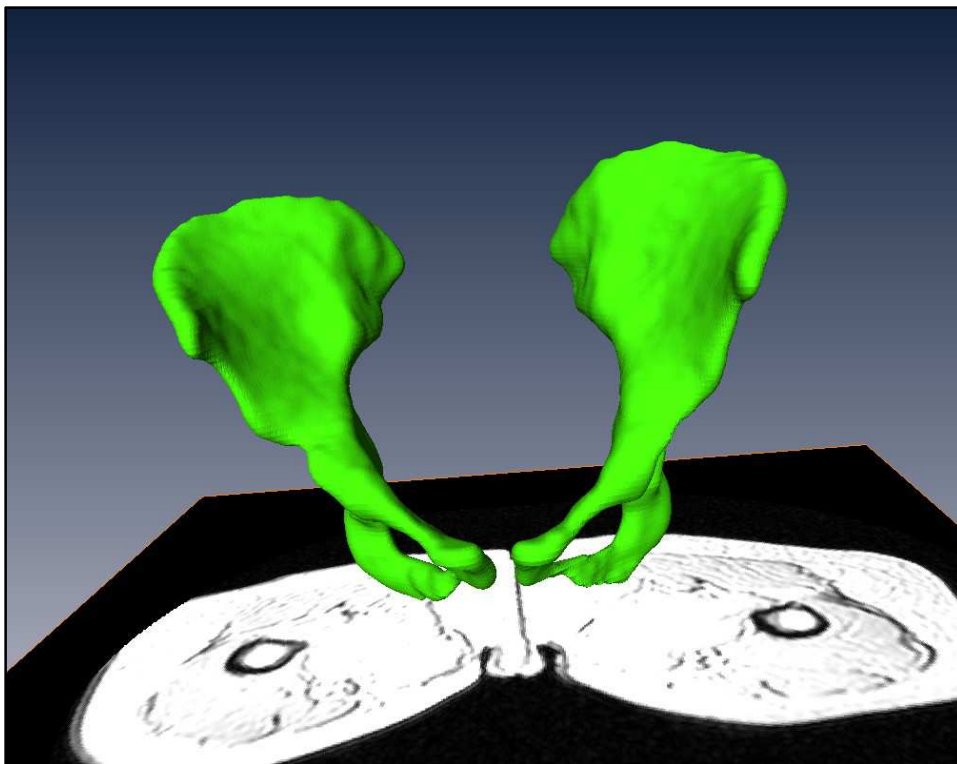


**Figure A2.2** – Digital model of the pelvic bones of a subject reconstructed using the AMIRA® software.

Four anatomical landmarks (right and left anterior superior, RASIS, LASIS, and posterior superior iliac spines, RPSIS, LPSIS) were virtually palpated on the digital bone using the written and pictorial instructions shown in Figure A1.3-4 (Van Sint Jan, 2007).

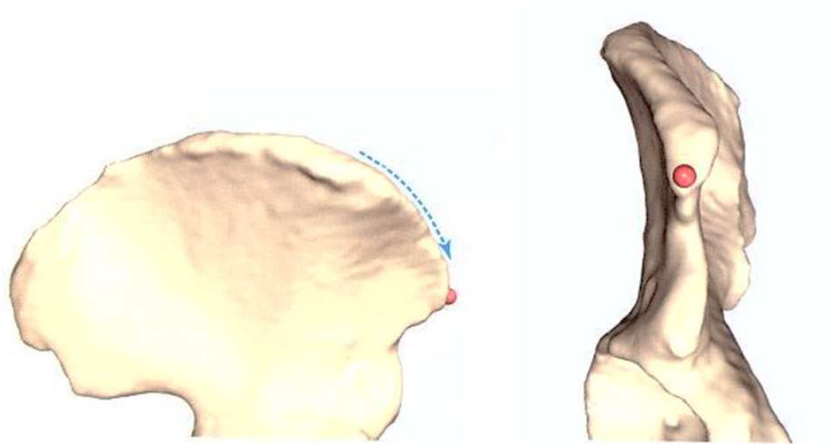


**Figure A2.3** – Identification of the prominent anterior and superior end of the iliac crest, or also called as anterior superior iliac spines (RASIS and LASIS, for the right and left side, respectively).

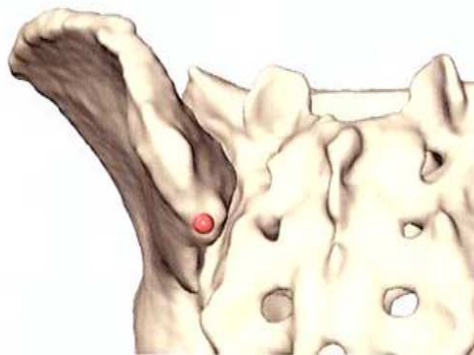


**Figure A2.4** – Identification of the prominent posterior and superior end of the iliac crest, or also called as posterior superior iliac spines (RPSIS and LPSIS, for the right and left side, respectively).

For the identification on the hip joint centre location, it was located as the centre of the sphere constructed in the acetabulum (Figure A1.5).



**Figure A2.4** – Identification of the hip joint centre position located in the middle of the joint cavity of the hip joint, the acetabulum.

---

Therefore, on each digital model of the bone six ALs were virtually identified as described above and shown as example in Figure A2.5. These points were used to define the pelvic bone anatomical frame (AF), as proposed by Cappozzo et al., (1995), and associated with the bone model.

In addition, for the UP-CAST procedure, a large number of unlabeled point (Figure A2.6) has to be identified over the prominent parts of the subject's bone (Donati et al., 2007). For this reason, on the digital model of the bone, also areas digitized used in the UP-CAST procedure were selected as shown in Figure A2.7.

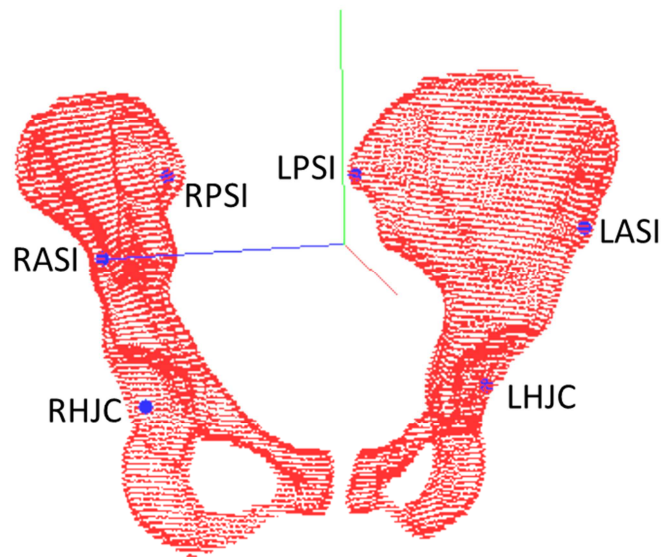


**Figure A2.5** – Position and acronyms of the selected anatomical landmarks, indicated with points: right and left anterior superior, (RASI, LASI), and posterior superior iliac spines, (RPSI, LPSI), and hip joint centre (RHJC, LHJC).

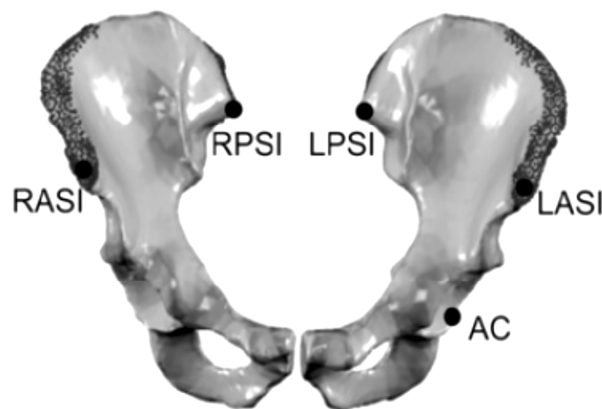


**Figure A2.6** – Position and acronyms pelvic anatomical landmarks, as in Figure A2.5 (the hip joint centre is indicated as the centre of the acetabulum) The darker points indicate the digitized areas used for the UP-CAST procedure.

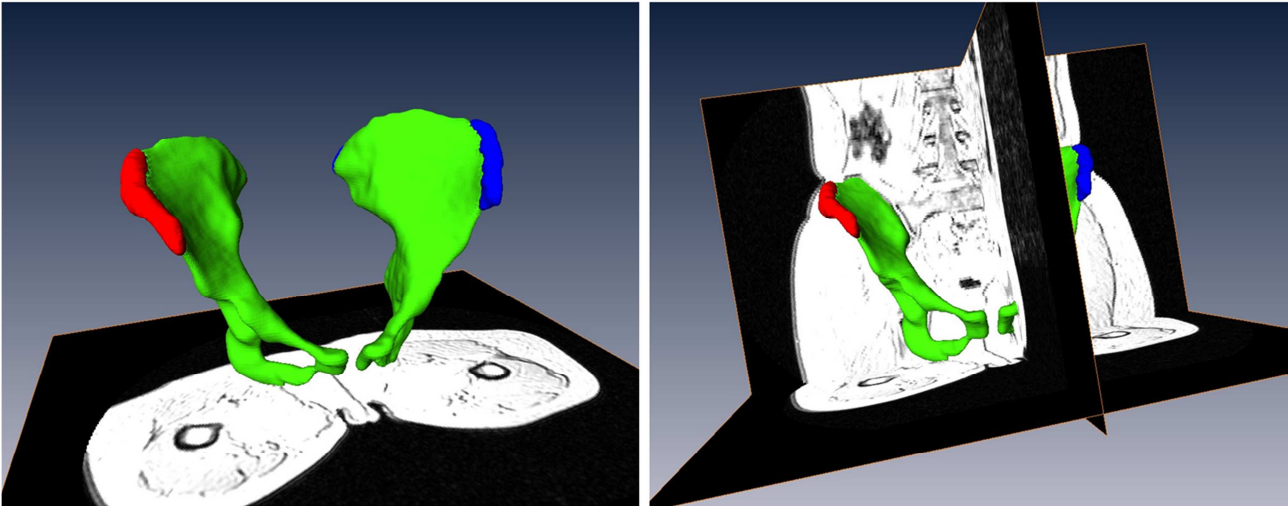


**Figure A2.7** – Digital model of the pelvic bones of a subject reconstructed using the AMIRA® software. The red and blue areas are the digitized ones used for the UP-CAST procedure, for the right and left part of the bone, respectively.

#### *Marker placement*

The subjects involved in the study performed also static photogrammetric acquisitions. A single operator performed all landmark identifications with a manual palpation. The location of the ALs was marked with a felt pen on the volunteer. The following pelvic ALs were identified: right and left anterior superior (RASIS, LASIS), and posterior superior iliac spines (RPSIS, LPSIS), and sacrum (SACR). Also the femur ALs were identified: medial and lateral epicondyle, for the right (RME, RLE) and left leg (LME, LLE).

Seven skin markers were glued on the pelvic segment and a cluster of four skin markers was glued on each lower limb of the volunteer (Figure A2.8).

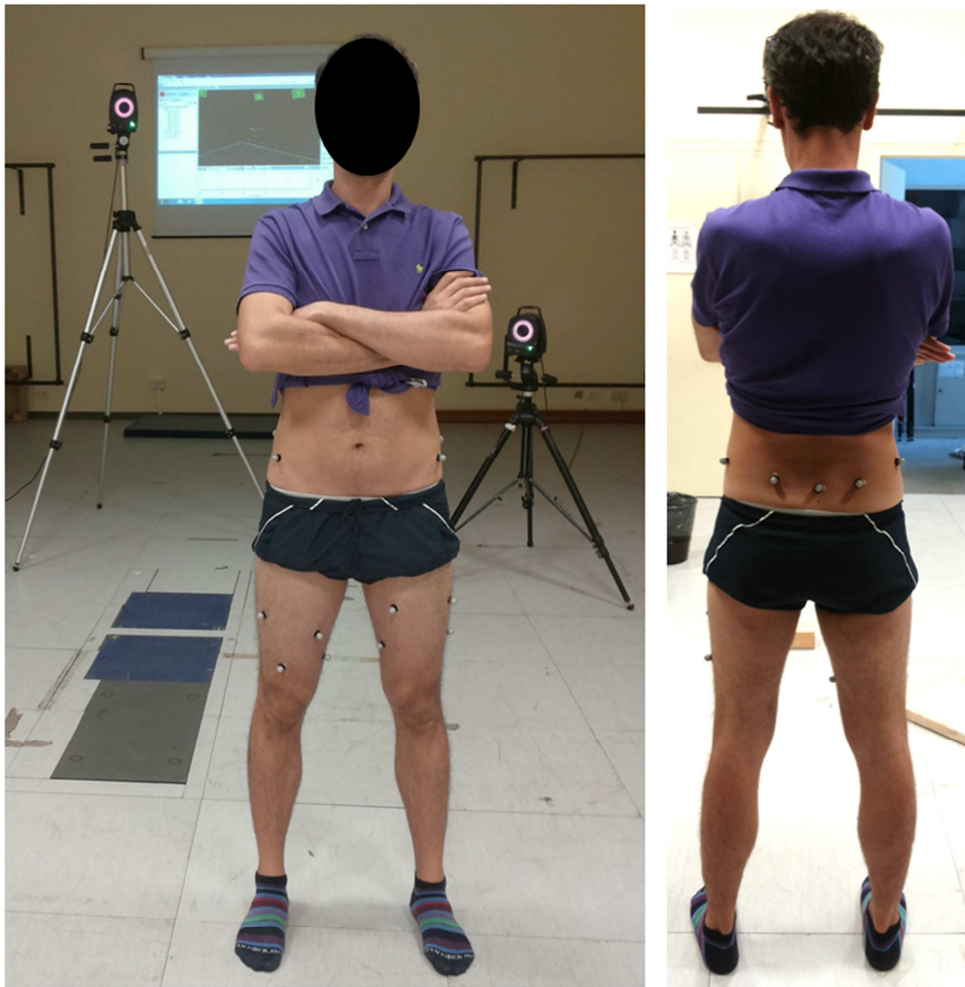


**Figure A2.7** – Skin marker location. Skin marker glued on the thigh segment were located close to the anatomical landmarks and on the iliac crests (left and right), which were marked with a felt pen on the subject.

#### *Data acquisition*

The instantaneous position of the skin markers were acquired (VICON MX, 100 frames/s) during multiple calibration trials in different posture (eight).

First, an orthostatic posture was acquired, as the one depicted in the Figure A2.7. Then, each subject stood five static postures assumed during the hip functional movement, *i.e.* “Star-arc movement” (Figure A2.8). Different supports were used to maintain the different position during the trial. The foot was supported, when required, and posture was maintained through active muscular contraction. Finally, also static postures which replicate the initial part of the gait was performed: each subject simulated the position assumed during the heel contact and the toe off (Figure A2.9).

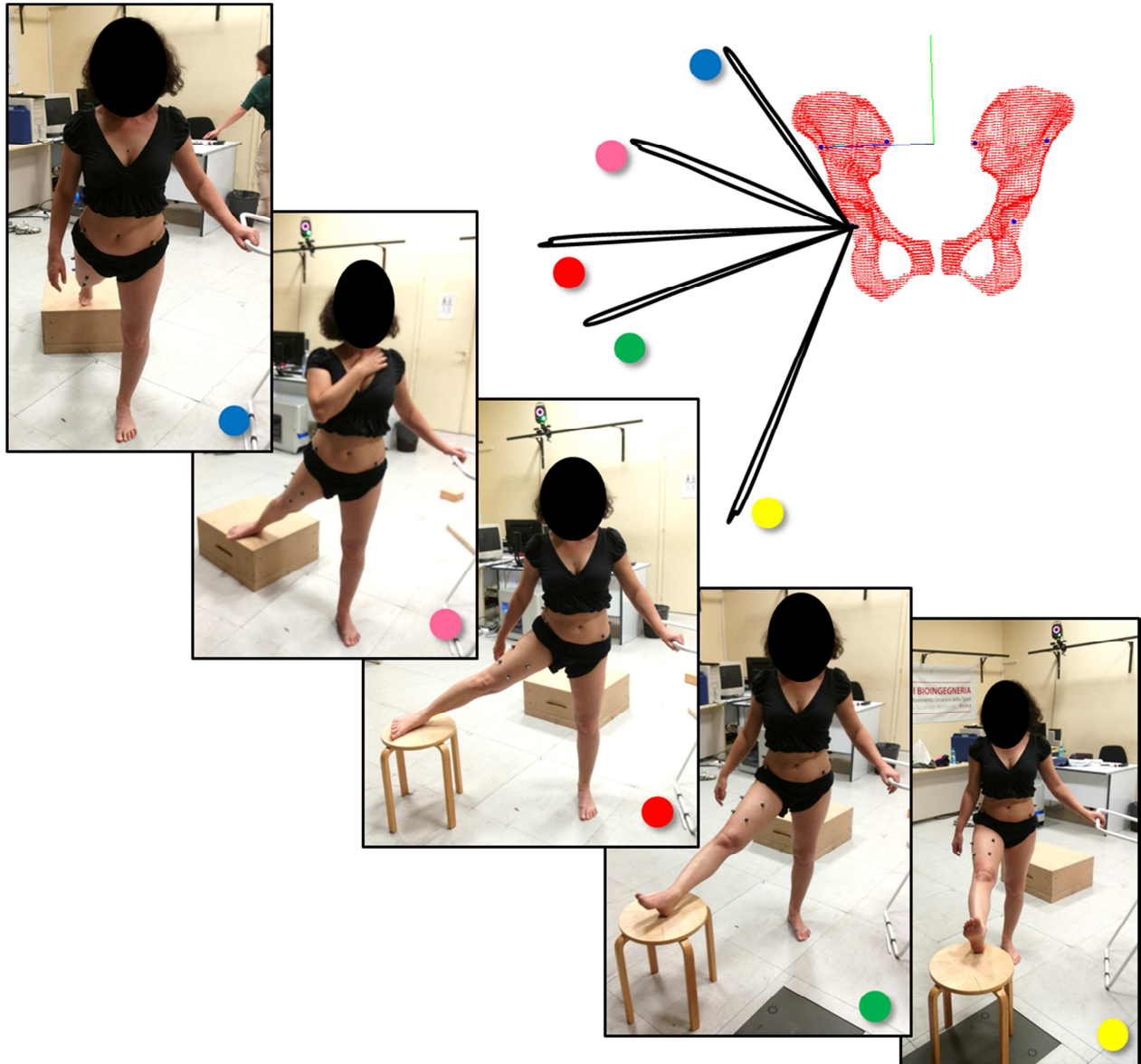


**Figure A2.8** – Five static postures assumed during the “Star-arc movement”. The different supports used to maintain the balance are also shown. The correspondence between the scheme of the movement (on the top of the figure, on the right side) and the different pictures is shown by circles with different colors.

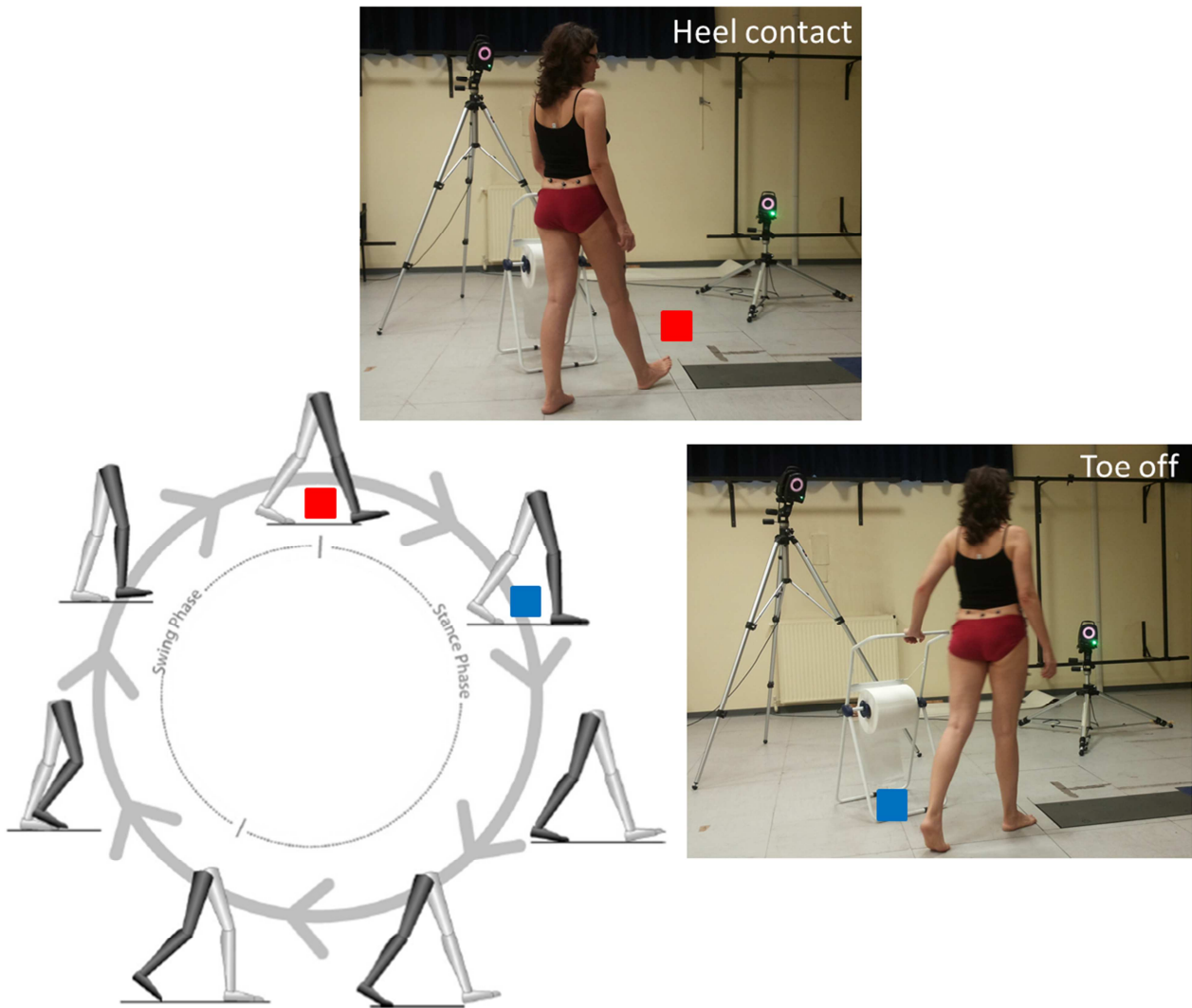


**Figure A2.9** – Two static positions assumed during the initial part of the gait. The support used to maintain the balance is also shown. The correspondence between the scheme of the gait phase movement (on the bottom of the figure, on the left side) and the different pictures is shown by squares with different colors.

For each subject and posture, a wand that carried three markers equipped with a rolling the tip was used to determine the position of clouds of unlabelled points over the prominent bony parts of the pelvis. This determination can be performed because the position of the tip with respect to the reference frame construct of the three markers on the wand is known. In addition, the positions of the pelvic marked ALs were determined with the wand, as shown for example in Figure A2.10. The femur ALs were identified only during the standing position of each subject. This information was obtained to estimate the relevant femur AF, and therefore estimate the hip angles as the relative motion between pelvic and femur AFs.



**Figure A2.10** – Identification procedure of the position of a pelvic AL during the toe-off posture of one subject using the wand equipped with three markers and a rolling tip.

*Data processing*

Seven skin markers glued on the pelvis were used to construct to build a technical frame (TF) during each posture of the different subjects (Figure A2.11).

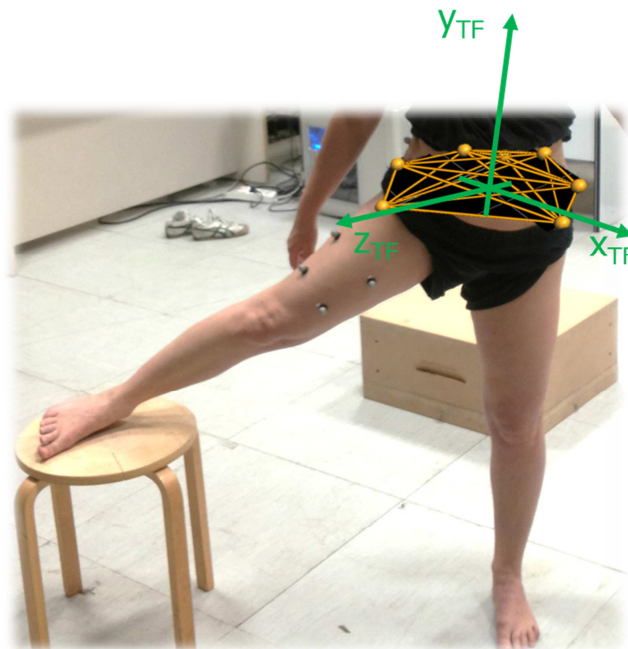


**Figure A2.11** – Definition of a technical reference frame during a static posture.

Through the UP-CAST method, the pelvis digital model was registered with the unlabelled point clouds. Acquiring the position of unlabelled points on the skin surface in the body segment areas where the soft tissue layer over the bone was sufficiently thin, the digitized surface could be

---

associated with the bone and the matching of these points with the digital model of the bone can be performed. Moreover, for each UP-CAST calibration, a new technical reference was defined excluding the markers close to the calibration area. Using a wand equipped with a cluster of three markers and a sphere on the tip that rolls over the surface to be digitized, the excluded skin markers showed a movement caused by the movement of the tip. The TF used for this acquisition, was then registered with the general one in a static trial.

The registration procedure was performed between digital bone and unlabelled points, both represented in the TF (Figure A2.12).

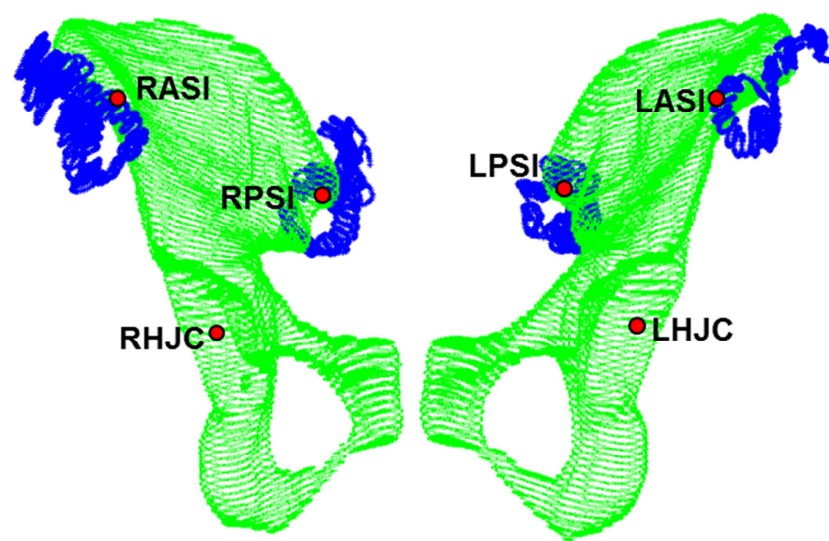


**Figure A2.12** – The registration procedure performed between digital model of the bone (subject-specific), represented with green points, and the unlabelled points, represented with blue points. Pelvic ALs were also shown, in red. This procedure was repeated for all the postures assumed by the different subjects.

The rigid transformation between TF and AF was thus obtained, and the position of the marked pelvic ALs were represented in the relevant AF.

To describe the STA of a given AL, the maximal distance between the positions assumed in the AF during the different postures was analysed for the different subjects. This distance was calculated for the different AF anatomical axes directions: x-anterior/posterior; y-inferior/superior; z-medio/lateral.

## Results

The relative movement between the ALs determined with the tip of the wand and the same AL virtually palpated on the bone digital model was defined. This represents the maximal displacement

between the positions of the AL in different calibration postures and its position identified in the orthostatic posture in the femur AF.

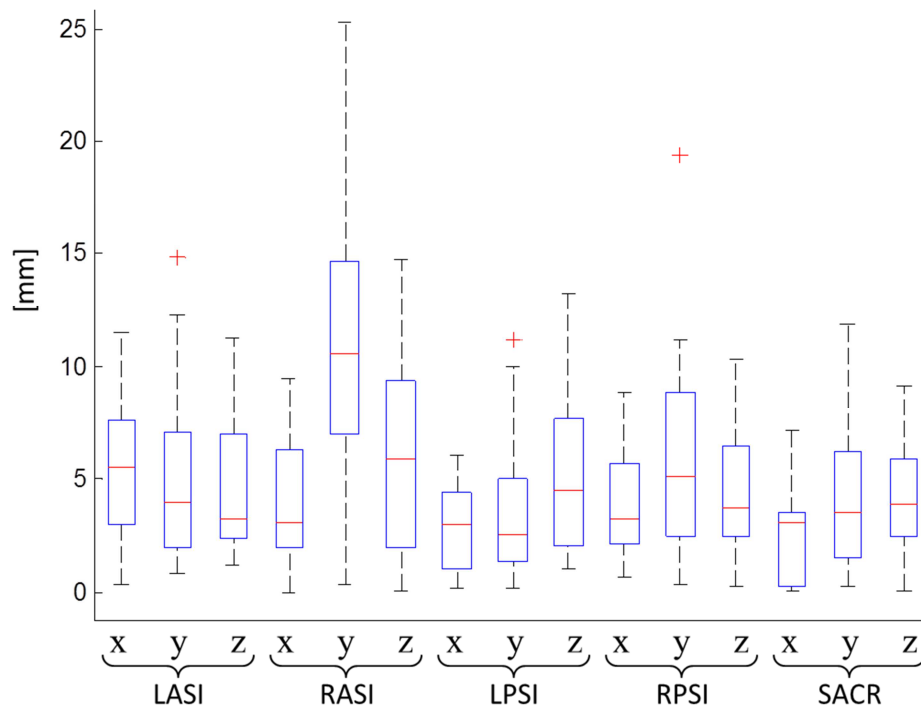


**Figure A2.13** – Soft tissue artefact displacement for the analysed hip position (“Star-Arc movement) with respect to the orthostatic one. Displacement represented for the pelvic ALs (right and left anterior superior (RASIS, LASIS), and posterior superior iliac spines (RPSIS, LPSIS), and sacrum (SACR)) and the different anatomical axes directions: x-anterior/posterior; y-inferior/superior; z-medio/lateral. Values represented using box-plots (minimum, lower quartile, median, upper quartile, and maximum) and expressed in mm. Statistics performed over all calibration trials and subjects. Outliers are also shown.

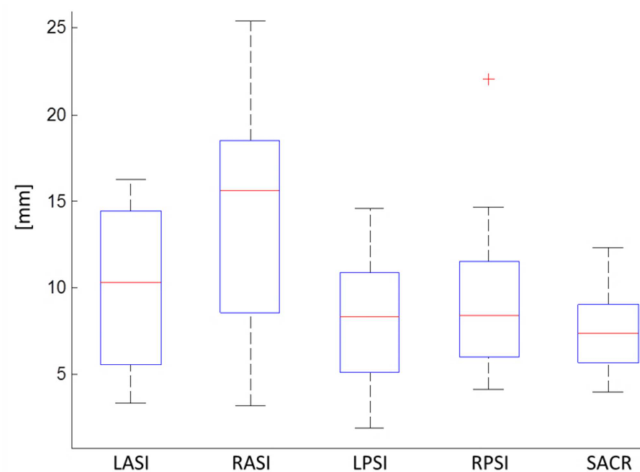


**Figure A2.14** –Soft tissue artefact displacement for the analysed hip position (“Star-Arc movement) with respect to the orthostatic one. Magnitude of the whole displacement represented for each pelvic ALs (right and left anterior superior (RASIS, LASIS), and posterior superior iliac spines (RPSIS, LPSIS), and sacrum (SACR)). Values represented using box-plots (minimum, lower quartile, median, upper quartile, and maximum) and expressed in mm. Statistics performed over all calibration trials and subjects. Outliers are also shown.

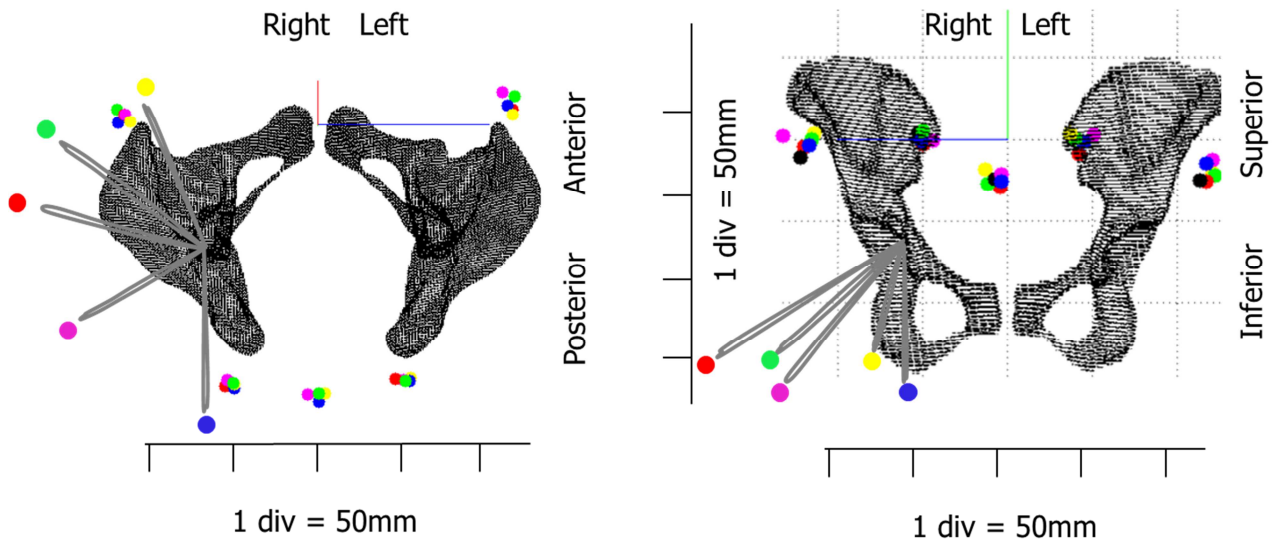


**Figure A2.15** – Soft tissue displacement of marked pelvic ALs (right and left anterior superior (RASIS, LASIS), and posterior superior iliac spines (RPSIS, LPSIS), and sacrum (SACR)). Position of these points represented with colored circles for the different hip hip position (“Star-Arc movement, Figure A2.8). The positions of the different points in the orthostatic posture are also shown with black circles.

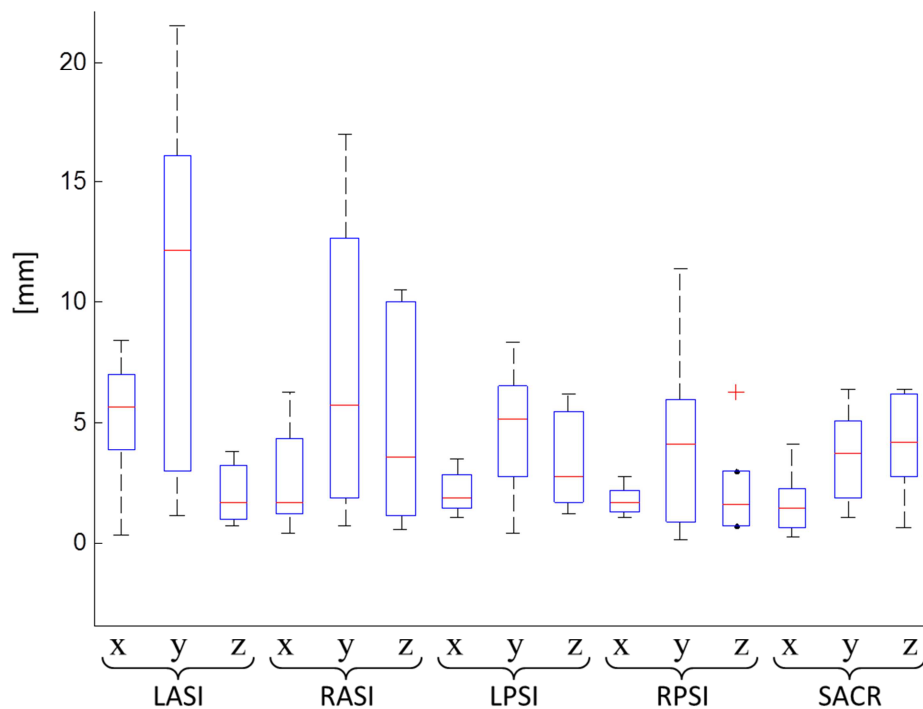


**Figure A2.16** – Soft tissue artefact displacement for the analysed two static positions assumed during the initial part of the gait with respect to the orthostatic one. Displacement represented for the pelvic ALs (right and left anterior superior (RASIS, LASIS), and posterior superior iliac spines (RPSIS, LPSIS), and sacrum (SACR)) and the different anatomical axes directions: x-anterior/posterior; y-inferior/superior; z-medio/lateral. Values represented using box-plots (minimum, lower quartile, median, upper quartile, and maximum) and expressed in mm. Statistics performed over all calibration trials and subjects. Outliers are also shown.

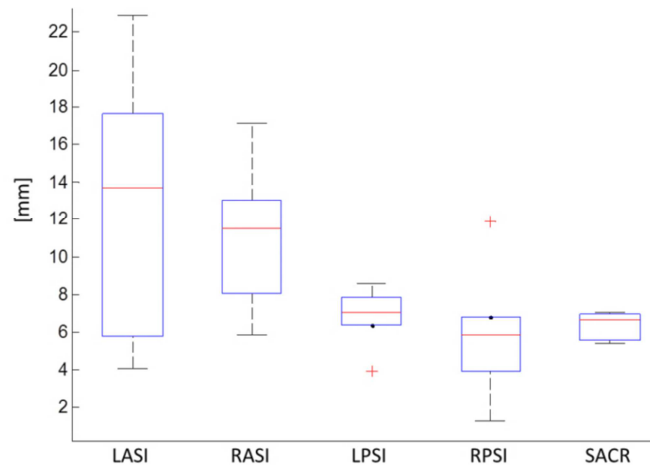


**Figure A2.17** – Soft tissue artefact displacement for the analysed two static positions assumed during the initial part of the gait with respect to the orthostatic one. Magnitude of the whole displacement represented for each pelvic ALs (right and left anterior superior (RASIS, LASIS), and posterior superior iliac spines (RPSIS, LPSIS), and sacrum (SACR)). Values represented using box-plots (minimum, lower quartile, median, upper quartile, and maximum) and expressed in mm. Statistics performed over all calibration trials and subjects. Outliers are also shown.

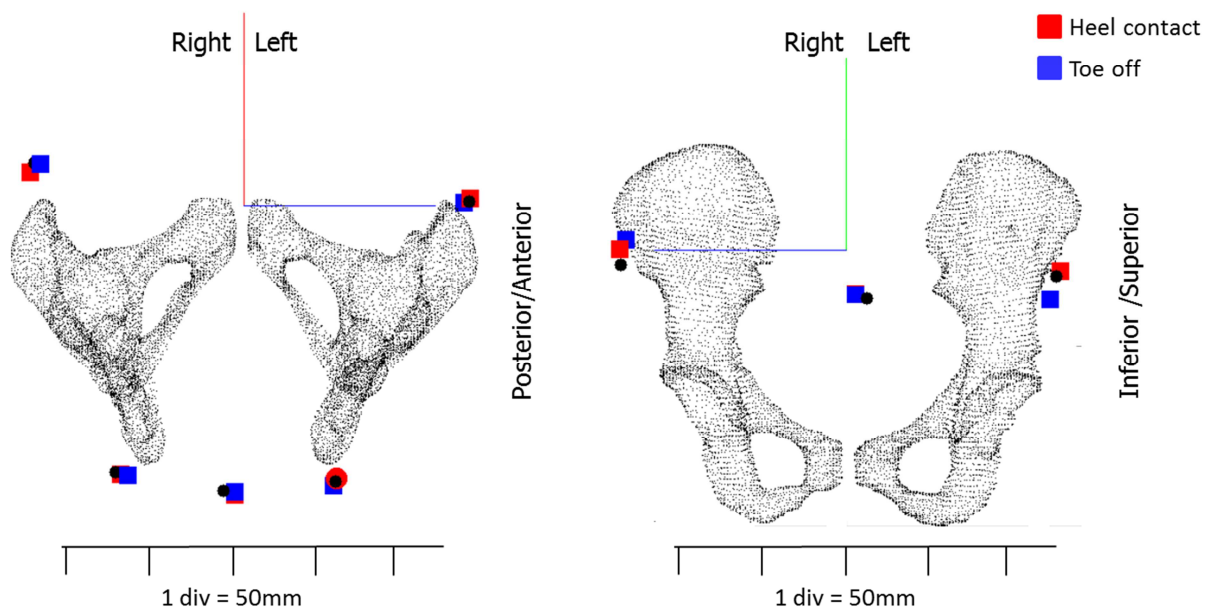


**Figure A2.18** – Soft tissue displacement of marked pelvic ALs (right and left anterior superior (RASIS, LASIS), and posterior superior iliac spines (RPSIS, LPSIS), and sacrum (SACR)). Positions of these points represented with colored squares for two static positions assumed during the initial part of the gait, in red is shown the heel contact and in blue the toe-off (Figure A2.9). The positions of the different points in the orthostatic posture are also shown with black circles.

---

## **Discussion**

The STA resulting from multiple static calibrations performed with the UP-CAST method was in the same range as assessed in Hara et al. (2014), except for the RASIS. To stabilize posture, the right leg on which the subject stood presented hip abductions wider than in gait, possibly causing a STA displacement larger than observed in Hara et al. (2014). The ASIS landmarks confirmed to have greater displacement than the PSIS, and the superior-inferior displacement to be wider than along the other directions as shown in Figures A2.13 and Figures A2.16. This is possibly due to hip abduction angles wider than in gait.

This proof of concept seems promising to enlarge current knowledge on pelvis STA, by performing further investigation on cohorts of subjects, possibly with different body mass indices.

Future work will entail enlarging the sample and further analysing the results in relation to the joint angles involved.

---

## References – A2

- Cappozzo, A., 1984. Gait analysis methodology. *Human Movement Science*, 3(1), 27–50.
- Cappozzo, A., Catani, F., Della Croce, U., Leardini, A., 1995. Position and orientation in space of bones during movement: anatomical frame definition and determination. *Clinical Biomechanics*, 10(4), 171–178.
- Della Croce, U., Leardini, A., Chiari, L., Cappozzo, A., 2005. Human movement analysis using stereophotogrammetry: Part 4: assessment of anatomical landmark misplacement and its effects on joint kinematics. *Gait & Posture* 21(2), 226–237.
- Della Croce, U., Cappozzo, A., Kerrigan, D.C., 1999. Pelvis and lower limb anatomical landmark calibration precision and its propagation to bone geometry and joint angles. *Medical & Biological Engineering & Computing*, 37(2), 155–161.
- Donati, M., Camomilla, V., Vannozzi, G., Cappozzo, A., 2007. Enhanced anatomical calibration in human movement analysis. *Gait & Posture* 26(2), 179–185.
- Donati, M., Camomilla, V., Vannozzi, G., Cappozzo, A., 2008. Anatomical frame identification and reconstruction for repeatable lower limb joint kinematics estimates. *Journal of Biomechanics*, 41(10), 2219–2226.
- Hara, R., Sangeux, M., Baker, R., McGinley, J., 2014. Quantification of pelvic soft tissue artifact in multiple static positions. *Gait & Posture* 39(2), 712–717.
- Leardini, A., Chiari, L., Della Croce, U., Cappozzo, A., 2005. Human movement analysis using stereophotogrammetry. Part 3. Soft tissue artifact assessment and compensation. *Gait & Posture*, 21(2), 212–225.
- Ramakrishnan, H.K., Kadaba, M.P., 1991. On the estimation of joint kinematics during gait. *Journal of Biomechanics*, 24(10), 969–977.
- Rozumalski, A., Schwartz, M., Novacheck, T., Wervej, R., Swanson, A., Dykes, D., 2008. Quantification of pelvic soft tissue artifact. In *Proceedings of the Gait and Clinical Movement Analysis Society*.
- Stagni, R., Leardini, A., Cappozzo, A., Benedetti, M.G., Cappello, A., 2000. Effects of hip joint centre mislocation on gait analysis results. *Journal of Biomechanics*, 33(11), 1479–1487.
- Van Sint Jan, S., 2007. *Color atlas of skeletal landmark definitions: guidelines for reproducible manual and virtual palpations*, Churchill. ed.